Jurnal Farmasi dan Ilmu Kefarmasian Indonesia

This journal is a peer-reviewed journal published three times a year on topics of excellence of research outcomes in the fields of pharmacy service and practise, community medicine, pharmaceutical technology, and health science disciplines that are closely related. This journal only accepts English-language submission. The following are the research areas that this journal focuses on

1. Clinical Pharmacy
2. Community Pharmacy
3. Pharmaceutics
4. Pharmaceutical Chemistry
5. Pharmacognosy
6. Phytochemistry

This journal receives a manuscript from the research results, systematic reviews and meta analyses that are closely related to the health sector, particularly the pharmaceutical field. Selected manuscripts for publication in this journal will be sent to two reviewers, experts in their field, who are not affiliated with the same institution as the author(s). Reviewers are chosen based on the consideration of the editorial team. Manuscripts accepted for publication are edited copies checked for the grammar, punctuation, print style, and format. The entire process of submitting manuscripts to make a final decision for publishing isconducted online.

Table of Content

Molecular Docking: Bioactive Compounds in Indramayu Mango (*Mangifera indica* L.) Peel Waste as NS5B Hepatitis C Virus (HCV) Inhibitor

Gusnia Meilin Gholam*, Mustika Luthfia, Iman Akhyar Firdausy
Department of Biochemistry, Faculty of Mathematics and Natural Sciences, Institut Pertanian Bogor, Bogor, Indonesia

*Corresponding author: gusnia_26@apps.ipb.ac.id

Abstract

Background: *Hepatitis C is caused by hepatitis C virus (HCV) infection. HCV infection is one of the biggest causes of chronic liver disease. About 60-80% of patients with acute hepatitis C will develop chronic hepatitis C.* ***Objective***: *This study aimed to analyze the potential of mango peel compounds as HCV NS5B inhibitors.* ***Methods***: *The methods in this study are ligand preparation, physicochemical and pharmacokinetic predictions, protein structure preparation, molecular docking, data analysis, and visualization.* ***Results***: *The results showed that the test ligands had binding free energies close to the reference ligands, namely Mangiferin -7.862 kcal/mol and respectively D-(+)-Maltose -6.453 kcal/mol, Dibutyl – phthalate -6.326 kcal/mol, bis-β-D-fructofuranose 1,2':2,3'-dianhydride -6.249 kcal/mol, 16-Heptadecyne-1,2,4-triol -5.476 kcal/mol, 3,4,5-trihydroxycyclohex-1-ene-1-carboxylic acid -5,360 kcal/mol, Trigonelline -4.905 kcal/mol, Hexitol -4.552 kcal/mol, α-Glucoheptitol -4.403 kcal/mol. All the test ligands bind the NS5B active site with hydrogen bonds. Furthermore, the ligand-receptor complex has a dissociation constant value and hydrogen bond length.* ***Conclusion***: *The results showed that Mangiferin was the most potential ligand in inhibiting NS5B HCV of all the test ligands used.*

Keywords: bioactive compound, hepatitis c virus, mango, molecular docking, NS5B

INTRODUCTION

Hepatitis C is caused by hepatitis C virus (HCV) infection. HCV infection is one of the biggest causes of chronic liver disease. About 60-80% of patients with acute hepatitis C will develop chronic hepatitis C when the HCV overcomes the body's innate and adaptive immune systems. Many people with chronic hepatitis C are unaware of their condition, as most have been asymptomatic for a long time (Rabaan et al., 2020). The HCV was detected using a serological enzyme immunoassay that measures anti-hepatitis C antibodies to indicate recent or past infection. Chronic hepatitis C is one of the main causes of liver disease worldwide, such as fibrosis, cirrhosis, and hepatocellular carcinoma (Castro et al., 2015). In 2019, an estimated 290,000 people died from hepatitis C, mostly from cirrhosis and hepatocellular carcinoma (WHO, 2021).

HCV is a single-stranded RNA virus in the family *Flaviviridae*. HCV has one open reading frame, which is translated to produce 3000 amino acids and cleaved to produce three structural proteins (core proteins, E1, and E2) and seven non-structural proteins (p7, NS2, NS3, NS4A, NS4B, NS5A, and NS5B) (Bukh, 2016). The HCV life cycle begins when the virion binds to a hepatocyte receptor, then gets internalized and releases *genomic* RNA into the cytoplasm. The HCV replication process is catalyzed by NS5B and several other proteins. NS3 assists the replication process by playing an important role in the RNA binding process, NS4B initiates the replication complex, and NS5A is important in regulating viral replication processes (Li & Lo, 2015).

NS5B is an *RNA-dependent RNA polymerase* (RdRp) protein that plays a role in replicating positive-strand genomic RNA of HCV. NS5B has a polymerase structure consisting of fingers, palms, and thumbs subdomains. The active site of this polymerase is located in the *palm* region (Sabariegos et al., 2021; Wei et al., 2016). NS5B can transcribe viral RNA, which functions for protein translation and the formation of progeny genomes. NS5B is considered an attractive drug target because mammalian cells do not have RdRp polymerase so that it can be selectively inhibited (Boyce et al., 2014). However, drugs to treat hepatitis are still relatively expensive, less effective, and cause various side effects (Shakya, 2019).

Nature provides various human needs, such as food, shelter, and medicinal compounds that can be used as alternative medicine. In addition to having fewer side effects than conventional drugs, plant compounds also have the potential to overcome these problems (Permata & Khoirunnisa, 2020; Zahra et al., 2022). Indonesia is a tropical country with a high number of mango plant commodities. The results of research by Luthfia et al. (2021) showed that there were several compounds isolated from mango peel, some of which were Citroflex A-4, D-(+)-Maltose, 16-Heptadecyne-1,2,4-triol, Mangiferin, 3,4,5-trihydroxycyclohex -1-ene-1-carboxylic acid, Hexitol, Trigonelline, bis-β-D-fructofuranose 1,2':2,3'-dianhydride, α-Glucoheptitol, and Dibuty phthalate. Mangiferin is a xanthone with antiviral, anticancer, antidiabetic, antiaging, antioxidative, and hepatoprotective activities (Imran et al., 2017). This study aimed to analyze the potential of mango peel compounds as HCV NS5B inhibitors.

MATERIALS AND METHODS
Materials

The materials used in this study were the NS5B structure of the Hepatitis C virus, which was downloaded from the Research Collaboratory for Structural Bioinformatics Protein Data Bank (RCSB PDB) (https: //www.rcsb.org/) with PDB ID code "3UPI". The test ligands were from bioactive compounds found in the Indramayu mango (*Mangifera indica* L.) peel waste (Table 1). All test ligands were downloaded from PubChem.

Tools

The equipment used in this study was a *hp* 250 G5 Notebook PC with Windows 10 Professional 64-bit operating system, Intel ® Core ™ i3-6006U processor specifications, and 4.00 GB RAM. The software used to conduct the research was YASARA structure (version 19.9.17) (Krieger & Vriend, 2014), Discovery Studio by Dassault Systems BIOVIA (Biovia, 2017) and PyMOL by Schrödinger.

Methods
Ligand preparation

The ligands structures were downloaded from the PubChem website (https://pubchem.ncbi.nlm.nih.gov/) in 3D and saved in (.pdb) format. Then, the ligand file was prepared using YASARA for energy minimization (*Options > Chose experiment > Energy minimization*) (Luthfia et al., 2021; Venkatachalam & Ettrich, 2021; Gholam et al., 2022). Hydrogens atom were added to all ligands (Gholam, 2022; Venkatachalam & Ettrich, 2021). The test ligands used in this study were Hexitol, Citroflex A-4, D-(+)-Maltose, 16-Heptadecyne-1,2,4-triol, Mangiferin, 3,4,5-trihydroxy cyclo hex-1-ene-1-carboxylic acid, Hexitol, Trigonelline, bis-β-D-fructofuranose 1,2':2,3'-dianhydride, α-Glucoheptitol, Dibutyl phthalate (Table 1). The reference ligand used was Dasabuvir (Shakya, 2019).

Physicochemical and pharmacokinetic prediction

Predictions of physicochemical and pharmacokinetics were performed on the reference and test ligands. The ligands structures were downloaded from the PubChem database (https://pubchem.ncbi.nlm.nih.gov/) in (.sdf) format. The Physicochemical predictions were carried out using the Lipinski rule of five on the SCFBio ITT Delhi website (http://www.scfbio-iitd.res.in/software/drugdesign/lipinski.jsp). The Lipinski rule of five parameters consists of molecular weight, hydrogen donor and hydrogen acceptor, the logarithm of octanol/water partition coefficient (log P), and molar refractivity (Lipinski et al., 1997). The pharmacokinetics prediction was performed by submitting the reference ligand and the test ligand SMILES structure to the pkCSM Biosig Lab website (http://biosig.unimelb.edu.au/pkcsm/prediction). A good ADMET pharmacokinetics profile is characterized by a compound that can be absorbed in the intestine, can be metabolized and excreted completely, and is not toxic (Fida et al., 2021; Luthfia et al., 2021; Pires et al., 2015).

Protein structure preparation

The three-dimensional crystallographic structure of NS5B polymerase bound to the 4, 5-dihydrofurano ligand was downloaded from the protein data bank (PDB ID: 3UPI) (Velázquez et al., 2012). The resolution of the crystallographic structure is 2.00 Å. Only chain B is used in this study, so the unused chains and residues are deleted (Shakya, 2019). Preparation was done using the YASARA structure. The NS5B polymerase receptor is energy-optimized. The optimized structure has the minimum energy for bonding with the test ligand. The crystallographic ligand in chain B has not been removed to determine the grid box area in the active site. It is also necessary to remove water molecules and add hydrogen molecules (Luthfia et al., 2021; Shakya, 2019; Venkatachalam & Ettrich, 2021).

Molecular docking

Validation is required before docking to determine the appropriate grid box. Validation was carried out by redocking the crystallographic ligands on the NS5B receptor. Validation was done using dock_run.mcr. macro from YASARA with runs=25 and Amber14 forcefield (Ali et al., 2020; Gholam & Firdausy, 2022). The grid box used is a cube-shaped 3Å grid box (X = 16.81, Y = 16.81, Z = 16.81). The parameter used is RMSD, with a valid score of less than 2 Å (Ali et al., 2020; Faridah et al., 2019).

The docking was done using the same command file as the validation process; it uses YASARA's dock_run.mcr (Krieger & Vriend, 2014), macro with runs=25, and Amber14 forcefield. YASARA implements AutoDock Vina (Ali et al., 2020; Trott & Olson, 2010; Venkatachalam & Ettrich, 2021). Amber14 forcefield is required to be able to calculate the ligands. Each docking run was ranked based on the strongest binding free energy (kcal/mol). The final result of the docking process shows the approximate binding free energy, dissociation constant (Kd), contact amino acid residues, and the binding conformational coordinates. The docking results are selected based on the lowest binding free energy. The (.yob) file was used to view the position of each ligand and contact amino acid residues through two-dimensional or three-dimensional visualization after being converted into (.pdb) format. (Ali et al., 2020; Venkatachalam & Ettrich, 2021).

Data analysis and visualization

The design for displaying the data in this study follows the research of Shakya (2019) by considering the binding free energy, conventional hydrogen bonds, hydrogen bond distances, and number of hydrogen bonds and visualizing both 2D and 3D conformations. The receptor's complex conformations, ligand interactions, and contact amino acid residues can be seen using the BIOVIA Discovery Studio in two dimensions (2D) (Komarudin et al., 2021). The three-dimensional (3D) visualization was done using PyMOL software (Zaelani et al., 2021).

Table 1. Selected bioactive compounds from Indramayu mango peel waste (Luthfia et al., 2021)

CID	Compound
10222764	Citroflex A-4
439186	D-(+)-Maltose
3015189	16-Heptadecyne-1,2,4-triol
5281647	Mangiferin
1094	3,4,5-trihydroxycyclohex-1-ene-1-carboxylic acid
453	Hexitol
5570	Trigonelline
440332	bis-β-D-fructofuranose 1,2':2,3'-dianhydride
101748	α-Glucoheptitol
3026	Dibutyl phthalate

Table 2. Lipinski prediction results

Compound	Parameter Lipinski rule of five					Application of Lipinski rule of five
	Molecular weight (<500 Da)	Hydrogen donor (<5)	Hydrogen acceptor (<10)	LogP (<5)	Molar refractivity (40-130)	
Dasabuvir (reference ligand)	493	1	5	3.141550	130.175186	Passed
Citroflex A-4	402	0	8	4.542399	107.939987	Passed
D-(+)-Maltose	342	8	11	0.779680	72.029884	Passed
16-Heptadecyne-1,2,4-triol	284	3	3	4.053739	92.266380	Passed
Mangiferin	422	7	11	1.100710	89.980591	Passed
3,4,5-trihydroxycyclohex-1-ene-1-carboxylic acid	174	4	5	0.250540	37.080692	Passed
Hexitol	182	6	6	0.326940	39.968788	Passed
Trigonelline	137	0	2	0.550850	32.389000	Passed
bis-β-D-fructofuranose 1,2':2,3'-dianhydride	324	6	10	1.014480	68.844788	Passed
α-Glucoheptitol	212	6	7	0.514430	46.122288	Passed
Dibutyl phthalate	278	0	4	3.439459	77.445992	Passed

RESULTS AND DISCUSSION

This study used bioactive compounds in Indramayu mango peel waste. Research by Luthfia et al. (2021) using LC-MS found several active compounds in Indramayu mango peel waste. Luthfia et al. (2021) also analysed the potential of the compounds that have the potential as an antiviral for SARS-CoV-2 with the target protein of *Angiotensin-converting enzyme* 2 (ACE2) *in silico*. The research proved that Mangiferin had the highest activity inhibiting ACE2. This study analysed the interaction of bioactive compounds in Indramayu mango peel waste as hepatitis C antiviral.

Physicochemical and pharmacokinetic prediction

Before molecular docking was performed, the pharmacokinetics and the physicochemical properties of the bioactive compounds in Indramayu mango peel waste were predicted. The physicochemical properties of the reference and test ligands were predicted using Lipinski rule of five. The parameters in Lipinski's rule of five were; molecular weight, number of hydrogen donors and acceptors, the partition coefficient value of octanol to water (log P), and molar refractivity. Compounds with good physicochemical properties had molecular weights <500 Da, number of hydrogen donors and acceptors <5 and <10, log P values <5, and molar refractivity value of 40-130 (Lipinski et al., 1997; *Lipinski Rule of Five*, n.d.). Compounds that did not violate a maximum of two parameters are considered a good drug candidates. The physicochemical predictions showed that the reference and test ligands passed the physicochemical predictions based on the Lipinski rule of five (Table 2).

The molecular weight of a compound plays a role in determining the permeability of the compound. Compounds with a molecular weight of less than 500 Da can easily penetrate cell membranes. The number of hydrogen donors and acceptors acts as a secondary determinant of fractional absorption because it affects the molecular interactions that will be formed with water molecules. The number of hydrogen acceptors and donors in a compound that is too high indicates poor permeability, which will affect the absorption and distribution process of the compound (Lipinski et al., 1997).

The log P value expresses a compound's lipophilic nature and solubility in the water. A good compound has low lipophilic properties, indicating that the compound is soluble in water. Meanwhile, molar refractivity determines the permeability of a compound. Molar refractivity values of 40-130 indicate that the body can absorb these compounds well (Lipinski et al., 1997; *Lipinski Rule of Five*, n.d.).

The test ligands' pharmacokinetic properties were predicted in absorption, distribution, metabolism, excretion, and toxicity (ADMET) using pkCSM Biosig Lab website (http://biosig.unimelb.edu.au/pkcsm/prediction). The absorption profile was determined by intestinal absorption and Caco2 permeability parameters. The steady-state volume of distribution (VDss) and the blood-brain barrier (BBB) parameters determined the distribution profile. The value of CYP2D6 inhibitors

and CYP3A4 inhibitors determined a metabolic profile. Meanwhile, the excretion profile can be determined based on the total clearance parameter, and the hepatotoxicity parameter can specify the toxicity profile (Pires et al., 2015).

A compound is considered to have good absorption if its absorption value in the intestine is 70-100%. Meanwhile, Caco2 permeability shows the ability of the compound to permeate the intestinal epithelium, which acts as a model for selecting candidates for oral administration. Caco2 permeability values with Ppap logs > 0.90 x 10^{-6} cm/s are considered to have high permeability (Singh, 2016). VDss shows the value of a total dose of a drug distributed thoroughly with the same concentration in blood plasma. Compounds with a high volume of distribution have a log VDss value > 0.45 and low if the log VDss value is < -0.15. The BBB parameter states the ability of a compound to penetrate the brain barrier, help reduce side effects and toxicity, and increase drug efficacy. A good compound has a log BBB value of > 0.3, and a bad one if the log BBB value is < -1 (Fida et al., 2021; Pires et al., 2015).

Metabolic profile is chemically changing drugs to form metabolites (detoxification). The liver carries this detoxification process using the cytochrome P450 (CYP) isoenzyme, consisting of CYP2D6 and CYP3A4. CYP2D6 plays a role in detoxifying drugs and xenobiotic substances in the body, while CYP3A4 plays of up to 50% in drug detoxification and is present in the small intestine and kidneys. The interaction of CYP inhibitors with the substrate can increase plasma levels (bioavailability), causing increased substrate activity and unwanted side effects (Fida et al., 2021; Pires et al., 2015).

Table 3. Predicted results of ADMET on test ligands

Compound	Absorption		Distribution		Metabolism		Excretion	Toxicity
	Intestinal absorption (%)	Caco2 permeability (log Ppap in 10^{-6} cm/s)	VDss (log L/kg)	BBB (log BB)	CYP2D6 inhibitor	CYP3A4 inhibitor	Total clearance	Hepatotoxicity
Dasabuvir (reference ligand)	85.507	-0.1111	-0.957	-1.03	No	Yes	0.735	Yes
Citroflex A-4	65.533	1.01	-0.071	-1.34	No	No	2.059	No
D-(+)-Maltose	6.412	-0.12	0.203	-1.024	No	No	1.545	No
16-Heptadecyne-1,2,4-triol	93.219	1.564	-0.369	-0.056	No	No	1.976	No
Mangiferin	46.135	-0.926	1.364	-1.573	No	No	0.347	No
3,4,5-trihydroxycyclohex-1-ene-1-carboxylic acid	46.681	-0.23	-0.618	-0.683	No	No	0.688	No
Hexitol	25.401	-0.441	-0.325	-1.309	No	No	0.919	No
Trigonelline	96.44	1.124	-0.758	-0.234	No	No	0.378	No
bis-β-D-fructofuranose 1,2':2,3'-dianhydride	32.563	0.448	0.281	-0.905	No	No	1.29	No
α-Glucoheptitol	21.174	-0.121	-0.304	-1.451	No	No	0.976	No
Dibutyl phthalate	95.044	1.622	-0.007	-0.054	No	No	0.93	No

Table 4. Crystallographic ligand redocking (validation)

Ligand	Binding free energy (kcal/mol)	RMSD (Å)	Contact amino acid residue
4,5-dihydrofurano	-11.26	0.00	PHE B:193, PRO B:197, ARG B:200, ASN B:316, ASP B:318, ASP B:319, CYS B:366, SER B:367, SER B:368, LEU B:384, GLY B:410, ASN B:411, MET B:414, TYR B:415, GLN B:446, ILE B:447, TYR B:448, GLY B:449, SER B:556

The total clearance parameter, a combination of hepatic and renal clearance determines the excretion profile. This relates to bioavailability and determines the dose to reach a steady state. It is also important to know the toxicity profile, one of which is hepatotoxicity. Hepatotoxicity is the primary manifestation of drug toxicity involving hepatocytes as an approach used in drug development (Fida et al., 2021; Pires et al., 2015). The pharmacokinetic prediction results showed that dasabuvir had a reasonably good pharmacokinetics profile but was hepatotoxic. Meanwhile, all tested ligands had a good pharmacokinetics and were not hepatotoxic (Table 3).

The physicochemical properties of the reference and test ligands were predicted using the Lipinski rule of five (Table 2). The physicochemical prediction results showed that the reference and test ligands met the Lipinski rule of five qualifications. The eleven ligands were followed by pharmacokinetics predictions of absorption, distribution, metabolism, excretion, and toxicity (ADMET). The pharmacokinetic prediction of dasabuvir (as a reference ligand) showed a relatively good pharmacokinetic profile but was hepatotoxic. Meanwhile, all tested ligands had a good pharmacokinetics and were not hepatotoxic (Table 3).

Molecular docking

The target enzyme is NS5B from the hepatitis C virus (HCV), which has a resolution of 2.00 Å (PDB ID: 3UPI) (Velázquez et al., 2012). Luthfia et al. (2021) explain that the quality of good protein structures ranges from 1.5 to 2.5 Å in molecular docking studies. NS5B is an RNA polymerase enzyme that plays an essential role in HCV replication (Shakya, 2019). The NS5B polymerase target receptor prepared using the YASARA structure has a structure composed of A and B chains. The A chain and water molecule were deleted. The B chain and the crystallographic ligand 4,5-dihydrofurano bound in the B chain are used to determine the grid box size. Ten test ligands from

Indramayu mango peel waste and one reference ligand were prepared using the YASARA structure. The three-dimensional structure is downloaded from the PubChem page in (.sdf) file format. The ligand energy was minimized and saved in the form of (_ligand.sdf) to be docked to the NS5B HCV protein receptor.

Before docking, validation was carried out to find the grid box size, with an RMSD value <2 Å to limit the movement area of the test ligands. This study used a grid box size of 3 Å (X = 16.81, Y = 16.81, Z = 16.81). The macro play option from the YASARA structure is used for the docking, using the dock.run macro (Gholam & Firdausy, 2022) with settings of runs=25 and Amber14 force field. Validation was carried out by redocking the crystallographic ligand,5-dihydrofurano, into the NS5B protein receptor. The results of the grid box validation can be seen in Table 4. This validation stage is intended to measure the validity of a molecular docking method. The parameter used is Root Mean Square Deviation (RMSD). RMSD is a parameter that shows the difference between the crystallographic ligand poses before and after redocking (Damayanti et al., 2021). Based on the validation results (Table 4), the resulting RMSD has an RMSD score of 0.00 Å. This result can be considered valid because the redocking process is able to mimic the initial pose of the crystallographic ligand when it is downloaded from the PDB (Damayanti et al., 2021). A grid box with a size of 3 Å is chosen to perform the molecular docking of the test ligand against the target protein. The results of the validation can be seen in Table 4.

The eleven ligands were docked on a 3 Å grid box (X = 16.81, Y = 16.81, Z = 16.81). The eleven ligands include Dasabuvir as a reference ligand and bioactive compounds from Indramayu mango peel waste consisting of Citroflex A-4, D-(+)-Maltose, 16-Heptadecyne-1,2,4-triol, Mangiferin, 3,4,5-trihydroxycyclohex-1-ene-1-carboxylic acid, Hexitol,

Trigonelline, bis-β-D-fructofuranose 1,2':2,3'-dianhydride, α-Glucoheptitol, Dibutyl phthalate as the test ligand. Eleven ligands were docked to inhibit the NS5B polymerase target receptor. Molecular docking was done using YASARA structure with play macro dock_run settings runs=25 and Amber14 force field (Ali et al., 2020; Gholam et al., 2022). The docking results using the YASARA structure are binding free energy (kcal/mol), the resultant file containing receptor-ligand complex and contact amino acid residues. The overall results that follow the parameters in the study by Shakya (2019) are presented in Table 5. In addition, this study also calculates the dissociation constant. The dissociation constant in YASARA structure docking results can be seen in Table 5, unchanged as in Srivastava et al. (2018) research. Visualization was carried out to show the various amino acid residues involved and three-dimensional visualization on the surface.

Molecular docking can be used to investigate the possibility of binding interactions between the test ligand and the protein at the binding site.(Srivastava et al., 2018). The results showed that amino acid residues that form hydrogen bonds in the ligand-receptor complex were ASN B:291, ASN B:316, ASP B:318, ASP B:319, CYS B:366, SER B:367, SER B:368, SER B:407, ASN B:411, TYR B:415, GLN B:446, TYR B:448, GLY B:449 (Table 5). The total number of these amino acid residues is thirteen. It is known that all thirteen amino acids that form hydrogen bonds occur at the binding site. This is known because Shakya (2019) has provided a series of amino acid residues that have the potential as binding sites on NS5B polymerase. This study's overall contact with amino acid residues also occurred in Chain B.

Table 5. Molecular docking results and interaction data

Compound	Binding free energy (kcal/mol)	Dissociation constant (pM)	Hydrogen bonds	Hydrogen bonds distance (Å)	Number of hydrogen bonds
Dasabuvir (reference ligand)	-9.175	188207.031	ASN B:291	1.90	5
			ASP B:318	1.60, 2.10, 2.50	
			GLN B:446	2.36	
Mangiferin	-7.862	1726146.25	ASP B:318	2.14	8
			ASP B:319	2.47, 2.98	
			CYS B:366	2.62, 4.69, 4.72	
			SER B:367	2.19	
			TYR B:415	1.99	
Hexitol	-4.552	460616768	SER B:407	2.10	5
			ASN B:411	2.39, 2.84	
			GLN B:446	1.92, 2.23	
3,4,5-trihydroxycyclohex-1-ene-1-carboxylic acid	-5.360	117779008	CYS B:366	2.49	2
			SER B:368	2.53	
Trigonelline	-4.905	253855936	ASN B:316	2.53	3
			CYS B:366	2.95, 4.97	
α-Glucoheptitol	-4.403	592322496	GLN B:446	2.58	1
D-(+)-Maltose	-6.453	18616082	CYS B:366	2.69, 2.99	5
			GLN B:446	2.19	
			TYR B:448	2.28	
			GLY B:449	2.71	
bis-β-D-fructofuranose 1,2':2,3'-dianhydride	-6.249	26267714	CYS B:366	2.35	6
			ASN B:411	2.66, 2.77, 3.01	
			TYR B:415	2.13	
			TYR B:448	2.35	
16-Heptadecyne-1,2,4-triol	-5.476	96836432	SER B: 407	2.16	3
			ASN B:411	2.48, 2.70	
Dibutyl phthalate	-6.326	23066438	TYR B:415	1.96	1

This study showed that the reference ligand Dasabuvir (CID_56640146) had the lowest binding free energy than the test ligand. Dasabuvir has a score of -9.175 kcal/mol. Dasabuvir forms hydrogen bonds in the amino acids residue ASN B:291, ASP B:318, and GLN B:446 with five hydrogen bonds (Fig 1). However, a test ligand has a binding score close to the reference ligand, Mangiferin (CID_5281647). Mangiferin has a binding free energy score of -7.862 kcal/mol. Mangiferin forms hydrogen bonds in the amino acids residue ASP B:318, ASP B:319, CYS B:366, SER B:367, and TYR B:415 with a total of eight hydrogen bonds (Fig 10). Mangiferin is the test ligand with the lowest docking score, and it should be noted in this study that all test ligands had a docking score. Consecutively D-(+)-Maltose (CID_439186) with a -6.453 kcal/mol binding score. Hydrogen bonds are formed at the amino acid residues CYS B:366, GLN B:446, TYR B:448, and GLY B:449 with a total of five bonds (Fig 6). Dibutyl phthalate (CID_3026) has a binding score of -6.326 kcal/mol with contact amino acid residues that form one hydrogen bond at TYR B:415 (Fig 9). bis-β-D-fructofuranose 1,2':2,3'-dianhydride (CID_ 440332) has a score of -6.249 kcal/mol. The amino acid residues forming hydrogen bonds, are CYS B:366, ASN B:411, TYR B:415, TYR B:448, with six hydrogen bonds formed (Fig 7). 16-Heptadecyne-1,2,4-triol (CID_3015189) with a docking score of -5.476 kcal/mol and residues that form hydrogen bonds are SER B:407, ASN B:411 with a total of three hydrogen bonds (Fig 8). 3,4,5-trihydroxycyclohex-1-ene-1-carboxylic acid (CID_1094) has a score of -5.360 kcal/mol. Hydrogen bonds are formed at residues CYS B:366, SER B:368 with two hydrogen bonds (Fig 3). Trigonelline (CID_5570) has a -4.905 kcal/mol score with amino acid residues that form hydrogen bonds at ASN B:316, and CYS B:366 and have a total of three hydrogen bonds (Fig 4). Hexitol (CID_453) has a -4.552 kcal/mol score with amino acid residues formed at SER B:407, ASN B:411, and GLN B:446 and has a total of five hydrogen bonds (Fig 2). α-Glucoheptitol (CID_101748) had the lowest binding score of all ligands with a -4.403 kcal/mol score. Also, this ligand only formed one hydrogen bond at residue GLN B:446 (Fig 5). Mangiferin has been shown to have scores close to the reference ligand Dasabuvir, but Mangiferin has more hydrogen bonds than Dasabuvir, which is eight bonds. The findings of this study provide a potential test ligand candidate for Mangiferin in its role of inhibiting NS5B. All data from the test ligands and reference ligands from the docking results are presented in Table 5.

Shakya (2019) explains that the minimum binding free energy, the greater the bond affinity in molecular docking studies. In addition, one of the main concerns of in silico studies is the presence of hydrogen bonds because the presence of bonds can determine the binding strength of the receptor-ligand (Shakya, 2019). This study found that the average presence of hydrogen bonds was caused by the interacting -OH (hydroxyl) group, which is also known to help stabilize the receptor-ligand complex (Weni et al., 2020; Gholam et al., 2022). This study also showed that the more hydrogen bonds, the stronger the bonds formed between the receptor-ligands complex. This is following the research of Uzzaman et al. (2019), which explains that a strong hydrogen bond is a significant contributing factor in increasing the affinity of drugs with receptors. Some literature states that strong hydrogen bonds have a distance of less than 2.3 Å (Uzzaman et al., 2021).

Visualization was carried out to analyze the receptor-ligand complex that forms a bond at each amino acid residue on the receptor. Visualization was done using BIOVIA Discovery Studio to visualize in two dimensions and PyMOL in three dimensions (surface). Visualization of the receptor-ligand complex can be seen in Figures 1 to 10. Visualization on the surface shows magenta colour in the ligand area. This is because the magenta indicates the visualization of the binding site area.

CONCLUSION

The results showed that of all the test ligands used, Mangiferin was predicted as the most potential ligand in inhibiting NS5B HCV. Each test ligand has a molecular interaction in the form of hydrogen bonds that bind the active site of NS5B HCV. The physicochemical and pharmacokinetic predictions of the test ligands also showed that the ligands used were in good criteria according to the specified parameters. This research needs to be proven *in vitro* and *in vivo*.

ACKNOWLEDGMENT

REFERENCES

Ali, N. S. M., Salleh, A. B., Leow, T. C., Abd Rahman, R. N. Z. R., & Ali, M. S. M. (2020). The Influence of Calcium toward Order/Disorder Conformation of Repeat-in-Toxin (RTX) Structure of Family I.3 Lipase from Pseudomonas fluorescens AMS8. *Toxins*, *12*(9), 579. https://doi.org/10.3390/toxins12090579

Biovia, D. S. (2017). *BIOVIA Discovery Studio Visualizer* (p. 936).

Boyce, S. E., Tirunagari, N., Niedziela-Majka, A., Perry, J., Wong, M., Kan, E., Lagpacan, L.,

Barauskas, O., Hung, M., Fenaux, M., Appleby, T., Watkins, W. J., Schmitz, U., & Sakowicz, R. (2014). Structural and Regulatory Elements of HCV NS5B Polymerase-β-loop and C-terminal tail - Are Required for Activity of Allosteric Thumb Site II Inhibitors. *PLoS ONE*, *9*(1), 1–12. https://doi.org/10.1371/journal.pone.0084808

Bukh, J. (2016). The History of Hepatitis C virus (HCV): Basic Research Reveals Unique Features in Phylogeny, Evolution and The Viral Life Cycle with New Perspectives for Epidemic Control. *Journal of Hepatology*, *65*(1), S2–S21. https://doi.org/10.1016/j.jhep.2016.07.035

Castro, R., Perazzo, H., Grinsztejn, B., Veloso, V. G., & Hyde, C. (2015). Chronic Hepatitis C: An Overview of Evidence on Epidemiology and Management from a Brazilian Perspective. *International Journal of Hepatology.* https://doi.org/10.1155/2015/852968

Damayanti, S., Khonsa, K., & Amelia, T. (2021). Antiviral Activity and Toxicity Prediction of Compounds Contained in Figs (Ficus carica L.) by In Silico Method. *Indonesian Journal of Pharmaceutical Science and Technology*, *8*(1), 21–33.

Faridah, Mumpuni, E., & Yunanto, Y. I. (2019). Analisis In-Silico Senyawa Kimia dalam Teh Hijau yang Bekerja pada Aktivator (PPAR-γ) sebagai Antiobesitas. *Jurnal Ilmu Kefarmasian Indonesia*, *17*(2), 251–254.

Fida, S., Dewi, A. R., & Damayanti, D. S. (2021). Studi In Silico Senyawa Aktif Daun Sirsak (Annona muricata L.) pada Aldose Reductase dan Glutathione Reductase untuk Menghambat Katarak Diabetik. *Jurnal Kedokteran Komunitas*, *9*(2), 1–14.

Gholam, G. M., Darmawan, N. I., Siregar, J. E., & Artika, I. M. (2022). Selected Polyphenols from Date (*Phoenix dactylifera*) as Anti-Virulence of *Candida albicans* Through Multiple Enzyme Targets. *Biointerface Research in Applied Chemistry*, *13*(4), 386. https://doi.org/10.33263/BRIAC134.386

Gholam, G. M. (2022). Molecular docking of the bioactive compound Ocimum sanctum as an inhibitor of Sap 1 Candida albicans. *Sasambo Journal of Pharmacy*, *3*(1), 18–24. https://doi.org/https://doi.org/10.29303/sjp.v6i1.264

Gholam, G. M., & Firdausy, I. A. (2022). Molecuar Docking Study of Natural Compounds from Red Betel (*Piper crocatum* Ruiz & Pav) as Inhibitor of Secreted Aspartic Proteinase 5 (Sap 5) in *Candida albicans,* *3*(2), 97-104. https://doi.org/10.29303/sjp.v3i2.145

Imran, M., Arshad, M. S., Butt, M. S., Kwon, J. H., Arshad, M. U., & Sultan, M. T. (2017). Mangiferin: A Natural Miracle Bioactive Compound Against Lifestyle Related Disorders. *Lipids in Health and Disease*, *16*(84), 1–17.

https://doi.org/10.1186/s12944-017-0449-y

Komarudin, A. D. P., Purnama, M. F. G., Sari, A. Y., Izzati, A., Sahila, E. N. M. R., Hidayat, S., Apriliya, T. N., & Muchtaridi. (2021). Studi In Silico Senyawa Tanaman Nerium oleander terhadap STAT-3 pada Kanker Payudara. *Jurnal Farmasi Udayana*, *10*(2), 149–155. https://doi.org/10.24843/jfu.2021.v10.i02.p07

Krieger, E., & Vriend, G. (2014). YASARA View - Molecular Graphics for All Devices - From Smartphones to Workstations. *Bioinformatics*, *30*(20), 2981–2982. https://doi.org/10.1093/bioinformatics/btu426

Li, H. C., & Lo, S. Y. (2015). Hepatitis C Virus: Virology, Diagnosis and Treatment. *World Journal of Hepatology*, *7*(10), 1377–1389. https://doi.org/10.4254/wjh.v7.i10.1377

Lipinski, C. A., Lombardo, F., Dominy, B. W., & Feeney, P. J. (1997). Experimental and Computational Approaches to Estimate Solubility and Permeability in Drug Discovery and Development Settings. *Advanced Drug Delivery Reviews*, *23*, 3–25. https://doi.org/10.1016/S0169-409X(96)00423-1

Lipinski Rule of Five. (n.d.). Retrieved July 19, 2022, from http://www.scfbio-iitd.res.in/software/drugdesign/lipinski.jsp

Luthfia, M., Eryandini, A., Geraldi, D., Narita, C., Miftahul, C., Jannah, & Ambarsari, L. (2021). Potency of Bioactive Compounds in Indramayu Mango Peel Waste to Inhibit ACE2. *Current Biochemistry*, *8*(2), 51–62.

Permata, E. I., & Khoirunnisa, Y. (2020). Efek Mangiferin dalam Mengatasi Masalah Kesehatan. *Jurnal Penelitian Perawat Profesional*, *2*(1), 31–38. https://doi.org/10.37287/jppp.v2i1.38

Pires, D. E. V, Blundell, T. L., & Ascher, D. B. (2015). pkCSM: Predicting Small-Molecule Pharmacokinetic and Toxicity Properties Using Graph-Based Signatures. *Journal of Medicinal Chemistry*, *58*, 4066–4072. https://doi.org/10.1021/acs.jmedchem.5b00104

Rabaan, A. A., Al-Ahmed, S. H., Bazzi, A. M., Alfouzan, W. A., Alsuliman, S. A., Aldrazi, F. A., & Haque, S. (2020). Overview of Hepatitis C Infection, Molecular Biology, and New Treatment. *Journal of Infection and Public Health*, *13*(5), 773–783. https://doi.org/10.1016/j.jiph.2019.11.015

Sabariegos, R., Albentosa-González, L., Palmero, B., Clemente-Casares, P., Ramírez, E., García-Crespo, C., Gallego, I., de Ávila, A. I., Perales, C., Domingo, E., & Mas, A. (2021). Akt Phosphorylation of Hepatitis C Virus NS5B Regulates Polymerase Activity and Hepatitis C Virus Infection. *Frontiers in Microbiology*, *12*, 3043. https://doi.org/10.3389/fmicb.2021.754664

Shakya, A. K. (2019). Natural Phytochemicals: Potential Anti-HCV Targets In Silico Approach. *Journal of Applied Pharmaceutical Science*, *9*(8),

94–100.
https://doi.org/10.7324/JAPS.2019.90813

Singh, D. (2016). Defining Desirable Natural Product Derived Anticancer Drug Space: Optimization of Molecular Physicochemical Properties and ADMET Attributes. *ADMET and DMPK*, *4*(2), 98–113. https://doi.org/10.5599/admet.4.2.291

Srivastava, S., Shree, P., Pandey, H., & Tripathi, Y. B. (2018). Incretin Hormones Receptor Signaling Plays The Key Role in Antidiabetic Potential of PTY-2 Against STZ-induced Pancreatitis. *Biomedicine & Pharmacotherapy*, *97*, 330–338. https://doi.org/10.1016/j.biopha.2017.10.071

Trott, O., & Olson, A. J. (2010). AutoDock Vina: Improving The Speed and Accuracy of Docking With a New Scoring Function, Efficient Optimization and Multithreading. *Journal of Computational Chemistry*, *31*(2), 455–461. https://doi.org/10.1002/jcc.21334.AutoDock

Uzzaman, M., Chowdhury, K., & Hossen, M. B. (2019). *Thermochemical , molecular docking and ADMET studies of aspirin metabolites*. *2*, 1–5. https://doi.org/10.15761/FDCCR.1000130

Uzzaman, M., Hasan, M. K., Mahmud, S., Yousuf, A., Islam, S., Uddin, M. N., & Barua, A. (2021). Physicochemical, Spectral, Molecular Docking and ADMET Studies of Bisphenol Analogues; A Computational Approach. *Informatics in Medicine Unlocked*, *25*, 100706. https://doi.org/10.1016/j.imu.2021.100706

Velázquez, F., Venkatraman, S., Lesburg, C. A., Rosenblum, S. B., Kozlowski, J. A., & Njoroge, F. G. (2012). Synthesis of New 4,5-Dihydrofuranoindoles and Their Evaluation as HCV NS5B Polymerase Inhibitors. *Organic Letters*, *14*(2), 556–559.

Venkatachalam, K. V, & Ettrich, R. H. (2021). Role of Aspartic Acid Residues D87 and D89 in APS Kinase Domain of Human with Phosphatases/Kinases. *Biochemistry and Biophysics Reports*, *28*, 101155. https://doi.org/10.1016/j.bbrep.2021.101155

Wei, Y., Li, J., Qing, J., Huang, M., Wu, M., Gao, F., Li, D., Hong, Z., Kong, L., Huang, W., & Lin, J. (2016). Discovery of Novel Hepatitis C Virus NS5B Polymerase Inhibitors by Combining Random Forest, Multiple e-Pharmacophore Modeling and Docking. *PLoS ONE*, *11*(2), 1–25. https://doi.org/10.1371/journal.pone.0148181

Weni, M., Safithri, M., & Seno, D. S. H. (2020). Molecular Docking of Active Compounds Piper crocatum on The Alpha-Glucosidase Enzyme as Antidiabetic. *Indonesian Journal of Pharmaceutical Science and Technology*, *7*(2), 64–72.

WHO. (2021). *Hepatitis C*. World Health Organization. https://www.who.int/news-room/fact-sheets/detail/hepatitis-c

Zaelani, B. F. D., Safithri, M., & Andrianto, D. (2021). *Molecular Docking of Red Betel (Piper crocatum Ruiz & Pav) Bioactive Compounds as HMG-CoA Reductase Inhibitor*. *24*(3), 101–107. https://doi.org/10.14710/jksa.24.3.101-107

Zahra, H., Haridas, R. B., Gholam, G. M., & Setiawan, A. G. (2022). Aktivitas Antiulseratif Berbagai Tanaman Herbal dan Prospek Masa Depan Sebagai Tanaman Budidaya. *Jurnal Sains Dan Kesehatan*, *4*(3), 343–353. https://doi.org/10.25026/jsk.v4i3.1046

Molecular Docking of Bicycloproline Derivative Synthetic Compounds on Envelope Protein: Anti-SARS-CoV-2 Drug Discovery

Syaiful Prayogi[1,2], Binar Asrining Dhiani[1], and Asmiyenti Djaliasrin Djalil[1]*
[1]Department of Pharmacy, Faculty of Pharmacy, Universitas Muhammadiyah Purwokerto, Purwokerto, Indonesia
[2]Department of Pharmacy, Faculty of Science and Technology, University of Peradaban, Brebes, Indonesia

*Corresponding author: asmiyentidjaliasrindjalil@ump.ac.id

Abstract

Background*: Although a SARS-CoV-2 vaccine is readily available, new cases of COVID-19 are still occurring. New drug discovery is needed to treat COVID-19. Protein E is one of the potential targets. Two synthetic compounds of bicycloproline derivatives have the potential to be developed.* ***Objective:*** *This study aimed to estimate the interaction of bicycloproline compounds to protein E in-silico.* ***Methods:*** *There were two bicycloproline-derived compounds, MI-09 and MI-30, used in docking. Remdesivir was used as a reference ligand. The crystal structure of the E protein was created using homology modeling, while the test compound was drawn using the Marvin Sketch. MOE 2022.02 and BDS 2021 were used for docking and visualization processes.* ***Results:*** *The pentamer of the SARS-CoV-2 E protein obtained a clash score (1.06); poor rotatomer (0.00%); favored rotamers (98.11%); Ramachandran favored (96.43%); Ramachandran outlier (1.78%); Rama Z-score (-1.08); and mol probity (1.04). Research shows promising inhibition potential of the MI-09 and MI-30. The MI-30 has the best binding energy of -10.3326 kcal/mol.* ***Conclusion:*** *The docking results show that MI-30 has potency as an inhibitor of protein E and can be developed in treating COVID-19. Further research is needed to confirm the result by in vitro and in vivo studies.*

Keywords*: COVID-19, homology modeling, envelope protein, bicycloproline, molecular docking*

How to cite this article:

Prayogi, S., Dhiani, B. A., & Djalil, A. D. (2023). Molecular Docking of Bicycloproline Derivative Synthetic Compounds on Envelope Protein: Anti-SARS-CoV-2 Drug Discovery. *Jurnal Farmasi dan Ilmu Kefarmasian Indonesia,* 10(1), 11-21. http://doi.org/10.20473/jfiki.v10i12023.11-21

INTRODUCTION

Although a vaccine for Severe Acute Respiratory Syndrome Coronavirus 2 (SARS-CoV-2) is already available, new cases of COVID-19 are still occurring due to low immunization coverage and emerging new variants. Therefore, new drugs are needed to treat severe COVID-19. CoV is a sheathed virus consisting of a single-stranded RNA as its genome. The genome size ranges from 26 to 32 kilobases, considered one of the largest among retroviruses (Woo et al., 2010). Pore-forming proteins in the SARS-CoV-2 envelope protein use amphipathic α-helix for pore formation. Pore openings are essential for transporting ions, toxins, and viroporin activity (Khader & Mohideen, 2021). For this reason, knowledge about the SARS CoV-2 protein is essential.

SARS-CoV-2 is a class of betacoronaviruses that have the polyproteins ORF1a and ORF1ab as well as 4 structural proteins: spike glycoprotein (S), membrane (M), nucleocapsid (N), and envelope (E) (Abdelrahman et al., 2020; M et al., 2020; Prajapat et al., 2020). Among these components, protein E is an ideal protein target for molecular docking (Chernyshev, 2020; Das et al., 2021). Research on the drug development of COVID-19, which targeted the SARS-CoV-2 E protein, was still limited. Some research was focused on drug repurposing of existing antiviral drugs. Therefore, drug development initiated with molecular docking targeting protein E of SARS-CoV-2 has significant novelty value.

In previous studies, many researchers have done extensive work uncovering SARS-CoV structural proteins. Structural proteins of SARS-CoV, such as proteins E, S, and M, can be suitable candidates for studying target drug interactions (J. Torres et al., 2006). Comparable to SAR-CoV, the SARS CoV-2 E protein plays a role in the infection process Protein E plays a role in the infection process (Alsaadi & Jones, 2019), virus assembly, virion release, and pathogenesis (Schoeman & Fielding, 2019) and, together with the M protein, plays a role in the spike maturation of SARS-CoV-2 (Boson et al., 2021). Its involvement in various aspects of protein targeting potentially stops the spread of infection while reducing symptoms and managing complications such as *Acute Respiratory Distress Syndrome (ARDS)* in severe SARS-CoV-2 infection (Schoeman & Fielding, 2020). Among the other structural proteins of SARS-CoV-2, the E protein has not received much investigation. We, therefore, have exploited to target the viral *E* protein as a therapeutic intervention against COVID-19. Some drug candidates that inhibit the SARS-CoV-2 E protein have been discovered from the ab initio-designed drugs based on structure characterization (Chernyshev, 2020; Das et al., 2021).

Meanwhile, a research group from China reported the activity of bicycloproline-derived compounds in inhibiting Mpro SARS-CoV-2 with an IC50 value of 7.6-748 nM. A total of 32 compounds (MI-01 to MI-32) were successfully synthesized by modifying the antiviral structure of telaprevir-boceprevir (Qiao et al., 2021). Mpro plays a role in the process of replication and transcription of viruses (Prajapat et al., 2020; Zhang et al., 2020). Protease can divide and produce proteins needed for virus survival (Jo et al., 2019). Two compounds (MI-09 and MI-30) among them have the potential to be developed and explored for possible targets of other proteins, including protein E (Li & Huang, 2021).

The primary purpose of this study was to trace other targets of synthesized bicycloproline derivative compounds (MI-09 and MI-30) against the E protein of SARS-CoV-2. Although the crystal structure of protein E of different organisms is predetermined, structural information is still needed. Therefore, this study is also focused on homological modeling of the SARS-CoV-2 E protein. Molecular docking was carried out between the E protein of SARS-CoV-2 and 2 compounds derived from bicycloproline to study protein-ligand interactions by adopting an in-silico strategy to explain its antiviral properties.

MATERIALS AND METHODS

Hardware applied for calculation, molecular modeling, and docking molecule were a personal computer with a specification of OS Windows 10 Pro-64-bit; Processor: Intel ® Core™ i5-10400 CPU @2.9GHz (12 CPUs); RAM 8192 MB DDR4; Direct 12; 1 TB HDD; 802.11b/g WLAN; Display: NVIDIA GeForce 210 Display Mode: 1366 x 768 (32bit) (60Hz). The program package Molecular Operating Environment MOE 2022.02 was the software applied. Program package MOE dock applied for and draws up parameter docking and simulation of process docking. Program Bio Discovery Visualization 2021 was applied to view the interaction of the ligand with macromolecules.

Protein preparation

Because there is no crystal structure of SARS-CoV-2 E protein eligible for docking, homology modeling was carried out. The monomer and pentamer structure of the SARS-CoV-2 E protein was built using the SWISS-MODEL web server

(https://swissmodel.expasy.org). *Wuhan-1 isolate* (GenBank ID: QHD43418.1) (National Library of Medicine) was used to predict *the sequence of the E protein* of SARS-CoV-2 (Dey et al., 2020). The E protein structure of the SARS-CoV (PDB ID: 5X29) was used as a template. The model with the best QMEAN was selected for follow-up. GalaxyRefine server was used to fine-tune the model (Heo, Park, and Seok 2013). The selected SARS-CoV-2 E protein monomer was constructed into a pentamer model (Chernyshev, 2020) using the GalaxyHomomer server (https://galaxy.seoklab.org) (Baek et al., 2017). MolProbity (http://molprobity.biochem.duke.edu) was used to validate the SARS-CoV-2 protein E pentamer (Chen et al., 2010). The generated protein structure was energy minimized using MOE with CHARMM27 Forcefield parameters; Gradient 0.1 RMS kcal/mol/A^2; and refinement to RMS Gradient: 0.001 kcal/mol/A to improve the protonated state of amino acid residues and add polar hydrogen using MOE.

Ligand preparation

This study used 2 bicycloproline derivative compounds (Figure 1) that actively inhibit SAS-CoV-2 in vitro from previous studies by Qiao and team (Qiao et al., 2021). Remdesivir molecule is used as a ligand for protocol validation. The 2D model of the compound structure was drawn using Marvin-Sketch software and stored in the *.mol extension. The 2D model converted to 3D. Furthermore, geometry optimization was carried out using the Semi-Empirical AM1 method (Asmara and Dwi 2015) via command compute-geometry optimization with parameters convergance limit: 0.01; iteration limit: 32767; algorithm: Polak-Ribiere (conjugate gradient); RMS gradient of: 0.01 kcal/(Å

mol) or 32767 maximum cycle. Then the ligands were stored in mol format.

Docking

Molecular docking was performed using MOE. Docking was focused at the docking site obtained using MOE software with the command 'Compute-Site Finder,' selected dummy atoms. The location of the ligand's pocket was focused on the area of amino acids responsible for forming interactions with ligands. The previous studies identified *Asn15, Leu19, Ala22, and Phe26 as the amino acids responsible for forming the interaction with the ligand (Dey et al., 2020; Park et al., 2021).*

Before docking the bicycloproline derivative compounds, the protocol and algorithm were validated by docking the remdesivir to the target protein. Process docking was done to apply two scoring methods: the GBVI/WSA dG scoring function and the london dG scoring function in dock MOE. There were several settings during docking: the placement method was triangle matcher, and the refinement was rigid receptor. The result of the process docking was then kept in mdb format. The *root-mean-square deviation* (RMSD) (<2 Å) suggested that the method could consistently predict the natural conformation of the complex ligand-protein.

Compounds were studied for their interaction with receptors by carrying out molecular docking. The observed parameter was the affinity energy between ligands and receptors which was assessed through the scoring bond energy and compound conformation at the binding site in the form of a mode of interaction between two molecules, such as hydrophobic interaction, electrostatic interaction, and hydrogen bond formed. The molecules' docking results were visualized using Biovia Discovery Studio 2021 (Dassault Systèmes, 2021).
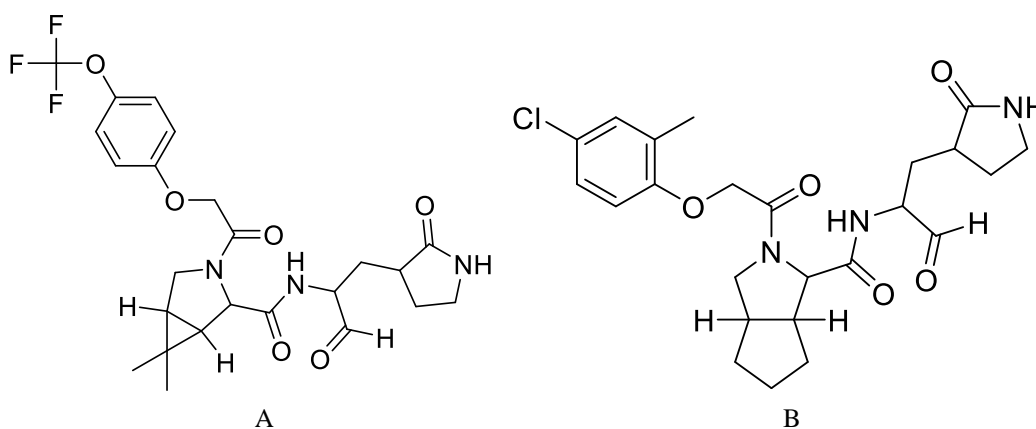

Figure 1. 2D structure of compound. MI-09 (A) and MI-32 (B)

RESULTS AND DISCUSSION

Modeling envelope protein SARS-CoV-2

Homology modelling of SARS CoV-2 E protein was done which showed the sequence identity of 91.38% with the template PDB ID:5X29 (SARS CoV)) (Figure 2). The SARS-CoV-2 E protein was already available in the PDB repository (PDB ID: 7K3G), but the structure was obtained using the solid-state NMR method (Mandala et al., 2020). The validation results show that the E structure has a high clash score and side chain outlier value. The results indicate that the NMR model wass less precise. Therefore, we tried to build a homology model in this study.

The monomer structure of the SARS-CoV-2 E protein with the lowest QMEAN (0.46) and Seq Identity (91.38%) was selected for refining. QMEAN is a combined assessment function that can determine global (i.e., for the entire structure) and local (i.e., per amino acid residue) total quality estimates based on a single model. The QMEAN terms range from 0 to 1, where a value of 1 indicates good agreement. The values were converted to Z-Scores to correlate with what we expect from high-resolution X-ray structures. The identity of seq will affect the proximity of the model to the actual state. The greater the percentage of identity values, the more similar the model will be to the actual state (Komari et al., 2020).

The final model was selected with a clash score (1.0), Rama favored (96.4%), and MolProbity (1.039). A favored value of 96.4% indicates that the protein has a structure with a quality that most amino acids are in the favored region than the outlier (Sharma et al., 2013). MolProbity combines log-weighted clash scores, Ramachandran outlier, and poor side-chain rotamer. The MolProbity value of 1.039 indicates that the model is quite good. If the model structure has a lower MolProbity than the actual crystallography resolution, then the model is said to be better in quality. This score shows one value expected to describe crystallographic resolution (Chen et al., 2010). As the SARS-CoV-2 E protein forms pentamer in physiological conditions (Pervushin et al., 2009), we built the SARS-CoV E protein pentamer structure using the GalaxyHomomer

server (Baek et al., 2017; Pervushin et al., 2009). The final validation of the SARS-CoV-2 E protein pentamer obtained a clash score (1.06), poor rotatomer (0.00%), favored rotamers (98.11%), Ramachandran favored (96.43%), Ramachandran outlier (1.78%), rama Z-score (-1.08), and MolProbity (1.04). Outlier residues with a maximum value of 2% can be improved to obtain a better model through energy minimization preparations (Agnihotry et al., 2022). The resulting homology modeling of SARS-CoV-2 E protein is shown in Figure 3. The value of the parameters obtained shows that the modeling proteins can be used for the docking process (Bordoli et al. 2009; Fiser 2010; Komari et al. 2020; Sharma et al. 2013). The SARS-CoV-2 E pentamer model has completed docking preparations (energy minimization) (Ramasami, 2020).

Molecular docking

A research group from China revealed that oral or intraperitoneal treatment with two compounds of 32 new SARS-CoV-2 Mpro inhibitors (MI-09 and MI-30) showed effective antiviral activity in a transgenic mouse model of SARS-CoV-2 infection. Therefore, we were interested to investigate the interaction of these two compounds against the SARS-CoV-2 E protein (Li & Huang, 2021; Qiao et al., 2021).

The MI-09 and MI-30 compounds can bind to the SARS-CoV-2 protein envelope. The binding energy was close to remdesivir (Table 1-2). Remdesivir was the first small-molecule antiviral drug approved by the FDA to treat SARS-CoV-2 infection. The mode of action of remdesivir was to inhibit RdRp (RNA-dependent RNA polymerase) during viral pathogenesis in patients (Gö Tte, 2021). As of today, we could not find any other FDA-approved drug for SARS-CoV-2 SAR with a mechanism of action on the E protein of SARS-CoV-2, remdesivir used as a reference ligand to validate the docking protocol. The interactions of potential drug candidates against SARS-CoV-2 protein E were ranked based on posing and scoring parameters. Binding affinity is used to determine the final rank of the ligand docking pose.
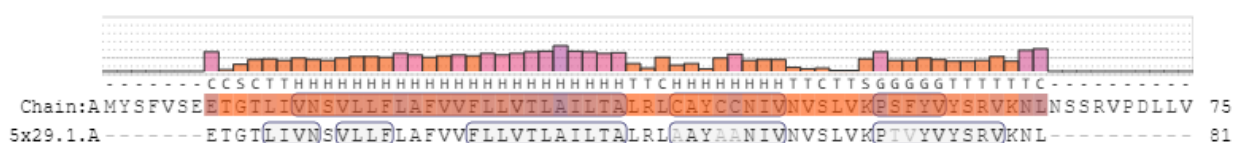
Figure 2. Sequence envelope modeling
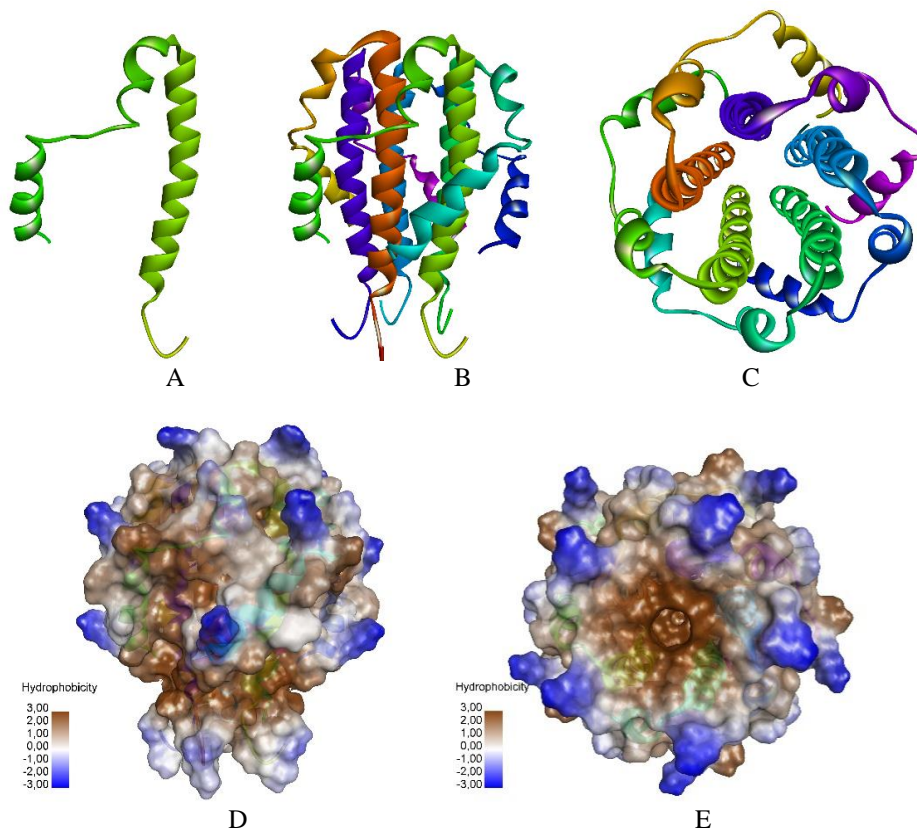
Figure 3. Protein E is the result of modeling. (A) monomer structure of E protein, (B) pentamer structure of E protein, (C) upper-view pentamer structure of E protein, (D) surface pentamer structure of E protein, (E) upper-view surface pentamer structure of E protein
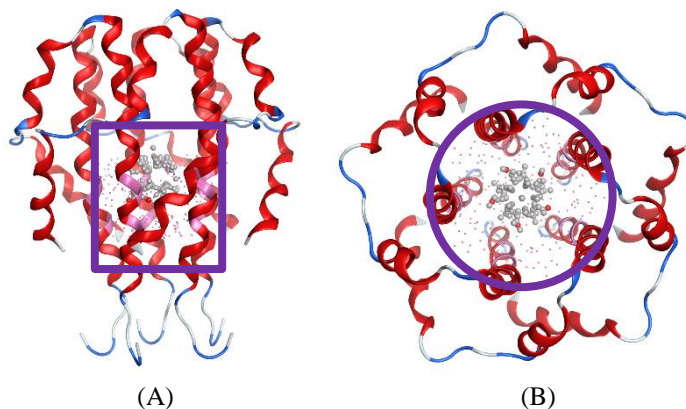
Figure 4. Site docking position. (A) view site docking, (B) upper-view site docking.

Table 1. Reference ligand docking results against SARS-CoV-2 protein envelope

Compound	S (kcal/mol)	RMSD (Å)	Hydrogen Bond	Active Site
Remdesivir	-10.8653	1.6114	Leu A: 19; Leu D: 19; Phe C:23	Hidrophobic: Leu B:19; Leu E:19; Ala E:22; Phe A:23; Phe C:23; Phe A:26; Phe B:26 Electrostatic: Phe C:26

The docking site was predetermined based on previous publications (Dey et al., 2020; Park et al., 2021). *The study* identified *Asn15, Leu19, Ala22, and Phe26 as the amino acids responsible for forming the interaction with the ligand.* The docking of remdesivir give RMSD value of 1.6114 Å (< 2 Å). The interaction visualization was depicted in Figure 4.

The bicycloproline derivative compounds were docked against the SARS-CoV-2 E protein through the same docking method and conditions. Protein-ligand binding occurs only when the free energy change is negative. The free energy of the bond was proportional to the stability of the protein-ligand interaction. Therefore, protein ligands occur with low binding affinity energies in the system (Afriza, Suriyah, and Ichwan 2018; Du et al. 2016; Sergeev, Dolinska, and Wingfield 2014). The binding affinity energy of the bond indicates the stability of the ligand-protein complex, which is an essential characteristic of drug efficacy (Mohamad Rosdi et al., 2017). The results showed that all compounds could bind to the envelope protein of SARS-CoV-2. The binding energy was close to remdesivir (-10.8653 kcal/mol) (Table1 and Figure 5). MI-30 has the lowest bond energy (-10.3326 kcal/mol) (Table 2 and Figure 6). The result indicates that MI-30 has the most spontaneous tendency to bind to protein E compared to MI-09.

In addition to bond energy, types of molecular interactions such as hydrogen bonds, hydrophobic, and electrostatic interactions, with essential amino acid residues exhibiting docking ligands in conformation into parameters to consider (Hariono et al., 2016). Remdesivir forms 3 hydrogen bonds and 7 hydrophobic bonds SARS-CoV-2 E protein. Both MI-30 and MI-09 form hydrogen bonds, which are formed between H and O atoms. The proton carrier pair (the so-called hydrogen bond donor) in the biological system (protein/receptor) is usually the NH_3 or OH group. The bond reaches excellent strength because the hydrogen atoms of the donor group are bound to highly electronegative atoms, where the electron density of hydrogen atoms shifts to neighboring atoms (Klebe, 2013). The bond between O... H is strong enough (Itoh et al., 2019; N Baker 2006; Panigrahi and Desiraju, 2007). It shows that both compounds have a reasonably good bond strength, with the greatest strength being MI-30, with a more significant number of hydrogen bonds.
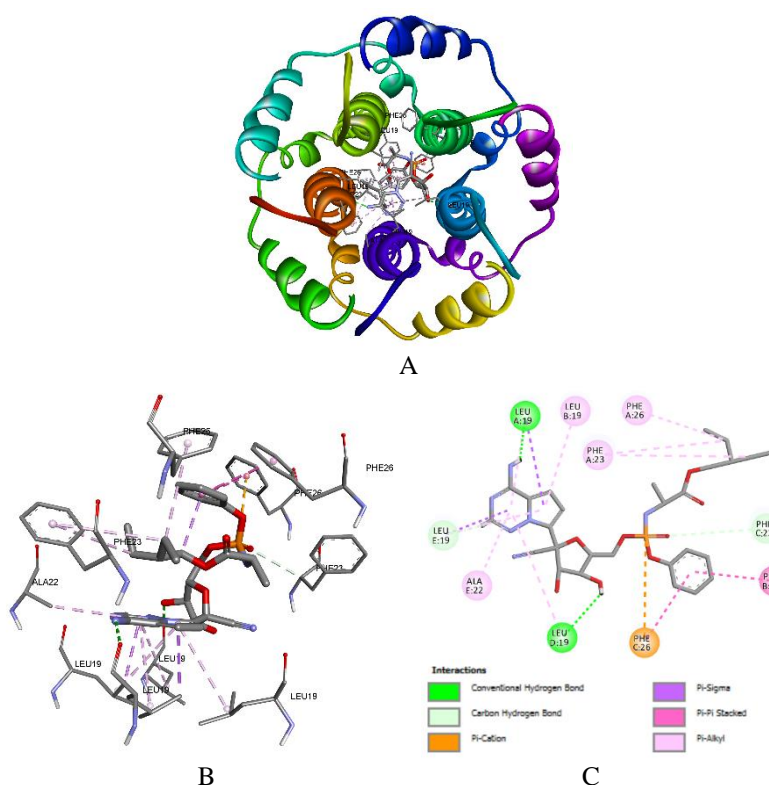

Figure 5. Docking interaction of remdesivir with SARS-CoV-2 E protein. A. Bottom view of ligand-protein, B. 3D display of ligand interaction with amino acid residue, and C. 2D display of ligand interaction with amino acid residue.

Table 2. Docking parameters of MI-09 and MI-30 compounds against protein E

Compound	S (kcal/mol)	Hydrogen Bond [Distance] {Atom Ligand-Atom Protein}	Hydrophobic Interactions	Electrostatic Interactions
MI-30	-10.3326	Leu A:19 [2.55] {H --- O} Leu A:19 [2.44] {H --- O} Leu E:19 [2.61] {H --- O} Phe A:23 [3,06] {O --- H}	Ala E:22(Alkyl); Ala A:22(Pi-Alkyl); Phe A:23(Pi-Alkyl); Phe E:23(Pi-Alkyl); Phe A:26(Pi-Alkyl); Phe B:23(Pi-Pi T-shaped)	-
MI-09	-10.0403	Leu A:19 [3.02] {O --- H} Leu E:19 [2.57] {H --- O} Phe B:23 [2.39] {O --- H}	Leu D:19(Alkyl; Halogen F, Alkyl); Leu E:19(Alkyl); Ala D:22(Alkyl); Ala E:22(Alkyl); Phe E:26(Pi-Alkyl) Phe D:26(Pi-Alkyl) Phe C:26(Pi-Alkyl, Pi-Alkyl) Phe B:26(Pi-Alkyl) Phe A:26(Pi-Alkyl) Ala C:22(Alkyl) Leu C:19(Alkyl, Pi-Alkyl) Ala B:22(Pi-Alkyl) Leu B:19(Pi-Alkyl)	-

In addition to hydrogen bonds, both MI-30 and MI-09 form hydrophobic bonds. The most hydrophobic bond type is alkyl. Hydrophobic interactions are the main contributors to protein stability compared to hydrogen bonds. Hydrogen bonds also support protein stability, but to a lesser extent than hydrophobic bonds (Pace et al., 2011). Hydrophobic bonding is also vital in combining drug molecules' non-polar regions with biological receptors' non-polar regions. The non-polar regions of drug molecules that are insoluble in water and the surrounding water molecules will combine through hydrogen bonds to form quasi-crystalline structures (icebergs) (Patrick, 2013; Siswandono, 2016). Therefore, hydrophobic bonds are the main determinants of complex equilibrium(Pace et al., 2011). Previous studies suggest that tretinoin compounds form hydrophobic interactions with protein E involving the Leu18 (Chain C, D), Leu21 (Chain C), Ala22 (Chain C), Val25 (Chain C), and Phe26 (Chains A-E), which may be the primary ligand binding site in the SARS-CoV-2 E protein. Blocking of SARS-CoV-2 E ion channels by small molecules can inhibit the activity of viroporin's E activity and consequently eliminates its contribution to viral assembly (Dey et al., 2020). In other previous NMR studies on the SARS-CoV-2 E, protein has shown inhibitor-mediated binding of residue hydrophilic interactions (Glu8, Thr9, Thr11, and Asn15) primarily by Asn15 hexamethylene ameloride (HMA) (Park et al., 2021; Pervushin et al., 2009). The E protein plays a multifunctional role in infection, viral assembly, virion release, and pathogenesis. E protein plays a role in the spike in SARS-CoV-2 maturation (Alsaadi & Jones, 2019; Boson et al., 2021; Schoeman & Fielding, 2020). Being involved in various aspects of the SARS-CoV-2 cycle, targeting this protein can potentially stop the spread of infection, reduce symptoms, and manage complications such as Acute Respiratory Distress Syndrome in SARS-CoV-2 infection (Schoeman & Fielding, 2020).
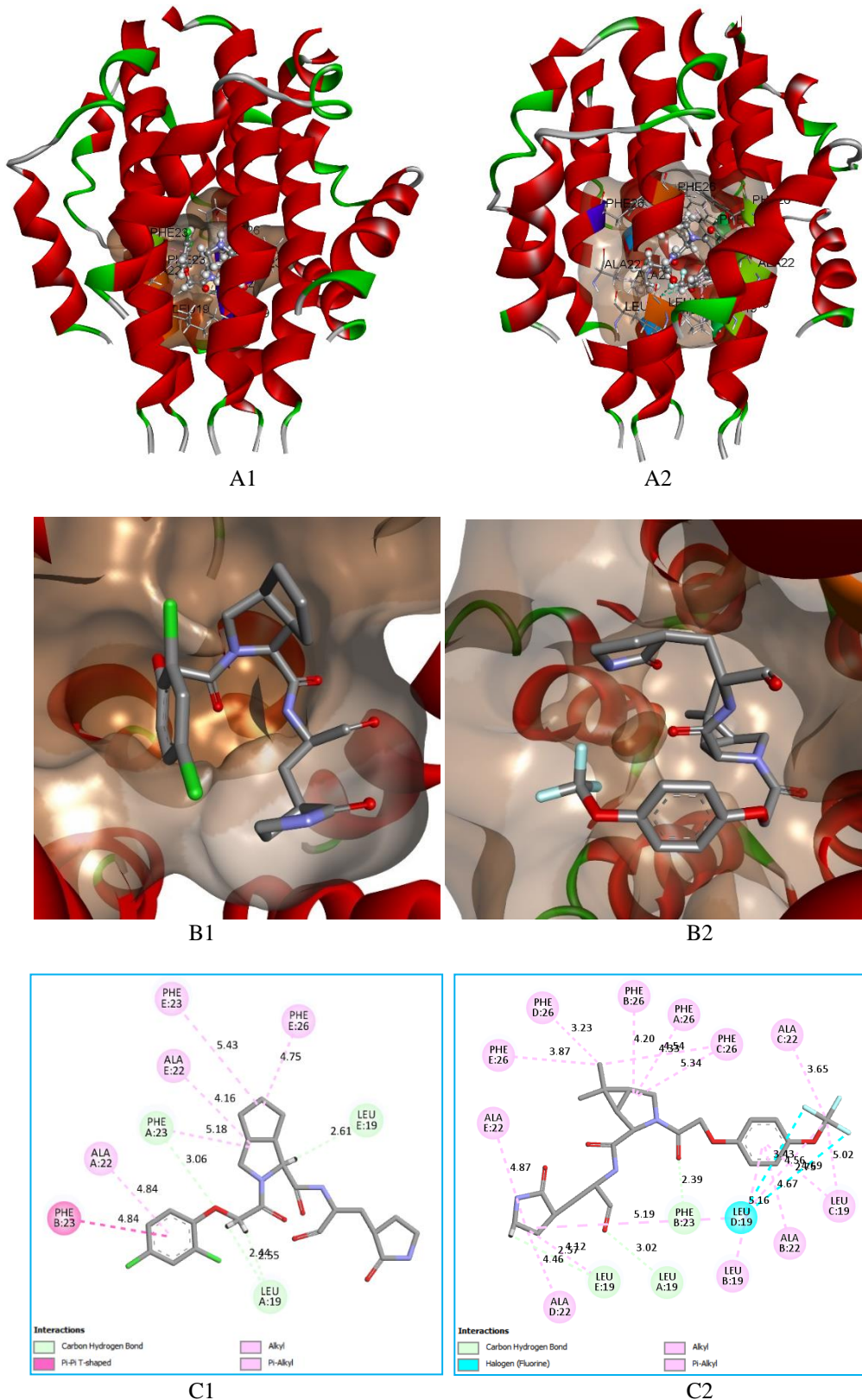
Figure 6. Docking interaction of MI-30 and MI-09 with SARS-CoV-2 E protein. A1-B1. The position of the ligand on the docking site of MI-30, A2-B2. The position of the ligand on the docking site of MI-09, C1. Ligand interaction with amino acid residues of MI-30, C2. Ligand interaction with amino acid residues of MI-09.

CONCLUSIONS

The bicycloproline compound MI-30 showed the best docking results with the lowest binding energy (-10.3326 kcal/mol) compared to MI-09 (-10.0403 kcal/mol). MI-30 forms a complex with the E protein of SARS-CoV-2 firmly and stably with the most hydrogen and hydrophobic bonds with successive amounts of 4 and 6 bonds. Meanwhile, the protein-ligand interaction of MI-09 with SARS-CoV-2 E protein formed 3 hydrogen bonds and 13 hydrophobic interactions. Overall, this discovery provides new knowledge about the possible mechanisms of inhibition of two bicycloproline-derived compounds to block the E protein cycle of SARS-CoV-2. Nonetheless, modifications of the compound, in-vitro as well as in-vivo investigations are needed to confirm this discovery.

ACKNOWLEDGMENT

REFERENCES

Abdelrahman, Z., Li, M., & Wang, X. (2020). Comparative Review of SARS-CoV-2, SARS-CoV, MERS-CoV, and Influenza A Respiratory Viruses. *Frontiers in Immunology*, *11*(September). https://doi.org/10.3389/fimmu.2020.552909

Afriza, D., Suriyah, W. H., & Ichwan, S. J. A. (2018). In silico analysis of molecular interactions between the anti-apoptotic protein survivin and dentatin, nordentatin, and quercetin. *Journal of Physics: Conference Series*, *1073*(3). https://doi.org/10.1088/1742-6596/1073/3/032001

Agnihotry, S., Pathak, R. K., Singh, D. B., Tiwari, A., & Hussain, I. (2022). Protein structure prediction. *Bioinformatics*, 177–188. https://doi.org/10.1016/B978-0-323-89775-4.00023-7

Alsaadi, E. A. J., & Jones, I. M. (2019). Membrane binding proteins of coronaviruses. *Future Virology*, *14*(4), 275. https://doi.org/10.2217/FVL-2018-0144

Asmara, A. P., & Dwi. (2015). Analisis Hubungan Kuantitatif Struktur Dan Aktivitas Senyawa Turunan Triazolopiperazin Amida Menggunakan Metode Semiempirik AM1. *Elkawnie*, *1*(2), 125–138.

Baek, M., Park, T., Heo, L., Park, C., & Seok, C. (2017). GalaxyHomomer: a web server for protein homo-oligomer structure prediction from a monomer sequence or structure. *Nucleic Acids Research*, *45*(W1), W320–W324. https://doi.org/10.1093/NAR/GKX246

Bordoli, L., Kiefer, F., Arnold, K., Benkert, P., Battey, J., & Schwede, T. (2009). Protein structure homology modeling using SWISS-MODEL workspace. *Nature Protocols*, *4*(1), 1–13. https://doi.org/10.1038/NPROT.2008.197

Boson, B., Legros, V., Zhou, B., Siret, E., Mathieu, C., Cosset, F.-L., Lavillette, D., & Denolly, S. (2021). The SARS-CoV-2 envelope and membrane proteins modulate maturation and retention of the spike protein, allowing assembly of virus-like particles. *The Journal of Biological Chemistry*, *296*, 100111. https://doi.org/10.1074/JBC.RA120.016175

Chen, V. B., Arendall, W. B., Headd, J. J., Keedy, D. A., Immormino, R. M., Kapral, G. J., Murray, L. W., Richardson, J. S., & Richardson, D. C. (2010). MolProbity: all-atom structure validation for macromolecular crystallography. *Acta Crystallographica Section D: Biological Crystallography*, *66*(Pt 1), 12. https://doi.org/10.1107/S0907444909042073

Chernyshev, A. (2020). Pharmaceutical targeting the envelope protein of SARS-CoV-2: the screening for inhibitors in approved drugs. *ChemRxiv*, 1–13. https://chemrxiv.org

Das, G., Das, T., Chowdhury, N., Chatterjee, D., Bagchi, A., & Ghosh, Z. (2021). Repurposed drugs and nutraceuticals targeting envelope protein: A possible therapeutic strategy against COVID-19. *Genomics*, *113*(1), 1129–1140. https://doi.org/10.1016/J.YGENO.2020.11.009

Dassault Systèmes. (2021). *BIOVIA DISCOVERY STUDIO VISUALIZAION* (No. 2021). Dassault Systèmes. https://3ds.com/products-services/biovia/products

Dey, D., Borkotoky, S., & Banerjee, M. (2020). In silico identification of Tretinoin as a SARS-CoV-2 envelope (E) protein ion channel inhibitor. *Computers in Biology and Medicine*, *127*, 104063. https://doi.org/10.1016/J.COMPBIOMED.2020.104063

Du, X., Li, Y., Xia, Y. L., Ai, S. M., Liang, J., Sang, P., Ji, X. L., & Liu, S. Q. (2016). Insights into Protein–Ligand Interactions: Mechanisms, Models, and Methods. *International Journal of Molecular Sciences*, *17*(2). https://doi.org/10.3390/IJMS17020144

National Library of Medicine. (n.d.). *Envelope Protein [Severe acute respiratory syndrome coronavirus 2] - Protein - NCBI*. Retrieved April 1, 2022, from https://www.ncbi.nlm.nih.gov/protein/QHD43418.1?report=fasta

Fiser, A. (2010). Template-Based Protein Structure Modeling. *Methods in Molecular Biology (Clifton, N.J.)*, *673*, 73. https://doi.org/10.1007/978-1-60761-842-3_6

Gö Tte, M. (2021). *Remdesivir for the treatment of Covid-19: the value of biochemical studies*. https://doi.org/10.1016/j.coviro.2021.04.014

Hariono, M., Abdullah, N., Damodaran, K. v., Kamarulzaman, E. E., Mohamed, N., Hassan, S.

S., Shamsuddin, S., & Wahab, H. A. (2016). Potential New H1N1 Neuraminidase Inhibitors from Ferulic Acid and Vanillin: Molecular Modelling, Synthesis and in Vitro Assay. *Scientific Reports 2016 6:1*, *6*(1), 1–10. https://doi.org/10.1038/srep38692

Heo, L., Park, H., & Seok, C. (2013). GalaxyRefine: protein structure refinement driven by side-chain repacking. *Nucleic Acids Research*, *41*(W1), W384–W388. https://doi.org/10.1093/NAR/GKT458

Homology Modeling. (n.d.). Retrieved August 3, 2022, from https://www.umass.edu/molvis/workshop/homol mod.htm#readymade

Itoh, Y., Nakashima, Y., Tsukamoto, S., Kurohara, T., Suzuki, M., Sakae, Y., Oda, M., Okamoto, Y., & Suzuki, T. (2019). N+-C-H⋯O Hydrogen bonds in protein-ligand complexes. *Scientific Reports*, *9*(1). https://doi.org/10.1038/S41598-018-36987-9

Jo, S., Kim, S., Shin, D. H., & Kim, M.-S. (2019). Inhibition of SARS-CoV 3CL protease by flavonoids. *Https://Doi.Org/10.1080/14756366.2019.169048 0*, *35*(1), 145–151. https://doi.org/10.1080/14756366.2019.1690480

Khader, A., & Mohideen, S. (2021). *Molecular Docking Analysis of Phytochemical Thymoquinone as a Therapeutic Agent on SARS-Cov-2 Envelope Protein Molecular Docking Analysis of Phytochemical Thymoquinone as a Therapeutic Agent on SARS-Cov-2 Envelope Protein View project Molecular Docking An*. *11*(1), 8389–8401. https://doi.org/10.33263/BRIAC111.83898401

Klebe, G. (2013). Protein–Ligand Interactions as the Basis for Drug Action. *Drug Design*, 61–88. https://doi.org/10.1007/978-3-642-17907-5_4

Komari, N., Hadi, S., & Suhartono, E. (2020). Pemodelan Protein dengan Homology Modeling menggunakan SWISS-MODEL. *Jurnal Jejaring Matematika Dan Sains*, *2*(2), 65–70. https://doi.org/10.36873/JJMS.2020.V2.I2.408

Li, L., & Huang, S. (2021). Newly synthesized Mpro inhibitors as potential oral anti-SARS-CoV-2 agents. *Signal Transduction and Targeted Therapy*, *6*(1), 3–4. https://doi.org/10.1038/s41392-021-00560-0

M, T. U. Q., SM, A., MA, A., & LL, C. (2020). Structural basis of SARS-CoV-2 3CL pro and anti-COVID-19 drug discovery from medicinal plants. *Journal of Pharmaceutical Analysis*, *10*(4), 313–319. https://doi.org/10.1016/J.JPHA.2020.03.009

Mohamad Rosdi, M. N., Mohd Arif, S., Abu Bakar, M. H., Razali, S. A., Mohamed Zulkifli, R., & Ya'akob, H. (2017). Molecular docking studies of bioactive compounds from Annona muricata Linn as potential inhibitors for Bcl-2, Bcl-w and Mcl-1 antiapoptotic proteins. *Apoptosis 2017 23:1*, *23*(1), 27–40. https://doi.org/10.1007/S10495-017-1434-7

N Baker, B. E. (2006). *22.2. Hydrogen bonding in biological macromolecules*.

Pace, C. N., Fu, H., Fryar, K. L., Landua, J., Trevino, S. R., Shirley, B. A., Hendricks, M. M. N., Iimura, S., Gajiwala, K., Scholtz, J. M., & Grimsley, G. R. (2011). Contribution of Hydrophobic Interactions to Protein Stability. *Journal of Molecular Biology*, *408*(3), 514. https://doi.org/10.1016/J.JMB.2011.02.053

Panigrahi, S. K., & Desiraju, G. R. (2007). Strong and weak hydrogen bonds in the protein–ligand interface. *Proteins: Structure, Function, and Bioinformatics*, *67*(1), 128–141. https://doi.org/10.1002/PROT.21253

Park, S. H., Siddiqi, H., Castro, D. v., de Angelis, A. A., Oom, A. L., Stoneham, C. A., Lewinski, M. K., Clark, A. E., Croker, B. A., Carlin, A. F., Guatelli, J., & Opella, S. J. (2021). Interactions of SARS-CoV-2 envelope protein with amilorides correlate with antiviral activity. *PLOS Pathogens*, *17*(5), e1009519. https://doi.org/10.1371/JOURNAL.PPAT.100951 9

Patrick, G. L. (2013). An Introduction to Medicinal Chemistry Fifth Edition. In *Oxford University Press* (5th Ed.). OXFORD. https://doi.org/10.1016/0307-4412(76)90096-0

Pervushin, K., Tan, E., Parthasarathy, K., Lin, X., & Jiang, F. L. (2009). Structure and Inhibition of the SARS Coronavirus Envelope Protein Ion Channel. *PLoS Pathog*, *5*(7), 1000511. https://doi.org/10.1371/journal.ppat.1000511

Prajapat, M., Sarma, P., Shekhar, N., Avti, P., Sinha, S., Kaur, H., Kumar, S., Bhattacharyya, A., Kumar, H., Bansal, S., & Medhi, B. (2020). Drug targets for corona virus: A systematic review. *Indian Journal of Pharmacology*, *52*(1), 56. https://doi.org/10.4103/IJP.IJP_115_20

Qiao, J., Li, Y.-S., Zeng, R., Liu, F.-L., Luo, R.-H., Huang, C., Wang, Y.-F., Zhang, J., Quan, B., Shen, C., Mao, X., Liu, X., Sun, W., Yang, W., Ni, X., Wang, K., Xu, L., Duan, Z.-L., Zou, Q.-C., … Yang, S. (2021). SARS-CoV-2 Mpro inhibitors with antiviral activity in a transgenic mouse model. *Science*, *371*(6536), 1374–1378. https://doi.org/10.1126/SCIENCE.ABF1611

Ramasami, P. (2020). *Computational Chemistry Methods: Applications* (P. Ramasami, Ed.). De Gruyter. https://doi.org/https://doi.org/10.1515/978311063 1623

Schoeman, D., & Fielding, B. C. (2019). Coronavirus envelope protein: current knowledge. *Virology Journal 2019 16:1*, *16*(1), 1–22. https://doi.org/10.1186/S12985-019-1182-0

Schoeman, D., & Fielding, B. C. (2020). Is There a Link Between the Pathogenic Human Coronavirus Envelope Protein and Immunopathology? A Review of the Literature. *Frontiers in Microbiology*, *0*, 2086. https://doi.org/10.3389/FMICB.2020.02086

Sergeev, Y. v., Dolinska, M. B., & Wingfield, P. T. (2014). The thermodynamic analysis of weak protein interactions using sedimentation equilibrium. *Current Protocols in Protein Science / Editorial Board, John E. Coligan ... [et Al.]*, *77*, 20.13.1. https://doi.org/10.1002/0471140864.PS2013S77

Sharma, S., Sarkar, S., Paul, S. S., Roy, S., & Chattopadhyay, K. (2013). A small molecule chemical chaperone optimizes its unfolded state contraction and denaturant like properties. *Scientific Reports*, *3*. https://doi.org/10.1038/SREP03525

Siswandono. (2016). *Medicinal Chemistry* (Siswandono, Ed.; 2nd ed.). Airlangga University Press.

Torres, J., Parthasarathy, K., Lin, X., Saravanan, R., Kukol, A., & Ding, X. L. (2006). Model of a Putative Pore: The Pentameric α-Helical Bundle of SARS Coronavirus E Protein in Lipid Bilayers. *Biophysical Journal*, *91*(3), 938. https://doi.org/10.1529/BIOPHYSJ.105.080119

Woo, P. C. Y., Huang, Y., Lau, S. K. P., & Yuen, K. Y. (2010). Coronavirus Genomics and Bioinformatics Analysis. *Viruses*, *2*(8), 1804. https://doi.org/10.3390/V2081803

Zhang, L., Lin, D., Sun, X., Rox, K., & Hilgenfeld, R. (2020). X-ray Structure of Main Protease of the Novel Coronavirus SARS-CoV-2 Enables Design of α-Ketoamide Inhibitors. *BioRxiv*, 2020.02.17.952879. https://doi.org/10.1101/2020.02.17.952879

Anti-Inflammatory Effect of Red Dragon Fruit (*Hylocereus polyrhizus*) Peel on Male White Rat

Pazri Yuna, Chrismis Novalinda Ginting, and Linda Chiuman*
Biomedical Science Magister Program, Faculty of Medicine, Dentistry, and Health Science, Prima Indonesia University, Medan, Indonesia

*Corresponding author: lindachiuman@unprimdn.ac.id

Abstract

Background: *The side effects of synthetic anti-inflammatory drugs have become a known problem in medicine as well as in the general public. These side effects problems drive patients to seek alternatives to common anti-inflammatory drugs, especially natural alternatives. Phytochemicals such as flavonoids, alkaloids, and many different others have been identified as potential anti-inflammatory agents. Red dragon fruit (Hylocereus polyrhizus) is one source of such phytochemicals. Whilst the consumption of the flesh of red dragon fruit is very common, utilization of the peel is very rare and often becomes waste.* **Objective**: *This study aimed to explore the potential of red dragon fruit peel as an anti-inflammatory agent.* **Methods**: *This experimental study with a control group post-test-only design. This study involved in-vitro (protein denaturation inhibition using bovine serum albumin) and in-vivo (carrageenan-induced inflammation on an air-pouch model on 25 white rats) experiment.* **Results**: *This study showed that the red dragon fruit peel extract contains flavonoid, alkaloid, saponin, and tannin compounds. Administration of red dragon fruit peel extract suspension was found to be effective at inhibiting protein denaturation and reducing white blood count in the inflammation exudates, and the effectiveness is increasing along with the dose.* **Conclusion**: *It can be concluded that the red dragon fruit peel extract was effective as an anti-inflammatory agent, especially at a higher dose.*

Keywords: *dragon fruit peel, anti-inflammatory, phytochemicals, flavonoid*

INTRODUCTION

Hylocereus polyrhizus, which is commonly known as red dragon fruit (in English-speaking countries) or *pitaya* or *pitahaya* (in Mexico, Central, and South America) or *buah naga* (in Malaysia and Indonesia) is a plant from the cactus family, Cactaceae (Saenjum et al., 2021; Muhammad et al., 2020). This plant is native to Central and South America, and Mexico in North America but is currently being cultivated in almost every tropical part of the world (Luu et al., 2021; Saenjum et al., 2021). Red dragon fruit (*H. polyrhizus*) got its name from the distinct red color of the fruit flesh, with pink-to-red peel (Luu et al., 2021; Saenjum et al., 2021). The part of red dragon fruit that people commonly consumed is the flesh or pulp of the fruit, while the peel is usually thrown away and becomes waste due to a lack of understanding of its utility value (Niah and Baharsyah, 2018; Paramita et al., 2015; Muhammad et al., 2020).

The potency of dragon fruit feel in the food industry as well as its pharmaceutical properties have been explored (Muhammad et al., 2020; Liana et al., 2019; Saenjum et al., 2021; Luu et al., 2021). For pharmaceutical use, the phytochemical content of the dragon fruit, including its peel already shows a positive sign. Multiple studies found that red dragon fruit peel has several phytochemical compounds such as betacyanin, flavonoid, phenol, terpenoid, carotene, phytoalbumin, vitamins B1, B3, B6, and B12, and vitamins A, C, and E (Hendra et al., 2019; Kartikawati et al., 2020; Muhammad et al., 2020; Saenjum et al., 2021; Liana et al., 2019; Luu et al., 2021; Sinaga et al., 2015). This large multitude of phytochemicals has many different effects on the physiological process in humans. For example, betacyanin (the compound responsible for the red color of the dragon fruit peel) is known to be an effective protective agent for cells and tissue from damage by free radicals and oxygen-reactive species and thus works as analgetic (Kartikawati et al., 2020). Meanwhile, flavonoid compounds work as anti-inflammatory agents by inhibiting cyclooxygenase and lipoxygenase (Hendra et al., 2020). Meanwhile, another study found that dragon fruit peel extracts are effective as an anti-inflammatory agent through the inhibition of hyaluronidase by the phenolic and flavonoid compounds of the extract (Liana et al., 2019). The dragon fruit possess great potency as anti-inflammatory agent by inhibiting the cyclooxygenase and lipoxygenase, as well as the hyaluronidase by its multiple compounds,. Both studies also only use the peel of the red dragon fruit. One study found that red dragon fruit peel contains more flavonoid and phenolic content compared to the flesh (Saenjum et al., 2021).

MATERIALS AND METHODS
Material

A fresh specimen in the form of fresh red dragon fruit procured from a traditional market in Medan and then identified by Herbarium Medanense at the Faculty of Mathematics and Natural Sciences of Sumatera Utara University to be *H. polyrhizus* through identification number 018/MEDA/2022.

Animal subject

For *in vivo* experiment in this study, 25 white male rats of Wistar strain, aged 5 months old, with the weight between 160-200 grams were divided into 5 separate groups, where each group received the same induction, but different interventions according to their group. All rats were put into an acclimatization state for 14 days and fed with food pellets and water. The first group was the negative control group (1 mL of suspension base), the second group was the positive control group (10 mL/kg of diclofenac sodium suspension), and the other three groups were the extract group with three different doses (500 mg/kg, 750 mg/kg, and 1000 mg/kg suspension). After the study was finished, all rats were euthanized using carbon dioxide gas inside a sealed chamber. The carcasses were disposed of per the Integrated Laboratory of Prima Indonesia University guidelines. This study and its experiment protocol were reviewed and approved by the Health Research Ethical Committee of Prima Indonesia University through ethics declaration number 027/KEPK/UNPRI/III/2022.

Methods
Extraction

Following cleaning the red dragon fruit under running water, the fruit was peeled and the peel was then cut into cubes, dried, and powdered. The extraction method used in this study was the maceration method which began by weighing 500 grams of powdered red dragon fruit peel and putting it into a glass container and mixing it with 1.5 liters of methanol, stirred, sealed, and kept in the dark chamber for three days. After three days, the mix was filtered and the filtrate was kept in a separate container while the residue was put back into the extraction jar. The extraction process was repeated twice using the residue. All the filtrate is then combined into a total volume of ~4.5 liters. This filtrate was then evaporated using a rotary evaporator to remove most of the methanol and increase the concentration of the extract, followed by further reduction with a water bath

until it turned into red dragon fruit peel extract (RDFPE) with a thick consistency.

Phytochemical screening

In this study, only qualitative phytochemical screening was conducted. This phytochemical screening was conducted to screen the presence of alkaloids, flavonoids, saponins, tannins, glycosides, steroids, and triterpenoid compounds. In order to detect the presence of alkaloid compounds, four different detection methods using four different reagents were carried out, Bouchardat's test, Mayer's test, Dragendorff's test, and Wagner's test. Each of these tests was conducted by adding each corresponding reagent into a sample of the filtrate inside a test tube. The presence of alkaloids is signified by the color of the precipitate, which is colored differently according to the reagent used in the test. The color of the precipitates in the Bouchardat's, Mayer's, Dragendorff's, and Wagner's tests was brownish-black, yellow, red, and reddish-brown, respectively (Egbuna et al., 2019). To detect steroids, the aqueous extract was mixed with chloroform and H_2SO_4 (Salkowski test). The formation of red chloroform layer and a greenish-yellow acid layer showed the presence of steroids (Egbuna et al., 2019). Liebermann-Burchard's test was carried out to detect the presence of triterpenoid by mixing the extract with ethanol, acetic anhydrate, and H_2SO_4 to produce a pink to violet color, signified the triterpenoid presence in the extract (Egbuna et al., 2019). To detect the presence of saponin, in a test tube, the extract and distilled water were mixed and shaken to produce froth. If the froth stable/persist for at least 10 minutes and did not diminish after HCl was added, then there was saponin in the extract. Just like alkaloid screening, flavonoid screening is also carried out using four different methods, each using a different reagent, $FeCl_3$, $Mg_{(s)}HCl_{(p)}$ (Shinado's test), NaOH, and H_2SO_4. For the $FeCl_3$, NaOH, and H_2SO_4 test, each reagent was added to the extract and if the flavonoid was present, the mixture will change color into a bluish-black, yellow to orange color which turn colorless upon the addition of HCl, and orange color, respectively. Meanwhile, for Shinado's test, a mix of the extract, magnesium, and hydrochloric acid was heated to boil for 5 minutes and red coloration indicates the presence of flavonoid (Egbuna et al., 2019). For tannin detection, if the extract changes color into brownish-green or blue-black upon the addition of ferric chloride, then tannin was present (Egbuna et al., 2019). Meanwhile, to detect the presence of glycoside, the Molisch test was carried out. The Molisch test began by mixing the extract with the Molisch reagent, followed by adding sulfuric acid

through the test tube wall to prevent mixing. If a purple ring formed, then glycoside was present (Elzagheid, 2018). This phytochemical screening was conducted by the Laboratory of Organic Chemistry of Mathematics and Natural Sciences Faculty of Sumatera Utara University.

Preparation of control, standard, and extract solution

The control was prepared by adding 50 μL of methanol into a volumetric flask and then added with 0.2% BSA solution until 5 mL volume was achieved. Meanwhile, the standard was prepared by mixing 125 mg of diclofenac sodium with methanol by adding methanol into a volumetric flask to achieve 25 mL volume to produce the main standard with a 5000-ppm concentration. This main standard was then diluted into 100 ppm, 200 ppm, 400 ppm, 800 ppm, and 1600 ppm concentrations. To prepare the extract solution, 200 mg of red dragon fruit peel extract was dissolved in 10 mL methanol to create the main extract solution with 20000 ppm. This main extract solution was then diluted into 1000 ppm, 2000 ppm, 4000 ppm, 8000 ppm, and 16000 ppm concentrations, respectively (Abidin et al., 2019; Rahmawati et al., 2020).

Preparation of Oral Suspension

The base of the oral suspension used in this study was carboxymethyl cellulose sodium (Na CMC). This base was prepared by adding 10 mL of hot distilled water into 0.5 grams of Na CMC powder inside a mortar and letting it sit for 15 minutes and grinded until it turned into a gel mass. The Na CMC gel mass was then transferred into a 100 mL volumetric flask and diluted into 100 mL volume to produce 0.5% Na CMC suspension. This base act as an excipient for the positive control and the red dragon fruit peel extract and also as the negative control. To prepare the red dragon fruit peel extract suspension (ES), 1 gram of red dragon fruit peel was added into the mortar, and into it added the suspension base and grinded with a pestle to homogenize it and then transferred into a 10 mL volumetric flask. The mix was then diluted into a 10 mL volume to produce 10 % ES suspension.

To prepare the diclofenac sodium suspension, 1 mL of suspension base was added into 100 mg of diclofenac sodium powder in the mortar whilst grinding. After the diclofenac sodium and the suspension were mixed, it was transferred into a 10 mL volumetric flask and diluted to 10 mL volume to give 1% sodium diclofenac suspension.

Preparation of bovine serum albumin (BSA)

Preparation of BSA started by making tris buffer saline (TBS) solution. It was done by dissolving 0.87

grams of sodium chloride (NaCl) and 0.121 gram of tris base in 100 mL aquadest. This TBS solution pH was then measured and adjusted with glacial acetate acid to achieve a pH of around 6.2-6.5. Inside a volumetric flask, 0.2 grams of BSA powder dissolved into 100 mL TBS solution to give 0.2% BSA solution.

In vitro anti-inflammation activity evaluation

The anti-inflammation activity of red dragon fruit peel extract in this study was evaluated by protein denaturation assay. Into seven test tubes, 5 mL of 0.2% BSA solution was added. 50 μL of control was added to the first test tube, 50 μL of the standard into the second tube, and extract solution with different concentrations (10 ppm, 20 ppm, 40 ppm, 80 ppm, and 160 ppm) into the third to the seventh tubes respectively, then incubated at room temperature for 30 minutes followed by heating for 45 minutes at 100ºC temperature and let it sit for another 25 minutes at room temperature. After that, the test tube vortexed, and the absorbance was measured using UV-Vis Spectrophotometry at 660 nm wavelength. This absorbance measurement was conducted three times (Abidin et al., 2019; Rahmawati et al., 2020; Sriarumtias et al., 2020). The anti-inflammatory activity was calculated using the following equation:

$$\%denaturation\ inhibition$$
$$= \frac{Control\ absorbance - Extract\ solution\ absorbance}{Control\ absorbance}$$
$$\times 100\%$$

In vivo anti-inflammatory activity evaluation

Carrageenan induced air-pouch model was chosen to induce inflammation in the experiment subject in this study. In each experiment subject, 20 mL of air was injected subcutaneously into the intrascapular region under anesthesia. On the third and sixth days after the 20 mL air injection, another 10 mL of air was injected into the same area to keep the space air-filled. On the sixth day, 2 mL of 1% carrageenan solution was injected into the air pocket to induce inflammation. Two hours prior to carrageenan injection, each experiment subject was given intervention according to their group and repeated 24 hours after induction. Forty-eight hours after induction, a small incision was made on the carrageenan pocket to aspire the exudates and the total white blood cell was counted using a hemocytometer. The white blood count was then used to calculate the white blood cell recruitment inhibition using the formula: $(1-T/C) \times 100\%$, where T corresponds to the intervention white blood count and C corresponds to the negative control white blood count (Leite et al., 2022).

RESULTS AND DISCUSSION

Phytochemical screening of RDFPE in this study revealed the presence of alkaloid, saponin, tannin, and flavonoid compounds, while steroid, triterpenoid, and glycoside were not detected. Complete screening methods and the result are presented in Table 1. In this study, methanol was used as an extraction solvent because a study has shown that methanol was an optimal extraction solvent to obtain high content of phytochemical constituents, as well as high *in-vitro* anti-inflammatory constituents (Truong et al., 2019). While methanol is toxic for humans and can lead to blindness or even death, most of the methanol used in the extraction process was evaporated using a rotary evaporator and on the water bath, which leaves the extract with only residual methanol. This residual methanol is also regulated and should not be more than 3000 ppm (European Medicines Agency and Committee for Human Medicinal Products, 2019).

Table 1. Phytochemical Screening of Red Dragon Fruit Peel Extract (RDFPE)

Secondary Metabolite	Reagent/Methods	Result
Alkaloid	Bouchardat's	Detected
	Mayer's	Detected
	Dragendorff's	Detected
	Wagner's	Detected
Steroid dan Terpenoid	Salkowski test	Not Detected
	Liebermann-Burchard	Not Detected
Saponin	Distilled water + HCl	Detected
	$FeCl_3$ 5%	Detected
Flavonoid	$Mg_{(s)} HCl_{(p)}$	Not Detected
	NaOH 10%	Not Detected
	$H_2SO_{4(p)}$	Detected
Tannin	$FeCl_3$ 1 %	Detected
Glycoside	Molisch	Not Detected

In-vitro testing of the anti-inflammatory effect of RDFPE showed positive inhibition of protein (BSA) denaturation. *In-vitro* testing in this study found that higher concentration RDFPE has higher capability in inhibition of protein denaturation. However, the protein denaturation inhibition capability is not linear with concentration. This meant that doubling the concentration did not double the protein denaturation inhibition. For example, dragon fruit peel extract with 160 ppm concentration has average protein denaturation inhibition of 36.22%, while at 10 ppm concentration, the average protein denaturation inhibition is only about 8.19%. The average protein denaturation inhibition between the two was approximately 4 times, while the concentration difference between the two is 16 times greater. The complete percentage of protein denaturation inhibition amongst different concentration are shown in Table 2 and Figure 1. Different concentrations showed that each concentration compared to the other was significantly inhibit the denaturation of the protein and a higher concentration was significantly better at inhibiting protein denaturation ($p<0.05$). Denaturation inhibition greater than 20% is considered to be a potential anti-inflammatory agent (Drăgan et al., 2016), hence, only

extract with 80 ppm and 160 ppm concentration have potential anti-inflammatory activity.

In-vivo testing on white Wistar rats (*Rattus norvegicus*) showed that oral administration of dragon fruit peel extract suspension effectively works as an anti-inflammatory agent. Oral administration of dragon fruit peel extract suspension decreased the amount of total white blood cells (WBC) in exudates from the carrageenan induction and the effectivity was increased along with the dose. These findings are presented in Table 3. In the highest dose given (1000 mg/kg), dragon fruit peel extract suspension even outperformed diclofenac sodium in white blood count reduction. However, administration of 500 mg/kg dragon fruit extract suspension has no significant difference with Na CMC in the reduction effect of white blood counts. In Tukey HSD post-hoc test, there was no evidence to reject the null hypothesis between Na CMC and RDFPE 500 mg/kg and between diclofenac sodium and RDFPE 1000 mg/kg ($p>0.05$) (Table 4). This study has found that RDFPE at 1000 mg/kg dosage manages to inhibit white blood cell recruitment up to 71,84%, higher than the diclofenac sodium inhibition of 64,83%. Some studies suggest inhibition of more than 50% fulfilled the requirement as an anti-inflammation agent (Zaini et al., 2016; Astika et al., 2022).

Table 2. Percentage of Protein Denaturation Inhibition Between Different Concentrations of RDFPE

Concentration (ppm)	Average Absorbance*	Average Absorbance Standard Deviation	Average Inhibition Percentage
Control	0.828067	0.006232	0
10	0.760200	0.005940	8.19±0.71
20	0.733300	0.005650	11.43±1.18
40	0.680400	0.007700	17.82±1.43
80	0.629800	0.002000	23.93±0.45
160	0.527200	0.005710	36.32±0.92

*Acquired from the mean of three absorbance measurement replications.
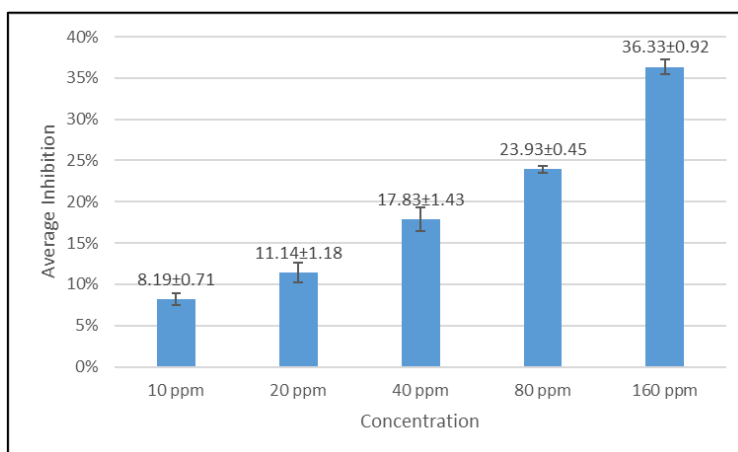

Figure 1. Protein Denaturation Inhibition Effectivity of Red Dragon Fruit Peel Extract in Different Concentrations. Represented as means ± SD of three replicates.

Table 3. Average White Blood Cell Count in Exudates in Different Groups

Group	n	Average Total WBC	Inhibition (%)
(-) Control	5	9,840.00±383.08	
(+) Control	5	3,460.00±736.04	64.83
RDFPE 1	5	9,130.00±719.03	7.21
RDFPE 2	5	7,820.00±646.72	20.52
RDFPE 3	5	2,770.00±757.13	71.84

(-) Control: Na CMC; (+) Control: Diclofenac sodium; RDFPE 1: 500mg/kg dose; RDFPE 2: 750mg/kg dose; RDFPE 3: 1000mg/kg dose.

Table 4. Mean Difference of Total White Blood Cells Between Different Groups

	(-) Control	(+) Control	RDFPE 1	RDFPE 2	RDFPE 3
(-) Control		-6380.00*	-710.00	-2020.00*	-7070.00*
(+) Control	6380.00*		5670.00*	4360.00*	-690.00
RDFPE 1	710.00	-5670.00*		-1310.00*	-6360.00*
RDFPE 2	2020.00*	-4360.00*	1310.00*		-5050.00*
RDFPE 3	7070.00*	690.00	6360.00*	5050.00*	

(-) Control: Na CMC; (+) Control: Diclofenac sodium; RDFPE 1: 500mg/kg dose; RDFPE 2: 750mg/kg dose; RDFPE 3: 1000mg/kg dose. *Significant mean difference

Many studies had found that red dragon fruit peel contains flavonoid, alkaloid, saponin, tannin, steroid, triterpenoid, and glycoside in varying concentrations (Ragab et al., 2018; Luo et al., 2014; Saenjum et al., 2021; Zain et al., 2019; Le, 2022). The difference in findings between this study and the other multiple studies is due to different methods of phytochemical analysis. Studies by others (Ragab et al., 2018; Luo et al., 2014; Saenjum et al., 2021; Zain et al., 2019; Le, 2022) were quantitative analyses, using different methods, whilst this study only uses qualitative screening and using a simple reagent, thus when the amount of the compound was not high enough for the reagent to detect, the result was negative.

This study finding is in accordance with findings by Nur et al, where dragon fruit extract was found to be effective in inhibiting BSA denaturation with 64,32±0,81 to 84,97±0,81% inhibition compared to the control group (Nur et al., 2022). Nur *et al.* study also found that different solvent of the extract affects the effectiveness of the protein denaturation inhibition effect. Aqueous extract (water solvent) is more effective at inhibiting protein denaturation compared to extract with ethanol or ethyl acetate solvent (Nur et al., 2022). These study findings are far lower compared to the findings by Nur et al (2022). However, the study by Nur *et al.* (2022) was using the whole fruit (peel, stem, and flesh), instead of just the dragon fruit peel like this study. While the peel contains a higher concentration of flavonoid content compared to the flesh when extract derived from peel, stem, and flesh will result in an extract with even higher flavonoid content. However, the effect of the difference can not be determined since

Nur *et al.* study did not specify the ratio of the different parts (Nur et al., 2022).

Eldeen *et al.* found that dragon fruit extract has an anti-inflammatory effect by involving both lipoxygenase and cyclooxygenase pathways (Eldeen et al., 2020). The extract effects on both lipoxygenase and cyclooxygenase pathways mean that the extract works lead to blockage of leukotriene and prostaglandin pathways (Eldeen et al., 2020). In their study, Eldeen *et al.* also found that dragon fruit extract with a higher concentration of betalains has higher anti-inflammatory potency. However, Eldeen *et al.* study was using white dragon fruit (*Hylocereus undatus*) instead of red dragon fruit (*Hylocereus polyrhizus*) like this study. This difference in dragon fruit species does not have a big difference in phytochemical contents, both generally contain similar phytochemical contents with a different concentration between the two species (Luo et al., 2014). Aside from betalains, flavonoid and tannin compounds in red dragon fruit peel most likely act as an anti-inflammatory, since both are known to have anti-inflammatory properties (Onyekere et al., 2019). However, since this study method of analysis of the phytochemical content of red dragon fruit peel was a qualitative analysis, this study cannot name a specific flavonoid or tannin compound which responsible for this anti-inflammation action.

CONCLUSION

This study has found that red dragon fruit contains alkaloids, saponins, tannins, and flavonoids. These multiple compounds have the potential as an anti-inflammatory agent, as an alternative to synthetic anti-inflammatory drugs. However, the dose at which this

extract work as an anti-inflammatory agent is way too high (1000 mg/kg), meanwhile the toxicity of this extract is still unknown. Further study to identify a specific compound that is responsible for this anti-inflammatory action and further action to isolate the compound(s) can reduce the dosage needed to perform effectively as an anti-inflammatory agent.

REFERENCES

Abidin, Zainal, Putri, Uni Angreni, and Widiastuti, Harti. 2019. "Potensi Anti-Inflamasi Fraksi Etil Asetat Ranting Patah Tulang (Euphorbia Tirucalli L.) Dengan Uji Penghambatan Denaturasi Protein." *Journal of Pharmaceutical Sciences* 2 (2): 49–54. https://doi.org/10.24252/djps.v2i2.11549.

Astika, Rahmila Yuni, Sani, Fathnur, and Elisma. 2022. "Uji Aktivitas Antiinflamasi Ekstrak Etanol Daun Kayu Manis (Cinnamomum Burmanni)Pada Mencit Putih Jantan." *Jurnal Ilmiah Manuntung* 8 (1): 14–23.

Drăgan, Maria, Stan, Cătălina Daniela, Pânzariu, Andreea, and Profire, Lenuţa. 2016. "Evaluation of Anti-Inflammatory Potential of Some New Ferullic Acid Derivatives." *Farmacia* 64 (2): 194–97.

Egbuna, Chukwuebuka, Ifemeje, Jonathan C., Maduako, Maryann Chinenye, Tijjani, Habibu, Udedi, Stanley Chidi, Nwaka, Andrew C., and Ifemeje, Maryjane Oluoma. 2019. "Phytochemical Test Methods: Qualitative, Quantitative and Proximate Analysis." In *Phytochemistry, Volume 1: Fundamentals, Modern Techniques, and Applications*. Waretown: Apple Academic Press Inc.

Eldeen, Ibrahim M S, Foong, Shin Y, Ismail, Noraznawati, and Wong, Keng C. 2020. "Regulation of Pro-Inflammatory Enzymes by the Dragon Fruits from Hylocereus Undatus (Haworth) and Squalene - Its Major Volatile Constituents." *Pharmacognosy Magazine* 16 (68): 81–86. https://doi.org/10.4103/pm.pm.

Elzagheid, Mohamed I. 2018. "Laboratory Activities to Introduce Carbohydrates Qualitative Analysis to College Students." *World Journal of Chemical Education* 6 (2): 82–86. https://doi.org/10.12691/wjce-6-2-1.

European Medicines Agency, and Committee for Human Medicinal Products. 2019. "ICH Guideline Q3C (R6) on Impurities: Guideine for Residual Solvents." Amsterdam.

Hendra, Rudi, Masdeatresa, Lidya, Abdulah, Rizky, and Haryani, Yuli. 2019. "Antibacterial Activity of Red Dragon Peel (Hylocereus Polyrhizus) Pigment." *Journal of Physics: Conference Series* 1351 (1). https://doi.org/10.1088/1742-6596/1351/1/012042.

Hendra, Rudi, Masdeatresa, Lidya, Almurdani, Muhammad, Abdullah, Rizky, and Haryani, Yuli.

2020. "Antifungal Activity of Red Dragon Peel (Hylocereus Polyrhizus)." *IOP Conference Series: Materials Science and Engineering* 833 (1): 12014.

Kartikawati, Endah, Deswati, Dytha Andri, and Pramudita, Bentari. 2020. "Uji Efek Analgetik Ekstrak Etanol Daun Asam Jawa (Tamarindus Indica L.) Pada Mencit Putih Jantan Galur Swiss Webster." *Jurnal Sabdariffarma* 1 (2): 11–18.

Le, Ngoc Lieu. 2022. "Functional Compounds in Dragon Fruit Peels and Their Potential Health Benefits: A Review." *International Journal of Food Science and Technology* 57 (5): 2571–80. https://doi.org/10.1111/ijfs.15111.

Leite, Leydianne, Patriota, De Siqueira, Brito, Dalila De, Ramos, Marques, Gama, Mariana, Caroline, Angela, Amorim, Lima, Ara, Yasmym, and Paiva, Guedes. 2022. "Inhibition of Carrageenan-Induced Acute Inflammation in Mice by the Microgramma Vacciniifolia Frond Lectin (MvFL)." *Polymers* 14 (1609): 1–12.

Liana, Rizal, Widowati, Wahyu, Fioni, Akbar, Khainir, Fachrial, Edy, and Lister, I Nyoman Ehrich. 2019. "Antioxidant and Anti-Hyaluronidase Activities of Dragon Fruit Peel Extract and Kaempferol-3-O- Rutinoside." *Jurnal Kedokteran Brawijaya* 30 (4): 247–52. https://doi.org/10.21776/ub.jkb.2019.030.04.3.

Luo, Hui, Cai, Yongqiang, Peng, Zhijun, Liu, Tao, and Yang, Shengjie. 2014. "Chemical Composition and in Vitro Evaluation of the Cytotoxic and Antioxidant Activities of Supercritical Carbon Dioxide Extracts of Pitaya (Dragon Fruit) Peel." *Chemistry Central Journal* 8 (1): 1–7.

Luu, Thi-thuy-hai, Le, Truc-linh, Huynh, Nga, and Quintela-alonso, Pablo. 2021. "Dragon Fruit : A Review of Health Benefits and Nutrients and Its Sustainable Development under Climate Changes in Vietnam." *Czech Journal of Food Sciences* 39 (2): 71–94.

Muhammad, N.W.F., Nurrulhidayah, A F, Hamzah, M.S., Rashidi, O., and Rohmad, A. 2020. "Physicochemical Properties of Dragon Fruit Peel Pectin and Citrus Peel Pectin: A Comparison." *Food Research* 4: 266–73.

Niah, Rakhmadhan, and Baharsyah, Riki Nirwan. 2018. "Uji Aktivitas Antioksidan Ekstrak Etanol Kulit Buah Naga Merah Super (Hyclocereus Costaricencis)." *Jurnal Pharmascience* 5 (1): 14–21. https://doi.org/10.20527/jps.v5i1.5781.

Nur, Ashaduzzaman, Uddin, M Rasel, Meghla, Nigar Sultana, and Uddin, M Jashim. 2022. "In Vitro Anti-Oxidant, Anti-Inflammatory, Anti-Bacterial, and Cytotoxic Effects of Different Extracted Colorants from Two Species of Dragon Fruit (Hylocereus Spp .)." *SSRN Electronic Journal* 61097.

Onyekere, Peculiar Feenna, Peculiar-Onyekere, Chioma Obianuju, Udodeme, Helen Ogechukwu, Nnamani, Daniel Okwudili, and Ezugwu, Chritopher Obodike. 2019. "Biological Roles of

Phytochemicals." In *Phytochemistry, Volume 1: Fundamentals, Modern Techniques, and Applications*. Waretown: Apple Academic Press Inc.

Paramita, Vita, Abidin, Zainal, Wikanta, Deddy K, Aini, Falasifah N, Adiatma, Afifta L, Teknik, Fakultas, and Diponegoro, Universitas. 2015. "Emulsifikasi Ekstrak Kulit Dan Buah Naga Merah Menggunakan Xanthan Gum: Analisis Kadar Fenolik, Kadar Flavonoid Dan Kestabilan Emulsi." *Metana* 11 (02). https://doi.org/10.14710/metana.v11i02.14753.

Ragab, Sabrin, Ibrahim, Mohamed, Mohamed, Gamal Abdallah, Ibrahim, Amgad, Khedr, Mansour, Fathalla, Mohamed, and El-kholy, Amal Abd-elmoneim Soliman. 2018. "Genus Hylocereus : Beneficial Phytochemicals , Nutritional Importance , and Biological Relevance — A Review." *Journal of Food Biochemistry* 42 (November 2017): 1–29. https://doi.org/10.1111/jfbc.12491.

Rahmawati, Rahmawati, Widiastuti, Harti, and Sulistya, Eka. 2020. "In Vitro Anti-Inflammatory Assay of Bitter Melon (Momordica Charantia L.) Ethanol Extract." *Jurnal Fitofarmaka Indonesia* 7 (3): 1–4. https://doi.org/10.33096/jffi.v7i3.655.

Saenjum, Chalermpong, Pattananandecha, Thanawat, and Nakagawa, Kouichi. 2021. "Antioxidative and Anti-Inflammatory Phytochemicals and Related Stable Paramagnetic Species in Different Parts of Dragon Fruit." *Molecules* 26 (3565).

Sinaga, Amanda Angelina, Luliana, Sri, and Fahrurroji, Andhi. 2015. "Losio Antioksidan Buah Naga Merah (Hylocereus Polyrhizus Britton and Rose)." *Pharmaceutical Sciences and Research (PSR)* 2 (1). https://doi.org/http://dx.doi.org/10.7454/psr.v2i1.3333.

Sriarumtias, Framesti Frisma, Ardian, Muhammad Egi, and Najihudin, Aji. 2020. "Uji Aktivitas Ekstrak Daun Jeruk Manis (Citrus x Aurantium L.) Sebagai Antiinflamasi." *PHARMACY: Jurnal Farmasi Indonesia (Pharmaceutical Journal of Indonesia)* 17 (1): 197. https://doi.org/10.30595/pharmacy.v17i1.6541.

Truong, Dieu-hien, Nguyen, Dinh Hieu, Thuy, Nhat, Ta, Anh, Bui, Anh Vo, and Do, Tuong Ha. 2019. "Evaluation of the Use of Different Solvents for Phytochemical Constituents , Antioxidants , and In Vitro Anti-Inflammatory Activities of Severinia Buxifolia." *Journal of Food Quality* 2019 (8178294): 9. https://doi.org/https://doi.org/10.1155/2019/8178294 Research.

Zain, Norashikin Mat, Nazeri, Muhd Azlan, and Azman, Nurul Aini. 2019. "Assessment on Bioactive Compounds and the Effect of Microwave on Pitaya Peel." *Jurnal Teknologi* 81 (2): 11–19. https://doi.org/10.11113/jt.v81.12847.

Zaini, Muhammad, Biworo, Agung, and Anwar, Khoerul. 2016. "Uji Efek Antiinflamasi Ekstrak Etanol Herba Lampasau (Diplazium Esculentum Swartz) Terhadap Mencit Jantan Yang Diinduksi Karagenin - Λ." *Jurnal Pharmascience* 03 (02).

Characterization of Spanlastic System Loaded Green Tea Extract as Antioxidant for Skin

Evelyne Santuso[1], Widji Soeratri[2]*, Tutiek Purwanti[2]
[1]Master Program in Pharmaceutical Science, Faculty of Pharmacy, Universitas Airlangga, Surabaya, Indonesia
[2]Department of Pharmaceutics, Faculty of Pharmacy, Universitas Airlangga, Surabaya, Indonesia

*Corresponding author: widji-s@ff.unair.ac.id

Abstract

Background: *Green tea possesses abundant polyphenols that exert antioxidant activity. However, green tea's hydrophilicity and instability limit its penetration into the skin layers. Recently, a non-ionic surfactant-based elastic nanovesicular system called spanlastic can enhance the delivery of hydrophilic and unstable substances. Spanlastic composed of vesicle builder and edge activator, which influence the characteristics of the vesicle.* **Objective**: *The study aimed to evaluate the influence of the ratio of the components on the characterization of green tea extract-loaded spanlastic using three different weight ratio of vesicle builder and edge activator that is 7:3, 8:2, and 9:1.* **Methods**: *Spanlastic is prepared by ethanol injection methods using Span 60 as vesicle builder (VB) and Tween® 60 as edge activator (EA). The characterization includes visually observed organoleptic, particle size (PS) and polydispersity index (PDI) using dynamic light scattering, entrapment efficiency (EE) and drug loading (DL) using total phenolic content assay. The most optimum ratio will be tested its zeta potential value using Zetasizer and viscosity using Brookfield Cone and Plate.* **Results**: *Selected spanlastic formula composed of Span 60 and Tween® 60 at a weight ratio of 8:2 has given characteristics as follows: entrapment efficiency 60.85±1.70%; drug loading 11.07±0.65%; the particle size is 419.70±7.42 nm; and PDI value 0.26±0.05. The prepared spanlastic has a greenish liquid form, with a zeta potential value of 28.53±2.78 mV and viscosity of 14.65±0.32 cP.* **Conclusion**: *The optimum weight ratio of vesicle builder and edge activator for green tea extract spanlastic is Span 60:Tween® 60 8:2.*

Keywords: *spanlastic, green tea extract, vesicle-based delivery system, characterization, antioxidants*

INTRODUCTION

Skin is the outermost part of the human body which mainly acts as a barrier against the external environment. It also protects the skin from microorganisms and prevents the water from evaporating from the skin (Martini, Nath and Bartholomew, 2018). As time passed, the natural process of skin aging occurred causing visible changes in the skin structure, such as loss of elasticity, fine lines, and dryness. The intrinsic factor such as cellular metabolism and external factors such as radiation of ultraviolet (UV) light can accumulate free radicals and induce matrix metalloproteinase production, which is known as the collagen degrading enzyme. When the amount of free radicals has exceeded the number of antioxidants, oxidative damage happened. Therefore, an antioxidant is essential to scavenge free radicals.

Antioxidants naturally present on plants, as secondary plant metabolites called polyphenols. The tea plant (Camellia sinensis L.) contains abundant polyphenols compound and shows potential as anti-aging. Polyphenols are especially present the most in green tea. Green tea polyphenols are dominated by catechin compounds: epigallocatechin-3-gallate (EGCG), epigallocatechin (EGC), epicatechin-3-gallate (ECG), and epicatechin (EC). The most abundant catechin compounds are EGCG, therefor its physicochemical characteristics is further used to represent green tea extract in this study . The physicochemical characteristics of EGCG are limiting the penetration to the skin, as it is very hydrophilic and unstable toward the light. Therefore green tea extract needs a suitable delivery system, to increase its penetration into the skin.

A non-ionic surfactant vesicular delivery system called spanlastic has been emerging as the novel delivery system suitable for delivering hydrophilic substances. The elasticity of the system has been shown to improve the entrapment efficiency of the active substances when compared with the conventional niosomes (Kakkar and Kaur, 2011a). The flexible membrane enables it to penetrate through small-sized pores of the skin, increasing active ingredients penetration. Besides that, the vesicle also act as penetration enhancer, increase penetration through fusion or adsorption with the stratum corneum, and through the hair follicle. The addition of an edge activator also increases skin diffusion by increasing the vesicle capacity to bind water, preventing water evaporation, and hydrating the skin enhancing its suitability to be applied on the skin for topical uses (Alaaeldin *et al.*, 2021; Rathod *et al.*, 2021).

Spanlastic is composed of a non-ionic surfactant as the vesicle builder and an edge activator that gives elasticity to the vesicle membrane. The formation of spanlastic is depends on three determining factors that is hydrophilic-lipophilic balance (HLB), critical packing parameter (CPP), and phase transition temperature (Tc). Span 60 is chosen as the non-ionic surfactant that fulfills all the requirements to form the vesicle. It has a low HLB value of 4.7 with a long alkyl chain. The CPP value also goes between 0.5-1.0 so it can form vesicles spontaneously. The Tc value of Span 60 is also pretty high at $53°C$ implying that the orderly stated bilayer molecules are present in the membrane (Ag Seleci *et al.*, 2016; Khoee and Yaghoobian, 2017; Mazyed *et al.*, 2021). Tween® 60 is chosen as the edge activator because of its hydrophilicity with an HLB value of 14.9 causing destabilization of the vesicles. The previous research also showed that a combination of Span 60 and Tween® 60 produces spanlastic with the highest entrapment of active ingredients (Alaaeldin *et al.*, 2021; Mazyed *et al.*, 2021).

Hence, the objective of this study was to prepare green tea extract-loaded spanlastic using various ratios of vesicle builder and edge activator to see how it influences the characterization of spanlastic. The characterization of spanlastic comprises entrapment efficiency, drug loading, particle size, polydispersity index, and zeta potential (Kakkar and Kaur, 2011a).

MATERIALS AND METHODS
Materials

Green tea leaf (Tea Heaven, Indonesia), Span 60 (Croda, UK), Tween® 60 (Croda, UK), Absolute Alcohol (Merck, Germany), Deionized water, Folin-Ciocalteu's phenol reagent (Merck, Germany), Sodium Carbonate (Merck, Germany), Gallic acid anhydrous (Merck, Germany).

Method
Preparation of green tea ethanol extract

Green tea leaf was processed using a grinder/blender to obtain a finely powdered green tea leaf. About 12 grams of powdered green tea leaf is weighed down and added with 720 ml 75% ethanol (1:60 w/v). The mixture was then heated in a thermostated water bath at $90°C$ for 10 minutes. After 10 minutes, the resultant infusion is filtered using the Buchner funnel vacuum filtration method with Whatmann filter paper 40. The filtrate was concentrated by a rotary evaporator under reduced pressure until the thick extract is obtained. Then, the extract continued to

be dried using a freeze dryer. The resultant powdered green tea ethanol extract is stored at room temperature in a dark bottle to prevent any light exposure (Hu, Zhou and Chen, 2009).

Preparation of green tea extract spanlastic

The ethanol injection method was employed to fabricate the spanlastic system. The method has been successfully developed in a spanlastic system in previous research. Accurately weight Tween® 60, as stated in Table 1, was added into deionized water and heated at 60°C. The organic phase consisting of Span 60 and powdered green tea extract dissolved in absolute ethanol was also prepared. The organic phase was injected dropwise into the water phase on continuous stirring until the milky dispersion is formed. The heating was continued for 30 minutes to evaporate the excess ethanol from the dispersion completely. The formed spanlastic was left overnight at 4°C for complete maturation until used in further studies (Fahmy *et al.*, 2018, 2019; Guimarães *et al.*, 2020; Mazyed *et al.*, 2021).

Characterization of green tea ethanol extract spanlastic

Organoleptic

The physical appearance of the green tea extract spanlastic was visually observed regarding its consistency, color, odor, and consistency soon after being kept refrigerated overnight.

Particle size and polydispersity index (PDI)

Green tea ethanol extract spanlastic was diluted with deionized water (1:100) and homogenized at 25°C, and then the particle size was determined using Malvern Zetasizer Nano.

Entrapment efficiency & drug loading

Entrapment efficiency was determined by analyzing the total phenolic compound on the spanlastic. About 1 ml of green tea ethanol extract spanlastic is centrifugated at 13,000 rpm for 30 minutes at 4°C to separate the free phenolic compound (Badria *et al.*, 2020). Then, the free phenolic compound on the supernatant was analyzed with the Folin-Ciocalteu method.

The standard curve of gallic acid was prepared to assess the total phenolic compound through a different concentration (20-100 ppm) of gallic acid standard solution in water. A saturated sodium carbonate solution (75 g/L) and 0.2 mol/L Folin-Ciocalteu's reagent was prepared. About 20 mL of 2 mol/L Folin-Ciocalteu's reagent was diluted with deionized water until the volume reaches 200 mL.

Precisely pipetted 0.5 ml of the green tea ethanol extract spanlastic supernatant sample and a standard solution are transferred to the amber vial and wrapped in aluminium foil, then added with 2.5 mL 0.2 mol/L Folin Ciocalteu's reagent. The mixture is left at room temperature for 4 minutes in the dark conditions. Then, about 2 mL of saturated sodium carbonate solution (75 g/L) was added to the mixture and left for 2 hours in the dark at room temperature. Deionized water was used as a blank solution. The absorbance was measured after 2 hours using UV-spectrophotometer at 764 nm against the blank solution. Then, total phenolic content was reported as gallic acid equivalent (GAE/gram) (Zhao *et al.*, 2019).

The total drug content, which consisted of the unentrapped and entrapped drug, was also determined to calculate the entrapment efficiency. About 1 mL of green tea ethanol extract spanlastic was added to 100 mL isopropyl alcohol. The mixture was homogenized and then processed to estimate the total phenolic content using the Folin-Ciocalteu method previously described (Mazyed *et al.*, 2021).

% EE was calculated based on equation %EE = (TD GTE-TF GTE)/TD GTE x 100

Drug loading was calculated using equation %DL = (TD GTE-TF GTE)/TS x 100 where TD was the total drug of green tea extract, TF was the total free green tea extract, and TS was the total surfactant used in the formula (Sallam *et al.*, 2021).

Table 1. Green tea extract-loaded spanlastic formula

Material	Function	Weight (w/w)		
		SPL 1 (9:1)	SPL 2 (8:2)	SPL 3 (7:3)
Green tea extract	Active ingredient	50 mg	50 mg	50 mg
Span 60	Vesicle builder	180 mg	160 mg	140 mg
Tween® 60	Edge activator	20 mg	40 mg	60 mg

Note:
SPL 1 = formula of green tea extract spanlastic with the weight ratio of 9:1
SPL 2 = formula of green tea extract spanlastic with the weight ratio of 8:2
SPL 3 = formula of green tea extract spanlastic with the weight ratio of 7:3
The total amount of surfactants used was 200 mg
Total volume of spanlastic was 25 ml

Zeta potential

The most optimal formula of green tea ethanol extract spanlastic was diluted with deionized water (1:100) and homogenized at 25°C, and the zeta potential was determined using Malvern Zetasizer Nano.

Viscosity

The viscosity of the green tea extract spanlastic was measured using the Brookfield Cone and Plate using spindle 41. Approximately 0.5-2.0 ml sample was put on the sample cup, then measured at 25°C.

Antioxidant activity by DPPH Radical Scavenging Method

The sample was separated first using a centrifuge at 13,000 rpm for 30 minutes. The resulting supernatant was used to make a series of concentrations to react with 0.004% DPPH ethanolic solution. About 2 ml of 0.004% DPPH ethanolic solution was added to the 2 ml sample. Then the mixture was left under dark conditions for 30 minutes. The absorbance measurement was performed at 517 nm using Spectrophotometer UV-Vis. The inhibition was calculated using the equation as follows % inhibition = (Ac-As)/Ac x100% where Ac was the absorbance of the control and As was the absorbance of the sample.

Data analysis

All measurements were conducted in triplicate, and data were expressed as mean ± SD. The data was analyzed using a One-way analysis of variance (ANOVA), followed by the Tukey test. A value of $P < 0.05$ was considered significantly different. The IBM SPSS Statistics 25 software was used for data analysis.

RESULTS AND DISCUSSION

Preparation of green tea extract spanlastic

The green tea extract-loaded spanlastic was successfully prepared using the ethanol injection method with Span 60 as the vesicle builder and Tween® 60 as the edge activator. Three main factors influenced the formation of spanlastic. The surfactant's hydrophilic-lipophilic balance (HLB) value and the critical packing parameter (CPP) needed to be considered. A surfactant with an HLB value between 4-8 and a CPP value between 0.5-1.0 reflected the ability of the surfactant to assemble vesicles by itself in the absence of cholesterol. Lastly, the phase transition temperature (Tc) was correlated with the permeability of the vesicle membrane. The higher the Tc value was, the more vesicle was stable and not porous.

The ethanol injection method was suitable for forming large unilamellar vesicles (LUV) of spanlastic, to be able to entrap more hydrophilic substances in its core (Durak *et al.*, 2020). Moreover, the addition of ethanol decreased the vesicle thickness, leading to an increase in drug partition and a smaller size of vesicles (Alnusaire *et al.*, 2021; Mahmoud A Elgewelly *et al.*, 2022).

Characterization of green tea ethanol extract spanlastic

Organoleptic

After being stored overnight, the green tea extract-loaded spanlastic was observed visually regarding color, odor, and consistency. The visually observed green tea extract-loaded spanlastic shown in Figure 1 showed no differences between its color, odor, or consistency even when formulated with different ratios of Span 60 (vesicle builder) and Tween® 60 (edge activator). All formula of green tea extract-loaded spanlastic depicted green-colored odorless liquid, as detailed in Table 2.
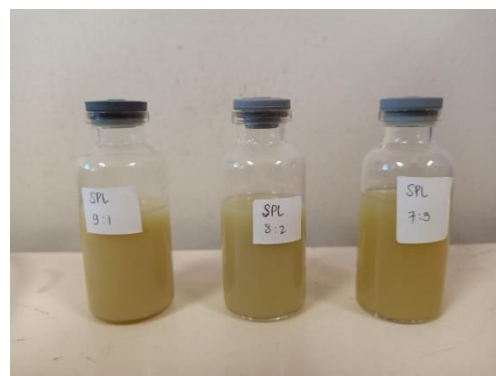
Figure 1. Green tea extract-loaded spanlastic with different ratios of vesicle builder and edge activator: SPL 1 (9:1); SPL 2 (8:2); and SPL 3 (7:3) from left to the right side

Table 2. Spanlastic formula organoleptic

Formula	Organoleptic Parameter		
	Color	Odor	Consistency
SPL 1 (Span 60: Tween® 60 9:1)	Green	Odorless	Liquid
SPL 2 (Span 60: Tween® 60 8:2)	Green	Odorless	Liquid
SPL 3 (Span 60: Tween® 60 7:3)	Green	Odorless	Liquid

Table 3. Result of particle size and polydispersity index measurement

Formula	Particle size ±SD (nm)*	PDI ±SD*
SPL 1 (Span 60: Tween® 60 9:1)	1283.05 ± 15.10	0.50 ± 0.04
SPL 2 (Span 60: Tween® 60 8:2)	419.70 ± 7.42	0.260 ± 0.05
SPL 3 (Span 60: Tween® 60 7:3)	244.20 ± 15.34	0.30 ± 0.01

*Particle size and PDI data were result from triplicate measurement

Table 4. Entrapment efficiency and drug loading of the green tea extract-loaded spanlastic

Formula	EE±SD (%)*	DL ±SD (%)*
SPL 1 (Span 60: Tween® 60 9:1)	61.46 ± 0.11	12.04 ± 0.09
SPL 2 (Span 60: Tween® 60 8:2)	60.85 ± 1.70	11.07 ± 0.65
SPL 3 (Span 60: Tween® 60 7:3)	39.95 ± 1.11	5.31 ± 0.28

*%EE and %DL data were result from triplicate measurement

Particle size and polydispersity index (PDI)

Designing a vesicular system within the nanometer range was essential to ensure the penetration of the system through the deeper skin layer. Several factors can affect the size of the vesicular system. Developing a small particle size will produce a larger surface area available for the diffusion process (Enas Elmowafy *et al.*, 2019; Alaaeldin *et al.*, 2021). Non-ionic surfactants, as the vesicle builder, can achieve a better entrapment of the active substances when incorporated in large amounts. But it also increased the diameter of the vesicle, resulting in a bigger vesicle size. A particle size below 700 nm has been reported to be able to penetrate the deeper skin layer and exert a beneficial effect on UVB treatment, psoriasis treatment, and anti-inflammatory effect (Farghaly *et al.*, 2017; Enas Elmowafy *et al.*, 2019; Elhabak, Ibrahim and Abouelatta, 2021)

From Table 3, increasing the Span 60 amount has significantly enlarged the diameter of the vesicle. While the concentration of Span 60 increased, the concentration of Tween® 60 decreased. This low concentration of edge activators was inadequate to cover the whole surface area, leading to the agglomeration of some vesicles to reduce their surface area, so the Tween® 60 will be sufficient to protect it. This agglomeration tendency will lead to the formation of a larger vesicle size. On the contrary, the increasing amount of edge activator, Tween® 60, has decreased particle size. This has been correlated to lower the surface tension between the two phases, leading to particle partition to a smaller vesicle. Another research also stated the possibility of mixed micelles formation in the presence of a high-concentration edge activator. It was also necessary to note that the preparation of spanlastic using ethanol has also affected the particle size (Shaaban *et al.*, 2019; Shamma *et al.*, 2019a; Badria and Mazyed, 2020). The addition of ethanol has decreased the vesicle membrane thickness, modifying

the net charge of the vesicle and providing steric stabilization, leading to a smaller vesicle size (Kakkar and Kaur, 2011b; Alaaeldin *et al.*, 2021).

The particle size distribution was reflected by the polydispersity index (PDI) value. The formulas showed PDI values ranging from 0.30-0.50, indicating a homogenous system with a low tendency toward aggregation (Abbas and Kamel, 2020; Elhabak, Ibrahim and Abouelatta, 2021).

Entrapment efficiency & drug loading

Entrapment efficiency is the essential factor that ensures the drug is successfully entrapped by the vesicle, to optimally deliver the drug. The non-ionic surfactant and edge activators, as the vesicular structure builder, is the essential determining factor of the system entrapment efficiency. Their amount together has shown significant effects on the entrapment efficiency of the system.

Based on Table 4, it can be observed that by increasing the amount of vesicle builder, Span has significantly increased the entrapment efficiency along with the drug loading. The only insignificant difference is the entrapment efficiency between SPL 1 and SPL 2, despite both having significantly different vesicle sizes. On the contrary, the negative effect is observed after increasing the amount of edge activator. The hydrophilic characteristic of edge activators leads to pore formation in the bilayer membrane, thus reducing its entrapment (Shamma *et al.*, 2019b; Elhabak, Ibrahim and Abouelatta, 2021).

The combination of the lipophilic and hydrophilic surfactant has developed a mixed HLB value. According to the literature, the best HLB value to prepare spanlastic is in the range of 4-8 (Ag Seleci *et al.*, 2016). It is essential to ensure that the concentration of edge activators should be at a certain point, since excess edge activators cause the formation of micelles and/or mixed micelles, instead of vesicle formation. The micellar structure will lead to drug leakage, resulting in

lower entrapment (Abbas and Kamel, 2020; Mahmoud A. Elgewelly *et al.*, 2022). While entrapment efficiency is not affected by the number of active substances added to the system due to the maximum capacity of the non-ionic surfactant to entrap the substances in a fixed amount (Elhabak, Ibrahim and Abouelatta, 2021).

Zeta potential

Based on the measurement result of particle size, PDI, %EE, and %DL it was concluded that SPL 2 has given the most suitable characteristic for the delivery of green tea extract. The measurement of zeta potential was undertaken on SPL 2 by using Malvern Zetasizer. Zeta potential value itself can reflect the stability of the system by measuring the net charge of the vesicles. The result obtained from the measurement is -28.53 ± 2.78 mV, as seen in Table 5. Despite the formula does not contain any charged molecules, the negative zeta potential was obtained as the result of dispersion medium hydroxyl ions adsorption on the vesicle surface. The charged vesicle is considered to have a low tendency towards aggregation and fusion because it will cause repulsion between vesicles. The system with a zeta potential value of around ± 30 mV is considered to be stable (E Elmowafy *et al.*, 2019; Badria and Mazyed, 2020; Elhabak, Ibrahim and Abouelatta, 2021).

Table 5. Zeta potential result of SPL 2

Formula	Zeta potential±SD (mV)
SPL 2 (Span 60: Tween® 60 8:2)	-28.53 ± 2.78

*data were result from triplicate measurement

Viscosity

Viscosity measurement is an essential parameter that reflects the system's suitability as the form of topical dosage. The result of viscosity measurement towards SPL 2 showed a low viscosity of 14.65 ± 0.32 cPs, as seen in Table 6. The watery texture of spanlastic is not suitable for the topical delivery dosage form, as it has a low residence time on the skin. Several previous research has stated that spanlastic incorporation into gel dosage form is increasing its adherence and spreadability on the skin, leading to better skin penetration (Goyal *et al.*, 2015; Enas Elmowafy *et al.*, 2019; Mahmoud A. Elgewelly *et al.*, 2022).

Table 6. Viscosity of SPL 2

Formula	Viscosity±SD (cPs)
SPL 2 (Span 60: Tween® 60 8:2)	14.65 ± 0.32

*data were result from triplicate measurement

Antioxidant activity by DPPH Method

The antioxidant activity is evaluated through the inhibition concentration of 50% DPPH radical (IC_{50}) value. The IC_{50} of green tea extract spanlastic and gallic acid as control shows a very strong antioxidant activity ($IC_{50} < 50$ ppm). The strong antioxidant activity related to the gallate group that present on position 3 EGCG catechin structure and hydroxyl group on 5' EGC structure (Guo *et al.*, 1999; Budiman *et al.*, 2019).

Table 7. IC_{50} value by DPPH Radical Scavenging Method

Formula	IC_{50}±SD (ppm)
Gallic acid (control)	3.34 ± 0.03
SPL 2	7.63 ± 0.07

*data are result from triplicate measurement
*data were result from triplicate measurement

CONCLUSION

In the present study, the green tea extract is successfully loaded in the vesicle-based delivery system spanlastic. The ratio of vesicle builder and edge activator does have an important role by significantly affecting the characterization of spanlastic. SPL 2 formula with an Span 60:Tween® 60 80:20 ratio showed the most optimal characteristic in particle size, PDI, entrapment efficiency, and drug loading for topical dosage forms. Moreover, through DPPH Radical Scavenging assay it has proven to possess a potent antioxidant activity with IC_{50} below 50 ppm that ensuring its effect as antiaging. However, spanlastic has a low viscosity, incorporation into another vehicle such as gel is encouraged to enhance its penetration into the skin. The described green tea extract-loaded spanlastic unravels its potential in future research to be used as the anti-aging topical dosage form.

ACKNOWLEDGMENT

REFERENCES

Abbas H, Kamel R. Potential role of resveratrol-loaded elastic sorbitan monostearate nanovesicles for the prevention of UV-induced skin damage. J Liposome Res 2020;30:45–53. https://doi.org/10.1080/08982104.2019.1580721

Ag Seleci D, Seleci M, Walter JG, Stahl F, Scheper T. Niosomes as nanoparticular drug carriers: Fundamentals and recent applications. J Nanomater 2016;2016. https://doi.org/10.1155/2016/7372306.

Alaaeldin E, Abou-Taleb HA, Mohamad SA, Elrehany M, Gaber SS, Mansour HF. Topical nano-vesicular spanlastics of celecoxib: Enhanced anti-inflammatory effect and down-regulation of tnf-α, nf-κb and cox-2 in complete freund's adjuvant-induced arthritis model in rats. Int J Nanomedicine 2021;16:133–45. https://doi.org/10.2147/IJN.S289828.

Alnusaire TS, Sayed AM, Elmaidomy AH, Al-Sanea MM, Albogami S, Albqmi M, et al. An in vitro and in silico study of the enhanced antiproliferative and pro-oxidant potential of olea europaea l. Cv. arbosana leaf extract via elastic nanovesicles (spanlastics). Antioxidants 2021;10:1–18. https://doi.org/10.3390/antiox10121860.

Badria F, Mazyed E. Formulation of Nanospanlastics as a Promising Approach for Improving the Topical Delivery of a Natural Leukotriene Inhibitor (3-Acetyl-11-Keto-β-Boswellic Acid): Statistical Optimization, in vitro Characterization, and ex vivo Permeation Study. Drug Des Devel Ther 2020;14:3697–721. https://doi.org/10.2147/DDDT.S265167.

Badria FA, Fayed HA, Ibraheem AK, State AF, Mazyed EA. Formulation of sodium valproate nanospanlastics as a promising approach for drug repurposing in the treatment of androgenic alopecia. Pharmaceutics 2020;12:1–27. https://doi.org/10.3390/pharmaceutics12090866.

Durak S, Rad ME, Yetisgin AA, Sutova HE, ... Niosomal drug delivery systems for ocular disease—recent advances and future prospects. Nanomaterials 2020.

Elgewelly MA, Elmasry SM, Sayed NS El, Abbas H. Resveratrol-Loaded Vesicular Elastic Nanocarriers Gel in Imiquimod-Induced Psoriasis Treatment: In Vitro and In Vivo Evaluation. J Pharm Sci 2022;111:417–31. https://doi.org/https://doi.org/10.1016/j.xphs.2021.08.023.

Elhabak M, Ibrahim S, Abouelatta SM. Topical delivery of l-ascorbic acid spanlastics for stability enhancement and treatment of UVB induced damaged skin. Drug Deliv 2021;28:445–53. https://doi.org/10.1080/10717544.2021.1886377

Elmowafy E, El-Gogary RI, Ragai MH, Nasr M. Novel antipsoriatic fluidized spanlastic nanovesicles: In vitro physicochemical characterization, ex vivo cutaneous retention and exploratory clinical

therapeutic efficacy. Int J Pharm 2019;568:118556. https://doi.org/10.1016/j.ijpharm.2019.118556.

Fahmy AM, El-Setouhy DA, Habib BA, Tayel SA. Enhancement of transdermal delivery of haloperidol via spanlastic dispersions: entrapment efficiency vs. particle size. AAPS Pharmscitech 2019. https://doi.org/10.1208/s12249-019-1306-2.

Fahmy AM, El-Setouhy DA, Ibrahim AB, Habib BA, Tayel SA, Bayoumi NA. Penetration enhancer-containing spanlastics (PECSs) for transdermal delivery of haloperidol: In vitro characterization, ex vivo permeation and in vivo biodistribution studies. Drug Deliv 2018;25:12–22. https://doi.org/10.1080/10717544.2017.1410262

Farghaly DA, Aboelwafa AA, Hamza MY, ... Topical delivery of fenoprofen calcium via elastic nano-vesicular spanlastics: Optimization using experimental design and in vivo evaluation. AAPS PharmSciTech 2017. https://doi.org/10.1208/s12249-017-0771-8.

Goyal G, Garg T, Malik B, Chauhan G, Rath G, Goyal AK. Development and characterization of niosomal gel for topical delivery of benzoyl peroxide. Drug Deliv 2015;22:1027–42. https://doi.org/10.3109/10717544.2013.855277.

Guimarães D, Noro J, Loureiro A, Lager F, Renault G, Cavaco-Paulo A, et al. Increased encapsulation efficiency of methotrexate in liposomes for rheumatoid arthritis therapy. Biomedicines 2020;8:1–15. https://doi.org/10.3390/biomedicines8120630.

Hu J, Zhou D, Chen Y. Preparation and antioxidant activity of green tea extract enriched. J Agric Food Chem 2009;57:1349–53.

Kakkar S, Kaur IP. Spanlastics-A novel nanovesicular carrier system for ocular delivery. Int J Pharm 2011a;413:202–10. https://doi.org/10.1016/j.ijpharm.2011.04.027.

Khoee S, Yaghoobian M. Niosomes: a novel approach in modern drug delivery systems. Elsevier Inc.; 2017. https://doi.org/10.1016/b978-0-323-46143-6.00006-3.

Martini FH, Nath JL, Bartholomew EF. Fundamentals of Anatomy & Physiology. 11th ed. Pearson; 2018.

Mazyed EA, Helal DA, Elkhoudary MM, ... Formulation and Optimization of nanospanlastics for improving the bioavailability of green tea epigallocatechin gallate. Pharmaceuticals 2021.

Rathod S, Arya S, Shukla R, Ray D, Aswal VK, Bahadur P, et al. Investigations on the role of edge activator upon structural transitions in Span vesicles. Colloids Surfaces A Physicochem Eng Asp 2021;627:127246. https://doi.org/10.1016/j.colsurfa.2021.127246.

Sallam NM, Sanad RAB, Ahmed MM, Khafagy ES, Ghorab M, Gad S. Impact of the mucoadhesive lyophilized wafer loaded with novel carvedilol

nano-spanlastics on biochemical markers in the heart of spontaneously hypertensive rat models. Drug Deliv Transl Res 2021;11:1009–36. https://doi.org/10.1007/s13346-020-00814-4.

Shaaban M, Nasr M, Tawfik AA, Fadel M, ... Novel bergamot oil nanospanlastics combined with PUVB therapy as a clinically translatable approach for vitiligo treatment. Drug Deliv … 2019. https://doi.org/10.1007/s13346-019-00653-y.

Shamma RN, Sayed S, Sabry NA, El-Samanoudy SI. Enhanced skin targeting of retinoic acid spanlastics: in vitro characterization and clinical evaluation in acne patients. J Liposome Res 2019a;29:283–90. https://doi.org/10.1080/08982104.2018.1552706

Zhao C, Tang G, Cao S, Xu X, Gan R, Liu Q. Phenolic Profiles and Antioxidant Activities of 30 Tea Infusions from Green , Black , Oolong , White , Yellow and Dark Teas. Antioxidants 2019:215

Study of Growth Curve of *Lactobacillus plantarum* FNCC 0026 and Its Antibacterial Activity

Safarini Marwah[1], Achmad Toto Poernomo[2], Esti Hendradi[2]*
[1]Master Program of Pharmaceutical Sciences, Faculty of Pharmacy, Universitas Airlangga, Surabaya, Indonesia
[2]Department of Pharmaceutical Sciences, Faculty of Pharmacy, Universitas Airlangga, Surabaya, Indonesia

*Corresponding author: esti-h@ff.unair.ac.id

Abstract

Background: *Lactobacillus plantarum is one of the lactic acid bacteria (LAB) with strong antibacterial activity. However, these bacteria show different growth for each strain. The turbidimetric bacterial growth curve approach is the most accurate, fastest, and most reproducible method for obtaining an overview of the bacterial life cycle. In addition, we also examined the antibacterial activity of each observation of the growth curve.* **Objective**: *The aim of the study was to determine the optimal incubation time with the highest biomass concentration and antibacterial activity of the Lactobacillus plantarum FNCC 0026.* **Method:** *Observations of optical density (OD) values were performed simultaneously on 10 points of Lactobacillus plantarum FNCC 0026 and performed every 12 hours. Antibacterial activity tested against Staphylococcus aureus ATCC 25923 and Escherichia coli ATCC 8739.* **Result:** *The Lactobacillus plantarum FNCC 0026 fermentation broth showed the highest OD value and antibacterial activity after 30 hours of incubation. The maximum diameter of the inhibition zone against Staphylococcus aureus ATCC 25923 and Escherichia coli 25923 were 17.08 ± 0.51 mm and 16.83 ± 0.54 mm.* **Conclusion**: *The results showed that the antibacterial activity had a linear relationship with the concentration of bacteria. In the Lactobacillus plantarum FNCC 0026, the optimum cultivation time is in the lag phase (24 – 30 hours).*

Keywords: *growth curve, Lactobacillus plantarum FNCC 0026, antibacterial activity*

INTRODUCTION

In the recent years, food is not only intended to overcome hunger and fulfill the body`s nutrition, but also to prevent chronic diseases and improve the quality of life. These terms are called functional foods and Nutraceuticals. Functional foods, according to the International Food Information Council (IFIC), can be defined as "foods that provide health benefits beyond basic nutrition". Nutraceuticals, on the other hand, are more accurately described as foods (or parts of foods) that provide medicinal or health benefits, including prevention and/or treatment of disease (Wang & Li, 2015). One of the functional foods with health benefits is probiotics.

Probiotics are live microorganisms that, when present in sufficient quantity, provide a benefit to the host. Most probiotics belong to the lactic acid bacteria (LAB) group (Daba & Elkhateeb, 2020). The LAB consists of a diverse group of Gram-positive, catalase-negative bacteria that produce lactic acid as their main product (Seddik et al., 2017). One of the LABs that has started to be widely applied in commercial products is *Lactobacillus plantarum*, which has great abilities in the fermentation process of various products (Seddik *et al.,* 2017).

Lactobacillus plantarum is considered a versatile bacterium because of their activities, including antioxidant, anticancer, anti-inflammatory, anti-proliferative, anti-obesity, anti-diabetic, antibacterial, and high environmental adaptability. The *Lactobacillus plantarum* is used as an antibacterial agent against *Bacillus cereus, Escherichia coli*, *Proteus vulgaris, Enterococcus fecalis* (Shim et al., 2016), *Staphylococcus aureus* (Layus et al., 2020). Furthermore, these bacteria inhibit the growth of antibiotic-resistant bacteria such as MRSA (Kumar et al.*,* 2017), ESBL *E.coli*, and Pseudomonas aeroginosa (Layus et al.*,* 2020).

In addition, *Lactobacillus plantarum* has an anti-adherent effect on bacteria, reducing the ability of pathogenic bacteria to adhere to host surfaces and preventing biofilm formation, which is important for the persistence and resilience of bacterial infections. It is also believed that the antibacterial activity of *Lactobacillus plantarum* is caused by the presence of organic acids and hydrogen peroxide and bacteriocins called plantaricin (Kumar, et al. 2017). Since the bactericidal activity of this peptide depends on the binding mechanism of the pathogenic mannose phosphotransferase permease (Man-PTS) to its MptC and MptD subunits. When these bacteriocins insert into the target cell membrane, they irreversibly open endogenous channels, allowing toxic ions to diffuse across the membrane and kill the target cell (Hernández-González et al., 2021).

The antibacterial activity of probiotics is greatly influenced by their viability. In general, probiotics show optimal activity when the viable cell count is at a concentration of approximately 106-109 colony-forming units (CFU)/mL, therefore the incubation time of the bacteria should be considered to reach the highest concentration (Slizewska & Chlebicx - Wojcik, 2020). The OD value of microorganisms is generally observed at a wavelength of 580 nm. However, the microbial growth of probiotics is strain-dependent, each bacterium has a different cell growth rate (Rezvani et al., 2017). Several approaches can be used to determine the rate of cell growth. Statistical approaches using bacterial growth parameters are highly accurate. The plating method is widely used, but this method cannot provide actual results and is time-consuming because it takes incubation time to determine the number of living cells. Other methods, such as turbidity measurements by OD measurements, by which real-time knowledge of bacterial populations, were used in this study (Rahman et al., 2017).

Therefore, the main objective of this study was to study the growth rate of *Lactobacillus plantarum* FNCC 0026 fermentation broth using OD measurements at different wavelengths and its antibacterial activity of *Lactobacillus plantarum* FNCC 0026 fermentation broth so that the optimum incubation time with the highest biomass can be determined.

MATERIAL AND METHODS
Materials

Materials used for this research are *Lactobacillus plantarum* FNCC 0026 culture from Pusat Studi Pangan dan Gizi Universitas Gajah Mada Yogyakarta; De Man, Rogosa, Sharp (MRS) broth medium (MERCK Millipore, USA), Nutrient agar medium (MERCK Millipore, USA); *Staphylococcus aureus* ATCC 25923 and *Escherichia coli* ATCC 8739 were provided by RSUD Dr. Soetomo.

Methods
Microbial preparation

One öse of *Lactobacillus plantarum* was mixed aseptically with 10.0 mL of MRS broth. Then the bacterial suspension in MRS broth was shaken using a rotary shaker at 150 rpm and 37°C during the test time.

Growth curve study of *Lactobacillus plantarum* FNCC 0026

The OD of 1.5 ml bacterial suspension was measured using a UV-Vis spectrophotometer at the same time every day after incubation. Suspension of *Lactobacillus plantarum* was measured at five different wavelengths (540, 570, 600, 630, and 660 nm). Observations were recorded simultaneously every 12 hours for 5 days after inoculation (Rahman et al., 2017).

Optimization of bacterial inhibitory test media

Optimization of test media was performed by combining two media, MRS broth and nutrient agar (NA), under three conditions. The combination concentrations used in MRS-NA medium were 75%:25% (w/v); 50%:50% (w/v); and 25%; 75% (w/v) respectively. Each combination was tested for probiotic inhibition against two test bacteria. The selected media combination is based on the growth of test organisms on the media and the presence of clear zones around the wells.

Antibacterial activity of *Lactobacillus plantarum* FNCC 0026

The bioassay was performed by the well agar diffusion method using selected modification (M) media. Test media were prepared by the pour method. 10-12 mL of melted M media (45-50 °C) was poured into an empty sterile Petri disc, allowing to solidify and used as a base layer media. The seed layer was prepared by adding 3-5 µL of 25% T bacterial inoculum into 8 mL of melted M media, vortex well, pouring over the surface and allowing it to solidify. The wells were made with a 7mm diameter drill bit. The reservoir of each well was filled with 50 µl of test solution. Incubation was at 37°C for 24 hours. The diameter of the growth inhibition zone was measured with a digital caliper (Isnaeni et al., 2017).

Statistical analysis

All results were subjected to analysis of variance (ANOVA) using a completely randomized design with three replications for all treatments. The differences between means were tested at a significance value of $p < 0.05$.

RESULT AND DISCUSSION
Growth curve study of *Lactobacillus plantarum* FNCC 0026

The growth phase of microorganisms consists of four phases: lag phase, exponential growth phase, stationary phase, and decline phase. The OD value approach can be directly correlated with cell concentration. The OD measurements calculate the amount of light lost due to scattering and absorption at a single wavelength (McBirney et al., 2016). The OD value of *Lactobacillus plantarum* FNCC 0026 cell suspension increased hourly until reaching the highest value at 30 hours incubation. The growth curve slopes or showed a steady value until 78 hours, called the stationary phase (Fig. 1). This was consistent with a previous study in which *Lactobacillus plantarum* reached maximum OD values by day 2 (36 hours) (Rahman et al., 2017). Therefore, it could be said that incubating *Lactobacillus plantarum* takes 30 hours to achieve optimal growth.

Wavelength selection is an important consideration for reading OD values. The maximum wavelength is unique to each bacterium due to differences in size and cell characteristic of each bacterium. In this study, there was no significant difference of OD values at different wavelengths during the early stages of growth. At a wavelength of 600 nm, the decline phase occurs after 78 hours, which is different from the other wavelengths. A wavelength of 600 nm is commonly used for bacterial analysis. Previous studies have shown that using a wavelength of 600 nm yields accurate and reproducible results (McBirney et al., 2016).
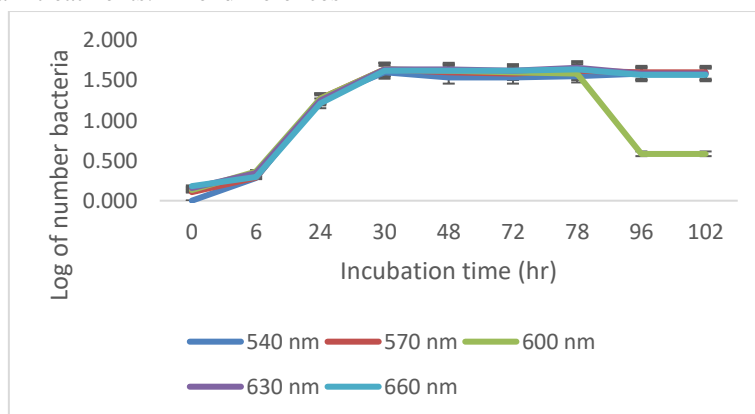

Figure 1. OD reading for *Lactobacillus plantarum* FNCC 0026 at different wavelengths from days 1 to 5. The highest OD value was on 30 hours.
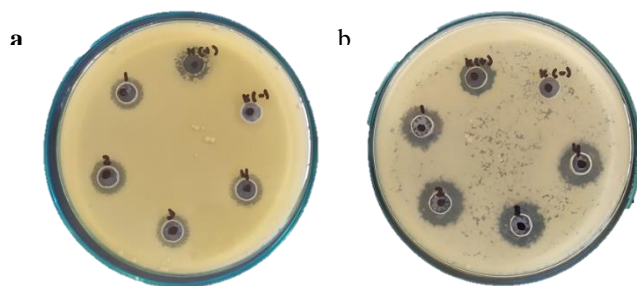
Figure 2. Antibacterial activity of Lactobacillus plantarum FNCC 0026 against a) *Staphylococcus aureus* ATCC 25923 and b) *Escherichia coli* ATCC 8739 was replicated four times. The positive control for SA bacteria ATCC 25293 was vancomycin, and for EC ATCC 8739 was ceftriaxone. The negative control used was MRS broth.

Table 1. Bacterial inhibitory test of each combination against *Staphylococcus aureus* ATCC 25923 and *Escherichia coli* ATCC 8739

Bacterial test : *Escherichia coli* ATCC 8739

Lactobacillus plantarum replication	Combination 1 (MRS-NA = 25%:75%)		Combination 2 (MRS-NA = 50%:50%)		Combination 3 (MRS-NA = 75%:25%)	
	Growth	Clear zone	Growth	Clear zone	Growth	Clear zone
Replication 1	+	-	+	+	+	+
Replication 2	+	-	+	+	+	+
Replication 3	+	-	+	-	-	-

Bacterial test : *Staphylococcus aureus* ATCC 25923

Lactobacillus plantarum replication	Combination 1 (MRS-NA = 25%:75%)		Combination 2 (MRS-NA = 50%:50%)		Combination 3 (MRS-NA = 75%:25%)	
	Growth	Clear zone	Growth	Clear zone	Growth	Clear zone
Replication 1	+	+	+	+	-	-
Replication 2	+	+	+	+	-	-
Replication 3	+	+	-	-	-	-

Note :

+ : formed

- : not formed

Optimization of bacterial inhibitory test media

Lactobacillus plantarum is a lactic acid bacterium with rich and complex nutritional requirements, so it requires a concentrated growth medium such as MRS medium for optimal growth (De Vos et al., 2009). The decrease in the pH of the medium to 5.7 and the addition of 0.14% sorbic acid to the MRS medium made this medium a suitable medium for probiotics. However, testing antimicrobial activity in a single concentrated medium can yield skewed results because pathogenic bacteria such as SA and E.coli cannot grow on MRS media. Therefore, a media combination between MRS and NA, which is a universal medium, is necessary to meet the needs of probiotics and test bacteria. The concentration in this combination of media differs for each strain according to the nutritional needs of the probiotics and test bacteria. Mixed media were selected based on their ability to grow the test bacteria and form a clear zone around the well. A clear zone indicates that Lactobacillus plantarum can live well so that it can provide inhibitory activity. The choice of combination medium for *Staphylococcus aureus* ATCC 25923 was combination 1 (MRS-NA = 25%:75%) which allowed test organisms to grow and a clear zone was seen around the wells. On the other hand, the selected combination medium for *Escherichia coli* ATCC 8739 was Combination 2 (MRS-NA = 50%:50%) had the most appropriate skills. *E. coli* grew well in combination medium 1 (MRS-NA = 25%:75%), but at this concentration, *Lactobacillus plantarum* could not provide any hindrance. In contrast, combination 3 (MRS-NA = 75%:25%) did not give the desired result for both SA and *E.coli* bacteria (Table 1). The pH of the medium affects the ability of the bacteria to live. MRS media concentrations that are high tend to be acidic, so they are not suitable for SA. while *E.coli* has metabolic flexibility that allows these bacteria to compete for

carbon and energy sources even though it is in unfavorable conditions (Alteri & Mobley, 2012).

Antibacterial Activity of *Lactobacillus plantarum* FNCC 0026

Antibacterial activity was tested against two pathogenic strains using an adequate diffusion assay (Fig. 2a,b). The difficulty of determining bacterial viability is one of the weaknesses of turbidity measurements. Therefore, activity tests should also be performed to confirm antimicrobial efficacy. Each OD measurement was tested to determine the highest antibacterial activity of *Lactobacillus plantarum* FNCC 0026. See Table 2 and Figure 3. Bacterial suspensions harvested after 30 h had the lowest OD values and the largest clear zones. A small OD value indicates the concentration of the bacterial suspension, it is expected that a high number of bacteria in the suspension. And the clear zone shows the inhibitory capacity of the bacterial suspension. The maximum inhibitory diameters for antibacterial activity against *S. aureus*

ATCC 25923 and *E. coli* ATCC 8739 were 17.08 ± 0.51 mm and 16.83 ± 0.54 mm, respectively.

Probiotic growth curves showed that *Lactobacillus plantarum* peaked at 30 hours of the lag phase and tended to decline in exponential antibacterial activity. The results of this study show that *Lactobacillus plantarum* FNCC 0026 can inhibit the growth of both Gram-positive and Gram-negative bacteria. The zone of inhibition diameter for commonly used antibiotics such as vancomycin in SA therapy is 11.97 ± 0.81 mm and ceftriaxone in E. coli therapy is 11.49 ± 0.98 mm. Probiotics have a larger zone of inhibition than antibiotics, indicating that *Lactobacillus plantarum* may replace antibiotics as the treatment of choice. As a functional food, this probiotic can exert advantages as a broad-spectrum antibiotic and acceptable taste than synthetic antibiotics. Therefore, probiotic production could be widely developed as a promising nutritional supplement.
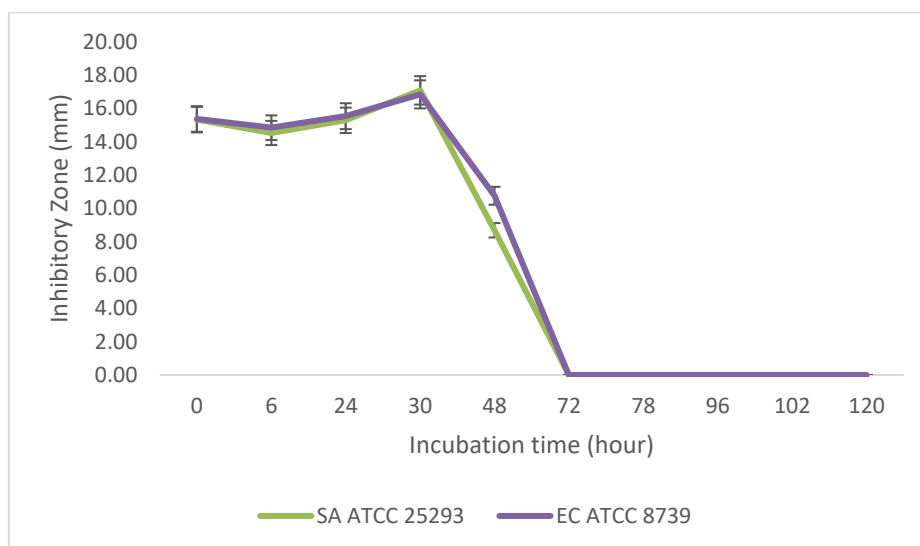

Figure 3. Inhibitory activity curve of Lactobacillus plantarum FNCC 0026 against two pathogenic bacteria (grey line: SA ATCC 25293 and yellow line: EC ATCC 8739) during the continuous incubation time. Each test was carried out three times for replication. And the highest inhibition zone was at 30 hours.

Table 2. Inhibitory activities of *Lactobacillus plantarum* FNCC 0026 against two pathogenic bacteria (mm)

Bacteria	0 h	6 h	24 h	30 h	48 h	72 h	78 h	96 h	102 h	120 h
Staphylococcus aureus ATCC 25923	15.32± 0.66	14.52 ± 0.75	15.28 ± 0.46	17.08 ± 0.51	8.68 ± 0.00	0.00	0.00	0.00	0.00	0.00
Escherichia coli ATCC 8739	15.36 ± 0.22	14.83 ± 1.41	15.52 ± 0.25	16.83 ± 0.54	10.75 ± 0.00	0.00	0.00	0.00	0.00	0.00

CONCLUSION

Lactobacillus plantarum is a lactic acid bacterium with a broad spectrum of activity and good antibacterial activity. The best performance of these bacteria is in lag phase (30 hours), after which decline phase was obtained significantly. Therefore, the incubation time for these bacteria should be considered to obtain optimal activity.

REFERENCES

Alteri, C.J., & Mobley, H.L.T. (2012). Escherichia coli physiology and metabolism dictates adaption to disverse host microenviroments. *Current Opinion Micribiology*, *15* (1), 3-9.

Daba, G. M., & Elkhateeb, W. A. (2020). Bacteriocins of lactic acid bacteria as biotechnological tools in food and pharmaceuticals: Current applications and future prospects. *Biocatalysis and Agricultural Biotechnology* , *28* (August), 101750.

De Vos, P., Garrity, G. M., Jones, D., Krieg, N. R., Ludwig, W., Rainey, F. A., *et al*., 2009. *Bergey's Manual Of Systematic Bacteriology 2nd Ed.* Athens: Springer.

Hernández-González, J. C., Martínez-Tapia, A., Lazcano-Hernández, G., García-Pérez, B. E., & Castrejón-Jiménez, N. S. (2021). Bacteriocins from lactic acid bacteria. A powerful alternative as antimicrobials, probiotics, and immunomodulators in veterinary medicine. *Animals* , *11* (4), 1-17.

Isnaeni, Andri A, and Muhammad.Y. (2017). Validation of thin- layer-chromatography-bioatutographic method for determination of streptomycin. *Jurnal Farmasi dan Ilmu Kefarmasian IndonesiaI.*, *4* (1): 32-38.

Kumar, L. M., Saad, W. Z., Mohamad, R., & Rahim, R. A. (2017). Influence of biofilm-forming lactic acid bacteria against methicillin-resistant *Staphylococcus aureus* (MRSA S547). *Asian Pacific Journal of Tropical Biomedicine* , *7* (12), 1107-1115.

Layus, B. I., Gerez, C. L., & Rodriguez, A. V. (2020). Antibacterial Activity of Lactobacillus plantarum CRL 759 Against Methicillin-Resistant *Staphylococcus* aureus and Pseudomonas aeruginosa. *Arabian Journal for Science and Engineering* , *45* (6), 4503-4510.

McBirney, S.E., Trinh, K., Wong-Beringer, A., Armani, A.M. (2016). Wavelength-normalized spestroscopic analysis of *Staphylococcus aureus* and *Pseudomonas aeruginosa* growth rates. *Biomedical Optics Express,7* (10), 4034-4042.

Rahman, N.A., Halim, M.R.A., Mahawi, N., Hasnudin, H., Al-Obaidi, J.R., Abdullah, N. (2017). Determination of the use of *Lactobacillus plantarum* and *Propionibacterium freudenreichii* application on fermentation profile and chemical composition of corn silage. *BioMes Research International,* ID 2038061, 1-8.

Rezvani, F., Ardestani, F., Najafpour, G. (2017). Growth kinetic models of five species of Lactobacilli and lactose consumption in batch submerged culture. *Brazilian Journal of Microbiology, 48*, 251 – 258.

Shim, Y. H., Lee, S. J., & Lee, J. W. (2016). Antimicrobial activity of lactobacillus strains against uropathogens. *Pediatrics International* , *58* (10), 1009-1013.

Seddik, H.A., Bendali, F., Ganeel, F., Fliss, I., Spano, G., Drider, D. (2017). *Lactobacillus plantarum* and its probiotic and food potentialities. *Probiotics & Antimicro. Prot., 9,* 111-122.

Slizewzka, K., Chlebicz-Wojcik, A. (2020). Growth kinetic of probiotic *Lactobacillus* strain in alternative, cost-efficient semi-solid fermentation medium. *Biology, 9* (432), 1-13.

Wang, C., & Li, S. (2015). Functional foods and nutraceuticals, Potential role in human health. In D. Ghosh, D. Bagchi, & T. Konishi, *Clinical aspects of functional foods and nutraceuticals* (pp. 51-76). NW: CRC Press, Taylor & Francis Group.

Effect of Different Lipid Ratios on Physicochemical Stability and Drug Release of Nanostructured Lipid Carriers Loaded Coenzyme Q10

Abdulloh Suyuti[1], Esti Hendradi[2,3]*, Tutiek Purwanti[2,3]

[1]Master Program in Pharmaceutical Science, Faculty of Pharmacy, Universitas Airlangga, Surabaya, Indonesia
[2]Department of Pharmaceutical Science, Faculty of Pharmacy, Universitas Airlangga, Surabaya, Indonesia
[3]Nanotechnology and Drug Delivery System Research Group, Faculty of Pharmacy, Universitas Airlangga, Surabaya, Indonesia

*Corresponding author: esti-h@ff.unair.ac.id

Abstract

Background*: For treatment or skin care via topical route, Coenzyme Q10 needs to permeate the epidermis which it is practically insoluble in water and a high molecular weight that make it difficult to penetrate the skin. Nanostructured Lipid Carriers (NLC) is chosen because of its ability to dissolve and solve the problem of low skin permeation. The type and ratio of solid and liquid lipids used in NLC affect the physicochemical characteristics, thus affecting the release profile and system stability.* ***Objective****: This study aimed to determine the effect of various ratios of Compritol 888 ATO as solid lipid and Miglyol 812 as liquid lipid on the physicochemical stability and Coenzyme Q10 release profile of NLC system.* ***Methods****: NLC was prepared using High Shear Homogenization method with three different lipid ratios. The ratio of Compritol 888 ATO : Miglyol 812 was 70:30, 80:20, and 90:10, respectively. NLC was evaluated for drug release and stability parameters including organoleptic, particle size, polydispersity index (PI), pH, viscosity, assay, and entrapment efficiency.* ***Results****: The stability test result for 90 days showed increments in the particle size and viscosity, whereas for assay and entrapment efficiency were decreased. The release test results showed no significant difference in the release parameters of the three tested formulas.* ***Conclusion****: During stability evaluation, NLC-CoQ10 systems did not significantly change pH and PI values, but statistically significantly changed particle size, viscosity, assay, and entrapment efficiency. The different in lipid ratios used in the formulas did not show significantly different results for release parameters.*

Keywords: coenzyme Q10, NLC, stability, release

INTRODUCTION

Endogenous antioxidant molecules are less likely to produce as a person gets older, which reduces their ability to protect the skin. Additionally, prolonged and excessive exposure to UV light might reduce antioxidant levels in the skin layer (Andarina & Djauhari, 2017). Exogenous antioxidant supplementation can be a substitute for restoring antioxidant deficiency while protecting the skin from damage and early aging caused by excessive UV exposure.

Various types of antioxidant compounds have been commonly applied topically to the skin, such as carotenoids, coenzyme Q10, essential oils, polyphenols, and vitamins. Topical administration of drugs offers many advantages over oral administration, including avoiding first-pass metabolism, targeting active ingredients for local effects, and improving patient compliance. Especially in the case of treatment or treatment for the skin, topical drug administration is very effective because it is directly applied to the targeted area thus allowing higher drug accumulation in the target area with minimal side effects compared to oral administration (Ryu *et al.,* 2020).

One of the antioxidants that are often associated with the aging process and aging-related diseases of the skin is coenzyme Q10 (Hernández-Camacho *et al.,* 2018). As people get older, their bodies produce less CoQ10, which lowers the quantities in their tissues and plasma. Because the skin is frequently exposed to environmental stressors including UV radiation and air pollution, CoQ10 levels in the skin declining. Many studies have shown that CoQ10 supplementation can increase the antioxidant properties of the skin, reduce reactive oxygen species, prevent premature aging, and is suitable for skin photoprotection (Sguizzato *et al.,* 2020). However, for administration through the skin, CoQ10 needs to overcome the skin's stratum corneum barrier and penetrate through the epidermis. Its practically insoluble in water and relatively high molecular weight (863.3 g/mol), make CoQ10 difficult to penetrate the skin despite its beneficial effect (Ryu *et al.,* 2020). In addition, CoQ10 is easily degraded when exposed to light *(Guedes et al.,* 2021). Therefore, a special delivery system is needed that can dissolve and overcome the problem of low skin permeation while providing stability to light. Developing a Nanostructured Lipid Carrier (NLC) is one alternative.

The lipid components of the carrier system are non-irritating and non-toxic, making NLC suitable for drug delivery applications through the skin. Lipid-based carrier systems are capable of providing drug protection from degradation after loading into the system, enabling controlled release, as well as enhanced skin penetration and retention *(Nene et al.,* 2021). The selection of the type and ratio of solid lipids and liquid lipids used in NLC affects the physicochemical characteristics, thus affecting the release profile and stability of the preparation.

This study aimed to determine the effect of various ratios of solid lipid Compritol 888 ATO and Miglyol 812 liquid lipids on the physicochemical stability and drug release profile of the NLC system. The ratio of solid lipid and liquid lipid is 70:30, 80:20, and 90:10 to a total lipid of 10% of the formula. Compritol 888 ATO was chosen because it is superior in terms of drug-trapping ability compared to homogeneous glycerides (Aburahma & Badr-Eldin, 2014). Research conducted by Nayak *et al.* (2017) prepared an NLC containing the active ingredient CoQ10 and retinaldehyde to treat wrinkles which were applied topically, showing that Compritol 888 ATO can dissolve CoQ10 better than some other lipid candidates. As for the liquid lipid component, Miglyol 812 was chosen because of its ability to increase the solubility of hydrophobic materials in the NLC system, thereby increasing drug loading capacity and preventing drug expulsion during storage (Ortiz *et al.,* 2021). The formulation of the NLC system containing CoQ10 in this study was intended for topical application as an anti-aging. The preparation was made at pH 6.0 ± 0.05 according to the skin pH specification range and the stability of the active ingredients. The method used for the manufacture of NLC is the high shear homogenization method because the process is simple, fast, and relatively low cost.

MATERIALS AND METHODS
Materials

Coenzyme Q10 (Kangcare Bioindustry - China), Compritol 888 ATO (Gattefosse - France), Miglyol 812 (Sigma Aldrich - USA), Poloxamer 188 (BASF - Germany), and propylene glycol (Dow Chemical Pacific - Singapore). All of these substances were pharmaceutical grade unless otherwise noted.

Tools

High shear homogenizer (T25 Ultra-Turrax IKA®), particle size analyzer (Delsa™ Nano), pH meter (Transinstrument WalkLAB HP9010), viscometer cone and plate (Brookfield), USP dissolution test apparatus 5 (Erweka DT820), double beam spectrophotometer UV-vis (Shimadzu UH5300).

Method

Preparation method of NLC

NLC loaded Coenzyme Q10 (NLC-CoQ10) was prepared using the High Shear Homogenization (HSH) method. The composition of the NLC-CoQ10 with various ratios of solid lipid and liquid lipid can be seen in Table 1. Using a hot plate set to 80°C, Compritol 888 ATO and Miglyol 812 were placed in a beaker glass and melted. Then put some CoQ10 into the mixture. Separately prepared surfactant solution (Poloxamer 188) in phosphate buffer solution and heated using a hot plate at 80°C. The water phase is added gradually into the oil phase. A high-speed homogenizer was then used to stir this mixture for 2 minutes at 3400 rpm. Then slowly added the mixture of propylene glycol and phosphate buffer solution which has been heated at 80°C using a hot plate. The mixture was homogenized by high shear homogenizer at 20,000 rpm for 5 minutes in three cycles with constant heating at 80°C after all the ingredients had been added. The result was cooled while stirring at 500 rpm until room temperature and the best NLC system was obtained.

Stability test

A stability test is used to predict system stability during the storage period. A stability test was performed using real-time conditions at room temperature (25 ± 2°C). The organoleptic, particle size, PDI, pH, and viscosity were evaluated on 1, 15, 30, 60, and 90 days. In addition, evaluation of assay and entrapment efficiency were also carried out at the beginning and end of storage.

Organoleptic

Organoleptic tests were carried out by visually determining the form, color, and odor of each formula.

Particle size and polydispersity index (PI) evaluation.

Measurement of particle size and PI were carried out using a Delsa™ nanoparticle size analyzer.

Approximately 50 mg of the sample was added with 50 mL of distilled water. It stirred using a magnetic stirrer for 10 minutes at a speed of 500 rpm. Then put 2 mL of solution and added distilled water up to 10 mL. The sample was placed in the glass cuvette and perform a measurement.

pH evaluation

In 20 mL of distilled water, approximately 1 g of NLC system was dissolved, then immersed the electrode into the sample. A digital pH meter was used to measure the pH value of the NLC preparations, which were already calibrated using a standard buffer solution.

Viscosity test

A cone and plate viscometer was used to determine the viscosity of the samples. About 2 mL samples were poured into the plate. Between the stationary plate and the rotating cone, the sample was in a shear.

Assay

About 100 mg of NLC systems was added by 10.0 ml of ethanol and sonicated for 20 minutes. The solution was transferred to a venoject tube and centrifuged at 2500 rpm for 15 minutes. The supernatant was taken at 1.0 ml and added with ethanol up to 10.0 ml. The assay was measured at 274 nm by spectrophotometry.

Entrapment efficiency test

The centrifugation technique was used to measure drug entrapment efficiency. The amount of free drug was measured to estimated amount of drug trapped, then the entrapment efficiency was calculated using the ratio of the amount of drug trapped to the total amount of drug added. About 2 g of NLC systems were centrifuged for 60 minutes at 3000 rpm. After phase separation, the supernatant was collected and 10.0 ml of ethanol was added. About 1 ml solution was taken and added with ethanol again up to 10.0 ml. The amount of drug was measured at 274 nm by spectrophotometry.

Table 1. The composition of NLC formulas (% w/w)

Composition	Function	Formula 1 (F1)	Formula 2 (F2)	Formula 3 (F3)
Coenzyme Q10	Active ingredient	2.4	2.4	2.4
Compritol 888 ATO	Solid lipid	7	8	9
Miglyol 812	Liquid lipid	3	2	1
Poloxamer 188	Surfactant	8	8	8
Propylene glycol	Co-surfactant	8	8	8
Phosphate buffer pH 6.0	Water phase	Until 100	Until 100	Until 100

Note :
Formula F1 = concentration ratio of solid lipid and liquid lipid 70:30
Formula F2 = concentration ratio of solid lipid and liquid lipid 80:20
Formula F3 = concentration ratio of solid lipid and liquid lipid 90:10

Drug Release test

The drug release test apparatus used was USP dissolution test apparatus 5 (paddle over disk). The apparatus consists of a paddle and vessel as used in dissolution tests, with the addition of a stainless steel disk designed as a transdermal dosage container at the bottom of the vessel. The disk form is a flat cylinder with the center space as a container which is closed with the membrane facing upwards. Due to insolubility of Q10 in water or a buffer solution, the dissolution medium was prepared with a mixture of 2.5% Tween 80 and 20% ethanol p.a in phosphate buffer pH 6.0 ± 0.05. The media was placed into a chamber and set to a temperature of 32 ± 0.5°C. About 2,5 g samples were inserted into the disk. The membrane used (cellulose acetate) closed in such a way that there were no air bubbles between the membrane and the sample surface. The prepared disk was placed at the bottom of the chamber. The bottom edge of the paddle should be 25 ± 2 mm from the disk. At each time interval, samples were taken from the middle zone between the surface of the media and the top of the paddle, not less than 1 cm from the vessel wall (United States Pharmacopoeia, 2007).

During operation, the paddle stirrer was rotated at 100 rpm and the media volume was 500 mL. About 5 mL of sample solution was taken and replaced with 5 mL of receptor medium using an injection syringe at 0, 5, 10, 15, 20, 25, 30, 45, 60, 90, 120, 150, 180, 210, 240, 270, 300, 330, and 360 minutes. Then the sample was analyzed with UV-Vis spectrophotometer at 274 nm. The drug concentration in the sample was calculated using the standard curve regression equation. To account for the 5 mL dilution of the release medium, the measured concentrations were corrected by following equation:

$$C_{n,corr} = C_n + \frac{Vs}{Vm} \int_{i=1}^{n-1} C_i$$

where $C_{n,corr}$ is the corrected concentration at sample interval n; Cn is the measured or uncorrected concentration at sample interval n; Vm is the original media volume in the dissolution vessel; Vs is the volume of sample removed at each time interval; and Ci is the uncorrected concentration at each previous sample interval i (Salt, 2021).

Statistical analysis

To statistically analyze the drug release parameter and initial data of physicochemical characteristics, if the data were homogenously and normally distributed, a one-way Analysis of Variance (ANOVA) technique

was utilized. But if the data were not homogenous or not normally distributed, statistics test was conducted with a non-parametric statistical test (Kruskal-Wallis). On the other hand, to statistically analyze the stability of each formula during storage, a repeated measure ANOVA or paired t-test technique was utilized. The stability test was not carried out by comparing between the different formulas, but a comparison between different time of measurement in each formula to find out whether there is a difference in the initial characteristics and after storage. The formula is declared stable if there is no significant difference from the measurement results after being stored. Thus repeated measure ANOVA is used if there are 5 observation days (days 1, 15, 30, 60, 90) and paired t-test if only measured on 2 observation days (days 1 and 90).

RESULTS AND DISCUSSION
Stability test result
Organoleptic

The organoleptic observation showed that the CoQ10- NLC was yellow, specific odor, and had a semisolid form and soft texture, as shown in Table 2. There was no change during storage except in Formula 3 on day 90 there was a separating layer at the bottom which indicated the presence of instability. This phase separation is probably due to the surfactant being less able to maintain the system in Formula 3 during the storage period.
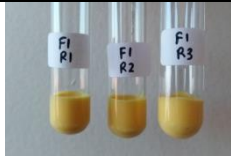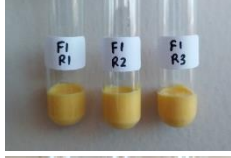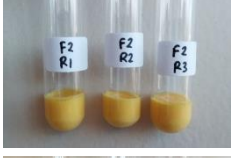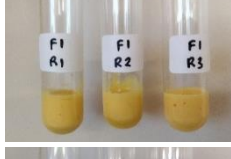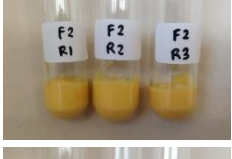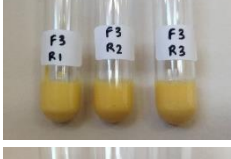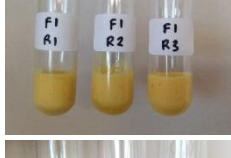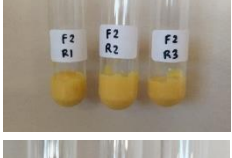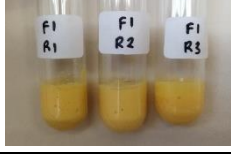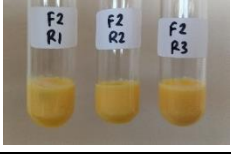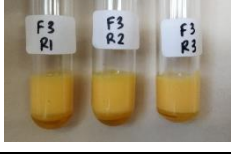
Particle size and polydispersity index (PI) evaluation.

Particle size is influenced by some factors such as the type of surfactant, concentration of surfactant, manufacture method, concentration, and ratio of liquid lipids and solid lipids (Salvi & Pawar, 2019). This study found that increasing liquid lipid ratio contributed to smaller particle size (Figure 1). Statistically, at initial day (1ˢᵗ day) showed a significant difference at least one pair between the groups of formulas F1, F2, and F3 at α = 0.05. The results of the post hoc test using Tukey HSD showed that the significantly different groups for particle size are F1 with F3, and F2 with F3. However, the particle size values show that there was a tendency for average particle size F1 < F2 < F3. Smaller particle size was obtained when the ratio of liquid lipids in the formula was increased. Liquid lipid helps to dissolve the drugs the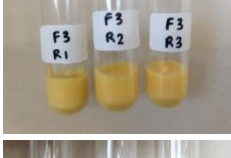reby allowing the system particle size to be smaller (Apostolou *et al.*, 2021). Particle size evaluation results during storage showed significantly increased size at 60ᵗʰ and 90ᵗʰ observation days, possibly due to particle coalescence. The presence of phase separation

that is visually visible on the organoleptic observation of F3 also has an impact on the particle size of F3 at 90th observation day which has a greater variation between replicates. However, during 90 days of storage, especially in formulas 1 and 2, the particle size was still below 600 nm, which is still able to deliver the encapsulated material into deeper layers of the skin (Danaei *et al.,* 2018).

Table 2. Visual observation of CoQ10-NLC systems during stability test

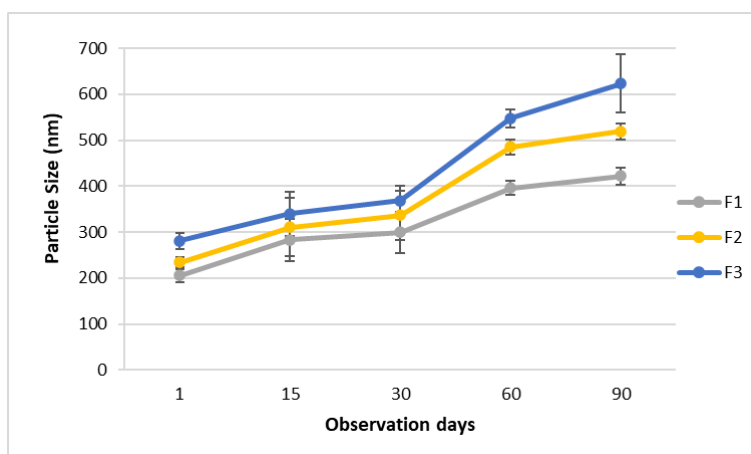| Observation Days	Formula 1 (F1)	Formula 2 (F2)	Formula 3 (F3)
1			
15			
30			
60			
90			

Figure 1. Stability test result for particle size during storage. Data is the mean of three replications ± SD
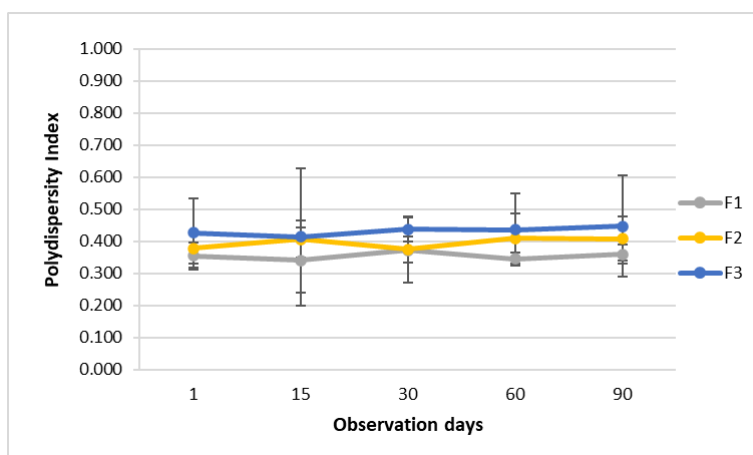
Figure 2. Stability test result for polydispersity index during storage. Data is the mean of three replications ± SD
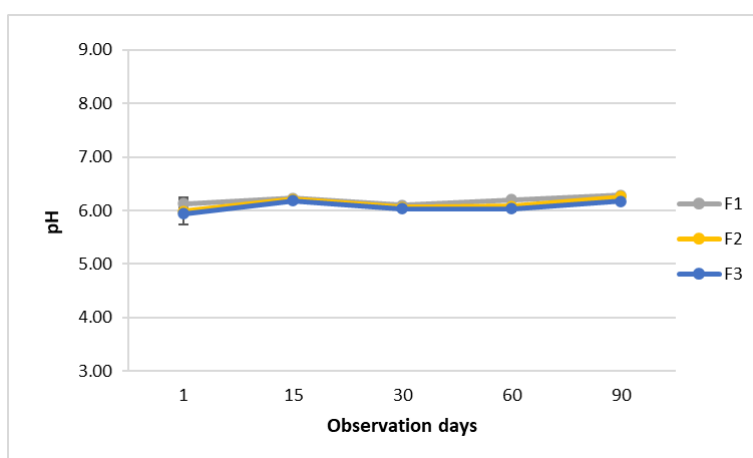

Figure 3. Stability test result for pH during storage. Data is the mean of three replications ± SD

The particle size distribution can be seen from the polydispersity index (PI). The PI indicates the uniformity of particle sizes within the sample population (Hendradi *et al.,* 2017). PI value that is lower than 0.5 indicates homogeneity and mono-dispersity formulation. If PI > 0.5 indicates a less homogeneous size variation or polydispersity in the formulation. However, the polydispersity index value < 1 is still acceptable because the colloidal carrier system is not always monodispersed (Salvi & Pawar, 2019). The polydispersity index obtained from this study shows a large variation between replicates. It was probably caused by variations in manufacture which are still perform manually. However, PI average result are < 0.5, which indicates a homogenous particle size distribution in the system (Figure 2). The statistical analysis of PI found no significant differences between all the formulas. Furthermore, there was no significant change during the storage period which indicates that all formulas remain homogeneous.

pH evaluation

The average pH of all formulas (Figure 3) was similar to the pH of the buffer solution (pH 6,00) used in the formulas. It was demonstrated that NLC systems can be used for topical administration in accordance with normal skin pH of 4 - 6 (Prakash *et al.,* 2017). The statistical analysis of pH found no significant differences between all the formulas. Furthermore, there was no significant change during the storage period which indicates that the pH of this system remains stable.

Viscosity test

The proper viscosity is required for NLC to adhere to the skin surface, thereby increasing drug penetration and residence time (Hendradi *et al.,* 2017). Viscosity can describe the ease of preparation when applied and predict the ease of moving molecules associated with drug release. Statistically, on initial day (1st day) the three groups of formulas showed significant differences in viscosity. On 1st day, the viscosity values show that there was a tendency F1 < F2 < F3 (Figure 4). Lower viscosity was obtained when the ratio of liquid lipids in the formula was higher. This is consistent with the

theory that a higher liquid lipid ratio can reduce the viscosity and reduce particle size, consequently results in a greater release of the drug and improved penetration ability (Apostolou *et al.,* 2021). Furthermore, there was no significant change during the storage period except for 90th day of storage. At that time, the viscosity value of the entire formula increased which was probably due to the coalesence between particles in the system and evaporation of the liquid during the storage period which resulted in a higher viscosity value. At 90th day, the viscosity value of F3 being lower than F2. It was probably due to the phase separation that occurs in F3 so that the consistency becomes slightly thinner.

Assay

An assay test during stability testing was useful for predicting the shelf life of a pharmaceutical preparation. The results of the assay test can be seen in Table 3. Based on the result of t-tes statistical analysis, it showed a significant difference among all formulas both for initial day (1st day) and end of storage (90th day). At the end of the storage period, the drug level was seen to decrease. This is probably due to the system being not stable enough so that drug degradation occurred.

Entrapment efficiency test

The results of the entrapment efficiency test can be seen in Table 3. Based on the result of t-tes statistical analysis, it showed a significant difference among all formulas both for initial day (1st day) and end of storage (90th day). The entrapment was increased with an increasing liquid lipid ratio. This is consistent with the theory that an increase in the liquid lipid ratio will improve the flexibility of the NLC core by influencing the imperfections in the crystal lattice, causing numerous drugs to be trapped in the system during the solidification of the lipid phase. This increase in the flexibility of the NLC core is also useful for preventing expulsion (Apostolou *et al.,* 2021). Miglyol 812's ability to increase the solubility of CoQ10 results in increased entrapment and penetration efficiency, making it a good choice for use in NLC formulations containing CoQ10. Miglyol can give a less perfect crystal shape to produce a larger space in the crystal. The enlarged crystal space can accommodate larger drugs so that the entrapment efficiency is greater (Annisa *et al.,* 2016). At the end of the storage period, the entrapment efficiency was seen to decrease. This is probably due to the system being not stable enough so that drug expulsion occurred.
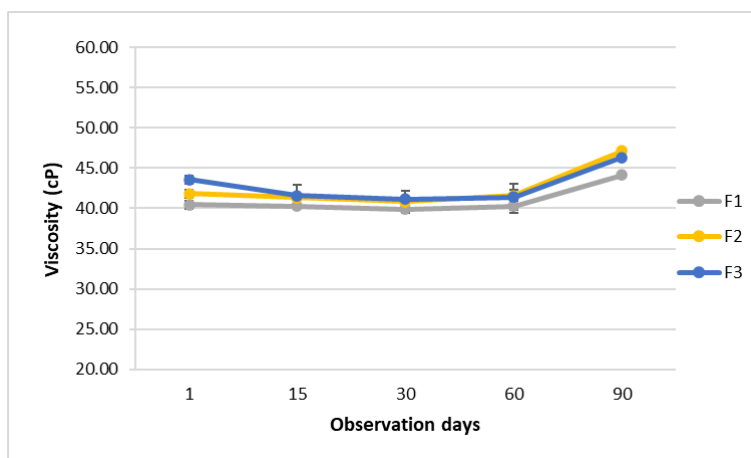
Figure 4. Stability test result for viscosity during storage. Data is the mean of three replications ± SD

Table 3. Stability test results for assay and entrapment efficiency of CoQ10-NLC systems during storage

Parameter	Formula	Before Storage (%)	After Storage (90 days) (%)
Assay	F1	92.66 ± 1.04	83.55 ± 4.40
	F2	92.35 ± 1.30	85.11 ± 4.28
	F3	91.60 ± 1.55	80.78 ± 3.18
Entrapment Efficiency	F1	92.73 ± 0.93	76.89 ± 1.03
	F2	87.90 ± 0.90	70.45 ± 1.90
	F3	84.60 ± 0.69	66.15 ± 1.41

Note: The data are represented as mean of three replicates ± SD

Figure 5. The relationship between the cumulative amount of Coenzyme Q10 released against time at 32°C in the dissolution medium. Data is the mean of three replications ± SD

Table 4. Regression line equations and correlation coefficient (r) of zero-order, first-order release kinetics, Higuchi model, and Korsmeyer-Peppas model

Release kinetics model		Formula 1 (F1)	Formula 2 (F2)	Formula 3 (F3)
Zero order	Regression equation	$y = 0.0217x + 1.3221$	$y = 0.0209x + 1.3673$	$y = 0.0204x + 1.0108$
	r	0.9705	0.9723	0.9663
First order	Regression equation	$y = 0.0028x + 0.1161$	$y = 0.0026x + 0.1654$	$y = 0.0036x - 0.1194$
	r	0.7833	0.8403	0.6885
Higuchi	Regression equation	$y = 0.4541x - 0.3046$	$y = 0.4374x - 0.2001$	$y = 0.4268x - 0.5207$
	r	0.9933	0.9953	0.9899
Korsmeyer-Peppas	Regression equation	$y = 0.5480x - 0.4901$	$y = 0.4917x - 0.3722$	$y = 0.7085x - 0.9094$
	r	0.8822	0.9284	0.7860

Drug release test result

This drug release test aims to determine the release kinetics and the rate of release (flux) of Coenzyme Q10 from the NLC system. The release rate (flux) is indicated by the slope v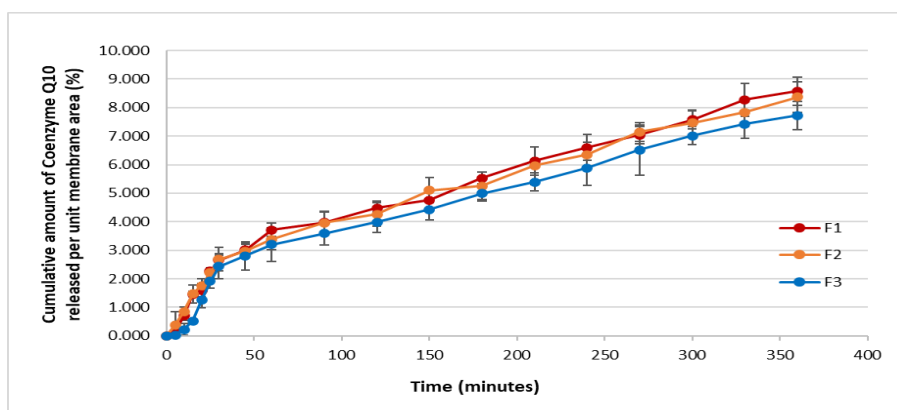alue in the regression equation between the amount of Coenzyme Q10 released per unit area of the membrane against time. The relationship between the cumulative amount of Coenzyme Q10 released against time can be seen in Figure 5. Statistically, it is known that there is no significant difference between the cumulative amount of Coenzyme Q10 regardless of the formulas F1, F2, and F3 at $\alpha = 0.05$.

The flux of Coenzyme Q10 from the NLC matrix was studied with various mathematical models to obtain the best model of the release kinetics of Coenzyme Q10 from the NLC matrix. Mathematical models used include zero-order kinetic models, first-order kinetic models, Higuchi models, and Korsmeyer-Peppas models. The result of regression line equations and correlation coefficient from some mathematical models can be seen in Table 4. The correlation coefficient (r) of

the Higuchi model is the highest, so the release kinetics of Coenzyme Q10 from the NLC matrix follows the release kinetics of the Higuchi model.

The flux is indicated by the slope value in the regression equation between the amount of Coenzyme Q10 released per unit of time. The result of flux calculation can be seen in Table 5. From the results of the test which was carried out for 6 hours, it was found that no significant differences between all the formulas. However, there was a tendency for cumulative drug release and release rate F1 > F2 > F3. The F1 release rate tends to be the highest because it has lowest viscosity. Formula 1 contains more liquid lipids which causes a thinner viscosity and smaller particle size, which theoretically affects the ease of drug ingredients to be separated from the base. The lower viscosity value will cause the molecules to move faster and give a greater release of the drug (Apostolou *et al.*, 2021). This trend is likely to be more significantly different if the difference in the ratio is enlarged, so there will be a significant difference between the three formulas.

Table 5. Coenzyme Q10 release rate from NLC with Higuchi model

Formula	Release rate (Flux) ($\mu g/cm^2/minutes$)
F1	0.4394 ± 0.0257
F2	0.4245 ± 0.0190
F3	0.4049 ± 0.0097

Note: The data are represented as mean of three replicates $\pm$ SD

CONCLUSION

The NLC-CoQ10 was successfully prepared using Compritol 888 ATO and Miglyol 812 as the lipid matrix. During stability evaluation, NLC-CoQ10 systems did not significantly change pH and PI values, but statistically significantly changed particle size, viscosity, assay, and entrapment efficiency. There were increments in the particle size and viscosity, which indicates the incorporation of small particles or coalescence. On the other hand, there was decrease in the assay and entrapment efficiency, which shows that the system is not stable enough so optimization is still needed to obtain the best system that has a long shelf life. From the results of the release test, it was known that NLC-CoQ10 was able to release the drug continuously but there was no statistically significant difference in the release parameters of the three tested formulas.

ACKNOWLEDGMENT

REFERENCES

Aburahma, M. H., & Badr-Eldin, S. M. (2014). Compritol 888 ATO: A multifunctional lipid excipient in drug delivery systems and nanopharmaceuticals. Expert Opinion on Drug Delivery, 11(12), 1865–1883. https://doi.org/10.1517/17425247.2014.935335

Andarina, R., & Djauhari, T. (2017). Antioksidan dalam Dermatologi. Jurnal Kedokteran Dan Kesehatan, 4(1), 39–48.

Annisa, R., Hendradi, E., & Melani, D. (2016). Pengembangan sistem nanostructure lipid carriers (NLC) meloxicam dengan lipid monostearin dan Miglyol 808menggunakan metode emulsifikasi. Journal of Tropical Pharmacy and Chemistry, 3(3), 156–169.

Apostolou, M., Assi, S., Fatokun, A. A., & Khan, I. (2021). The effects of solid and liquid lipids on the physicochemical properties of nanostructured lipid carriers. Journal of Pharmaceutical Sciences, 110(8), 2859–2872. https://doi.org/10.1016/j.xphs.2021.04.012

Danaei, M., Dehghankhold, M., Ataei, S., Hasanzadeh Davarani, F., Javanmard, R., Dokhani, A., Khorasani, S., & Mozafari, M. R. (2018). Impact of particle size and polydispersity index on the clinical applications of lipidic nanocarrier systems. Pharmaceutics, 10(2), 1–17. https://doi.org/10.3390/pharmaceutics10020057

Guedes, L. de S., Martinez, R. M., Bou-Chacra, N. A., Velasco, M. V. R., Rosado, C., & Baby, A. R. (2021). An overview on topical administration of carotenoids and coenzyme q10 loaded in lipid nanoparticles. Antioxidants, 10(7), 1–25. https://doi.org/10.3390/antiox10071034

Hendradi, E., Rosita, N., & Rahmadhanniar, E. (2017). Effect of lipid ratio of stearic acid and oleic acid on characteristics of nanostructure lipid carrier (NLC) system of diethylammonium diclofenac. Indonesian Journal of Pharmacy, 28(4), 198–204. https://doi.org/10.14499/indonesianjpharm28iss4pp198

Hernández-Camacho, J. D., Bernier, M., López-Lluch, G., & Navas, P. (2018). Coenzyme Q10 supplementation in aging and disease. Frontiers in Physiology, 9(FEB), 1–11. https://doi.org/10.3389/fphys.2018.00044

Nayak, K., Katiyar, S. S., Kushwah, V., & Jain, S. (2017). Coenzyme Q10 and retinaldehyde co-loaded nanostructured lipid carriers for efficacy evaluation in wrinkles. Journal of Drug Targeting, 26(4), 333–344. https://doi.org/10.1080/1061186X.2017.1379527

Nene, S., Shah, S., Rangaraj, N., Mehra, N. K., Singh, P. K., & Srivastava, S. (2021). Lipid based nanocarriers: A novel paradigm for topical antifungal therapy. Journal of Drug Delivery Science and Technology, 62(December 2020), 102397. https://doi.org/10.1016/j.jddst.2021.102397

Ortiz, A. C., Yañez, O., Salas-Huenuleo, E., & Morales, J. O. (2021). Development of a nanostructured lipid carrier (NLC) by a low-energy method, comparison of release kinetics and molecular dynamics simulation. Pharmaceutics, 13(4). https://doi.org/10.3390/pharmaceutics13040531

Prakash, C., Bhargave, P., Tiwari, S., Majumdar, B., &

Bhargava, R. K. (2017). Skin surface pH in acne. Journal of Clinical and Aesthetic Dermatology, 10(7), 33–39.

Ryu, K. A., Park, P. J., Kim, S. B., Bin, B. H., Jang, D. J., & Kim, S. T. (2020). Topical delivery of coenzyme Q10-loaded microemulsion for skin regeneration. Pharmaceutics, 12(4). https://doi.org/10.3390/pharmaceutics12040332

Salt, A. (2021). A data set to verify volume and sample removal correction calculations for dissolution testing. *Dissolution Technologies*, *28*(2), 16–20. https://doi.org/10.14227/DT280221P16

Salvi, V. R., & Pawar, P. (2019). Nanostructured lipid carriers (NLC) system: A novel drug targeting carrier. Journal of Drug Delivery Science and Technology, 51(990), 255–267. https://doi.org/10.1016/j.jddst.2019.02.017

Sguizzato, M., Mariani, P., Spinozzi, F., Benedusi, M., Cervellati, F., Cortesi, R., Drechsler, M., Prieux, R., Valacchi, G., & Esposito, E. (2020). Ethosomes for coenzyme Q10 cutaneous administration: From design to 3D skin tissue evaluation. Antioxidants, 9(6). https://doi.org/10.3390/antiox9060485

United States Pharmacopoeia Convention. (2020). The United States Pharmacopoeia 43 and The National Formulary 38. Philadelphia: United States Pharacopoeia Convention Inc.

The Effect of Polymers Ratio Carboxymethyl Chitosan, Polyvinyl Pyrolidone K-30, and Ethyl Cellulose N22 on Physico-Chemical Characteristics and Drug Release from Matrix Type Diclofenac Potassium Patch

Esti Hendradi*, Rahayuningtyas, Tristiana Erawati

Departement of Pharmaceutical Science, Faculty of Pharmacy, Universitas Airlangga University, Surabaya, Indonesia

*Corresponding author: esti-h@ff.unair.ac.id

Abstract

Background: *Diclofenac potassium is an NSAID drug that is used in the treatment of mild to moderate pain. The use of this drug orally can cause side effects in the gastrointestinal tract, and the drug will undergo extensive first-pass metabolism in the liver. Therefore, preparations for transdermal patches were made.* **Objective:** *Determining the effect of the polymer ratios of carboxymethyl chitosan, polyvinyl pyrolidone K-30, and ethyl cellulose N22 on the physicochemical characteristics and drug release of a matrix type diclofenac potassium patch.* **Methods**: *In this study, matrix type diclofenac potassium patches were made using a combination of carboxymethyl chitosan (CMC), polyvinyl pyrrolidone (PVP) K-30 polymer, and ethyl cellulose (EC) N22 in a ratio of 2:3:7 and 3:2:7. Patches are made by mixing the entire polymer matrix and diclofenac potassium together, which are then evaporated and dried.* **Results:** *The results showed that the different polymer compositions of CMC, PVP K-30, and EC N22 resulted in patches with physicochemical characteristics that were not significantly different. The combination of these polymers is able to control the release of the drug from the patch for a long time. It was also found that increasing the concentration of CMC was able to increase the rate of release of diclofenac potassium. Formula 2 with a ratio of 3:2:7 is claimed to be the best formula in terms of physical, chemical, and drug release characteristics from the patch. Further studies are needed, such as drug penetration tests into the skin.*

Keywords: *transdermal patch, diclofenac potassium, carboxymethyl chitosan, polyvinyl pyrrolidone K-30, and ethyl cellulose N-22*

INTRODUCTION

Diclofenac potassium is a phenylacetic acid derivative that belongs to the nonsteroidal anti-inflammatory drugs (NSAID) class of drugs. Diclofenac potassium has greater solubility and absorption than diclofenac sodium and is often recommended in the treatment of mild to moderate pain requiring a rapid onset of action. The drug's mechanism of action is as a non-selective cyclooxygenase (COX) inhibitor (Psimadas et al., 2012).

Oral use of diclofenac potassium can cause gastrointestinal side effects such as bleeding and peptic ulceration due to COX inhibition, which reduces prostaglandins in the gastric epithelium (Purnamasari et al., 2019). Diclofenac potassium has a short half-life of 1-3 hours and undergoes extensive first-pass metabolism in the liver that is only 50% of the systemically available oral dose (Rajabalaya et al., 2008).

Patches are transdermal dosage forms that deliver a specific dose of a drug into the bloodstream through the skin. The patch can release drugs slowly and steadily, with less change in drug levels than oral administration. It also avoids first-pass metabolism in the liver, keeps GI side effects to a minimum, and is easy for patients to use (Nalamachu and Gudin, 2020).

Transdermal patches are classified into two types: membrane patches and matrix patches. Matrix-type patches are thinner, lighter, and more flexible in the production process (Nalamachu and Gudin, 2020). Patch preparation is accomplished by thoroughly combining the active substances, polymers, and other components to be evaporated and dried.

Transdermal patches contain a drug, a polymer matrix, a penetration enhancer, adhesives, a backing layer, and additional excipients such as plasticizers (Al Hanbali et al., 2019). The drug crossing the skin process begins with drug release from the patch, followed by passive diffusion into the skin via the stratum corneum. Polymer is a crucial component of the patch since it influences and controls the rate of drug release from the patch (Nalamachu and Gudin, 2020).

Carboxymethyl chitosan (CMC) is a chitosan derivative that is hygroscopic, hydrophilic, has antibacterial activity, is biodegradable, biocompatible, non-toxic, has minimal immunogenicity, is affordable, and is easily accessible (Basmal et al., 2017 ; Shariatinia, 2018). Furthermore, CMC includes carboxymethyl groups, which may firmly bind water molecules via hydrogen bonds and improve their solubility in water, resulting in higher dissolution and bioavailability in the administration of drugs that are difficult to dissolve in water (Shariatinia, 2018). PVP is an amorphous synthetic polymer that is hygroscopic, non-toxic, and has a high swelling capacity. It also forms pores in the membrane that can aid release the drug from its base (Nurahmanto et al., 2018). Meanwhile, ethyl cellulose (EC) N-22 is a water-insoluble polymer that can maintain the drug in the preparation by generating a protective film (Nurahmanto et al., 2018).

The purpose of this study is to see how the combination of CMC, PVP K-30, and EC N-22 polymers in the ratios 2:3:7 and 3:2:7 affects the physicochemical properties and diclofenac potassium release from matrix type patches.

MATERIALS AND METHODS
Materials

Diclofenac potassium (obtained from PT. Dexa Medica), carboxymethyl chitosan (purchased from Xi'an Lyphar Biotech Co. Ltd), polyvinyl pyrrolidone K-30 (purchased from CV. Tristar Chemicals), ethyl cellulose N-22 (purchased from Dow Chemical Company), polyethylene glycol 400 (purchased from Indokemika Group), methyl methacrylate (purchased from Merck Schuchardt OHG), menthol, 96% ethanol and distilled water. The purity of the materials used was pharmaceutical grade.

Method
Preparation diclofenac potassium patch

The transdermal patch was prepared by mixing all the components of the material, consisting of the active ingredient, polymer, and other additives listed in Table 1. The manufacturing step begins with weighing each polymer in each formula. CMC was dissolved in 1.5 ml of aquadest, PVP K-30 was dissolved in 2 ml of 96% ethanol, and EC N-22 was dissolved in 2 ml of 96% ethanol. The three are stirred until homogeneous. Next, the PVP solution was mixed with the EC solution, and then the CMC solution was slowly added to the mixture and stirred at a constant speed until homogeneous. The next step is adding to the mixture a solution of menthol in 2 ml of 96% ethanol that has been mixed with diclofenac potassium. Then a total of 1.5 ml of PEG 400 was added to the mixed solution and stirred until homogeneous. Methyl methacrylate was also added to the mixture and stirred thoroughly. After all the mixing is complete, it is done overnight. The mixture is then poured into the mold with the inner diameter of the patch was 4 cm and the solvent evaporation process is carried out by placing it in a fume hood for 3 hours. Then it dried in an oven at 40 °C for 3 hours.

Table 1. Formula of diclofenac potassium patch matrix type

Compound	Function	Quantity (mg)	
		Formula 1 (KPE= 2:3:7)	Formula 2 (KPE= 3:2:7)
Diclofenac potassium	Active ingredient	16.4	16.4
CMC	Polymer	80	120
PVP K-30	Polymer	120	80
EC N-22	Polymer	280	280
PEG 400	Plasticizer	1,695	1,695
Methyl methacrylate	Adhesive	48	48
Menthol	Enhancer	6	6

Note: KPE = CMC: PVP K-30: EC N-22
Total polymer weight = 480 mg
Surface area of patch = 12.56 cm^2

Evaluation of the patch
Organoleptic examination

Organoleptic examination of diclofenac potassium patch was carried out by visually observing the color, smell, and surface texture.

Weight uniformity

Weight variations were tested by individually weighing diclofenac potassium patches on an analytical balance and calculating the average weight. The weight of each patch should not deviate significantly from the average weight and %KV ≤ 6% (Patel *et al.*, 2012).

Moisture content (MC)

The patches were weighed and kept at room temperature for 2.5 hours in a desiccator containing silica gel. The patch is then re-weighed to ascertain the preparation's moisture content. Percentage of moisture content can be calculated using the following formula:

$$\% \ Moisture \ content = \frac{(\text{Initial weight} - \text{Final weight})}{\text{Initial weight}} \times 100\%$$ *Viscosity test*

Acceptance requirements % moisture content of the patch are in the range of 2-10% (Shabbir et al., 2017).

Flatness

The flatness of the patch is determined by cutting the patch in the middle and two from each side of the patch with a size of 1x1 cm2. The length of the cut of each strip is measured before and after it is allowed to stand, and then the percent constriction is calculated using the formula:

$$\% \ Constriction = \frac{(L1 - L2)}{L1} \times 100\%$$

Information:
L2 = End length of each strip
L1 = Initial length of each strip

The constriction acceptance value is 0%, which means it is equivalent to 100% patch flatness (Shekade, 2021).

Thickness

The thickness of the transdermal patch is tested by measuring the preparation with a caliper at different points of each preparation. The replication of the test was carried out three times ±SD.

Determination of drug content

The goal of surface morphology observation is to determine the surface structure and pores created on the surface patch. Scanning Electron Microscopy (SEM) (Hitachi FLEXSEM 1000) was used for this test with magnification 250X.

Surface morphology

The determination of diclofenac potassium level was carried out by dissolving the patch at 500 rpm for 30 minutes in 100 ml of solvent (a mixture of 96% ethanol and phosphate buffer pH 7.4±0.05 in a 3:7 ratio) and centrifuging at 3000 rpm for 15 minutes. Furthermore, the content of the drug was analyzed by UV spectrophotometry. Acceptance levels for drugs are in the range of 85–115% (Hendradi et al., 2019).

Homogeneity of drug content

The test was carried out by cutting the patch into four equal-sized parts. Each part was dissolved in 25 ml of solvent (a mixture of ethanol and phosphate buffer in a ratio of 3:7) and stirred at 500 rpm for 30 minutes. The samples were then centrifuged and analyzed with a UV spectrophotometer set to its maximum wavelength. Acceptance levels for drugs are in the range of 85–115% (Hendradi et al., 2019).

In vitro drug release test

The first step is to make a standard potassium diclofenac working solution in phosphate buffer pH.7.4 ± 0.05. Standard working solutions were made with levels of 2 ppm, 8 ppm, 10 ppm, 14 ppm, and 20 ppm. Each absorbance was observed using a UV spectrophotometer at the maximum wavelength. The maximum wavelength obtained is 277 nm. Then a standard curve of diclofenac potassium was made by connecting the concentration (x axis) vs. absorbance (y axis) of each standard solution of work and obtaining the

linear equation y= ax+b. This equation can then be used to calculate the grade from the release test.

The release test was carried out in vitro with three replications of each formula. The test was performed with a USP-compliant dissolution apparatus, namely a 5-paddle over disk equipped with a diffusion cell and a paddle-type stirrer. Diffusion cells were used as a place for the transdermal patch to be placed before being closed by the cellophane membrane and then placed at the bottom of the vessel. A 500-mL phosphate buffer solution with a pH of 7.4 ±0.05 was used as the dissolution medium. The test temperature was kept constant at 37± 0.5 °C, and the paddle speed was set to 50 rpm. Sampling was carried out at 0, 15, 30, 60, 90, 120, 150, 180, 210, 240, 270, 300, 360, and 420 minutes by taking 5 ml of sample. Each sampling was replaced with a new dissolution medium containing the same amount. The samples taken were analyzed for drug content by measuring the absorbance at the maximum wavelength using a UV spectrophotometer. The obtained levels are then corrected using the Wurster and Taylor equations with the following formula:

$$Cn = C'n + \frac{a}{b} \sum_{s-1}^{n-1} Cs$$

Note:
Cn = Actual levels after correction (ppm)
C'n = Readable levels (calculated from the sample absorption values read on the spectrophotometer) (ppm)
Cs = Levels read from the previous sample
a = Volume of sample taken
b = Volume of media

The cumulative amount of diclofenac potassium released from the basis of the unit area of the membrane each time (μg/cm^2) is obtained by calculating the concentration obtained each time (μg/mL) times the amount of media dissolution (ml) divided by the surface area of the patch (cm^2). Furthermore, the release profile of diclofenac potassium can be determined with data on the cumulative amount released.

The diclofenac potassium release rate (flux) is the slope (y) of the linear regression line equation of the diclofenac potassium release profile depicted when it reaches steady state.

Data analysis

Data from the evaluation patch were analyzed using independent t-test with 95% confidence level or significance value (*a*) = 0.05. There is a significant difference symbolized by H_1, while the absence of a significant difference is symbolized as H_0. If the value of *a* < 0.05 is obtained, then H_1 is accepted.

RESULTS AND DISCUSSION
Organoleptic examination

Based on the results of organoleptic observations, formula 1 and formula 2 had the same visual appearance in terms of color, smell, texture, and patch. Patch is white, slightly smells of methyl methacrylate, has a smooth surface texture, is not brittle, and has a diameter of 4 cm. The results of the patch of the two formulas can be seen in Figure 1.
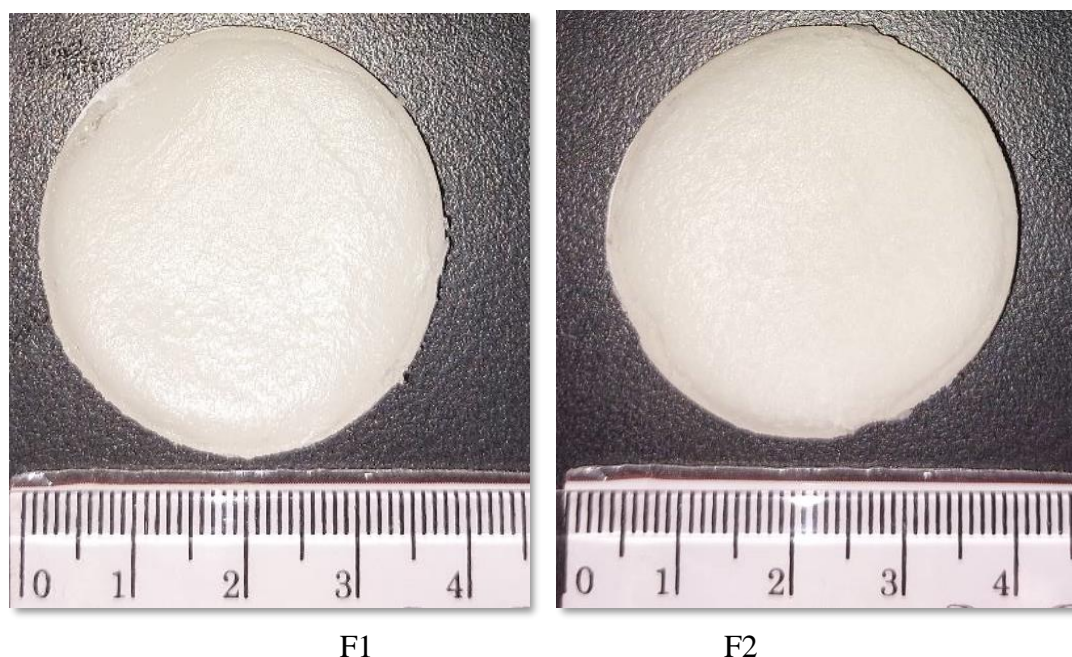

F1   F2

Figure 1. The visual appearance of patch in formulas 1 and 2 and the diameter of the preparation is 4 cm

Table 2. Results of the of the physico-chemical characteristics of diclofenac potassium patch

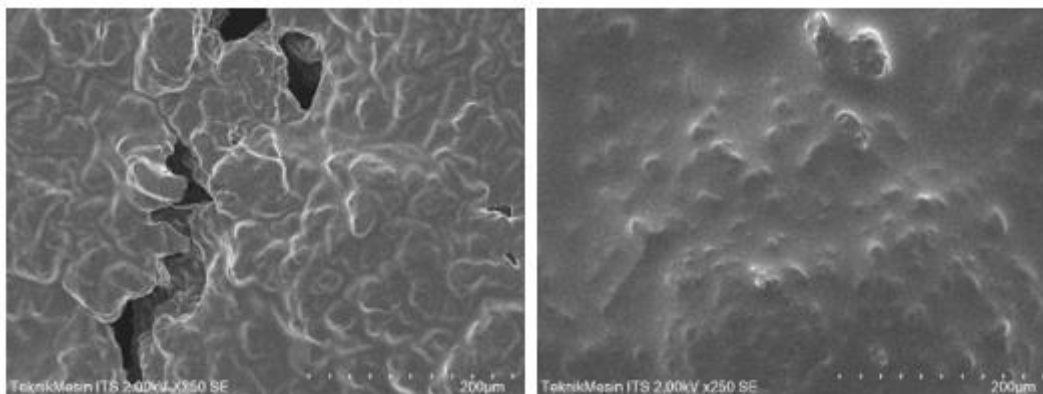| Formula	Weight uniformity (gram)	Moisture content (%)	Flatness (%)	Thickness (cm)	Drug content (%)
F1	2.3110 ± 0.008	4.53 ± 0.12	100	0.245 ± 0.004	91.18 ± 0.99
F2	2.3308 ± 0.021	4.68 ± 0.11	100	0.247 ± 0.001	92.92 ± 0.57

Figure 2. The surface morphology observation of diclofenac potassium patch using Scanning Electron Microscopy (SEM) (Hitachi FLEXSEM 1000) with magnification 250X

Table 3. Results of homogeneity drug content of diclofenac potassium patch

Formula	Part of the patch	Drug content (%)
F1	1	91.18 ± 0.75
	2	91.93 ± 0.37
	3	90.81 ± 0.99
F2	1	93.05 ± 1.12
	2	92.80 ± 0.94
	3	92.55 ± 0.57

The physico-chemical characteristics of the patch

The results of the evaluation of the The physico-chemical characteristics of the patch such as uniformity of weight, moisture content (MC), flatness, thickness, and drug content are presented in Table 2. Data is the average of 3 replications of the test ± SD. The % KV value of the two formulas in each evaluation has given a result of ≤ 6 % which indicates the uniformity of weight, MC, flatness, thickness, and drug content in both formulas. Tests for MC and drug levels in formula 1 and formula 2 also met the requirements, namely MC was in the range of 2-10%, while drug levels were in the range of 85-115% Hendradi et al., 2019 ; Shabbir et al., 2017). Statistical independent t-test each test has given a significance value of > 0.05, which means that there is no significant difference in weight, MC, flatness, thickness, and drug content between formulas 1 and 2. The result of the combination of carboxymethyl chitosan, polyvinyl pyrrolidone K-30, and ethyl cellulose N-22 2:3:7 and 3:2:7 on the characteristics still couldn't show the different characteristics. It takes a

combination with a large difference between CMC and PVA to show the different characteristics.

Surface morphology

The transdermal patch was observed using a Scanning Electron Microscopy (SEM). Tests were carried out at 250x magnification. The results of surface morphology observation of diclofenac potassium patch can be seen in Figure 2.

In formula 1 and formula 2 transdermal patch, there have been scattered particles that blend together and are evenly distributed on the entire surface patch. It was also observed in formula 1 that visible pores were clearly visible on the surface of the patch. These pores are formed due to the higher amount of PVP K-30 polymer in formula 1. PVP K-30 has the ability to form pores on the membrane so that it affects drug release from the preparation (Franco and De Marco, 2020).

Homogeneity of drug content

The evaluation result of the homogeneity of drug content in patch are presented in Table 3. The homogeneity test aims to determine the uniform distribution of diclofenac potassium in each part of the

patch. It is expected that if the drug is homogeneously distributed, the drug release can occur simultaneously in each part of the patch. The test results showed that the diclofenac potassium content in each patch met the requirements, which were in the range of 85-115% (Hendradi et al., 2019). Formula 1 and formula 2 also have a value of %KV $\leq$ 6%, which means that the drug content in each patch is uniform and is declared homogeneous. The result of statistical analysis independent t-test has given a significance value > 0.05, which means that there is no significant difference in diclofenac potassium content in each part of the patch between the two formulas.

In vitro drug release

The diclofenac potassium release test from the patch was carried out for 7 hours with a 5-paddle over disk apparatus. The results of the cumulative amount of diclofenac potassium released from the preparation at any time can be seen in Figure 3. The data is then used to determine the rate of drug release by connecting the cumulative amount of drug released (%) with the root of the time described when it reaches steady state. The release rate (flux) of diclofenac potassium is the slope of the linear regression equation on the curve. The release flux values in the two formulas are presented in Table 4.

In vitro drug release

The diclofenac potassium release test from the patch was carried
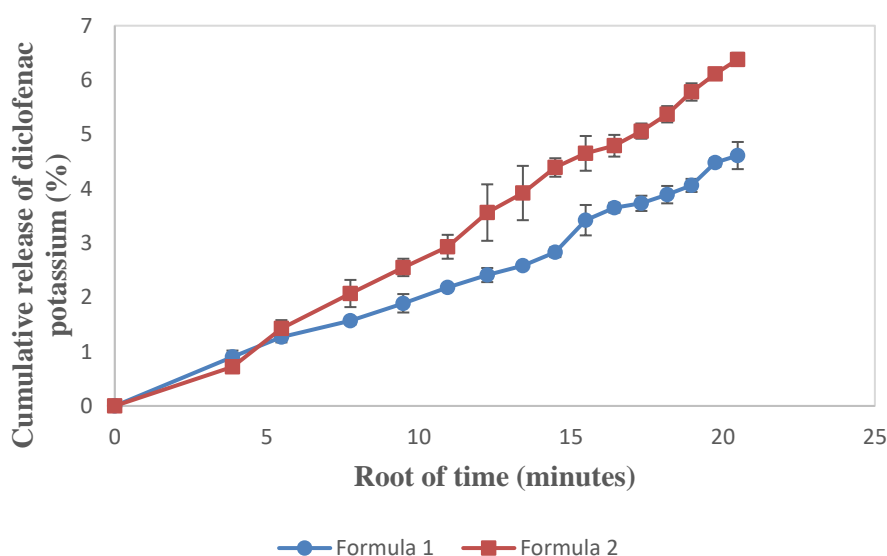
Figure 3. The curve of the cumulative amount of diclofenac potassium released in formulas 1 and 2. The data is the average of 3 replications ± SD

Table 4. Fluks of diclofenac potassium from patch

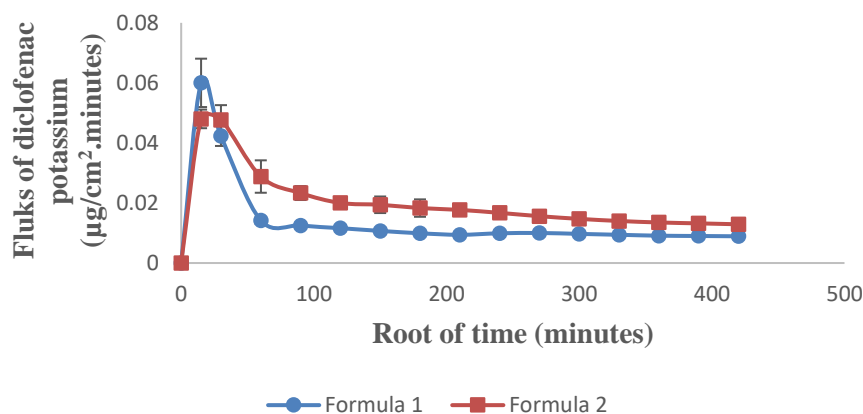| Formula	Fluks ($\mu g/cm^2$.minutes)
F1	0.2242 ± 0.0077
F2	0.3314 ± 0.0068

Figure 4. Controlled release curve of diclofenac potassium in formulas 1 and 2. Data is the mean of 3 replications ± SD

Table 5. Regression equaltions and correlation coefficient values for each diclofenac potassium release kinetics model

Formula	Higuchi	Zero order	Korsmeyer-Peppas
F1	y = 0.2513x – 0.6062, R^2 = 0.9868	y = 0.0087x + 1.0818, R^2 = 0.9828	y = 0.5132x – 0.7072, R^2 = 0.9776
F2	y = 0.3299x – 0.5105, R^2 = 0.9952	y = 0.0116x + 1.651, R^2 = 0.9842	y = 0.572x – 0.7038, R^2 = 0.9935

According to Table 4, formula 2 produces a greater flux value than formula 1, which produces 0.3314 g/cm^2.min. The independent t-test resulted in a significance value < 0.05, indicating that there is a difference in the fluks value between the two formulations. The fluks of diclofenac potassium from patch grow as the number of CMC rises. CMC has excellent hydrophilic characteristics, which allow it to absorb and bind water firmly. The more bound water there is, the more the polymer swells, resulting in quicker drug release (Shabbir et al., 2018). When a result, as the number of CMC grows, so do the fluks of diclofenac potassium from the patch.

The release fluctuation data were then correlated with time to prove the controlled release of diclofenac potassium in both formulas. Figure 4 depicts the curve relationship of time vs. average fluctuations at each time. The results show that the release of diclofenac potassium from the patch in Formulas 1 and 2 occurred in a controlled manner from the 150th minute until the end of the test, namely the 420th minute. Controlled release is generally expected to occur in patches. This is due to the use of a combination of hydrophilic and hydrophobic polymers that are able to provide controlled drug release for a long time (Shivalingam et al., 2014).

Furthermore, the determination of the release kinetics of diclofenac potassium from the patch preparation was carried out. The diclofenac potassium release profile was aggregated using the Highuchi model, the Zero order, and the Korsmeyer-Peppas model. Table 5 lists the regression equations for each kinetic model. The results reveal that the release kinetics of diclofenac potassium from patch formulas 1 and 2 follow the Higuchi model, which is reflected by the coefficient of variation that is the greatest and closest to one. The Higuchi model is frequently applied to transdermal medicine administration devices such as patches (Paarakh et al., 2019). Diffusion is the primary drug release mechanism in the Higuchi model (Shabbir et al., 2018).

CONCLUSION

The combination of carboxymethyl chitosan (KMK) polymer, polyvinyl pyrrolidone (PVP) K-30, and ethyl cellulose (EC) N-22 in the ratios 2:3:7 and 3:2:7 resulted in a patch that met the physicochemical requirements and was capable of providing controlled release over a long period of time using the Higuchi model kinetics. The amount of carboxymethyl chitosan (CMC) added had no effect on the physicochemical properties of the two formulae developed. However, an increase in CMC has a considerable influence on the value of the drug release flux, which rises as well. So formula 2 with a 3:2:7 ratio of carboxymethyl chitosan (CMC) polymer, polyvinyl pyrrolidone (PVP) K-30, and ethyl cellulose (EC) N-22 yielded a greater diclofenac potassium release flux, specifically 0.3314 µg/cm^2.minute.

REFERENCES

Al Hanbali, O. A., Khan, H. M. S., Sarfraz, M., Arafat, M., Ijaz, S., & Hameed, A. (2019). Transdermal patches: Design and current approaches to painless drug delivery. *Acta Pharmaceutica*, *69*(2), 197–215. https://doi.org/10.2478/acph-2019-0016

Basmal, J., Prasetyo, A., & Fawzya, Y. N. (2017). Pengaruh Konsentrasi Asam Monokloro Asetat Dalam Proses Karboksimetilasi Kitosan Terhadap Karboksimetil Kitosan Yang Dihasilkan. *Jurnal Penelitian Perikanan Indonesia*, *11*(8), 47. https://doi.org/10.15578/jppi.11.8.2005.47-56

Franco, P., & De Marco, I. (2020). The use of poly(N-vinyl pyrrolidone) in the delivery of drugs: A review. *Polymers*, *12*(5), 18–21. https://doi.org/10.3390/POLYM12051114

Hendradi, E., Riantiny, A. I. K. E., Hasiholan, J., & Miatmoko, A. (2019). The Effect of Different Ratios of the Hydrophilic Polymers Sodium Alginate 20cP and Hydroxy Propyl Methyl Cellulose

E15 on the Physicochemical Characteristics of Meloxicam Patch. *SSRN Electronic Journal*, 5–9. https://doi.org/10.2139/ssrn.3489586

Nalamachu, S., & Gudin, J. (2020). Characteristics of analgesic patch formulations. *Journal of Pain Research*, *13*, 2343–2354. https://doi.org/10.2147/JPR.S270169

Nurahmanto, D., Sabrina, F. W., & Ameliana, L. (2018). Optimasi Polivinilpirolidon Dan Carbopol Pada Sediaan Patch Dispersi Padat Piroksikam. *Jurnal Ilmiah Manuntung*, *3*(2), 197. https://doi.org/10.51352/jim.v3i2.129

Paarakh, M. P., Jose, P. A. N. I., Setty, C. M., & Peter, G. V. (2019). Release Kinetics – Concepts and Applications. *International Journal of Pharmacy Research & Technology*, *8*(1), 12–20. https://doi.org/10.31838/ijprt/08.01.02

Psimadas, D., Georgoulias, P., Valotassiou, V., & Loudos, G. (2012). Molecular Nanomedicine Towards Cancer : *Journal of Pharmaceutical Sciences*, *101*(7), 2271–2280. https://doi.org/10.1002/jps

Purnamasari, N., Alatas, F., & Gozali, D. (2019). Formulasi Dan Evaluasi Transdermal Patch Kalium Diklofenak. *Kartika : Jurnal Ilmiah Farmasi*, *7*(1), 43. https://doi.org/10.26874/kjif.v7i1.209

Rajabalaya, R., Khanam, J., & Nanda, A. (2008). Design of a matrix patch formulation for long-acting permeation of diclofenac potassium. *Asian Journal of Pharmaceutical Sciences*, *3*(1), 30–39.

Shabbir, M., Ali, S., Hamid, I., Sharif, A., Akhtar, M. F., Raza, M., Ahmed, S., Peerzada, S., & Amin, M. U. (2018). Influence of different formulation variables on the performance of transdermal drug delivery system containing tizanidine hydrochloride: In vitro and ex vivo evaluations. *Brazilian Journal of Pharmaceutical Sciences*, *54*(4), 1–12. https://doi.org/10.1590/s2175-97902018000400130

Shabbir, M., Ali, S., Raza, M., Sharif, A., Akhtar, M. F., Manan, A., Fazli, A. R., Younas, N., & Manzoor, I. (2017). Effect of hydrophilic and hydrophobic polymer on in vitro dissolution and permeation of bisoprolol fumarate through transdermal patch. *Acta Poloniae Pharmaceutica - Drug Research*, *74*(1), 187–197.

Shariatinia, Z. (2018). Carboxymethyl chitosan: Properties and biomedical applications. *International Journal of Biological Macromolecules*, *120*, 1406–1419. https://doi.org/10.1016/j.ijbiomac.2018.09.131

Shekade, M. S. V. (2021). *Journal Of Pharmacy And Experimental Medicine Niosome : A Novel Drug Delivery System*. 1–5. https://americanscietificreports.com/science-world/articlepdf/jpem-1-103.pdf

Shivalingam, M. R., Durgabhavani, G., Vaishnavi, K., & Priyanka, K. (2014). Formulation and evaluation of Diclofenac potassium transdermal patches for enhanced therapeutic efficacy. *Indian Journal of Research in Pharmacy and Biotechnology*, *2*(3), 1152–1157. http://www.ijrpb.com/current issues/1/v2_is3/ijrpb 2(3) 3 siva lingam 1152-1157.pdf

Characteristics and Physical Stability of Nanoemulsion as a Vehicle for Anti-Aging Cosmetics: A Systematic Review

Eva Syariefah Rachman, Widji Soeratri*, Tristiana Erawati
Departement of Pharmaceutics, Faculty of Pharmacy, Universitas Airlangga, Surabaya, Indonesia

*Corresponding author: widji-s@ff.unair.ac.id

Abstract

Background*: Skin aging can be overcome by applying anti-aging cosmetics. Many active ingredients that have anti-aging potential are derived from plants, and these materials must be delivered with a sound skin delivery system, namely nanoemulsion. The characteristics of nanoemulsion are closely related to physical stability.* ***Objective****: This study aims to conduct a systematic review of in vivo and in vitro study designs to examine the characteristics and physical stability of nanoemulsions used in topical anti-aging cosmetics.* ***Methods****: A systematic literature review based on the PRISMA statement was used to review the articles regarding nanoemulsions' characteristics and physical stability. The article search was accessed from an internet search database: Scopus, Pubmed, and Web of Science, published between January 2012 and June 2022.* ***Results****: Of the 244 articles, 44 were found to be related to the characteristics and physical stability of nanoemulsions in anti-aging cosmetics. These showed that active ingredients with antioxidant activity, filter UV rays, moisturizing agents, and cell-repairing agents are delivered by a nanoemulsion system with various types and ratios of surfactants, cosurfactants, and oil phases. Tween 80, Span 80, Transcutol HP, and Caprylic/capric triglyceride are the most widely used nanoemulsion compositions.* ***Conclusion****: The type and composition of the oil phase, surfactant, and cosurfactant affect the characteristics of the nanoemulsion (droplet size, polydispersity index, viscosity, zeta potential) and the physical stability of the nanoemulsion so that it can deliver active ingredients that have the potential as anti-aging well.*

Keywords*: Characteristics, Physical Stability, Nanoemulsions, Cosmetics, Skin Aging*

INTRODUCTION

Aging is a natural phenomenon of a decline in physiological function and skin structure that cannot be avoided but can be slowed down (Li et al., 2021) . Two factors, i.e. intrinsic factors such as genotype, endocrine metabolism, and hormone levels, and extrinsic factors such as air pollution, UV radiation, and nutritional levels, can influence skin aging (Ahmed et al., 2020). UV radiation is the main external factor that significantly influences the rapid occurrence of premature aging. When UV rays reach the skin surface, UV rays increase free radicals in the skin, causing damage to DNA, skin peroxidation, and protein cross-linking. Highly reactive molecules called free radicals have one or more unpaired electrons. Free-radical formation triggers signs of aging such as thinning of the epidermis and dermis layers, reduced elastic fibers, decreased collagen synthesis, and decreased number of fibroblasts (Cao et al., 2020).

Invasive and non-invasive treatments can be done to slow down the aging of the skin. Invasive treatment is an action that is carried out on the body through incisions, punctures or using a tool that goes into the skin(Cousins et al., 2019). The non-invasive treatment is a procedure that does not require a device that goes into the skin. One example of non-invasive anti-aging treatments is the use of topical anti-aging cosmetics. All circles of society can use topical cosmetics because it is easy to use and can be done anywhere. Therefore, anti-aging cosmetics are an easy alternative to treat skin aging. Based on the function, anti-aging cosmetics are divided into three categories: antioxidant cosmetics, moisturizing cosmetics, and biological activity of cosmetics (Li, 2015).

Several innovative cosmetic delivery systems are used in cosmetic products, one of which is nanoemulsion. Nanoemulsion is one type of drug delivery by mixing the water phase and the oil phase with the help of surfactants and co-surfactants with a certain HLB value to produce a droplet size of 20-500 nm, which varies depending on the composition of the nanoemulsion system and the method of manufacture (Harwansh et al., 2019). Nanoemulsions can deliver both lipophilic and hydrophilic drugs. There are several nanoemulsions, i.e. oil in water (O/W), water in oil (W/O) nanoemulsions, and double nanoemulsions such as oil in water in oil (O/W/O) or water in oil in water (W/O/W). W/O nanoemulsion is a nanoemulsion consisting of water as the dispersed phase or internal phase and oil as the dispersion medium or external phase. The W/O nanoemulsion can protect the degradation of hydrophilic drugs so that the hydrophilic drugs can become an internal phase protected by oil as an external phase, and vice versa O/W nanoemulsions can protect the degradation of lipophilic drugs.

Nanoemulsions are very attractive for cosmetics due to the aesthetic properties of nanoemulsions, i.e. stability, low viscosity, transparent visual aspect, and high surface area, enabling effective delivery of the active ingredients to the skin. Nanoemulsions are formed from the dispersion process from one liquid phase into another liquid phase to form droplets. Nanoemulsion has a tiny and homogeneous globule size that can prevent creaming, sedimentation, and coalescence. The advantage of using nanoemulsions as topical preparations is that more active substances can be formulated in one preparation due to an increase in solubility capacity and can increase the bioavailability of the active substance to increase the thermodynamic activity of the active substance on the skin. In addition, it has high effectiveness in penetrating the skin's stratum corneum (Marzuki et al., 2019). The composition and characteristics of the oil phase, surfactants, and cosurfactants affect nanoemulsions stability and oxidative stability. The characteristics of the physical properties of nanoemulsions can evaluate through several tests such as organoleptic, homogeneity, phase separation, nanoemulsion type, measurement of pH, percent transmittance, viscosity, droplet size, and polydispersity index. The characteristics of the nanoemulsion are related to physical stability and clarity because they will have an important effect on the resulting droplet size (Marzuki et al., 2019).

Studies related to nanoemulsions for topical anti-aging products have been carried out. However, to our knowledge, a systematic review that summarizes the characteristics and physical stability of nanoemulsions in topical anti-aging products has not been performed. Therefore, this systematic review intend to fill the gap by efficiently integrating accurate information and providing a basis for making a dicision from the related literature that systematically reviewed all available related studies for characteristics and physical stability of nanoemulsion systems for topical anti-aging products. This study aims to conduct a systematic review of *in vivo* and *in vitro* study designs of examine the characteristics and physical stability of nanoemulsions used in topical anti-aging cosmetics.

RESEARCH METHOD

This research is a systematic (Systematic Literature Review) using the PRISMA (Preferred Reporting Items for Systematic Review and Meta-analysis) method, which is carried out systematically by following or doing research. This systematic review technique consists of multiple parts, including 1) Establishing the background and objectives, 2) Formulating research questions, and 3) Conducting a literature search. 4) Criteria for selection, 5) Practice screens, 6) Checklist and quality procedures 6) Strategy for Data Extraction, and 7) Strategy for Data Synthesis.

Keywords

The search for articles relevant to this research topic was conducted using the keywords: 'cosmetics,' 'skincare,' 'skin aging,' 'stability,' 'characteristics,' and 'nanoemulsion.' These keywords are obtained through the formulation of PICO. Table 1 gives a detailed explanation of the search technique.

Eligibility criteria

Inclusion criteria were studies that used quantitative data obtained from experimental results with *in vitro* or *in vivo* study, products tested for topical use and no additional anti-aging therapy was used. Articles that discuss the characteristics and/or stability of nanoemulsions that contain ingredients that counteract free radicals can repair skin cells, provide moisture to the skin, and protect the skin from UVA/UVB rays.

Exclusion criteria were articles in the form of reviews, reports, or chapters in books, products tested for internal use and the presence of additional accompanying therapeutic methods. Research article on the topic of the problem is not related to the characteristics and/or stability of nanoemulsions that contain ingredients that counteract free radicals can repair skin cells, provide moisture to the skin, and protect the skin from UVA/UVB ray.

Literature searches and selection

The data collection process required in this study was obtained from three web databases: Scopus, Pubmed, and Web of Science, published between January 2012 and June 2022. Required data collection online in May - June 2022. No regional, language, or temporal restrictions were applied when searching for literature.

Data extraction

After obtaining the appropriate keywords, a search can be carried out on the database to be used through the official website of each database. After the search of the articles, screening was carried out on each article obtained. The screening was done through the Mendeley tools. In the first stage of screening, it was done by checking for duplication of search results. After separating the duplicate articles, it was continued by sorting based on the suitability of the title and abstract with the topic of this research, namely nanoemulsion in anti-aging topical preparations. Furthermore, the eligibility test was carried out, and each article filtered from the title and abstract selection will be read in its entirety to see whether it is in accordance with the inclusion criteria previously set.

Data analysis and reporting

Article review analysis was used to collect data so that it could produce findings to answer the objectives of this study. The data will be presented in the form of a table consisting of the authors, active ingredients, constituent materials (oil phase, surfactants, cosurfactants), characteristics (droplet size, polydispersity index, zeta potential), physical stability and research results.

RESULTS AND DISCUSSION
Results

A total of 244 articles were successfully obtained from searching in three databases, i.e. Scopus, Web of Science, and Pubmed. Furthermore, as many as 37 duplicate articles were issued, and there were 207 articles left in the screening process by reading the title and abstract. As many as 132 articles were rejected throughout the screening phase because they did not match the inclusion criteria; consequently, only 75 articles were included in the full-text reading assessment step. Furthermore, as many as four articles must be issued because they do not have full access to read the entire article, so 71 articles remain in the assessment process for eligibility. Finally, as many as 27 articles must be issued because they do not have exposure of interest to get 44 articles that meet all inclusion criteria used in the Systematic Literature Review as shown in Table 2.

Table 1. Description of search strategy

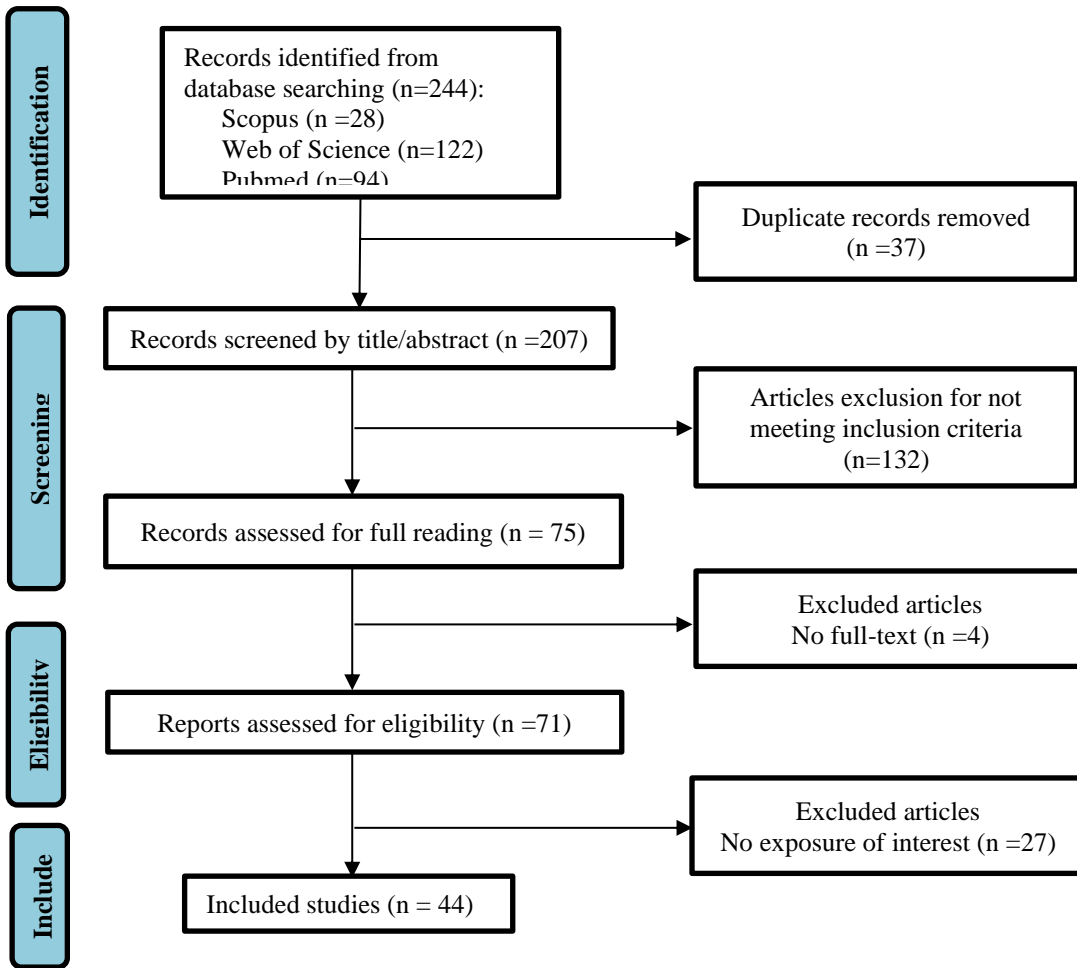| Database	Search Strategy
Scopus	[[('Cosmetics' or 'Skin Care' or 'Skin Aging') and ('Stability' or 'Characteristics') and ('Nanoemulsion')]
Pubmed	[[('Cosmetics' or 'Skin Care' or 'Skin Aging') and ('Stability' or 'Characteristics') and ('Nanoemulsion')]
Web of science	[[('Cosmetics' or 'Skin Care' or 'Skin Aging') and ('Stability' or 'Characteristics') and ('Nanoemulsion')]

Figure 1. Preferred Reporting Items for Systematic Reviews and Meta-Analyses (PRISMA) Flow Diagram of the study

Tabel 2. Summary of studies on characteristics and physical stability of nanoemulsion for anti-aging effects

Active Ingredients	Ingredients	Characteristics	Stability	Anti-aging Effects
Leaf and Stem *Vellozia squamata*	Oil phase: Babacu oil Surfactant: Sorbitan monoestearate, PEG- 40 hydrogenated castor oil	• Droplet size: Leaf 154.6±9.59 nm Stem 147.6±33.32 nm • Polydispersity Index: Leaf 0.284±0.034 Stem 0.351±0.254 •Viscosity: Stem 99.70 Cp Leaf 99.70 Cp	Accelerated stability assay: Thermal cycle • Droplet size after 7 days (stem 157.4±6.90 nm) (leaf 144.5±4.02 nm) • Polydispersity index after 7 days (stem 0.490±0.128) (leaf 0.310±0.022) (Quintão et al., 2013)	• The total phenol content in plant extracts is proportional to the free radical inhibition of the antioxidants. Both of these effects also depend on the concentration of the plant extract. • Hydroalcoholic extracts from *V. squamata* as potential natural ingredients with antioxidant properties.
Tocotrienol	Oil phase: Palm oil esters Surfactant: Tween 80, Span 80	-	Centrifugation test: Sedimentation rates at earth gravity decreased with the increased in the percentage of the oil phase (10%, 20% and 30%). (Han et al., 2013)	The greatest elasticity was produced by the nanoemulsion containing 30% oil.
• Octyl Methoxycinnamate (OMC) • Titanium Dioxide	Oil phase: Avocado oil Surfactant: Ultrol® L70, Ultrol® CE200	• 10 w/w % avocado oil and 12 and 14 w/w % Ultrol® L70 w/w: no nano size • 5 w/w % avocado oil and 12 and 14 w/w % Ultrol® L70: 6 – 10 nm but destabilized after 5 days • 12 and 14 w/w % Ultrol® CE200, with 5 w/w % avocado oil: 6-10 nm	Stability study was conducted by visual observation for 1 month. There was no precipitation in the nanoemulsion containing 5% avocado oil/0.25% TiO2/12% Ultrol® CE200/water. The average droplet size is in the range of 400 to 500 nm. (Silva et al., 2013)	The formulation containing (w/w) 5% avocado oil/12% nonionic surfactant/83% water, 1% w/w for chemicals (OMC) and 0.25% for Titanium Dioxide was a stable nanoemulsion formulation.

Active	Composition	Characterization	Reference	Note
• Ethyl Hexyltriazone (EHT) • Diethylamino Hydroxybenzoyl Hexyl Benzoate (DHHB) • Bemotrizinol (Tinosorb S) • Avobenzone (AVO) • Octyl Methoxycinnamate (OMC)	Oil phase: Miglyol 812 Surfactant: Pluronic F68	• Droplet size (nm) NE-OMC 190.6 ± 20.1 NE-AVO 170.4 ± 14.3 NE-EHT 198.4 ± 7.2 NE-TINO 191.2 ± 11.9 NE-DHHB 186.5 ± 20.3 NE-UVMIX 118.2 ± 4.4 Unloaded NE 290.4 ± 18.7 • Polydispersity Index NE-OMC 0.26 ± 0.02 NE-AVO 0.23 ± 0.03 NE-EHT 0.23 ± 0.03 NE-TINO 0.22 ± 0.01 NE-DHHB 0.23 ± 0.01 NE-UVMIX 0.22 ± 0.03 Unloaded NE 0.39 ± 0.04 • Zeta Zeta potential (-mV) NE-OMC 13.3 ± 0.5 NE-AVO 22.8 ± 1.1 NE-EHT 37.7 ± 1.5 NE-TINO 28.6 ± 1.2 NE-DHHB 27.2 ± 1.9 NE-UVMIX 20.5 ± 1.8 Unloaded NE 24.9 ± 0.6	- (Puglia et al., 2014)	Both NLC and nanoemulsion can protect the photostable active ingredients.
Retinyl Palmitate	Oil phase: Labrafac lipophile Surfactant: Labrasol Cosurfactant: Plurol oleique	Droplet size: 14.42±1.10 nm Polydispersity Index: 0.680 Viscosity 55.28 ± 0.08 mPas	- (Clares et al., 2014)	Nanoemulsion with Retinyl Palmitate loaded penetrate deeper than SLN and Liposome.

Propolis Extract	Oil phase: Rice bran oil Surfactant: Tween 80, KollipHor RH40 Cosurfactant: Glycerin, Propylene	Droplet size: 23.72 nm Polydispersity index: 0.338	After stability test for 63 days at 25^0C and passing through 6 cycles of Freeze Thaw test there was no separation, propolis nanoemulsion was a stable formula. Droplet size when thermal cycling test Cycle 0 18.4 ± 0.36 nm Cycle 6 23.53 ± 3.25 nm Polydispersity Index when thermal cycling test Cycle 0 0.29 ± 0.04 Cycle 6 0.4 ± 0.14 (Mauludin et al., 2015)	Propolis nanoemulsion consisting of 26.25% KollipHor RH40; 8.75% glycerin; 5% RBO; 3% EEP; and 57% water can reduce 58% of DPPH free radicals.
Fullerene	Oil phase: Palm kernel oil esters Surfactant: Span 80, Tween 80	Droplet size: 140 - 170 nm	Fullerene nanoemulsion showed good stability by visual observation. (Ngan et al., 2015)	Fullerene could increase collagen production, skin hydration by observing collagen score and corneometric units.
Swiftlet Nest	Oil phase: Jojoba oil, Olive oil Surfactant: Tween 80	Droplet size: 136.35 nm Zeta potential: 40.2 mV	There was no separation after centrifugation and during 3 months of storage, this indicates that formulation was stable. (Mohd Taib et al., 2015)	Stable formula with homogenization time of 17 minutes consisted of 3.99% Tween 80; 90.03% deionized water and 3.4% other ingredients and contains 2.58% Swifle Nest.

Opuntia ficus-indica (L.) Mill Extract	Oil phase: Capric/Caprilic triglycerides Surfactant: Tween 80, Span 80	Droplet size: 92.2 - 233.6 nm Polydispersion Index: 0.200 Zeta potential: −26.71- −47.01 mV	•Droplet size (nm) at t0 119.0±7.4 at 4°C 121.6±8.8 at 25°C 233.6±30.1 at 45°C 92.71±6.1 •Polydispersity Index at t0 0.257±0.038 at 4°C 0.251±0.020 at 25°C 0.305±0.126 at 45°C 0.228±0.044 •Zeta potential (mV) at t0 -26.71±6.67 at 4°C -41.71±4.55 at 25°C -39.77±5.99 at 45°C -41.21±6.02 (Ribeiro et al., 2015)	Nanoemulsion 1% *Opuntia ficus-indica* (L.) Mill hydroglycolic extract can enhance the water content in the stratum corneum with the mechanism of action of humectants.
Quercetin	Oil phase: Capric/Caprilic triglycerides Surfactant: Oleth-20, Oleth-3, Cetyl Trimethyl Ammonium Chloride (CTAC)	-	Quercetin nanoemulsion was stable at low and room temperature. (Dario et al., 2016)	Nanoemulsion has good capability as a topical formulation and has low skin irritation.
Clinacanthus nutans (L.) Leaves	Oil phase: Guava seed oil/palm kernel oil Surfactant: Tween 80, Span 80	Droplet size 97.38±1.63 nm Zeta potential -25.1±0.57 mV Polydispersity index 0.25±0.01	During different storage conditions for 90 days (room temperature and 45 °C), visual inspection revealed no phase separations, indicating the nanoemulsion's stability. (Che Sulaiman et al., 2016)	A good Clinacanthus nutans nanoemulsion formula consisted of 8.13% of surfactant, 5% of oil, 1% of xanthan gum, 84.97% of water, 0.1% of bioactive extract, and 0.8% of preservative.

B-D Glucan Polysaccharides Extract	Oil phase: Palm olein Surfactant: KollipHor®RH40 (Polyoxyl 40 Hydrogenated Castor Oil)	Droplet size: 263 nm Polydispersity index: 1.85 Viscosity: 0.244 cP	After 24 h Droplet size: 289.6 nm Polydispersity Index: 0.312 At a concentration of less than 1%of β-D-glucan, the nanoemulsion showed better stability compared to a concentration of 85% of β-D-glucan at storage for 90 days at 4 °C and at 25 °C. (Alzorqi et al., 2016)	A good nanoemulsion formulation consists of 85% water and an oil/surfactant ratio of 3, using ultrasonic for 300 seconds and a power of 700 W.
Quercetin	Oil phase: Capric/Caprilic triglycerides Surfactant: Oleth-20, oleth-3, Cetyl Trimethyl Ammonium Chloride (CTAC).	Droplet size: 19.99±0.07 nm Polydispersity Index: 0.082 Zeta potential: 19.6±2.2 mV Viscosity: 7.1 cP	Ostwald ripening occurred in an accelerated stability test for 90 days at 45ºC with an increase in droplet size of 1000%, but observations were not carried out at room temperature. (Dario et al., 2016)	The optimum 0.5% Quercetin nanoemulsion formula was 5.6 % Oleth-20 and 3.4% Oleth-3, CTAC 1% using surfactant mixture HLB equal to 12.5.
Ethoxylated Lanolin (El) Acetylated Lanolin (Al)	Oil phase: Rubus idaeus (Raspberry seed Oil), Passiflora edulis seed oil, Prunus persica (Peach kernel oil) Surfactant: Sorbitan Monooleate, PEG 36 Castor Oil	Droplet size 48.0±7.2 nm	There was no change in droplet size in the formula containing 6.0% EL but at the addition of 2.0% AL, the droplet size increased. (Pereira et al., 2016)	The nanoemulsion formula containing 6.0% EL was more stable than the nanoemulsion formula with 2.0% AL which contained lanolin derivatives.
Thistle Oil	Oil phase: Thistle oil Surfactant: Tween 80, Decyl Glucoside	• 4% Decyl glucoside Droplet size 189.0 ± 5 - 179.8 ± 10 nm Polydispersity index • 0.216 - 0.303 Viscosity: 580 ± 50- 562 ± 30 mpa • 4% Tween 80 Droplet size: 191.1 ± 9 nm Polydispersity index: 0.335 Viscosity: 690 ± 100 mpa • 6% Tween 80 Droplet size: 159.5 ± 8 nm	After 60 days • 4% Decyl glucoside Droplet size 168 ± 9 - 233 ± 12 nm Polydispersity index 0.232 - 0.325 • 4% Tween 80 Droplet size 201 ± 3 nm Polydispersity index 0.269 • 6% Tween 80 Droplet size 164 ± 6 nm Polydispersity index 0.295 (Miastkowska et al., 2016)	More amount of Tween 80 up to 6% could decrease droplet size. The concentration of Decyl glucoside as natural surfactant needed lower amount to obtain optimal formula.

		Polydispersity index: 0.257 Viscosity: 587 ± 22 mpa		
Vitamin E	Oil phase: palm olein Surfactant: Polyoxyethylene (4) Lauryl Ether (Brij 30)	Droplet size O/S ratio 4:6 31.45±0.06 - 46.50±3.83 nm Droplet size O/S ratio 5:5 28.63±6.97 - 42.66±7.25 nm Viscosity 0.04 - 0.07 Pa.S	Formulas with added vitamin E and without added vitamin E were stable by visual observation during 12 h storage with four freeze-thaw cycle tests at 4 °C, 25 °C, and 40 °C. (Ramli et al., 2017)	The right formula for carrying vitamin E was an oil:surfactant ratio of 4:6, 5:5 and 6:4 and contains 20-50% by weight of water.
Agave sisalana	Oil phase: Caprylic/Capric Triglyceride Surfactant: Tween 80, Span 80	• Nanoemulsion with extract Droplet size 155.0 ± 1.29 nm Polydispersity Index I 0.10 ± 0.01 Zeta potential -17.67 ±0.40 mV pH 4.47±0.09 • Nanoemulsion with extract and polysaccharide-enriched fraction Droplet size 155.80 ± 3.99 nm Polydispersity Index 0.09 ± 0.02 Zeta potential −20.41 ± 2.58 mV pH 5.01 ± 0.05	Accelerated stability test after 24 h and 90 days • Nanoemulsion with extract Droplet size t0 171. 23 ± 3.49 nm 4 °C 165.0 ± 4.27 nm 25 °C 174.86 ± 2.29 nm 45 °C 237. 84 ± 3.84 nm Polydispersity Index t0 0.12 ± 0.02 4 °C 0.09 ± 0.02 25 °C 0.09 ± 0.01 45 °C 0.08 ± 0.03 Zeta Potential t0 −15. 77 ± 2.20 mV 4 °C −18. 02 ± 1.78 mV 25 °C −16. 10 ± 2.73 mV 45 °C −18. 91 ± 3.14 mV • Nanoemulsion with extract and polysaccharide-enriched fraction Droplet size t0 174. 81 ± 5.37 nm 4 °C 172.71 ± 10.6 nm 25 °C 175.97 ± 6.19 nm 45 °C 215.79 ± 11.11 nm Polydispersity Index t0 0.11 ± 0.02 4 °C 0.09 ± 0.03	The formula containing *Agave sisalana* extract with an additional 0.5% polysaccharide-enriched fraction was considered safe for the skin. The formula contained 40% oil phase, 50% water phase, and 10% surfactant additive.

			25 °C 0.10 ± 0.02 45 °C 0.09 ± 0.04 Zeta Potential t0 −23. 03 ± 1.94 mV 4 °C −20.78 ± 2.19 mV 25 °C −22. 78 ± 3.04 mV 45 °C −19.04 ± 2.31 mV (Barreto et al., 2017)	
Coffee Oil Algae Oil	Oil phase: Coffee oil/Algae oil Surfactant:Tween 80, Span 80	Droplet size: 36.7±0.2 nm	Droplet size during storage for 1 day and 90 days 4°C 37.7±0.3 and 31.9±0.2 nm 25°C 37.5±0.2 and 35.3±0.2 nm 40°C 36.8±0.2 and 47.5±1.2 nm Polydispersity Index during storage for 1 day and 90 days 4°C 0.065 and 0.087 25°C 0.093 and 0.124 40°C 0.076 and 0.050 (Yang et al., 2017)	0.1% coffee oil-algae oil nanoemulsion could decrease water loss and erythema the HLB value 12.86
• Curcumin • Benzylisothiocyanate	Oil phase: a-tocopherol Surfactant: Sodium Stearoyl Lactate, Tween 80 Cosurfactant: Ethanol	• Droplet size Pure NE: 38 ± 3 nm BITC loaded: 45 ± 2 nm Curcumin loaded: 49 ± 3 nm BITC + curcumin: 53 ± 2 nm • Viscosity Pure NE: 1.41 ± 0.01 cP Curcumin loaded: 1.46 ± 0.02 cP BITC loaded: 1.45 ± 0.01 cP BITC + curcumin: 1.48 ± 0.01cP	• NE with addition of ethanol has good stability than NE without ethanol. • At 25⁰C, NE without ethanol showed increasing of droplet size. • At 4⁰C, NE showed increased size both NE and NE without ethanol. • BITC was loaded in NE showed high stability in alkaline conditions. Pure NE was stable under acidic and neutral condition. (Kaur et al., 2017)	When compared with empty nanoemulsion and curcumin nanoemulsion, benzilisothiocyanate nanoemulsion acted as a better antioxidant. The smallest droplet size was obtained at a concentration of 2% ethanol.

Jaboticaba (*plinia peruviana*) Extract	Oil phase: Caprylic/Capric Triglyceride Surfactant: Tween 80	Droplet size: 184.5 ± 3.96 nm Polydispersity Index: 0.185 ± 0.012 Zeta potential: -15.5 ± 5.37 mV	Stability studies of nanoemulsion were performed at room temperature over 120 days: Zeta potential nanoemulsion with extract: -21.5 - -36.7 mV (Mazzarino et al., 2017)	The nanoemulsion formula with 10% jaboticaba extract consisted of 5 % oil, 1 % surfactant, and 500 bar of homogenization pressure and also contained high phenolic activity.
Ubiquinone (Co-Q10)	Oil phase: Virgin Coconut Oil Surfactant: Tween 80, Span 80 Cosurfactant: Ethanol	Droplet size: 93.2 ± 2.78 nm Viscosity: 8.5 cPas	- (Erawati et al., 2018)	Co-Q10 nanoemulsion formula penetrated deeper than Co-Q10 emulsion formula.
Co-Q10	Oil phase: Isopropyl Myristate Surfactant: Tween 80 Cosurfactant: Transcutol HP	Droplet size: 11.76 ± 1.1 nm Polydispersity Index: 0.228 Zeta potential: 14.7 ± 1.23 mV Viscosity 199.05 ± 0.35 cP	18 formulations with various Surfactants: Co-surfactant ratio and drug concentration were evaluated for their thermodynamic stability using centrifugation, heating-cooling, and freeze-thaw tests, and a formula that passed three of the tests was selected. (El-Leithy et al., 2018)	The right formula to deliver Co-Q10 was a formula containing 10% w/w isopropyl myristate (Oil phase), 60% w/w of Tween 80: Transcutol HP mixture (S/cosmix) at ratio 2:1, 30% w /w water and 2% w/w Co-Q10.
Ellagic Acid	Oil phase: Isopropyl Myristate Surfactant: EL -40 Cosurfactant: Glycerol	Droplet size: 24.28 nm Zeta potential: −2.93 mV	The stability study consisted of the constant-temperature accelerated test, the high-speed centrifugation test, and the high-temperature test, after which no precipitation and no change in droplet size were observed in EA nanoemulsion. (Zhang et al., 2018)	Higher concentration of ellagic acid nanoemulsion,greater anti-aging effects.
• Caffeine (CAF) • Ethyl Ximenynate (EXM)	Oil phase: Isononanoate (EI), Dicaprylyl Ether (DE) Surfactant: Potassium Lauroyl Wheat Amino Acids, Palm Glycerides, Capryloyl Glycine	Droplet size: 30 - 50 nm	The stability of the nanoemulsion at room temperature (RT), 4^0C and 50 °C over 3 months was conducted to 15 formulas and 2 formulas was chosen with each 0.4% CAF and 0.8% EXM by visual inspection. Both of them were stable. (Musazzi et al., 2018)	Higher Dicaprylyl Ether concentration, higher clearness of system. Better EXM release When water content is higher at different oil and water ratios. Even though EXM and CAF have different polarities, there was no significant difference in permeation.

Tetraselmis tetrathele extract	Oil phase: Palm Kernel Oil Esters (PKOEs) Surfactant:Tween 80	Droplet size: 102.3 - 249.5 nm Zeta potential: - 33.2 to - 71.7 mV Viscosity: 79.19 Pa.s	In the 10-week stability test at 4, 25, and 45 °C T1 (20 wt% Tween 80) and T2 (15 wt% Tween 80) were stable but T3 (10 wt% Tween 80) precipitated at week eight. Of the three formulas, T1 has the best stability. (Farahin et al., 2019)	1% of *Tetraselmis tetrathele* extract was chosen in formula with 20% tween 80 and 8%.
Sunflower Oil	Oil phase: Sunflower oil Surfactant: Tween 80 Cosurfactant: Sorbitol	Droplet size: 124.47 nm Viscosity: 225 ± 25 cP	3 formulas were observed stability of its droplet size during 12 weeks and F1 was stable than others: • Droplet size F1 0-week 124.47 nm 6 weeks 307.17 nm 12 weeks 393.78 nm • Viscosity F1 0 week 225.0 ± 25.00 4 weeks 437.5 ± 21.65 6 weeks 562.5 ± 0.00 12 weeks 750.0 ± 50.00 (Arianto & Cindy, 2019)	For 12 weeks of storage at room temperature, low temperature, and high temperature, a nanoemulsion mixture containing 5% sunflower oil with a ratio of 38:22 surfactant Tween 80 and sorbitol with an SPF value of 5.43±0.03 demonstrated good stability.
Grape Seed Oil	Oil phase: Grape Seed Oil Surfactant: Tween 80 Cosurfactant: PEG 400	Droplet size: 163.82 nm Viscosity: 210 cP	Physical stability was observed during 8 weeks storage: Droplet size 438.50 nm Viscosity 550 cp (Sumaiyah & Leisyah, 2019)	F3 with 6% grape seed oil was chosen from 3 formulas of nanoemulsion due to its highest improvement in anti-aging activity (moisture, evenness and pore, spots, and wrinkles).
• Centella Asiatica • *Lycopersicon esculentum* Mil. • *Moringa oleifera* Lam. Extract	Oil phase: Virgin Coconut Oil Surfactant: Tween 80	Droplet size: 197 ± 2.18 nm Polydispersity Index: 0.23 ± 0.01 Zeta potential: -17.1 ± 0.26 mV Viscosity: 2.55 ± 0.03 cP	At a temperature of 25°C, droplet size and polydispersity index values were constant while the zeta potential value changed for 3 days. However, at low temperature and high temperature, droplet size increases. Thus, the appropriate temperature for nanoemulsion stability is 25°C. (Limthin & Phromyothin, 2019)	A good formulation is a nanoemulsion containing 1% extract with a ratio of water, virgin coconut oil and surfactant Tween 80 is 80:10:10 with a homogenization of 4000 rpm for 20 minutes.

Sucupira Oil	Oil phase: Sucupira oil Surfactant: Span 80, Tween 80	Droplet size: 150 nm Polydispersity Index: 0.2 Conductivity: 90 to 100 µs/cm	Stability Droplet size Day 1 4°C: 152.4±5.7 nm 25°C: 151.1±4.1 nm 45°C: 149.6±6.0 nm Day 90 4°C: 150.9±5.2 nm 25°C: 149.8±4.5 nm 45°C: 161.6±5.9 nm (Pacheco et al., 2019)	Treatment with a concentration of 5 g/ml Sucupira could significantly inhibit interleukin IL-6 and IL-8 in irradiated keratinocytes. It was very suitable for UVA radiation treatment.
• Retinyl Palmitate • Dead Sea Water	Oil phase: Sunflower Seed Oil, Arlamol™ HD oil Surfactant: Brij 96	Droplet size: 50 to 180 nm	- (Garcia-Bilbao et al., 2020)	4.2%, w/w of Retinyl Palmitate (mixed with sunflower seed oil) dissolved in 15.8% w/w of Arlamol™ HD oil); 7% w/w of Dead Sea Water, 7% w/w of Brij 96, and 66% w/w of triple distilled water was chosen as final formula of nanoemulsion.

• Gotu kola
• Mangosteen Rind
• Cucumber
• Tomato Extract
	Oil phase: Avocado oil
	Surfactant: Tween 80, Span 80
		Droplet size: 1.64 ± 0.99 µm
		Viscosity: 1638 ± 1294 cP
			• Viscosity after 60 days
			  5 °C: 2180 cP
			  Ambient: 830 cP
			  40 °C: – (not stable)
			• Droplet size after 60 days
			  5°C: 822.2 nm
			  Ambient: 836.3 nm
			  40°C: 6511.7 nm
			(Septiyanti & Meliana, 2020)
				2% Gotu kola extract, 2% mangosteen rind extract, 2 % tomato extract and 4% cucumber extract with 2 % of avocado oil was chosen as suitable anti-aging formula.

Mangostin Peel Extract	Oil phase: Virgin Cocunut Oil (VCO)-PG Surfactant:Tween 20, Span 20	Droplet size: 28.67 ± 0.58 nm Polydispersity Index: 0.37 ± 0.01 Zeta potential: -48.50 ± 2.27 mV	After freeze-thaw cycle test, droplet size of formula with HLB value of 15.1 increased not significant. (Sungpud et al., 2020)	Ratio Span 20 and Tween 20 is 4:1 having an HLB value of 15.1 with 10% extract and VCO-PG was chosen as best formula.

• Vitamin C • Vitamin E • Curcumin (CAC)	Oil phase: Capmul MCM C8 (CA) Surfactant: Bacillus Subtilis as Surfactin Cosurfactant: Transcutol	• Droplet size (nm) SF:TR:CA 69.3±1.4 SF:TR:Vitamin C 176.46±0.50 SF:TR:Vitamin E 183.9±7.64 SF:TR: CAC 89.18±1.35 • Polydispersity Index SF:TR:CA 0.084±0.019 SF:TR:Vitamin C 0.108±0.014 SF:TR:Vitamin E 0.328±0.01 SF:TR: CAC 0.371±0.02 • Zeta potential (mV) SF:TR:CA -77.36±1.61 SF:TR:Vitamin C -82.7±1.9 SF:TR:Vitamin E -95.03±5.11 SF:TR: CAC -43.57±7.10	Stability was observed for 195 days at 25^0C, formula of curcumin (CAC) was not stable. Droplet size of Vitamin C formula increased: 190.57±0.3 nm Droplet size of Vitamin E decreased: 147.6 ± 1.9 nm Polydispersity index of Vitamin C: 0.183±0.06 Polydispersity index of Vitamin E: 0.126 ± 0.016 Zeta potential of Vitamin C: - 77.57±0.8 mV Zeta potential of Vitamin E: - 89.7±1.14 mV (Lewińska et al., 2020)	50% surfactin from Bacillus subtilis as surfactant, 30% Transcutol as cosurfactant and 20% Capmul MCM C8 (CA) as oil phase was the suitable formula to carry vitamin C and vitamin E which has anti-aging effects.
Ocimum Sanctum Linn	Oil phase: Tea seed oil Surfactant: Tween 20 Cosurfactant: PEG-400	Droplet size: 170.0±0.6 nm Polydispersity index: 0.143±0.010 Potential Zeta: -24.0±0.6 mV	Droplet size, PI and Zeta potential was stable and remained constant after heating-cooling cycles was conducted. (Chaiyana et al., 2020)	15% tea seed oil; 7.5% Tween 20; 7.5% PEG 400 and 70% Water was nanoemulsion formula to encapsulate 0.1% w/w *O. Sanctum* ethanolic extract.
Cordyceps Militaris	Oil phase: Sea buckthorn oil Surfactant: Tween 80 Cosurfactant: Chitosan	Droplet size: 87.0±2.1 nm Polydispersity Index: 0.089±0.023 Zeta potential: -26.20±2 mV	• Droplet size (nm) RT 87.0±2.1 4^0C 87.1±3 25^0C 114.5±2 60^0C 161.8 • Polydispersity Index RT 0.089±0.023 4^0C 0.100±0.030 25^0C 0.122±0.04 60^0C 0.106±0.04 • Zeta potential (mV) RT -26.20±2 4^0C -25.94±0.7 25^0C -19.81±0.5 60^0C -12±1.2 (Rupa et al., 2020)	88% Water (*Cordyceps*); 6% sea buckthorn oil; 6% surfactant; 0.1% chitosan cosurfactant is safe for topical use that contain good antioxidant.

Microbial Carotenoids	Oil phase: Buriti oil Surfactant:Tween 80, Span 80 Cosurfactant: Propylene glycol	Droplet size: 142.11 ± 0.92 nm Polydispersity index: 0.198 ± 0.017	Stability was conducted during 30 days Droplet size 0 day 142.11 ± 0.92 nm 15 days 148.47 ± 2.68 nm 30 days 147.72 ± 1.63 nm Polydispersity index 0 day 0.198 ± 0.161 15 days 0.133 ± 0.018 30 days 0.092 ± 0.011 (Mansur et al., 2020)	12% Tween 80; 3% Span 80; 2% Propylene glycol; 3% Buriti oil; 0.2% Microbial carotenoids and 0.1% Vitamin E with 10% OMC; 3% EHMC and 3% BZF-3 had SPF of 36 ± 1.5.
Retinyl Palmitate	Oil phase: Capryol 90 and Captex 355 Surfactant: KollipHor EL Cosurfactant: Transcutol HP	Droplet size: 16.71 nm Polydispersity index: 0.015 Zeta potential: -20.6 mV Viscosity: 77.48±1.73 cp	Stability of droplet size and polydispersity index was observed during 90 days at ambient conditions then no significant changes were observed. Droplet size: 16 nm Polydispersity index: 0.05 (Algahtani et al., 2020)	10% oil phase (ratio 2:1); 30% KollipHor EL; 15% Transcutol HP and 45% Water was chosen as best formula with drug content 98.87±0.55%.
Cordyceps militaris Extracts	Oil phase: Sugar squalene Surfactant: Tween 85	Droplet size: 157.1±2.6 nm Zeta potential: -15.8±0.3 mV	After heating-cooling cycle test, the droplet size increased that were less than 300 nm and polydispersity index was less than 0.4. (Marsup et al., 2020)	5% Tween 85; 10% Sugar squalene with 1% of *Cordyceps militaris* extract was chosen as best formulation of nanoemulsion that potent to deliver high amount extract to skin layer.
Curcumin	Oil phase: Medium Chain Triglycerides, Eucalyptol Surfactant: Tween 80 Cosurfactant: Soybean lecithin	Droplet size: 69 - 128 nm	- (Nikolic et al., 2020)	5% MCT; 5% Eucalyptol; 1% soybean lecithin; 9% Tween 80; 80% water was best formula and monoterpene eucalyptol could modify nanoemulsion strongly.
Green Coffee Beans Extract	Oil phase: Green Coffee Oil Surfactant: Poloxamer Cosurfactant: Soy lecithin	Droplet size: 224±0.98 Polydispersity index: 0.204±0.01 Zeta potential: −37.4±0.49 mV	- (Buzanello et al., 2020)	Higher content of green coffee oil, higher its antioxidant activity.

Carrot Seed Oil	Oil phase: Carrot Seed Oil Surfactant: Tween 80 Cosurfactant: Sorbitol 40 and 20	Droplet size: 338.34 nm Viscosity: 499.00±0.00 mpa	• Droplet size 4-weeks 411.86 nm 8-weeks 512.27 nm Viscosity 4-weeks 454.33±1.15 mpa 8-weeks 439.00±1.73 mpa (Arianto et al., 2021)	4% carrot seed oil; 40% Tween 80; 20% sorbitol as best formula had SPF value 20.28±0.218.
Bakuchiol	Oil phase: Bakuchiol Rich Extract Surfactant: Coco betaine, Surfactin	Droplet size: 221±4 nm Polydispersity index: 0.182±0.01 Zeta potential: 73±5 mV	Stability test with freeze-thaw 6 cycles was observed by visual inspection if there was no precipitation. (Lewińska et al., 2021)	The best formula of nanoemulsion was 5% Surfactant (Coco betaine: Surfactin = 4:1); 1% Oil phase and 94% water phase.
Ceramide-Like Molecule	Oil phase: Oleic acid Surfactant: Tween 80	Droplet size: 231 – 277 nm Polydispersity index: 0.137 – 0.365 Zeta potential: – (29±3) to – (34±5) mV	30 days stability test resulted that nanoemulsion preparation was stable by visual inspection. (Guzman et al., 2021)	Oil: surfactant ratio was 1 and 73% water could encapsulated up to 2.0% ceramide-like molecule.
Levan	Oil phase: Ascorbyl Tetraisopalmitate Surfactant: Sodium Surfactin Powder Cosurfactant: Transcutol HP	Droplet size: 143.9±74 - 385.2±26.6 nm Polydispersity Index: 0.171±0.02 – 0.430±0.01 Zeta potential: – 18.04±0.42 to 40.34±0.84 mV	After 90 days Droplet size: 91.6±5.5 – 195.7±7.5 nm Polydispersity Index: 0.094±0.010 – 0.650±0.120 Zeta potential: – 14.07±1.36 to 38.27±1.26 mV (Lewińska et al., 2021)	50% sodium surfactin powder;30% Transcutol HP; 20% ascorbyl tetraisopalmitate was a formula of nanoemulsion and this formula was added by pentylene glycol, 1.2-hexanediol and butylene glycol as preservatives to enhance its stability during 90 days.

Discussion

The stability of the nanoemulsion is determined by the composition and characteristics of the oil phase, surfactant, and cosurfactant. Stability tests on nanoemulsions were carried out to investigate the stability of the droplet size and to observe changes in stability, such as no phase separation. Stability consists of physical and chemical stability. The stability of nanoemulsion can be interpreted that the preparation does not change or change within the permissible limits related to physical, chemical, microbiological, therapeutic, and toxicological characteristics (Rai et al., 2018). Physical and chemical stability is one of the important criteria for the success of a preparation. Physical stability was observes physical changes in preparation such as organoleptic examination, pH, homogeneity, specific gravity, and changes in nanoemulsion characteristics. Physical stability can be reviewed by comparing the physical properties of the preparation before and after the centrifugation test, thermal cycling, and real-time methods (Zothanpuii et al., 2020) .

The instability of nanoemulsions occurs through several mechanisms such as gravity separation, flocculation, coalescence, and ostwald ripening. This instability affects the increase in droplet size. Gravity separation occurs were characterized by the appearance of creaming and sedimentation because the density of internal phase is lower or higher than the surrounding environment. Gravity separation can be overcome by adding a thickening agent so that the viscosity of the nanoemulsion increases. Flocculation and coalescence are aggregating droplet events and can be prevented by increasing repulsion rather than attraction (Bhattacharjee, 2019).

Table 2 shows ingredients that function as antioxidants, UV rays filters, moisturizing agents, and cell repairing agents that can help skin cope with aging in accordance with topical anti-aging functions (Li, 2015). Leaf and stem of Vellozia Squamata (Quintão et al., 2013), Tocotrienol (Han et al., 2013), propolis extract (Mauludin et al., 2015), quercetin (Dario, Oliveira, et al., 2016), vitamin E (Ramli et al., 2017), *Clinacanthus nutans* (L.) leaves (Che Sulaiman et al., 2016), β-D-glucan polysaccharides extract (Alzorqi et al., 2016), curcumin (Nikolic et al., 2020) and benzyl isothiocyanate (Kaur et al., 2017), Jaboticaba (*Plinia peruviana*) extract (Letícia Mazzarino et al., 2018), *Tetraselmis tetrathele* (Farahin et al., 2019), grape seed oil (Sumaiyah & Leisyah, 2019), Centella Asiatica/*Lycopersicon esculentum* Mill./*Moringa oleifera* Lam. extract (Limthin & Phromyothin, 2019), Gotu kola/mangosteen rind/cucumber/tomato extract (Septiyanti & Meliana, 2020), Mangostin peel extract (Sungpud et al., 2020), *Cordyceps militaris* (Marsup et al., 2020; Rupa et al., 2020) and Green coffee beans extract (Buzanello et al., 2020), vitamin C/vitamin E (Lewińska et al., 2020) are an antioxidant compounds that play a role in protecting the skin from UV radiation, cigarette smoke and also hypoxia. Antioxidants can protect the skin from free radicals that cause aging by increasing collagen production. Antioxidants are stable compounds that donate electrons to reactive free radicals and neutralize them, reducing their capacity to damage surrounding cells. Antioxidants delay or inhibit cell damage. Free radicals come from endogenous sources (fibroblast, respiratory chain, inflammatory cells, epithelial cells) as well as from exogenous sources such as exposure to ultraviolet light, smoking, air pollution, and industrial chemicals. Antioxidants have two mechanisms for carrying out their functions. The first mechanism is chain cleavage, in which primary antioxidants give electrons to free radicals. The second mechanism is to help regenerate primary antioxidants, deactivate singlet oxygen, absorb ultraviolet radiation, bind metal ions, and reduce free radicals (Gulcin, 2020).

Cell repairing agents are retinyl palmitate (Clares et al., 2014), fullerene (Ngan et al., 2015), swiftlet nest (Taib et al., 2015), coffee oil/algae oil (Yang et al., 2017), co-Q10 (El-Leithy et al., 2018; Erawati et al., 2018), ellagic acid (Zhang et al., 2018), caffeine (CAF)/ethyl ximenynate (EXM) (Musazzi et al., 2018), *Ocimum sanctum* Linn (Wantida Chaiyana et al., 2020), bakuchiol (Lewińska et al., 2021), ceramide-like molecule (Guzman et al., 2021), and thistle oil (Miastkowska et al., 2016). The cell repairing agent stimulates and increases skin collagen production by increasing the ability to proliferate old dermis fibroblast cells (Li, 2015). When collagen production decreases with increasing age, the result is an increase in the process of "dry skin" and its elasticity properties.

Levan (Lewińska et al., 2021), *Opuntia ficus-indica* (L.) Mill Extract (Ribeiro et al., 2015), Ethoxylated Lanolin (EL)/Acetylated Lanolin (AL) (Pereira et al., 2016), and *Agave sisalana* (Barreto et al., 2017) are some of the active compounds from the articles in Table 2 which function as moisturizing agents. Moisturizing agents help maintain water in the skin's uppermost layer to prevent it from dry out. Based on the mechanism of action, moisturizers are divided into three types: occlusive, humectant, and emollient (Dini & Laneri, 2021). The action of occlusive moisturizer is to prevent transepidermal water loss (TEWL) in the stratum corneum so that dehydration does not occur in the skin. The mechanism of action of humectants as moisturizers is to attract water from the environment to enter the skin to be able to hydrate the stratum corneum. Emollients work by softening and filling cracked skin with oil droplets.

Exposure to UV rays on the skin can cause thinning of the skin barrier, the appearance of wrinkles, and also damage the DNA structure, causing skin cells to reduce their ability to regenerate to form new cells (Cao et al., 2020). Using an ultraviolet light scattering agent or UV absorber can reduce the negative impact of UV exposure. Hence, sunscreen to slow down aging is needed. From the selected articles, several active compounds that act as ultraviolet light scattering agents or UV absorbers are octyl methoxycinnamate (OMC)/titanium dioxide (Silva et al., 2013), ethyl hexyltriazone (EHT)/diethylamino hydroxy benzoyl hexyl benzoate (DHHB)/bemotrizinol (Tinosorb

S)/avobenzone (AVO)/ octyl methoxycinnamate (Puglia et al., 2014), sucupira oil (Pacheco et al., 2019), sunflower oil (Arianto & Cindy, 2019), retinyl palmitate and dead sea water (Garcia-Bilbao et al., 2020), microbial carotenoids (Mansur et al., 2020), and carrot seed oil (Arianto et al., 2021).

Furthermore, Table 2 describes the different types of surfactants, cosurfactants, and oil phases used in each study. The most important factors to avoid unstable formulas are surfactants, cosurfactants, and the oil phase. Surfactants are the first factor that plays a major role in the creation of nanoemulsions by reducing the interfacial tension between two immiscible liquids and causing them to become miscible as a result of the hydrophilic and hydrophobic groups that are present at the head and tail of each surfactant, respectively. The choice of surfactant depends on its solubility in oil and water, the HLB value, and its non-irritating properties to the skin (Rai et al., 2018). Table 1 shows several articles using two types of surfactants, single surfactants and the addition of cosurfactants with various oil phases. The combination of tween 80 and span 80 was the most commonly utilized surfactant among the 44 selected articles (Barreto et al., 2017; Erawati et al., 2018; Han et al., 2013; Mansur et al., 2020; Ngan et al., 2015; Pacheco et al., 2019; Ribeiro et al., 2015; Septiyanti & Meliana, 2020; Sulaiman et al., 2016; Yang et al., 2017). Next, among the ten articles that used a combination of tween 80 and span 80, the smallest droplet size of nanoemulsion with 36.7±0.2 nm was conducted by adding 0.1% coffee oil/algae oil phase (Yang et al., 2017) and it was stable at storage condition for 90 days by visual observation and the largest particle size of nanoemulsion with 170 nm was conducted with a palm kernel oil ester as the oil phase by Ngan et al. (2015) and the polydispersity index (PI) value close to zero which means the particle size distribution is good, so that showed good stability during 90 days of storage by centrifugation and freeze-thaw cycle tests. Tween 80 is a hydrophilic nonionic surfactant with an HLB value of 15.0, and Span 80 is a lipophilic nonionic surfactant with an HLB value of 4.3. In addition to its non-irritating nature, combining these two types of nonionic surfactants can reduce droplet size by providing steric stabilization. Steric stabilization is produced by nonionic surfactants having long polyoxyethylene chains with polar groups on the surfactant head. The polyoxyethylene chain of Tween 80 and the ring of Span 80 can form steric stabilization. The smaller the droplet size resulted in the smaller the aggregation rate, so this nanoemulsion is difficult to coalesce. In addition, the small particle size can be stored longer, is not easily damaged, the texture is not easy to change, and is easily absorbed by the skin.

The use of a single surfactant is also not infrequently used in nanoemulsion formulations such as tween 80 (Farahin et al., 2019; Guzman et al., 2021; Limthin & Phromyothin, 2019; L Mazzarino et al., 2018; Mohd Taib et al., 2015), tween 85 (Marsup et al., 2020), kolliphor®RH40 (polyoxyl 40 hydrogenated castor oil) (Alzorqi et al., 2016), brij 96 (Garcia-Bilbao

et al., 2020) and pluronic F68 (Puglia et al., 2014). Among these studies, research by Garcia-Bilbao et al. (2020) produced the smallest droplet size of 50 nm with 7% brij 96 as a surfactant, a mixture of sunflower seed oil and arlamol™ HD oil as the oil phase, and the largest droplet size from the research conducted by (Guzman et al., 2021) of 277 nm with a ratio of oleic acid and Tween 80 of 1, the polydispersity index value of 0.365, the zeta potential value of (-34±5) mV and also stable at storage for 30 days. The electrostatic repulsion between the scattered droplets close to each other is directly connected to the zeta potential, which is the difference between tightly bonded surface ions around a solution-neutral droplet (Marzuki et al., 2019). A high zeta potential value indicates that the emulsion is both physically and chemically stable, as repulsive forces tend to prevent flocculation. A good zeta potential value (positive and negative charge) indicates a stable nanoemulsion system, thereby reducing the droplet aggregation potential by 30 mV. If the zeta potential is positive, it implies that the positively charged particles in the suspension are dispersed. On the other hand, a negative zeta potential means that the negatively charged in the suspension is dispersed.

The second factor is the cosurfactant; cosurfactants are amphiphilic in a state without a tendency to be partitioned in large quantities at the surfactant interfacial monolayer (Harshitha et al., 2020). The cosurfactants commonly used are short to medium-chain alcohols (C3-C8), which assist the solubility of solutes in the dispersion medium by increasing the flexibility of the layer around the droplet area and lowering the surface free energy so that stability can be maintained. In addition, with the use of cosurfactants, the concentration of surfactant used can be reduced to reduce the risk of irritation that can be caused. In the articles reviewed, the most commonly used cosurfactant was Transcutol HP (Algahtani et al., 2020; El-Leithy et al., 2018; Lewińska et al., 2021; Agnieszka Lewińska et al., 2020) and ethanol (Buzanello et al., 2020; Erawati et al., 2018; Kaur et al., 2017) as well as several articles using sorbitol (Arianto et al., 2021; Arianto & Cindy, 2019), glycerine (Mauludin et al., 2015; Zhang et al., 2018), propylene glycol (Mauludin et al., 2015), PEG-400 (W. Chaiyana et al., 2020; Sumaiyah & Leisyah, 2019), chitosan (Rupa et al., 2020) and plurol oleique (Clares et al., 2014). Nanoemulsion with Transcutol HP as cosurfactant, ascorbyl tetraisopalmitate as oil phase, and sodium surfactin powder as surfactant had the largest droplet size of 385.2±26.6 nm, polydispersity index 0.430±0.01 and zeta potential value –18.04±0.42 (Lewińska et al., 2021). The polydispersity index value from this study is classified as polydispersity, indicating an extensive droplet size distribution so that the droplet size is very diverse and sedimentation is prone to occur. According to Stokes' Law, the speed of deposition is directly proportional to the size of the diameter of the particle, where if the diameter of the particle is small, then the speed of deposition is also low (long). The zeta potential value, smaller than 30 mV, also indicates less stability (Rai et al., 2018). Furthermore, the smallest

droplet size was 11.76 ± 1.1nm, Zeta potential - 14.7 ± 1.23mV, and Viscosity 199.05 ± 0.35 cp with Transcutol HP as cosurfactants, Tween 80 as surfactant, and isopropyl myristate as the oil phase (El-Leithy et al., 2018). The study showed good stability by visual observation.

From the above explanation, using single and combined surfactants produced good nanoemulsion characteristics, but the resulting stability was different. Nanoemulsions with combined surfactants produce better stability than single surfactants because they can provide a better balance of HLB values according to the desired type of nanoemulsion. The addition of cosurfactants is not something that must be added in a nanoemulsion system, but the cosurfactant itself can positively impact the nanoemulsion's stability (Sadoon & Ghareeb, 2020). Cosurfactants can increase the hydrocarbon tail's mobility so that the oil's penetration in the tail becomes greater.

When compared with studies using two surfactants and a single surfactant, the addition of cosurfactants and also the increase in surfactant concentration as in the study of El-Leithy et al. (2018) that 60% of the surfactant Tween 80 and cosurfactant Transcutol HP resulted in smaller emulsion droplet sizes due to the increase in surfactant molecules to absorb around the interface area to reduce the oil-water interfacial tension and dissolve large amounts of hydrophilic surfactants or hydrophobic drugs on the nanoemulsion system. Transcutol HP has advantages over other cosurfactants because it is non-volatile, almost odorless and transparent (Osborne & Musakhanian, 2018). When compared to ethanol, Transcutol HP has a higher boiling point so it does not limit the processing temperature.

The third most important factor is the selection of the type of oil; oil selection also plays an important role in nanoemulsion characteristics and stability. Oils contain long-chain triglycerides (LCT) because they contain more than 12 carbon chains. Apart from LCT, there are two other triglycerides classifications: medium-chain triglycerides (MCT) containing 6-12 carbon chains and short-chain triglycerides (SCT) containing less than six carbon chains (Zulkanain et al., 2020). Based on Table 2, the most frequently used type of oil is caprylic/capric triglyceride (Barreto et al., 2017; Dario et al., 2016; Mazzarino et al., 2017; Ribeiro et al., 2015). 19.99±0.07 nm is the smallest droplet size among research articles using caprilyc/capric triglyceride as the oil phase, oleth-20, oleth-3, cetyltrimethylammonium chloride as a surfactant (Dario et al., 2016). This study showed a positive zeta potential (+19.6±2.2 mV). These were due to the presence of the cationic surfactant cetyltrimethylammonium chloride. The polydispersity index value of 0.082 is classified as polydispersity, which means that the particle size distribution in the system varies. Caprylic/capric triglycerides are triglyceride oils from coconut oil or fatty acids and glycerin. This oil spreads easily and doesn't feel occlusive.

The lowest viscosity was 7.1 cP because Caprilyc/capric triglyceride was only 5% (Dario et al.,

2016). Caprylic/capric triglycerides are classified as medium-chain triglycerides (MCT). MCTs have unique physical properties. For example, MCTs are more polar than LCTs, so MCTs are more soluble in water. Oils with medium chain triglycerides (MCT) are stable at low and high temperatures, have low viscosity, and produce smaller droplet sizes than nanoemulsions with high viscosity oils (Erawati et al., 2018). This study showed the occurrence of ostwald ripening in the preparation during 90 days of storage. Although it produces a small droplet size, ostwald ripening also affects the stability of the nanoemulsion due to its low viscosity. Based on stokes' law (McClements, 2005), the lower the viscosity, the more distant the distance between the droplets, so they tend to bond with each other, and the kinetic energy will increase so that the deposition rate is high. Oils that have short to medium chains are more stable than long chains. These are because oils with short to medium chains are easier to break the chain and produce clearer formula when compared to oils with long chains.

The largest droplet size was 277 nm with oleic acid as its oil phase, tween 80 as a single surfactant with 75% water percentage, and a potential zeta value (-29±3) mV (Guzman et al., 2021). However, when the water percentage decreased to 73%, the percentage of oleic acid and surfactant was increased, the droplet size became smaller, and increased the encapsulation of the ceramide-like molecule. These are because the solubility of the ceramide-like molecule to oleic acid increases so that the ceramide-like molecule is easily trapped in the oleic acid, and the concentration of surfactant used can reduce the surface tension so that it has good stability. Oleic acid (C18:1) is an unsaturated fatty acid that is lipophilic and non-polar (Rowe et al., 2006). These are in accordance with the statement of Harshitha et al. (2020) that the oil phase used can also affect the droplet size and stability of the formed nanoemulsion. The oil phase in the nanoemulsion acts as a carrier that can dissolve hydrophobic active substances and form droplets in the dispersion medium in the presence of surfactants and cosurfactants. The fatty acids generate a negative charge on the zeta potential in oleic acid (Zhao et al., 2010). Due to the wide range of absolute zeta potential values, limiting zeta potential values cannot be used to predict the stability of nanoemulsions. The physical stability of the produced emulsion may be partially determined by the zeta potential.

CONCLUSION

The effectiveness of anti-aging ingredients like antioxidants, photoprotective agents, moisturizing agents, and cell repairing agents could be improved by using nanoemulsions as carriers. The physical stability of nanoemulsions is affected by factors such as droplet size, zeta potential, polydispersity index, and viscosity. The composition and characteristics of the oil, surfactant, and cosurfactant have an impact on the characteristics and physical stability of the nanoemulsion itself. According to the findings of the

literature research, Tween 80, Span 80, Transcutol HP, and caprylic/capric triglyceride, which is referred to as MCT oil, were found to be the most often used surfactants, cosurfactants, and oils in the review articles. The type of surfactant and cosurfactant used, as well as their ratio, influence the characteristics and stability of nanoemulsions. Since the oil's physicochemical characteristics (molecular weight, polarity, and viscosity) have a significant impact on the nano emulsification spontaneously, nanoemulsion droplet size, and drug solubility, the oil phase plays a key role in the nanoemulsion formulation. The oil chosen for the nanoemulsion formulation is one that can produce nanoemulsions with tiny droplet sizes and can dissolve the drug as much as possible. The characteristics of the nanoemulsion also affect the physical stability. According to Stokes' law, physical stability is affected by particle size and viscosity. Characteristics that include particle size and viscosity will affect the physical stability of a preparation. As stated by Stokes' law, particle size and viscosity are important characteristics because they determine the homogeneity of the formed system, namely: the separation rate increases with increasing particle size, the more significant the difference between the density of the medium and the particles and the decrease in viscosity.

LIMITATIONS

Some articles published in 2022 are not fully accessible, and the author did not investigate the chemical stability of these articles; Chemical stability is one of the stabilities regarding the length of time a preparation maintains its chemical content and potency.

CONTRIBUTION

The author states that a potential conflict of interest does not exist in this article review.

ACKNOWLEDGEMENT

REFERENCES

Ahmed, I. A., Mikail, M. A., Zamakshshari, N., & Abdullah, A. S. H. (2020). Natural Anti-Aging Skincare: Role and Potential. *Biogerontology*; *21*(3); 293–310. https://doi.org/10.1007/s10522-020-09865-z

Algahtani, M.S., Ahmad, M. Z., & Ahmad, J. (2020). Nanoemulgel for Improved Topical Delivery of Retinyl Palmitate: Formulation Design and Stability Evaluation. *Nanomaterials*; *10*(5); 848. https://doi.org/10.3390/nano10050848

Alzorqi, I., Ketabchi, M. R., Sudheer, S., & Manickam, S. (2016). Optimization of Ultrasound Induced Emulsification on the Formulation of Palm-Olein Based Nanoemulsions for the Incorporation of Antioxidant β-d-Glucan Polysaccharides. *Ultrasonics Sonochemistry*; *31*; 71–84.

https://doi.org/10.1016/j.ultsonch.2015.12.004

Arianto, A., Bangun, H., Sumaiyah., & Siregar, C. N. D. Y. P. (2021). The Use of Carrot Seed Oil (Daucus Carota L.) to Formulate Nanoemulgels as an Effective Natural Sunscreen and Skin Anti-Aging. *International Journal of Applied Pharmaceutics*; *14*(1); 124–129. https://doi.org/10.22159/ijap.2022v14i1.43481

Arianto, A., & Cindy, C. (2019). Preparation and Evaluation of Sunflower Oil Nanoemulsion as a Sunscreen. *Open Access Macedonian Journal of Medical Sciences*; *7*(22); 3757–3761. https://doi.org/10.3889/oamjms.2019.497

Barreto, S. M. A. G., Maia, M. S., Benicá, A. M., de Assis, H. R. B. S., Leite-Silva, V. R., da Rocha-Filho, P. A., de Negreiros, M. M. F., de Oliveira Rocha, H. A., Ostrosky, E. A., Lopes, P. S., de Farias Sales, V. S., Giordani, R. B., & Ferrari, M. (2017). Evaluation of In Vitro and In Vivo Safety of the By-Product of Agave Sisalana as a New Cosmetic Raw Material: Development and Clinical Evaluation of a Nanoemulsion to Improve Skin Moisturizing. *Industrial Crops and Products*; *108*; 470–479. https://doi.org/10.1016/j.indcrop.2017.06.064

Bhattacharjee, K. (2019). Importance of Surface Energy in Nanoemulsion. *Nanoemulsions - Properties, Fabrications and Applications*; 1–20. https://doi.org/10.5772/intechopen.84201

Buzanello, E. B., Pinheiro Machado, G. T. B., Kuhnen, S., Mazzarino, L., & Maraschin, M. (2020). Nanoemulsions Containing Oil and Aqueous Extract of Green Coffee Beans with Antioxidant and Antimicrobial Activities. *Nano Express*; *1*(1); 010058. https://doi.org/10.1088/2632-959X/ab9c47

Cao, C., Xiao, Z., Wu, Y., & Ge, C. (2020). Diet and Skin Aging—from the Perspective of Food Nutrition. *Nutrients*; *12*(3); 1–29. https://doi.org/10.3390/nu12030870

Chaiyana, W., Anuchapreeda, S., Somwongin, S., Marsup, P., Lee, K. H., Lin, W. C., & Lue, S. C. (2020). Dermal Delivery Enhancement of Natural Anti-Ageing Compounds from Ocimum Sanctum Linn. Extract by Nanostructured Lipid Carriers. *Pharmaceutics*; *12*(4); 309. https://doi.org/10.3390/pharmaceutics12040309

Che Sulaiman, I. S., Basri, M., Fard Masoumi, H. R., Ashari, S. E., & Ismail, M. (2016). Design and Development of a Nanoemulsion System Containing Extract of Clinacanthus Nutans (L.) Leaves for Transdermal Delivery System by D-Optimal Mixture Design and Evaluation of Its Physicochemical Properties. *RSC Advances*; *6*(71); 67378–67388. https://doi.org/10.1039/C6RA12930G

Clares, B., Calpena, A. C., Parra, A., Abrego, G., Alvarado, H., Fangueiro, J. F., & Souto, E. B. (2014). Nanoemulsions (NEs), Liposomes (LPs) and Solid Lipid Nanoparticles (SLNs) for Retinyl Palmitate: Effect on Skin Permeation.

International Journal of Pharmaceutics; *473*(1–2); 591–598. https://doi.org/10.1016/j.ijpharm.2014.08.001

Cousins, S., Blencowe, N. S., & Blazeby, J. M. (2019). What is an Invasive Procedure? A Definition to Inform Study Design, Evidence Synthesis and Research Tracking. *BMJ Open*; *9*(7); 2018–2020. https://doi.org/10.1136/bmjopen-2018-028576

Dario, M. F., Oliveira, C. A., Cordeiro, L. R. G., Rosado, C., Mariz, I. de F. A., Maçôas, E., Santos, M. S. C. S., Minas da Piedade, M. E., Baby, A. R., & Velasco, M. V. R. (2016). Stability and Safety of Quercetin-Loaded Cationic Nanoemulsion: In Vitro and In Vivo Assessments. *Colloids and Surfaces A: Physicochemical and Engineering Aspects*; *506*; 591–599. https://doi.org/10.1016/j.colsurfa.2016.07.010

Dario, M. F., Santos, M. S. C. S., Viana, A. S., Arêas, E. P. G., Bou-Chacra, N. A., Oliveira, M. C., da Piedade, M. E. M., Baby, A. R., & Velasco, M. V. R. (2016). A High Loaded Cationic Nanoemulsion for Quercetin Delivery Obtained by Sub-PIT Method. *Colloids and Surfaces A: Physicochemical and Engineering Aspects*; *489*; 256–264. https://doi.org/10.1016/j.colsurfa.2015.10.031

Dini, I., & Laneri, S. (2021). The New Challenge of Green Cosmetics: Natural Food Ingredients for Cosmetic Formulations. *Molecules*; *26*(13); 3921. https://doi.org/10.3390/molecules26133921

El-Leithy, E. S., Makky, A. M., Khattab, A. M., & Hussein, D. G. (2018). Optimization of Nutraceutical Coenzyme Q10 Nanoemulsion with Improved Skin Permeability and Anti-Wrinkle Efficiency. *Drug Development and Industrial Pharmacy*; *44*(2); 316–328. https://doi.org/10.1080/03639045.2017.1391836

Erawati, T., Soeratri, W., & Rosita, N. (2018). Skin Penetration of Ubiquinone (Co-Q10) in Nanoemulsion Delivery System using Virgin Coconut Oil (VCO). *International Journal of Drug Delivery Technology*; *8*(2); 77–79. https://doi.org/10.25258/ijddt.v8i2.13871

Farahin, A. W., Yusoff, F. M., Basri, M., Nagao, N., & Shariff, M. (2019). Use of Microalgae: Tetraselmis Tetrathele Extract in Formulation of Nanoemulsions for Cosmeceutical Application. *Journal of Applied Phycology*; *31*(3); 1743–1752. https://doi.org/10.1007/s10811-018-1694-9

Garcia-Bilbao, A., Gómez-Fernández, P., Larush, L., Soroka, Y., Suarez-Merino, B., Frušić-Zlotkin, M., Magdassi, S., Goñi-de-Cerio, F., Gomez-Fernandez, P., Larush, L., Soroka, Y., Suarez-Merino, B., Frusic-Zlotkin, M., Magdassi, S., & Goni-de-Cerio, F. (2020). Preparation, Characterization, and Biological Evaluation of Retinyl Palmitate and Dead Sea Water Loaded Nanoemulsions toward Topical Treatment of Skin Diseases. *Journal of Bioactive and Compatible Polymers*; *35*(1); 24–38. https://doi.org/10.1177/0883911519885970

Gulcin, İ. (2020). Antioxidants and Antioxidant Methods: An Updated Overview. *Archives of Toxicology*; *94*(3); 651-715. https://doi.org/10.1007/s00204-020-02689-3

Guzman, E., Fernandez-Pena, L., Rossi, L., Bouvier, M., Ortega, F., Rubio, R. G., Guzmán, E., Fernández-Peña, L., Rossi, L., Bouvier, M., Ortega, F., & Rubio, R. G. (2021). Nanoemulsions for the Encapsulation of Hydrophobic Actives. *Cosmetics*; *8*(2); 45. https://doi.org/10.3390/cosmetics8020045

Han, N. S., Woi, P. M., Basri, M., & Ismail, Z. (2013). Characterization of Structural Stability of Palm Oil Esters-Based Nanocosmeceuticals Loaded with Tocotrienol. *Journal of Nanobiotechnology*; *11*(1); 27. https://doi.org/10.1186/1477-3155-11-27

Harshitha, V., Swamy, M. V., Kumar, D. P., Rani, K. S., & Trinath, A. (2020). Nanoemulgel: A Process Promising in Drug Delivery System. *Research Journal of Pharmaceutical Dosage Forms and Technology*; *12*(2); 125. https://doi.org/10.5958/0975-4377.2020.00022.1

Harwansh, R. K., Deshmukh, R., & Rahman, A. (2019). Nanoemulsion: Promising Nanocarrier System for Delivery of Herbal Bioactives. *Journal of Drug Delivery Science and Technology; 51*; 224-233. https://doi.org/10.1016/j.jddst.2019.03.006

Kaur, K., Kaur, J., Kumar, R., & Mehta, S. K. (2017). Formulation and Physiochemical Study of α-Tocopherol based Oil in Water Nanoemulsion Stabilized with Non Toxic, Biodegradable Surfactant: Sodium Stearoyl Lactate. *Ultrasonics Sonochemistry*; *38*; 570–578. https://doi.org/10.1016/j.ultsonch.2016.08.026

Lewińska, A., Domżał-Kędzia, M., Kierul, K., Bochynek, M., Pannert, D., Nowaczyk, P., & Łukaszewicz, M. (2021). Targeted Hybrid Nanocarriers as a System Enhancing the Skin Structure. *Molecules*; *26*(4); 1063. https://doi.org/10.3390/molecules26041063

Lewińska, A., Domżał-Kędzia, M., Jaromin, A., Łukaszewicz, M., Lewinska, A., Domzal-Kedzia, M., Jaromin, A., & Lukaszewicz, M. (2020). Nanoemulsion Stabilized by Safe Surfactin from Bacillus Subtilis as a Multifunctional, Custom-Designed Smart Delivery System. *Pharmaceutics*; *12*(10); 953. https://doi.org/10.3390/pharmaceutics12100953

Lewińska, A., Domżał-Kędzia, M., Maciejczyk, E., Łukaszewicz, M., & Bazylińska, U. (2021). Design and Engineering of "Green" Nanoemulsions for Enhanced Topical Delivery of Bakuchiol Achieved in a Sustainable Manner: A Novel Eco-Friendly Approach to Bioretinol. *International Journal of Molecular Sciences*; *22*(18); 10091. https://doi.org/10.3390/ijms221810091

Li, X. (2015). Anti-Aging Cosmetics and Its Efficacy Assessment Methods. *IOP Conference Series: Materials Science and Engineering*; *87*(1); 4–9.

https://doi.org/10.1088/1757-899X/87/1/012043

Li, Z., Zhang, Z., Ren, Y., Wang, Y., Fang, J., Yue, H., Ma, S., & Guan, F. (2021). Aging and Age-Related Diseases: From Mechanisms to Therapeutic Strategies. *Biogerontology*; *22*(2); 165–187. https://doi.org/10.1007/s10522-021-09910-5

Limthin, D., & Phromyothin, D. (2019). Improving Stability of Nanoemulsion Containing Centella Asiatica, Lycopersicon Esculentum Mil. and Moringa Oleifera Lam. Extract. *Materials Today: Proceedings*; *17*; 1852–1863. https://doi.org/10.1016/j.matpr.2019.06.223

Mansur, M. C. P. P. R., Campos, C., Vermelho, A. B., Nobrega, J., da Cunha Boldrini, L., Balottin, L., Lage, C., Rosado, A. S., Ricci-Júnior, E., & dos Santos, E. P. (2020). Photoprotective Nanoemulsions Containing Microbial Carotenoids and Buriti Oil: Efficacy and Safety Study. *Arabian Journal of Chemistry*; *13*(8); 6741–6752. https://doi.org/10.1016/j.arabjc.2020.06.028

Marsup, P., Yeerong, K., Neimkhum, W., Sirithunyalug, J., Anuchapreeda, S., To-Anun, C., & Chaiyana, W. (2020). Enhancement of Chemical Stability and Dermal Delivery of Cordyceps Militaris Extracts by Nanoemulsion. *Nanomaterials*; *10*(8); 1565. https://doi.org/10.3390/nano10081565

Marzuki, N. H. C., Wahab, R. A., & Hamid, M. A. (2019). An Overview of Nanoemulsion: Concepts of Development and Cosmeceutical Applications. *Biotechnology & Biotechnological Equipment*; *33*(1); 779–797. https://doi.org/10.1080/13102818.2019.1620124

Mauludin, R., Primaviri, D. S. S., & Fidrianny, I. (2015). Nanoemulsion of Ethanolic Extracts of Propolis and Its Antioxidant Activity. *AIP Conference Proceedings*; *1677*; 100011. https://doi.org/10.1063/1.4930769

Mazzarino, L., da Silva Pitz, H., Lorenzen Voytena, A. P., Dias Trevisan, A. C., Ribeiro-Do-Valle, R. M., & Maraschin, M. (2017). Jaboticaba (Plinia Peruviana) Extract Nanoemulsions: Development, Stability, and In Vitro Antioxidant Activity. *Drug Development and Industrial Pharmacy*; *44*(4); 643–651. https://doi.org/10.1080/03639045.2017.1405976

McClements, D. J. (2005). Food Emulsions: Principles, Practicies, and Techniques. Boca Raton: CRC Press.

Miastkowska, M. A., Banach, M., Pulit-Prociak, J., Sikora, E. S., Głogowska, A., & Zielina, M. (2016). Statistical Analysis of Optimal Ultrasound Emulsification Parameters in Thistle-Oil Nanoemulsions. *Journal of Surfactants and Detergents*; *20*(1); 233–246. https://doi.org/10.1007/s11743-016-1887-7

Mohd Taib, S. H., Abd Gani, S. S., Ab Rahman, M. Z., Basri, M., Ismail, A., & Shamsudin, R. (2015). Formulation and Process Optimizations of Nano-

Cosmeceuticals Containing Purified Swiftlet Nest. *RSC Advances*; *5*(53); 42322–42328. https://doi.org/10.1039/C5RA03008K

Musazzi, U. M., Franze, S., Minghetti, P., & Casiraghi, A. (2018). Emulsion versus Nanoemulsion: How Much is the Formulative Shift Critical for a Cosmetic Product? *Drug Delivery And Translational Research*; *8*(2); 414–421. https://doi.org/10.1007/s13346-017-0390-7

Ngan, C. L., Basri, M., Tripathy, M., Abedi Karjiban, R., & Abdul-Malek, E. (2015). Skin Intervention of Fullerene-Integrated Nanoemulsion in Structural and Collagen Regeneration Against Skin Aging. *European Journal of Pharmaceutical Sciences*; *70*; 22–28. https://doi.org/10.1016/j.ejps.2015.01.006

Nikolic, I., Mitsou, E., Pantelic, I., Randjelovic, D., Markovic, B., Papadimitriou, V., Xenakis, A., Lunter, D. J., Zugic, A., & Savic, S. (2020). Microstructure and Biopharmaceutical Performances of Curcumin-Loaded Low-Energy Nanoemulsions Containing Eucalyptol and Pinene: Terpenes' Role Overcome Penetration Enhancement Effect? *European Journal of Pharmaceutical Sciences*; *142*; 105135. https://doi.org/10.1016/j.ejps.2019.105135

Osborne, D. W., & Musakhanian, J. (2018). Skin Penetration and Permeation Properties of Transcutol®—Neat or Diluted Mixtures. *AAPS PharmSciTech*; *19*(8); 3512–3533. https://doi.org/10.1208/s12249-018-1196-8

Pacheco, M. T., Silva, A. C. G., Nascimento, T. L., Diniz, D. G. A., Valadares, M. C., & Lima, E. M. (2019). Protective Effect of Sucupira Oil Nanoemulsion against Oxidative Stress in UVA-Irradiated HaCaT Cells. *Journal of Pharmacy and Pharmacology*; *71*(10); 1532–1543. https://doi.org/10.1111/jphp.13148

Pereira, T., Guerreiro, C., Maruno, M., Ferrari, M., & Rocha-Filho, P. (2016). Exotic Vegetable Oils for Cosmetic O/W Nanoemulsions: In Vivo Evaluation. *Molecules*; *21*(3); 248. https://doi.org/10.3390/molecules21030248

Puglia, C., Damiani, E., Offerta, A., Rizza, L., Tirendi, G. G., Tarico, M. S., Curreri, S., Bonina, F., & Perrotta, R. E. (2014). Evaluation of Nanostructured Lipid Carriers (NLC) and Nanoemulsions as Carriers for UV-Filters: Characterization, In Vitro Penetration and Photostability Studies. *European Journal of Pharmaceutical Sciences*; *51*(1); 211–217. https://doi.org/10.1016/j.ejps.2013.09.023

Quintão, F. J. O., Tavares, R. S. N., Vieira-Filho, S. A., Souza, G. H. B., & Santos, O. D. H. (2013). Hydroalcoholic Extracts of Vellozia Squamata: Study of Its Nanoemulsions for Pharmaceutical or Cosmetic Applications. *Revista Brasileira de Farmacognosia*; *23*(1); 101–107. https://doi.org/10.1590/S0102-695X2013005000001

Rai, V. K., Mishra, N., Yadav, K. S., & Yadav, N. P.

(2018). Nanoemulsion as Pharmaceutical Carrier for Dermal and Transdermal Drug Delivery: Formulation Development, Stability Issues, Basic Considerations and Applications. *Journal of Controlled Release;* *270*; 203-225. https://doi.org/10.1016/j.jconrel.2017.11.049

Ramli, S., Norhman, N., Zainuddin, N., Ja'afar, S. M., & Rahman, I. A. (2017). Nanoemulsion Based Palm Olein as Vitamin E Carrier. *Malaysian Journal of Analytical Sciences*; *21*(6); 1399–1408. https://doi.org/10.17576/mjas-2017-2106-22

Ribeiro, R., Barreto, S., Ostrosky, E., Rocha-Filho, P., Veríssimo, L., & Ferrari, M. (2015). Production and Characterization of Cosmetic Nanoemulsions Containing Opuntia Ficus-Indica (L.) Mill Extract as Moisturizing Agent. *Molecules*; *20*(2); 2492–2509. https://doi.org/10.3390/molecules20022492

Rowe, R., Sheskey, P., & Owen, S. (2006). Handbook of Pharmaceutical Excipients Fifth Edition. Chicago: APhA Publications.

Rupa, E. J., Li, J. F., Arif, M. H., Yaxi, H., Puja, A. M., Chan, A. J., Hoang, V.-A. A., Kaliraj, L., Yang, D. C., & Kang, S. C. (2020). Cordyceps Militaris Fungus Extracts-Mediated Nanoemulsion for Improvement Antioxidant, Antimicrobial, and Anti-Inflammatory Activities. *Molecules*; *25*(23); 5733. https://doi.org/10.3390/molecules25235733

Sadoon, N. A., & Ghareeb, M. M. (2020). Formulation and Characterization of Isradipine as Oral Nanoemulsion. *Iraqi Journal of Pharmaceutical Sciences*; *29*(1); 143–153. https://doi.org/10.31351/vol29iss1pp143-153

Septiyanti, M., & Meliana, Y. (2020). Characterization of Nanoemulsion Gotukola, Mangosteen Rind, Cucumber and Tomato Extract for Cosmetic Raw Material. *Journal of Physics: Conference Series*; *1442*; 012046. https://doi.org/10.1088/1742-6596/1442/1/012046

Silva, F. F. F., Ricci-Júnior, E., & Mansur, C. R. E. (2013). Nanoemulsions Containing Octyl Methoxycinnamate and Solid Particles of TiO 2: Preparation, Characterization and In Vitro Evaluation of the Solar Protection Factor. *Drug Development and Industrial Pharmacy*; *39*(9); 1378–1388. https://doi.org/10.3109/03639045.2012.718787

Sulaiman, I. S. C., Basri, M., Fard Masoumi, H. R., Ashari, S. E., & Ismail, M. (2016). Design and Development of a Nanoemulsion System Containing Extract of Clinacanthus Nutans (L.) Leaves for Transdermal Delivery System by D-Optimal Mixture Design and Evaluation of Its Physicochemical Properties. *RSC Advances*; *6*(71); 67378–67388. https://doi.org/10.1039/C6RA12930G

Sumaiyah, & Leisyah, B. M. M. (2019). The Effect of Antioxidant of Grapeseed Oil as Skin Anti-Aging in Nanoemulsion and Emulsion Preparations. *Rasayan Journal of Chemistry*; *12*(3); 1185–1194.

https://doi.org/10.31788/RJC.2019.1235337

Sungpud, C., Panpipat, W., Chaijan, M., & Yoon, A. S. (2020). Techno-Biofunctionality of Mangostin Extractloaded Virgin Coconut Oil Nanoemulsion and Nanoemulgel. *PLoS One*; *15*(1); 1–22. https://doi.org/10.1371/journal.pone.0227979

Yang, C.-C., Hung, C. F., & Chen, B. H. (2017). Preparation of Coffee Oil-Algae Oil-Based Nanoemulsions and the Study of Their Inhibition Effect on UVA-Induced Skin Damage in Mice and Melanoma Cell Growth. *International Journal of Nanomedicine*; *12*; 6559–6580. https://doi.org/10.2147/IJN.S144705

Zhang, H., Zhao, Y., Ying, X., Peng, Z., Guo, Y., Yao, X., & Chen, W. (2018). Ellagic Acid Nanoemulsion in Cosmetics: The Preparation and Evaluation of a New Nanoemulsion Method as a Whitening and Antiaging Agent. *IEEE Nanotechnology Magazine*; *12*(1); 14–20. https://doi.org/10.1109/MNANO.2017.2780859

Zhao, Y., Wang, C., Chow, A. H. L., Ren, K., Gong, T., Zhang, Z., & Zheng, Y. (2010). Self-Nanoemulsifying Drug Delivery System (SNEDDS) for Oral Delivery of Zedoary Essential Oil: Formulation and Bioavailability Studies. *International Journal of Pharmaceutics*; *383*(1–2); 170–177. https://doi.org/10.1016/j.ijpharm.2009.08.035

Zothanpuii, F., Ravindran, R., & Kanthiah, S. (2020). A Review on Stability Testing Guidelines of Pharmaceutical Products. *Asian Journal of Pharmaceutical and Clinical Research*; *13*(10); 3–9. https://doi.org/10.22159/ajpcr.2020.v13i10.38848

Zulkanain, N. I., Ab-Rahim, S., Camalxaman, S. N., & Mazlan, M. (2020). Medium-Chain Fatty Acids in Nutritional Therapy: A Review. *Malaysian Journal of Fundamental and Applied Sciences;* *16*(3); 318–323. https://doi.org/10.11113/mjfas.v16n3.1610

Growth Inhibitory Effects of Red and Yellow Passion Fruits against MRSA and ESBL-producing Bacteria

Aprelita Nurelli Dwiana[1,2], Achmad Toto Poernomo[1], Iif Hanifa Nurrosyidah[3], Isnaeni[5], Dian Rahmawaty[4], Idha Kusumawati[1*]

[1]Department of Pharmaceutical Sciences, Faculty of Pharmacy, Universitas Airlangga, Surabaya, Indonesia
[2]Master Student of Study Program of Magister Sciences, Faculty of Pharmacy, Universitas of Airlangga, Surabaya, Indonesia
[3]Doctoral Student of Doctoral Program, Faculty of Pharmacy, Universitas of Airlangga, Surabaya, Indonesia.
[4]Department of Microbiology, Faculty of Medicine, Universitas of Airlangga, Surabaya, Indonesia.
[5]Department of Health Science, Faculty of Health Science, Universitas Muhammadiyah Surabaya, Surabaya, Indonesia.

*Corresponding author: idhakusumawati.unair@gmail.com

Abstract

Background: *Red passion fruit (Passiflora edulis Sims) and yellow passion fruit (Passiflora edulis f. flavicarpa) are native Indonesian fruits with numerous health benefits. This study used de Man, Rogosa, and Sharpe (MRS) medium for fermentation. Probiotics are beneficial microorganisms obtained from fermented food or drink (Hamid et al., 2020). Probiotics and lactic acid bacteria, which are known to have various benefits, particularly as antibacterial, are among the active components identified in passion fruit pulp.* **Objective:** *This study examined the antibacterial activity of red and yellow passion fruits.* **Methods:** *Freshly collected passion fruit pulps were fermented in MRS medium in a shaker incubator for 48 hours at 24°C. The filtrates from the fermented broth were tested against clinical isolates of methicillin-resistant Staphylococcus aureus (MRSA) and extended-spectrum beta-lactamase (ESBL)-producing bacteria. The analyses applied the streak plate method and the total plate count method.* **Results:** *The Minimum Inhibitory Concentrations (MICs) of red passion fruit ferment filtrate against MRSA 10 and MRSA 11 were 50% and 60%, respectively, and of yellow passion fruit ferment filtrate against MRSA 10 and MRSA 11 were both 30%. Meanwhile, the MICs of red passion fruit ferment filtrates were 35% against ESBL 41 and ESBL 43 and 25% against ESBL 45 and ESBL 47, whereas the MICs of yellow passion fruit (Passiflora edulis f. favicarpa) ferment filtrates were 25% against ESBL 41 and ESBL 43, and 12.5% against ESBL 45 and ESBL 47. Red passion fruit (Passiflora edulis Sims) and yellow passion fruit (Passiflora edulis f. flavicarpa) ferment filtrates became growth inhibitors against the clinical isolates of MRSA and ESBL-producing bacteria with an optimal fermentation time of 24 hours and an optimal concentration of 75%.* **Conclusion:** *The results of this study found that the fermented filtrates of red and yellow passion fruits in MRS media could be developed as an antibacterial against MRSA and ESBL-producing bacteria.*

Keywords: *Passiflora, Methicillin-resistant Staphylococcus aureus, and Extended-spectrum beta-lactamase.*

INTRODUCTION

Indonesia is home to a plethora of plant species, many of which are fruit trees, including the *Passiflora edulis* plant, which produces passion fruit or granadilla. The *Passifloraceae* family consists of over 500 species in the genus *Passiflora*. Yellow and red passion fruits are common throughout Indonesia, particularly in West Java and West Sumatra. Unripe red passion fruit is red with white spots; the rind is rather thick and hard. Red passion fruit can bear quite a lot; the fruit is round to slightly oval in shape, and the juice has a sweet and sour taste with a guava-like aroma (Karsinah and Manshur, 2010). Meanwhile, unripe yellow passion fruit is light green, and the ripe one is golden yellow with white spots; the rind is tough and thick. Besides containing protein, fat, carbohydrates, fibre, vitamins, and minerals, passion fruit is also rich in flavonoids (Karsinah and Manshur, 2010; Shiamala et al., 2013). According to Cushnie and Lamb (2005), flavonoids can reduce the synthesis of nucleic acids, the function of cell membranes, and energy expenditure.

It is fascinating to study how the phenolic chemicals in yellow passion fruit, which have antibacterial and antioxidant properties, can be used as a source of medicine (Shiamala et al., 2014). A prior study by Joachim et al. (2016) also found that the triterpene components in the methanol extract of passion fruit can prevent the growth of several bacteria, including *E. coli, Enterobacter aerogenes, Klebsiella pneumoniae, Pseudomonas euginosa*, and *Providencia stuartii*. In addition, *Passiflora edulis* seed oil rich in unsaturated fatty acids has been shown to have antibacterial activity against *Escherichia coli, Salmonella enteritidis, Staphylococcus aureus,* and *Bacillus cereus* (Marlene et al., 2019). Furthermore, Marwah et al. (2019) revealed that yellow passion fruit ferment

Figure 1 : The yellow passion fruit

filtrate could inhibit the growth of *Escherichia coli,* methicillin-resistant *Staphylococcus aureus* (MRSA), and extended-spectrum beta-lactamase (ESBL)-producing bacteria.

This study aims to determine the MIC and antibacterial activity of yellow passion fruit ferment filtrates and red passion fruit ferment filtrates against MRSA and ESBL-producing bacteria.

MATERIALS AND METHODS

Materials

This study used distilled water, de Man, Rogosa, and Sharpe (MRS) media, MRSA 4, MRSA 10, MRSA 11, MRSA 23, ESBL 41, ESBL 43, ESBL 45, and ESBL 47 from Jombang Regional General Hospital (RSUD Jombang), red passion fruit ferment filtrate, yellow passion fruit ferment filtrate, Nutrient Agar (Merck), and NaCl p.a (Merck).

Tools

The tools used in this study were analytical balance (Sartorius-Werke GMBH type 2472), autoclave (Huxley HV-340 Speedy), ultrasonic vibrators (Julabo), vortex (Thermo), micrometer syringes (Hamilton), pH paper (Macherey-Nagel), pH meter (S1 Analytics), öse wire, 15 cm diameter petri dish, and 0.2 µm membrane filters (Minisart).

Plant source and determination

In August 2020, yellow and red passion fruits were collected from Krembung, Sidoarjo, East Java, Indonesia. A botanist from the Faculty of Science and Technology, Universitas Airlangga, verified the identification of the yellow passion fruit (Figure 1), and a botanist from Herbarium Malangensis, Department of Biology, Faculty of Mathematics and Natural Sciences, Universitas Negeri Malang verified the identification of red passion fruit (Figure 2).

Figure 2 : The red passion fruit

Preparation of fermentation media

To make MRS broth, 52 grams of MRS broth powder was dissolved in 1 liter of distilled water and mixed well. After that, it was sterilized in an autoclave at 121°C for 15 minutes.

Preparation of growth media

Growth media were prepared by dissolving 18 g of nutrient agar (NA) powder (Oxoid) in 1 L of distilled

water, then divided into 10 mL and autoclaved for 15 minutes at 121°C for sterilization.

Preparation of samples

Red and yellow passion fruits were cleaned and dried. Then, 10 g of the fruit pulps were weighed and added to 200 mL of MRS broth media. The samples were then fermented with a rotary shaker for 48 hours at 150 rpm and filtered with a 0.2 m filter membrane after

48 hours of fermentation. Lastly, the passion fruit ferment filtrates were put into the vial.

Preparation of bacterial test

All bacteria were collected from RSUD Jombang; each of which was then inoculated and allowed to grow in nutrient agar medium for 24 hours at 37°Celsius. To produce a bacterial suspension for the OD measurement, 10 mL of sterile saline (0.9 percent NaCl) was added to the culture and then vortexed until all colonies were removed from the surface of the agar medium. A spectrophotometer was used to perform OD measurements at a wavelength of 580 nm.

Methods
Streak Plate Method

For the analysis using the Streak Plate method, 5 mL of yellow and red passion fruit filtrates with concentrations of 6.25%, 12.5%, 25%, 30%, 35%, 40%, 45%, 50%, 55%, 60%, 65%, 70%, 75%, 80%, 85%, 90%, and 100% according to dilution in distilled water (v/v) were added to 5 mL of diluted nutrient agar and then vortexed until homogeneous. The samples were then divided into four equal portions in a sterile petri, each for a different type of bacteria. After the nutrient agar was solid, the next step was to streak the bacteria 1

cm wide with three replications for each type of bacteria. The temperature was maintained at 37°Celsius for 24 hours during the incubation period. After incubation, the progress of bacterial growth was checked. This experiment was repeated with 48-hour incubation.
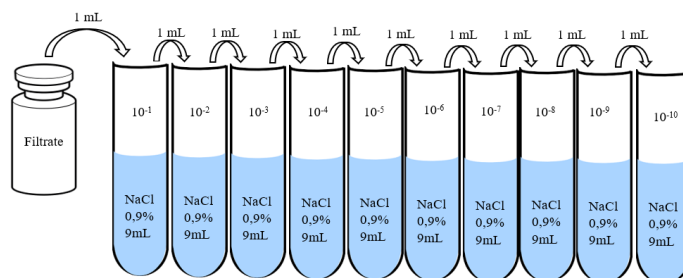
Total Plate Count Method

Aside from the Streak Plate method, the Total Plate Count method was also applied in this study. For passion fruit ferment filtrate with a concentration of 100%, 9 mL of 0.9% sterile saline was taken and labelled 10^{-1} until 10^{-10}. As much as 1 mL of 100% ferment filtrate was then added to a 10^{-1} saline solution and vortexed until homogenous. The next step was to transfer it from 10^{-1} to 10^{-2} and vortex it until homogeneous. These steps were repeated until 10^{-10}. The result was then added to 10 mL diluted nutrient agar, vortexed until homogeneous, poured into a sterile petri dish and allowed to solidify. The same procedure was applied for ferment filtrate with a concentration of 75%. The temperature was maintained at 37°Celsius for 24 hours during the incubation period. After incubation, the progress of bacterial growth was checked.

Figure 3: Schematic diagram of Total Plate Count

RESULTS AND DISCUSSION

Granadilla, which is another name for passion fruit (*Passiflora edulis*) or *markisa* in Indonesian, is a member of the *Passifloraceae* family which consists of over 500 species. This tropical fruit is rich of protein, fat, carbohydrates, fibre, vitamins, minerals, and flavonoids (Karsinah and Manshur, 2010; Ramaiya et al., 2013). Numerous investigations have proven that flavonoid molecules are antimicrobial, whose antibacterial activity can be divided into three categories: 1) inhibitor of nucleic acid production, 2) inhibitor of cell membrane function, and inhibitor of energy-producing metabolic processes (Cushnie and Lamb, 2005).

Botanical, chemical, and pharmacological reports on the genus *Passiflora* have been reviewed in previous studies. In addition, several in vitro and in vivo pharmacological studies have discovered the promising bioactivities in purple passion fruit (*P. edulis* Sims f. *edulis*), such as antioxidant, antimicrobial, anti-inflammatory, antihypertensive, hepatoprotective and lung-protective activity, anti-diabetic, sedative, and antidepressant activity, as well as anxiolytic activity. Most of the pharmacological effects of *P. edulis* Sims f. *edulis* are due to its bioactive compounds, i.e., polyphenols, triterpenes, and polysaccharides (He et al., 2020).

A previous study by Nurrosyidah et al. (2020) revealed that red passion fruit can inhibit the growth of MRSA and ESBL-producing bacteria.
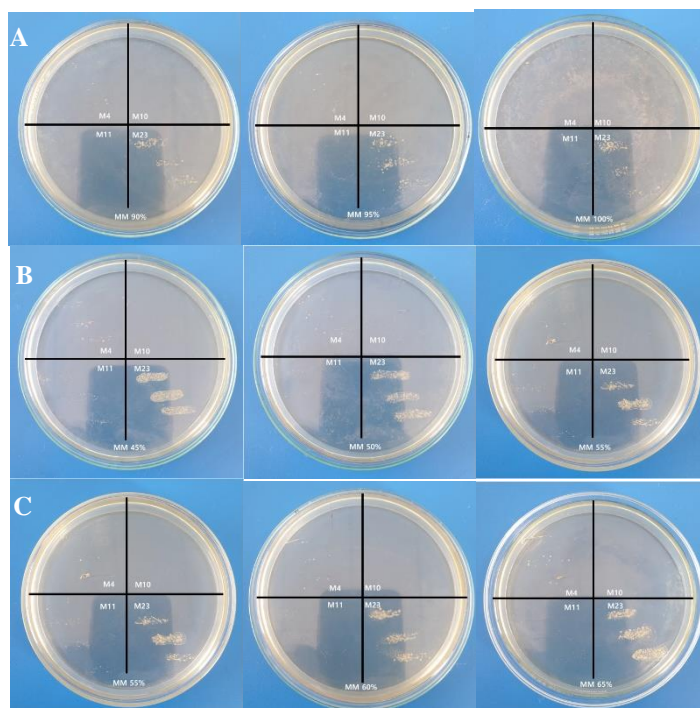
Figure 4: Streak Plate Method. A) MRSA 4 and MRSA 23 in 90%(+), 95%(+), and 100%(+) red passion fruit ferment filtrates; B) MRSA 10 in 45%(+), 50%(+), and 55%(-) red passion fruit ferment filtrates; and C) MRSA 11 in (55% (+), 60%(+), and 65%(-) red passion fruit ferment filtrates

This study used the streak plate method to determine the antibacterial activity of yellow and red passion fruit ferment filtrates. The screening results of red passion fruit ferment filtrate and yellow passion fruit ferment filtrate determined that MRSA 4 and MRSA 23 bacteria were negative or resistant. This is indicated by the growth of both bacteria, which continued up to a concentration of 100%. The MIC value for inhibiting the growth of MRSA and ESBL-producing bacteria was lower in yellow passion fruit ferment filtrate than in red passion fruit ferment filtrate, signifying that yellow passion fruit was more effective in inhibiting MRSA and ESBL-producing bacteria. The MICs of red passion fruit (*Passiflora edulis* Sims) ferment filtrate against MRSA 10 and MRSA 11 were 50% and 60%, respectively; and yellow passion fruit (*Passiflora edulis* f. *flavicarpa*) ferment filtrate against MRSA 10 and MRSA 11 were both 30%. Meanwhile, the MICs of red passion fruit ferment filtrate were 35% against ESBL 41 and ESBL 43 and 25% against ESBL 45 and ESBL 47, whereas the MICs of yellow passion fruit ferment filtrate were 25% against ESBL 41 and ESBL 43 and 12.5% against ESBL 45 and ESBL 47.

This study applied the total plate count method to compare the percentages of inhibition of bacterial growth after 24-hour and 48-hour incubations at concentrations of 100% and 75%. The results indicated that 24 hours was optimal for the ferment filtrate.

Within 48 hours, MRSA 4 and MRSA 23 bacteria entered the death phase, while MRSA 10 and MRSA 11 bacteria experienced a 99.99% decrease in growth. The comparison of 24-hour and 48-hour incubation times showed that MRSA and ESBL-producing bacteria in the ferment filtrates were harvested after 24 hours, not 48 hours, as the bacteria died after 48 hours (entering the death phase).

A comparison of the percentage of inhibition between 100% ferment filtrate and 75% ferment filtrate is shown in Table 1 and Table 2.

Table 1. Percentage of Inhibition of red passion fruit (MM) and yellow passion fruit (MK) against MRSA with 3 replication

NO	Bacteria	Percentage of Inhibition			
		MM 100%	MM 75%	MK 100%	MK 75%
1	MRSA 10	91,61%	100%	97,82%	100%
		+ 143,77	+ 0	+ 133,39	+ 0
2	MRSA 11	100%	100%	100%	100%
		+ 0	+ 0	+ 0	+ 0

Table 2. Percentage of Inhibition of red passion fruit (MM) and yellow passion fruit (MK) against ESBL-producing bacteria with 3 replication

NO	Bacteria	Percentage of Inhibition			
		MM 100%	MM 75%	MK 100%	MK 75%
1	ESBL 41	98,16%	98,31%	99,99%	99,99%
		+ 141,01	+ 135,94	+ 108,8	+ 117,84
2	ESBL 43	76,74%	97,09%	45,98%	99,98%
		+ 133,33	+ 137,76	+ 133,63	+ 134,32
3	ESBL 45	85,98%	92,94%	86,81%	100%
		+ 137,85	+ 134,63	+ 132,42	+ 0
4	ESBL 47	57,31%	88,01%	99,99%	99,99%
		+ 138,54	+ 139,40	+ 13,8	+ 94,79
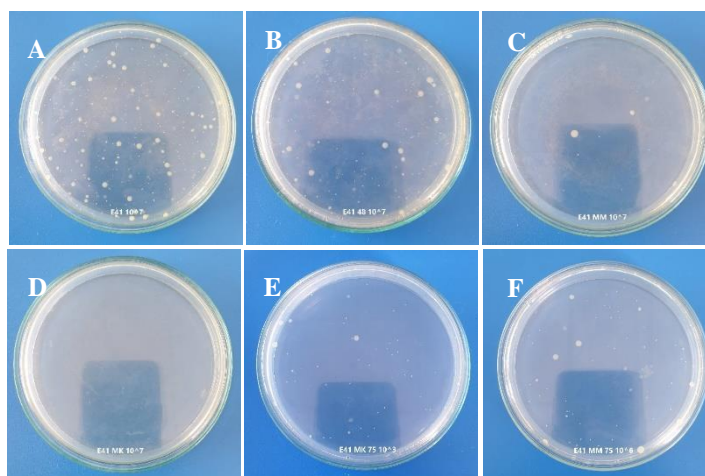
Figure 5: Total Plate Count Method. A) ESBL after 24 hours; B) ESBL 41 after 48 hours; C) 100% red passion fruit (MM) against ESBL 41 after 24 hours; D) 100% yellow passion fruit (MK) against ESBL 41 after 24 hours; E) 75% red passion fruit (MM) against ESBL 41 after 24 hours; and F) 75% yellow passion fruit (MK) against ESBL 41 after 24 hours

The 75% ferment filtrate was more effective for inhibiting the growth of MRSA and ESBL-producing bacteria. As seen in Table 1, the percentage of inhibition of 75% ferment filtrate is higher than 100% ferment filtrate, meaning that 75% ferment filtrate is more effective than 100% ferment filtrate.

In conclusion, the best time and concentration for the ferment filtrates of red passion fruit (*Passiflora edulis* Sims) and yellow passion fruit (*Passiflora edulis* f. *flavicarpa*) as growth inhibitors against the clinical isolates of extended-spectrum beta-lactamase (ESBL)-producing *E.coli* and methicillin-resistant *Staphylococcus aureus* are 24 hours and 75%, respectively. At lower concentrations, many of the phenols formed are undissociated, more hydrophobic, can bind to hydrophobic regions of membrane proteins, and dissolve well in the lipid phase of bacterial membranes. This affects the integration of the cytoplasmic membrane, leading to intracellular leakage, which in turn causes lysis by activating enzymes that require more energy, resulting in less energy for antimicrobial activity.

CONCLUSION
This study examined red passion fruit (*Passiflora edulis* Sims) and yellow passion fruit (*Passiflora edulis* f. *flavicarpa*) ferment filtrate in MRS media. The results may lead to the discovery of new antibacterial agents against methicillin-resistant *Staphylococcus aureus*

(MRSA) and extended-spectrum beta-lactamase (ESBL). Furthermore, characterization and identification of red and yellow passion fruits are absolutely necessary to determine the antimicrobial compounds that can be produced so that they can be used as antibacterials in the future.

References
Cushnie, T. P. T., & Lamb, A. J. (2005). Antimicrobial activity of flavonoids. International Journal of Antimicrobial Agents, 26(5), 343–356. https://doi.org/10.1016/j.ijantimicag.2005.09.002

Dzotam, J. K., Touani, F. K., and Kuete, V. (2016). Antibacterial and antibioticmodifying activities of three food plants (Xanthosoma mafaffa Lam., Moringa oleifera (L.) Schott and Passiflora edulis Sims) against multidrug-resistant (MDR) Gram-negative bacteria. BMC Complement. Altern. Med

He, X., Luan, F., Yang, Y., Wang, Z., Zhao, Z., Fang, J., Wang, M., Zuo, M., & Li, Y. (2020). Passiflora edulis: An Insight Into Current Researches on Phytochemistry and Pharmacology. Frontiers in Pharmacology, 11(May), 1–16. https://doi.org/10.3389/fphar.2020.00617

Joachim KD, Francesco KT, Victor K. .(2016). Antibacterial and antibioticmodifying activities of

three food plants (Xanthosoma mafaffa Lam., Moringa oleifera (L.) Schott and Passiflora edulis Sims) against multidrug-resistant (MDR) Gram-negative bacteria. BMC Complement. Altern. Med 16 (9). [DOI: 10.1186/s12906-016-0990-7] [PMID] [PMCID].

Jusuf, Nelva K., Putra, Imam Budi., Dewi, Nani Kumala. (2020). Antibacterial Activity of Passion Fruit Purple Variant (Passi fl ora edulis Sims var . edulis) Seeds Extract Against Propionibacterium acnes. 5–10.

Karsinah, Hutabarat R. C. dan Manshur A. (2010). *Markisa* Asam (Passiflora edulis) Buah Eksotik Kaya Manfaat Balai Penelitian Tanaman Buah. Balai Penelitian Tanaman Buah Tropika : Sumatera Barat, pp 30-35.

Marlene GP, et al. , (2019). Effect of extraction process on composition, antioxidant and antibacterial activity of oil from Yellow Passion Fruit (Passiflora edulis Var. Flavicarpa) Seeds. Waste and Biomass Valorization. 10(9):1-15. [DOI :10.1007/s12649-018-0269-y].

Marwah, Safarini., Rosyidah, Iif H., Mertaniasih, Ni M., Hamzah, Muhammad N.S.B., Novianti, Kholis A., Primaharinastiti, Riesta., Rahmawaty, Dian., Isnaeni., (2020). In vitro Antibacterial Activity of Cell Free Fermentation Supernatant of Passiflora edulis forma flavicarpa Sims. Fruit Fermented by de Man, Rogosa and Sharp Media. Fakultas Farmasi Universitas Airlangga. Indonesia : pp 1-8.

Ministry of Health of the Republic of Indonesia. Indonesia Pharmacopoeia (6th edition). (2020). Jakarta: Ministry of Health of the Republic of Indonesia.

Nurrosyidah, Iif Hanifa., et al. (2020). Inhibitory activity of fermentation filtrate of red passion fruit pulp (Passiflora edulis sims.) againts Extended spectrum beta-lactamase (ESBL) and Methicillin-Resistant Staphylococcus aureus (MRSA). Berkala Penelitian Hayati Volume 26 No.1 Desember 2020.

Pereira, M. G., Maciel, M. G., Haminiuk, G. M., Hamerski, C. W. I., Bach, F., Hamerski, F., et al. (2019). Effect of extraction process on composition, antioxidant and antibacterial activity of oil from Yellow Passion Fruit (Passiflora edulis Var. Flavicarpa) Seeds. Waste Biomass Valorizati. 10.

Ramaiya, S. D., Bujang, J. S., Zakaria, M. H., King, W. S., & Shaffiq Sahrir, M. A. (2013). Sugars, ascorbic acid, total phenolic content and total antioxidant activity in passion fruit (Passiflora) cultivars. Journal of the Science of Food and Agriculture, 93(5), 1198–1205. https://doi.org/10.1002/jsfa.5876

Ramaiya, Shiamala Devi*., et al. (2012).* Sugars, ascorbic acid, total phenolic content and total antioxidant activity in passion fruit (Passiflora) cultivars. Journal of the Science of Foo and Agriculture.

Shiamala DR, Japar SB, Muta HZ, Wong SK, Muhd ASS. (2013). Sugars, ascorbic acid, total phenolic content and total antioxidant activity in passion fruit (Passiflora) cultivars. Journal of the Science of Food and Agriculture. 2013 Mar 30;93(5):1198-205. [DOI: 10.1002/jsfa.5876] [PMID].

Shiamala DR, Japar SB, Muta HZ.Assessment of total phenolic, antioxidant, and antibacterial activities of Passiflora species. (2014). ScientificWorldJournal 2014;2014:167309 [DOI: 10.1155/2014/167309] [PMID] [PMCID].

Cost of Illness Study in Thyroid Patients: A Systematic Review

Seisye Junita Miru[1], Libriansyah[2], Mufarrihah[3], Yunita Nita[3]*

[1]Master of Pharmaceutical Science Program, Faculty of Pharmacy, Universitas Airlangga, Surabaya, Indonesia
[2]Department of Internal Medicine, Dr. Ramelan Navy Hospital, Surabaya, Indonesia
[3]Department of Pharmacy Practice, Faculty of Pharmacy, Universitas Airlangga, Surabaya, Indonesia

*Corresponding author: yunita-n@ff.unair.ac.id

Abstract

Background: *The thyroid has a vital role in growth, neurodevelopment, reproduction, and metabolism. About 300 million people around the world had been reported to be suffering from thyroid disorders, but more than half were unaware. The factors of sex, age, weight of disease, and other accompanying conditions should be considered, otherwise, it will cause a long time treatment period in which the cost will become higher from year to year.* **Purpose**: *The systematic review aims to provide an overview of the financial burden caused by thyroid disease for the communities, governments and health care providers.* **Method**: *A systematic review of publications in several databases, namely PUBMED, SCIENCE DIRECT, DOAJ, SCOPUS and GOOGLE SCHOLAR. Results: Six research articles were obtained from publications selected for systematic review. The reviewed articles show overviews of the cost of thyroid disease in several countries. The financial burden of thyroid patients in some countries varies, with different perspectives. The lowest to highest cost ranges from 0.125 USD/patient – 8106 USD/patient. Conclusion: The study in this review illustrates the various costs in different countries; the cost of screening, and thyroid surgery has the largest contribution compared to other costs; research on the financial burden suffered by thyroid patients in the future must be carried out continuously and periodically to be able to estimate the cost of therapy more appropriately to provide a useful data for health care providers, governments and the community. Direct medical costs are the largest proportion.*

Keywords: *thyroid, cost of disease, cost analysis, the economic cost burden*

INTRODUCTION

Thyroid gland disease is a public health problem worldwide. The imbalance in the hormone system can lead to many diseases, from raised bumps to life-threatening diseases, such as thyroid cancer (Awad *et al*., 2016). Iodine deficiency is the most common cause of thyroid disease. Iodine deficiency has several side effects on human growth and development, called *iodine deficiency disorders (IDDs),* resulting from inadequate thyroid hormone production. The *iodine deficiency disorders (IDDs) mitigation* program started from the decade of 1990 through the *salt* iodization strategy or "berry salt for all" (Zimmermann & Andersson, 2021).

The manifestations of thyroid disorders vary greatly and depend on the type of thyroid hormone disorder. The manifestations of thyroid disorders differ, particularly hyperthyroidism and hypothyroidism. Factors affecting TSH and thyroid hormone include genetic factors, demographic factors such as age and gender, intrinsic factors (stress), drugs and environmental/*lifestyle factors* (*smoking*, alcohol consumption) (Leko et al., 2021). Symptoms in patients with hyperthyroidism disorders are anxiety, confusion, diarrhoea, palpitations, chest pain, hair loss, and diplopia, while in hypothyroidism, the symptoms are fast tiredness, slow mind, dry skin, constipation, increased weight, not resistant to cold (Indonesian Thyroid Association, 2022).

Hypothyroidism, hyperthyroidism (thyrotoxicosis), and nodular goitre are just a few hormonal manifestations and functions of different thyroid disorders (National Institute for Health and Care Excellence, 2019). Thyroid dysfunction, including hyperthyroidism and hypothyroidism, can affect the circulatory system by affecting cardiac output, contractility, blood pressure, vascular resistance, and rhythm disturbances, ultimately resulting in heart failure, fibrillation, and congestive heart failure (Awad *et al.,* 2016).

According to epidemiological studies, the prevalence of hyperthyroidism and hypothyroidism ranges from 0.1 to 1.25% and 0.25 to 4.20% worldwide (Taylor *et al.*, 2018). The prevalence of thyroid nodules rises with age and body mass index, and they are four times more common in women than in men. Approximately 90 to 95% of thyroid nodules are benign (Kant *et al.,* 2020).

Thyroid cancer incidence nearly tripled from 4.9 cases per 100,000 people in 1975 to 14.3 cases per 100,000 people in 2009. Since the middle of the 1990s, there has been a significant rise in thyroid cancer cases, with 53,990 cases predicted to occur in the United States in 2018 (Ioachimescu, 2019). According to data from the European Network of Cancer Registries, women had a three times higher incidence rate of cancer in 2012 than men (9.3 cases versus 3.1 cases per 100,000 person-years, respectively) (Filetti *et al.,* 2019). Therefore, thyroid gland disease is one of the endocrine cancers and accounts for between 1% and 1,5% of all new cancer cases diagnosed each year in the United States. Its incidence has also steadily increased globally over the past three decades (Awad *et al.*, 2016).

To increase overall survival and quality of life (QoL) is the main goal of all cancer treatments. Contrary to many other cancers, thyroid cancer has a prognosis that is generally favourable. A preoperative risk assessment is used to determine the primary course of treatment for thyroid cancer patients, which usually entails surgery to lift the thyroid tissue (Ju *et al.,* 2016; Filetti *et al.,* 2019).

Longer thyroid treatments will result in significant price increases. The overall cost of thyroid treatment in the US in 2008 for females over 18 reached $4.3 billion. According to the Endocrine Society (2015), the average cost of treating thyroid disease was $343, the average cost of outpatient visits was $409, and the average cost of prescription drugs was $16.21. One study conducted in Korea discovered that the total cost of thyroid disease collected from 2002 to 2010 was 224.2 billion won in 2002, 303.4 billion won in 2004, 400.3 billion won in 2006, 570.4 billion won in 2008, and 762.2 billion won in 2010. Thyroid disease-related costs in Korea increased three and a half times between 2002 and 2010 (Hyun *et al.,* 2014).

Patients with hypothyroidism utilize medical resources and pay much higher medical costs than those with euthyroid control *(*Hepp *et al.,* 2021). The estimated annual medical costs for each patient in the United States related to hypothyroidism range from $460 to $2.555. An investigation into the cost analysis of hyperthyroid patients was carried out in one of the hospitals in Indonesia, and the breakdown of cost components was discovered. As much as Rp 42,842,900 in annual drug costs, Rp 465,683 on average per patient, or 83% of the overall cost for thyroid patients, laboratory costs make up the most significant portion of these expenses (Saharah *et al.,* 2020).

There hasn't been enough research done on the thyroid's cost of illness (C.O.I.). Policymakers and the general public can make decisions about thyroid control programs to enhance the long-term health of thyroid

patients by using C.O.I. evaluation to understand the financial burden better. This systematic review aims to provide an overview of the financial costs associated with thyroid disease for the community, the government, and healthcare providers.

MATERIALS AND METHODS
Search strategy

The literature search was conducted on several databases: PUBMED, SCIENCE DIRECT, DOAJ, SCOPUS. The keywords used are a combination of the keywords "cost of disease", "thyroid" contained in the title or abstract of the databases. For searches in English, the keywords used are *"cost of disease", "burden of disease", "cost analysis", "cost for treatment", "thyroid disease"*. A manual search with GOOGLE SCHOLAR was also performed. Both the database search and manual search were conducted in September 2021. The literature search is restricted to articles that use either English or Indonesian.

Inclusion and exclusion criteria

Articles that meet the inclusion criteria are related to C.O.I. from various thyroid dysfunctions, both hyperthyroidism and thyroid cancer. However, for other economic evaluations besides the analysis of disease costs, for example the study of *cost effectiveness Analysis (C.E.A.), cost-benefit analysis (C.B.A.), cost utility analysis (C.U.A.)* are included in exclusion criteria. Moreover, studies that are inaccessible to the full text or only available abstracts are excluded for papers, case reports.

Data extraction and analysis

On one article will be reviewed if the same articles were obtained in the databases. The articles that have been obtained from the search results with the combination keywords of *"cost of illness", "cost analysis", "cost for treatment", "thyroid disease"*, *"cost of disease"* contained in the title or abstract of the database were gathered. Then, from the results of the literature search, an evaluation was carried out to ensure that the article was relevant to the purpose of the study. Abstracts from articles obtained were then evaluated independently, and the whole text of the article was also evaluated and filtered to obtain articles that meet the research inclusion criteria. Then, the list of articles to be reviewed and data extraction was carried out. The steps in this systematic review are described in *prism flow* which maps the number of articles identified, the number of articles included and excluded as well as the reason for exclusion. In this study, quality of the research was critically evaluated following previous

C.O.I. related research (Patty *et al.,* 2021). This study used a 10-point checklist; it will be given a score of 2 if all criteria were met, a score of 1 if only some criteria were met, and a score of 0 if only a few criteria were met. The maximum score was 20, with three studies of good quality, two of moderate quality and one of poor quality.

RESULTS AND DISCUSSION
Search result

Search results from the database with the keywords used resulted in 755 articles for the initial search. After identifying and removing the duplication of articles, eight articles and abstracts relevant to the study's purpose were generated. A total of three articles were then excluded because one article only displayed an abstract while the full text was unavailable. The other two articles were excluded because they belonged to C.E.A. studies. In the end, the remaining five articles met the research objectives and could be used in *a systematic review*. A manual search was also conducted on google scholar, one relevant article was obtained. Therefore, six articles were analyzed in this *systematic review* (Fig. 1).

Characteristics of the study

The six articles acquired are C.O.I. studies carried out across several nations, including Germany, Korea, Indonesia, Denmark, and the United States. The term "burden of illness" (C.O.I.), also known as "burden of disease" (B.O.D.), refers to the various ways that disease can affect how people feel about their health in a nation, particular regions, communities, and even as individuals. The C.O.I. category can include both direct and indirect costs, as well as the incidence or prevalence of a disease and its effects on age, morbidity, health status, quality of life (QoL), and financial aspects (Jo, 2014). This study focuses heavily on seeing C.O.I. from thyroid diseases with various thyroid diseases, namely *benign* and *malignant* thyroid plus hyperthyroid (n=2), *papillary thyroid cancer* (n=1), hyperthyroid (n=1), thyroid cancer plus hyperthyroid and hypothyroid (n=1), and *primary hyperparathyroidism* (n=1). These articles on the *systematic review* were published between 2002 and 2020. All studies were conducted in hospitals, inpatients, outpatients, and both. The average data collection was carried out retrospectively using medical record data, financial institution details data, SIM-RS data and insurance claim data. This study calculated the cost using the payer perspective (n=3), society (n=1) and hospital (n=2). The research characteristics of the 6 articles are shown in Table 1.
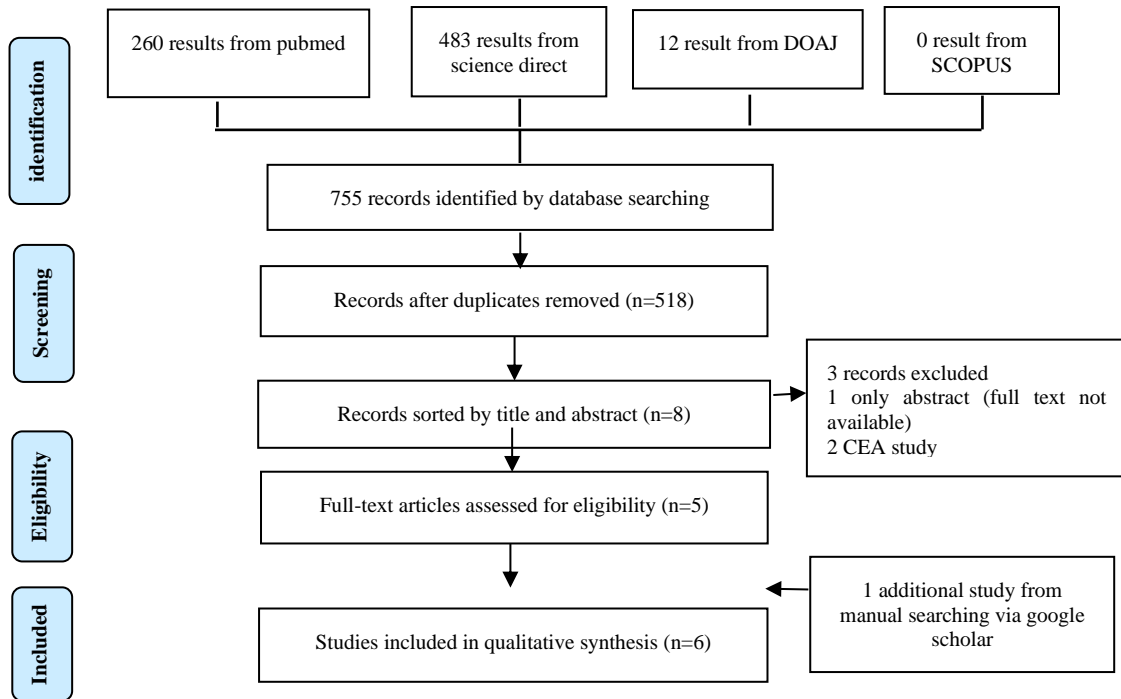
Figure 1. *Systematic review of flow diagrams*

Table 1. Characteristics of Research Articles

Authors	City	Number of Samples	Study size	Epidemiological approach	Methods of resource qualification	Study period	Type of Disease	Data Source	Settings	Study design	Study Prespective
Kahaly & Dietlein, 2002	Ger	5932	32 locations	Prevalence	Drummond Checklist	1981-2001	Benign and malignant thyroiditis, hyperthyroid	Cost breakdown data from insurance companies and government departments	I & O	R	P
Kim *et al,* 2018	Kor.	33	2120	Incidence	Drummond Checklist	2010-2015 (5 year periods	Papillary thyroid cancer (TPC)	Medical record data, cost breakdown data, follow-up outpatient data after surgery	I & O	R	P
Hyun *et al.,* 2014	Kor.	-	-	Incidence	Drummond Checklist	2-year intervals during the last 10 years	Malignant and benign thyroid tumors, functional abnormalities inflammation, thyroid abnormalities in newborns	Medical records, details of direct and indirect medical costs	I & O	R	S
(Saharah *et al.,* 2020	IND	92	1139	Prevalence	Drummond Checklist	January 2017 to December 2018	Hyperthyroidism	Medical record data, SIM-RS, INA-CBG package	(O)	R	H
Møllehave *et al.,* 2018	Den	100,000	5,330,119 persons	Incidence	Drummond Checklist	1995–2015 in Denmark, i.e., before and after the introduction of mandatory IF in 2000	Thyroid cancer, hypothyroidism, hyperthyroidism	Medical records data, cost breakdown data, e Danish health care system	I & O	R	P
Hollenbeak *et al.,* 2007)	US	4863	8510	Incidence	Drummond Checklist		Primary hyperparathyroidism	cost breakdown data from business departments, literature search	I & O	R	H

Note: **GER** = Germany; **KOR** = Korea; **IND** = Ind; **DEN** = Denmark; **US** = United States; **I** = Inpatient;

O = Outpatient; **R =** Retrospective; **P** = Third party payer; **H** = Hospital; **S** = Society

Table 2. Screening and Thyroid Surgery Cost

Authors	Screening, Thyroid surgery	Cost
Hollenbeak et al., 2007	Minimally invasive parathyroidectomy	7228 USD/patient
	Parathyroid surgery with routine preoperative thyroid ultrasonography and further thyroid treatment	8098 USD/patient
	Bilateral neck exploration (B.N.E.)	8106 USD/ patient
Kahaly & Dietlein, 2002	Lobectomy	120 USD/patient
	Subtotal unilateral thyroidectomy	88 USD/patient
	Subtotal unilateral thyroidectomy with contralateral lobectomy	96 USD/patient
	Total thyroidectomy	107 USD/patient
	Total cervical and transtoracal thyroidectomy lymphadenectomy	344 USD/patient
Kim *et al.,* 2018	Hemithyroidectomy	0.774 USD ± 0.096 USD/patient
	Total thyroidectomy	1.31 USD ± 0.187 USD/ patient
	Total thyroidectomy with R.N.D.	1.92 USD ± 0.445 USD/ Patient
	Total bilateral thyroidectomy with radical neck dissection and mediastinal dissection	21.8 USD ± 7.6 USD/ Patient

Research in various countries causes differences in costs because the currencies used are different so that a cost adjustment calculation is needed. The cost obtained in the study reviewed in this study will be converted into USD currency in 2020, where to adjust the cost must calculate *consumer price index* and *purchasing power parities*.

$$P.P.P. = \frac{cost\ on\ the\ article}{PPP\ in\ 2020} = Relative\ cost\ after$$
converting to P.P.P.

$$C.P.I. = Yield\ \frac{CPI\ in\ 2020}{CPI\ in\ the\ year\ in\ the\ article} \times P.P.P.$$
= Value in USD in 2020

The consumer price index (C.P.I.) is a calculation of consumer purchasing power by looking at purchasing power in a country in various years. Whereas *Purchasing power parities (P.P.P.)* is a calculation of purchasing power by comparing purchasing power of each country by eliminating differences in price levels between countries (OECD, 2020) (BANK, 2020).

Cost of thyroid disease

The six studies showed the cost in thyroid patients with various types of diseases, namely thyroid cancer, hyperthyroid and hypothyroid. The observed costs were direct medical costs, direct non medical

costs, and indirect costs for both inpatients and outpatients. Some costs were calculated from both the yearly average cost and the cost per procedure - mainly on operating procedures. The screening and thyroid surgery cost articles are shown in Table 2.

Meanwhile, a research in Indonesia conducted on hyperthyroid patients shows that an average cost for each patient per year is 125.71 USD. Unlike payments that use BPJS, the average cost of each patient is 41.68 USD per year, which is the highest cost component and is about 83%. There is a difference in cost between the hospital rate and the INA-CBGs rate of 84.03 USD per patient (Saharah *et al.,* 2020)

In some countries, the cost of surgical measures is the highest, particularly in Germany, which is around 374 USD± 120.50 USD/patient (Kahaly & Dietlein, 2002). In Korea and Denmark, the average cost of operating measures is almost the same. The average *thyroid surgery* in Denmark is 0.500 USD – 0.741 USD/per surgery (Møllehave et al., 2018). For Korea, *hemithyroidectomy* procedure costs 0.382 USD ± 0.094 USD/patient, *total* thyroidectomy costs 0.452 USD ± 0.062 USD/patient, *total thyroidectomy ipsilateral radical neck dissection* costs 0.772 USD ± 0.140 USD/patient, and t*otal thyroidectomy with bilateral*

R.N.D. and mediastinal dissection costs 7.76 USD ± 6.67 USD/patient (Kim *et al.,* 2019)

In a study conducted in Denmark, the total cost of drugs and hospital costs for thyroid disease amounted to 12501.59 USD per 100,000 people from 1995 to 2015 (can be seen in Table 4), with an average cost of antithyroid drugs of 11.73 USD (Møllehave *et al.,* 2018). Meanwhile, in Indonesia, the average cost of drugs is 3.22 USD/patient (Saharah *et al.,* 2020). For patients treated with radioiodine in Germany anaverage of 205 USD ± 77.34 USD/patient was obtained (Kahaly & Dietlein, 2002), while for radioiodine therapy in patients in Denmark, it was 89.19 USD - 0.32 USD/patient (Møllehave *et al.,* 2018). The lowest cost is in Germany, which is around 0.125 USD/patient. While the highest cost is found in the United States, the cost of *bilateral action neck exploration (B.N.E.)* which is 8106 USD/patient. Details of thyroid treatment costs can be seen in Table 3.

Thyroid disease and disorders have a large economic impact on patients, governments and healthcare providers. Thyroid disease is more prevalent in women than in men (Endocrine Society, 2015). This study uses several perspectives in accordance with the respective research objectives, but some studies have not yet been fully conducted for non-medical and indirect costs. Systematic review related to C.O.I. in thyroid patient is still unavailable, and there is still little research. In *systematic review* not only focuses on C.O.I. from patients with hyperthyroid or hypothyroid disorders but also looks at C.O.I. in patients with thyroid cancer or other thyroid dysfunction.

The study's perspectives vary from health care providers, the government, and society. Studies from different angles, covering slightly different cost items in turn, can result in various outcomes for the same disease. The costs for a specific group are usefully disclosed by each perspective. The societal perspective is preferred because it allows a thorough analysis of all costs incurred due to the disease and is advised for potential cost analyses like C.B.A., C.E.A., and C.U.A. It is the most comprehensive because it covers all direct medical costs and indirect costs for all members of the specific society in which they are involved (Jo, 2014)

For the population groups reviewed by each study, it varies, and also in most large populations. This can affect cost differences between countries. These results can present the conditions of each country. Several studies show a long period and each data is analyzed annually to see the COI. One of the studies in this study did not mention how many total samples were analyzed, because the data was seen every two years in 2002, 2004, 2006, 2008, and 2010. The data was seen from age <19 years to >80 years where based on the age of patients 50 years had the largest portion (27.6%), then followed by 40 years (25.3%) and 30 years (18.0%) (Hyun *et al.,* 2014)

For the design study used in this *systematic review*, the average uses retrospective studies obtained from patient medical record data, patient cost detail data and also data from the insurer. This study looks at an overview of a condition or a disease. One study discussed the cost of thyroid in patients with hyperthyroidism, where the cost components measured were administration costs, doctor's consultation costs, laboratory costs, and drug costs (Saharah *et al.,* 2020). Hyperthyroidism can occur at a vulnerable age of 20-40 years because it is in fertile age with high productivity, causing anxiety, stress and depression. Hyperthyroidism has been associated with increased psychiatric morbidity; increased thyroid hormones in the blood can cause anxiety and depression (Bang *et al.,* 2014)

An important factor determining the patient's direct medical costs is the length of hospitalization (Rae H, 2013). This results in a reasonably high cost because compared to outpatients, the condition of patients in hospitalization is much more complex, requiring more examination through laboratory and doctor control costs. In addition, it is also deducted from the cost of the patient's surgical measures and the cost of the patient's medication (Kahaly & Dietlein, 2002). Surgical facility and hospital costs affect how much healthcare costs vary from country to country. Comparing the costs of treating thyroid cancer in the United States and France reveals that the former is three times more expensive than the latter, with hospital expenses and other treatment costs accounting for the majority of the difference rather than the price of the surgery itself (Finnerty *et al.,* 2014). Indirect costs also show a large cost, especially related to losing patient productivity (Kahaly & Dietlein, 2002). Treating thyroid dysfunction generates high medical costs for patients and families and can result in patients losing productivity.

Table 3. Cost of Thyroid Disease Disorders

First Authors, Year	Year of cost estimation	Type of Disease	Total	Direct Cost	Indirect cost
Kahaly, 2002	1981-2001	Hyperthyroidism (Graves Disease)	Thyroid surgery (4631 USD) Radioiodine Therapy (5241 USD)	The cost of inpatient care in Germany is approximately 250 million/year/10,000 members (43345 USD/ patient/year)	Loss of work productivity due to thyroid disorders approximately 240 million/year/10,000 members (41624 USD/member/year)
		Toxic nodular goiter	Thyroid surgery (4186 USD) Radioiodine Therapy (4342 USD)		
		Benign and malignant thyroiditis, hyperthyroid	Average cost of Thyroid surgery 374 USD ± 120.50 USD /patient Average cost of R.A.I. 205 USD ± 77.34 USD/patient		
Kim, 2018	Data from Jan 2010 and Dec 2010 Fol 5 years 2010-2015	Papillary thyroid cancer (TPC)	Total overall cost hemithyroidectomy 0.774 USD ± 0.096 USD/patient total thyroidectomy 1.31 USD ± 0.187 USD/ patient total thyroidectomy with RND 1.92 USD ± 0.445 USD/ Patient total bilateral thyroidectomy with R.N.D. and MD. 21.8 USD ± 7.6 USD/ Patient	hemithyroidectomy (0.382 USD ± 0.094 USD/patient) total thyroidectomy (0.452 USD ± 0.062 USD/patient) total thyroidectomy with R.N.D. (0.772 USD ± 0.140 USD/patient) total bilateral thyroidectomy with R.N.D. and MD. (7.76 USD ± 6.67 USD/patient)	
Hyun, 2014	2002-2010	Malignant and benign thyroid tumors, functional abnormalities inflammation, thyroid abnormalities in newborns	2002 (301 USD) 2004 (408 USD) 2006 (537 USD) 2008 (766 USD) 2010 (1024 USD)	2002 (193 USD) 2004 (280 USD) 2006 (369 USD) 2008 (561 USD) 2010 (770 USD)	2002 (108 USD) 2004 (127 USD) 2006 (169 USD) 2008 (206 USD) 2010 (255 USD)

Saharah, 2020	Jan 2017 - Dec 2018	Hyperthyroidism	Total Real Costs (125.71 USD/patient) INA-SBG Package (Q-5-44-0) (41.68 USD/ patient)	Laboratory 104.63 USD/patient Doctor/ patient consultation 15.58 USD/patient Drug costs 3.22 USD/patient Administration fee 2.27 USD/patient
Molehave, 2018	1995-2015	Thyroid cancer, hypothyroidism, hyperthyroidism	EUR 80,000 per 100,000 people from 1995 – 2015 (12475.20 USD/ 100,000 patients) (0.125 USD/patient)	Average cost of OAT 11.7 USD/patient/tahum The average of thyroid hormone therapy 5.5 USD/patient/year TS 0.500 USD – 0.741 USD/operation RAI 89.19 USD- 0.32 USD/ patient
Hollenbeak, 2007	1974-2004	Primary hyperparathyroidism	M.I.P. (7228 USD/patient) Parathyroid surgery with U.S. and further thyroid (8098 USD/patient) B.N.E. (8106 USD/patient)	OR ($20/minute) SI (968 USD/scan) U.S. (212 USD) F.S.P. (127 USD) Rapid testing of PTH levels ($38/test)

Description: TS = Thyroid Surgery; **RAI** = Radioiodine Therapy; RND = ipsilateral radical neck dissection; **MD** = Mediastinal dissection; **JAN** = January; **DEC** = December; fol = Follow up; **oat** = Anti thyroid drug; **MIP** = Minimally invasive parathyroidectomy; **BNE** = Bilateral neck exploration; **US** = Ultrasonography; **SI** = Sestamibi Imaging; **OR** = Operating room; **FSP** = frozen section preparation

The number of days spent in the hospital and for outpatient visits (by sex, age, and year) for thyroid treatment is multiplied by the daily average wage (by sex, age, and year) from the Survey Report on Labor Conditions by Job Type to estimate the loss of productivity when the patient is unable to work as a result. The number of deaths (based on gender and age) is multiplied by the per capita loss from the year after the death to the year of life expectancy (based on gender and age) to determine the future income loss due to premature death (Hyun *et al.,* 2014).

This review has limitations due to differences between countries, differences in perspectives, few articles, and currency differences. This can lead to bias, and the review results cannot be generalized.

CONCLUSION

Estimating the costs associated with thyroid disease is critical to evaluation and illustration for governments and communities going forward. The study in this review illustrates the different costs in different countries; the cost of screening and thyroid surgery has the largest contribution compared to other costs. In estimating costs in each country using different methods. Treatment for thyroid patients over a long period entails increasingly high costs. It is evident in a financial burden that continues to increase from year to year in some countries. This has an impact on society, especially social impacts and economic impacts. The analysis related to the cost burden of thyroid patients in the future must be carried out in order to be able to estimate the cost of more specific therapies in order to provide useful data for health care providers, the government and the community.

ACKNOWLEDGEMENTS

REFERENCES

Awad, S. A. S., Ashraf, E. M., Khaled, A. S., Salih, B. S., Yousef, S., Abeer, A. S., & Anna, A. (2016). The epidemiology of thyroid diseases in the Arab world: A systematic review. *Journal of Public Health and Epidemiology*, *8*(2), 17–26. https://doi.org/10.5897/jphe2015.0713

Bang, K., Watt, T., & Hegedüs, L. (2014). *Anxiety and Depression Are More Prevalent in Patients with Graves' Disease.* 173–178. https://doi.org/10.1159/000365211

Endocrine Society. (2015). *Endocrine Facts and Figures First Edition Thyroid.*

Filetti, S., Durante, C., Hartl, D., Leboulleux, S., Locati, L. D., Newbold, K., Papotti, M. G., & Berruti, A. (2019). Thyroid cancer: ESMO Clinical Practice Guidelines for diagnosis, treatment and follow-up. *Annals of Oncology*, *30*(12), 1856–1883. https://doi.org/10.1093/annonc/mdz400

Finnerty, B. M., Brunaud, L., Mirallie, E., & Mcintyre, C. (2014). Cost disparity between health care systems — it's not the surgeons : A cost analysis of thyroid cancer care between the United States and France. *Surgery*, *159*(1), 132–141. https://doi.org/10.1016/j.surg.2015.06.049

Hepp, Z., Lage, M. J., Espaillat, R., & Gossain, V. V. (2021). The direct and indirect economic burden of hypothyroidism in the United States: a retrospective claims database study. *Journal of Medical Economics*, *24*(1), 440–446. https://doi.org/10.1080/13696998.2021.1900202

Hollenbeak, C. S., Lendel, I., Beus, K. S., Ruda, J. M., & Stack, B. C. J. (2007). The cost of screening for synchronous thyroid disease in patients presenting with primary hyperparathyroidism. *Archives of Otolaryngology--Head & Neck Surgery*, *133*(10), 1013–1021. https://doi.org/10.1001/archotol.133.10.1013

Hyun, K. R., Kang, S., & Lee, S. (2014). Cost-of-illness trends associated with thyroid disease in Korea. *Endocrinology and Metabolism*, *29*(3), 257–269. https://doi.org/10.3803/EnM.2014.29.3.257

Indonesian Thyroid Association. (2022). *KAPITA SELEKTA TIROID edisi 1.*

Ioachimescu, A. G. (2019). Thyroid Cancer. *Endocrinology and Metabolism Clinics of North America*, *48*(1), xv–xvi. https://doi.org/10.1016/j.ecl.2018.12.002

Jo, C. (2014). Cost-of-illness studies: concepts, scopes, and methods. *Clinical and Molecular Hepatology*, *20*(4), 327–337. https://doi.org/10.3350/cmh.2014.20.4.327

Kahaly, G. J., & Dietlein, M. (2002). Cost estimation of thyroid disorders in Germany. *Thyroid : Official Journal of the American Thyroid Association*, *12*(10), 909–914. https://doi.org/10.1089/105072502761016548

Kant, R., Davis, A., & Verma, V. (2020). Thyroid nodules: Advances in evaluation and management. *American Family Physician*, *102*(5), 297–304. http://dx.doi.org/

Kim, S. Y., Kim, S. M., Chang, H., Kim, B. W., Lee, Y. S., Kwon, S. S., Shin, H., Chang, H. S., & Park, C. S. (2019). Cost for treatment and follow-up of thyroid cancer increases according to the severity of disease. *Head and Neck*, *41*(7), 2376–2379. https://doi.org/10.1002/hed.25706

Leko, M. B., Gunjača, I., Pleić, N., & Zemunik, T. (2021). Environmental factors affecting thyroid-stimulating hormone and thyroid hormone levels. *International Journal of Molecular Sciences*, *22*(12). https://doi.org/10.3390/ijms22126521

Møllehave, L. T., Linneberg, A., Skaaby, T., Knudsen, N., Ehlers, L., Jørgensen, T., & Thuesen, B. H. (2018). Trends in Costs of Thyroid Disease Treatment in Denmark during 1995-2015. *European Thyroid Journal*, *7*(2), 75–83. https://doi.org/10.1159/000485973

National Institute for Health and Care Excellence. (2019). Thyroid disease: assessment and management. *National Institute for Health and Care Excellence Guideline, November 2019*, 1–55.
https://www.nice.org.uk/guidance/ng145/resources/thyroid-disease-assessment-and-management-pdf-66141781496773

Patty, Yohana Febriani Putri Peu, Mufarrihah, and Nita, Yunita. "Cost of illness of diabetes mellitus in Indonesia: a systematic review" *Journal of Basic*

and Clinical Physiology and Pharmacology, vol. 32, no. 4, 2021, pp. 285-295. https://doi.org/10.1515/jbcpp-2020-0502

Saharah, S., Lorensia, A., & Suyanto, S. (2020). Analysis of Real Costs and INA-CBG of Hyperthyroidism in Hasanuddin University Hospital. *Media Kesehatan Masyarakat Indonesia*, *16*, 421–429. https://doi.org/10.30597/mkmi.v16i4.10990

Taylor, P. N., Albrecht, D., Scholz, A., Gutierrez-Buey, G., Lazarus, J. H., Dayan, C. M., & Okosieme, O. E. (2018). Global epidemiology of hyperthyroidism and hypothyroidism. *Nature Reviews Endocrinology*, *14*(5), 301–316. https://doi.org/10.1038/nrendo.2018.18

Zimmermann, M. B., & Andersson, M. (2021). Global perspectives in endocrinology: Coverage of iodized salt programs and iodine status in 2020. *European Journal of Endocrinology*, *185*(1), R13–R21. https://doi.org/10.1530/EJE-21-0171.

In Vitro Release Ability of Nanoparticles Poly-Lactic-Co-Glycolic-Acid (PLGA) Gel Containing Pegagan Leaves Ethanolic Extract (*Centella asiatica L.*)

Mardiyanto, Elsa Fitria Apriani*, M. Pandu Kalingga Jati
Department of Pharmacy, Faculty of Mathematics and Natural Sciences, Sriwijaya University, Ogan Ilir, Indonesia

*Corresponding author: elsafitria@mipa.unsri.ac.id

Abstract

Background: Pegagan (Centella asiatica L.) leaves are proven to contain high concentrations of flavonoid compounds as antioxidants. Flavonoids are unstable compounds due to environmental influences such as light, humidity, pH, and oxygen. The stability of pegagan extract was proven to be improved by making the extract into nanoparticle preparations. Objective: This study aims to formulate nanoparticles of pegagan into gel preparations and determine their release ability with the Franz diffusion test using a cellophane membrane compared to pegagan gel not formulated into nanoparticles. Methods: Nanoparticles were made using poly-lactic-co-glycolic acid polymers and then formulated into gels with various concentrations of Carbopol 934, namely 1, 1.5 and 2%. The gel nanoparticles were then subjected to the characterization of the preparation, stability test and release test of the preparation. Results: A concentration of 1% Carbopol 934 provides the best evaluation of gel preparations where the gel produced was homogeneous, pH was around 6.2, viscosity was 3417.12 cPs, spreadability was 5.1 cm, and adhesion was 209.33 seconds. The stability test showed no significant organoleptic and pH changes (p>0.05). The release kinetics model occurs at zero order. F1 has a higher reaction kinetics constant (k) than the other formulations, so drug release occurs faster. Conclusion: The best formula of pegagan (F1) nanoparticle gel was proven to have good physical stability and release ability.

Keywords: Centella asiatica L; Nanoparticles; Gel; Franz Diffusion

INTRODUCTION

The development of herbal medicine in Indonesia is growing rapidly. One of the plants that are widely used in health is *Centella asiatica* L. leaves. *Centella asiatica* L. leaves are known to have an anti-inflammatory (Park *et al*., 2017), neuroinflammatory (Gelders *et al*., 2018), antioxidant (Jiang *et al*., 2016), anti-obesity (Rameshreddy *et al*., 2018), antidiabetic (Zheng *et al*., 2018), wounds healing (Sawatdee *et al*., 2016), anti-hypertension (Liu *et al*., 2017), etc. The ethanolic extract of pegagan leaves was proven to contain alkaloids, glycosides, terpenoids, steroids, flavonoids, tannins, and reducing sugars (Arumugam *et al*., 2011). Flavonoids are the main compounds found in pegagan leaves. Based on research conducted by Quyen *et al*. (2020), the total flavonoid content of *Centella asiatica* L. leaves was higher than the total phenolic content, namely 23.03 ± 2.89 mgQE/g and 2.14 ± 0.29 mgGAE/g, respectively.

Flavonoids are phenolic compounds with a C6-C3-C6 chemical structure (Panche et al., 2016). Flavonoids are beneficial for health because they can protect the body from reactive oxygen species. Flavonoids will oxidize free radicals to become more stable and less reactive (Panche et al., 2016). However, the effectiveness of flavonoids can be reduced because flavonoids are less-stable compounds. Flavonoids are compounds sensitive to light, oxygen, pH, and temperature (Ioannou et al., 2012). Based on the research of Ioannou et al. (2020), the antioxidant activity of flavonoids was significantly reduced when flavonoids were exposed to excess heat for 2 hours. In addition, research by Ramesova et al. (2011) also proved that flavonoids degrade when exposed to atmospheric oxygen. To increase the stability of the flavonoids, the ethanolic extract of *Centella asiatica* L. leaves was formulated into nanoparticles.

Nanoparticles is a technology that aims to develop the dosage form size in the nano range, namely 200-500 nm (Mardiyanto et al., 2018). The polymer used is Poly-lactic-co-glycolic Acid (PLGA). While the stabilizer used is Polyvinyl Alcohol (PVA), which protects the nanoparticle preparation from the influence of temperature (Mardiyanto et al., 2018). The nanoparticles of *Centella asiatica* L. were then formed into a gel preparation.

Gel preparations have several advantages because they have a higher water component, making drug dissolution easier. Gels consisting of one phase have a faster drug release than creams consisting of two phases. This is evidenced by the research of Patel et al. (2009), where the release profile of psoralen gel preparations was greater than psoralen cream, namely $48.11 \pm 2.1\%$ and 25.96 ± 1.2. The release of active substances in gel preparations is also strongly influenced by gelling agents. The greater the concentration of the gelling agent used will produce a thick gel preparation that makes it difficult to release the active substance (Forestryana et al., 2020). The gelling agent used in this study was Carbopol 934. Carbopol 934 is a gelling agent that is commonly used because it has high compatibility and stability. In addition, the use of Carbopol 934 also provides a good release of active substances (Madan and Singh, 2010).

Based on the description above, the researchers formulated a nanoparticle gel of *Centella asiatica* L. with variations in carbopol 934 concentration. The gel was characterized and tested for release ability using the Franz Diffusion Cell method and measurement of flavonoid content using UV-Vis Spectrophotometry.

MATERIALS AND METHODS
Materials

The materials used were *Centella asiatica* L. Leaves (Palembang, Indonesia), Poly-Lactic-Co-Glycolic Acid (Sigma Aldrich, Singapore), Polyvinyl alcohol (Sigma Aldrich, Singapore), cellophane membrane (Merck, Indonesia), KH_2PO_4 (Merck, Indonesia), NaOH (Merck, Indonesia), glycerin (Bratachem, Indonesia), methylparaben (Bratachem, Indonesia), propylparaben (Bratachem, Indonesia), aquadest (Bratachem, Indonesia), quercetin (Sigma Aldrich, Singapore), carbopol 934 (Multisera Indos, Indonesia), and 96% ethanol (Bratachem, Indonesia)

Tools

The tools used in this study were analytical balances with readability of 0.001 g and 0.0001 g (Nesco®), pH meter (Thermo Scientific ®), rotary evaporator (IKA), franz diffusion cell (Pyrex®), Cup and Bob viscometer (Grace M3400®), and UV-Vis spectrophotometry (Biobase®).

Preparation of Centella asiatica L. leaves ethanolic extract

Centella asiatica L. leaves are obtained from Palembang, Indonesia. Leaves were made into a herbarium and identified at the Plant Conservation Center at the Purwodadi LIPI Botanical Garden. *Centella asiatica* L. leaves are dried to obtain dry simplicia. The simplicia was then macerated using 96% ethanol in a ratio of 1:5 for five days while stirring occasionally (Apriani et al., 2021). The filtrate obtained

was then concentrated using a rotary evaporator at a temperature of 60°C to get a thick extract.

Preparation of nanoparticles of Centella asiatica L.

The manufacture of nanoparticles following the research of Apriani et al. (2022). The nanoparticles were made using the Emulsion Solvent Evaporation Method. A total of 158 grams of extract and 50 grams of PLGA were dissolved in ethyl acetate solvent and acted as oil phase. In a different container, 40 mg of PVA was dissolved in aquadest and served as the aqueous phase. The oil phase was added drop by drop into the water phase above the homogenizer at a speed of 750 rpm for 1 hour. Next, aquadest was added up to 25 ml. The resulting solution was then evaporated for 24 hours.

Preparation of nanoparticles gel

The gel preparation in this study refers to the research of Mardiyanto et al. (2022) with modifications. The concentration of the materials used can be seen in Table 1. Carbopol 934 was dispersed in distilled water and added TEA to form a gel mass. Methylparaben and propylparaben were dissolved in glycerin and put into a gel mass. Nanoparticles of pegagan were added little by little and stirred until homogeneous. After homogeneous, add the remaining distilled water up to 100 mL.

Table 1. Formula for nanoparticles gel

Materials	Concentration Formula (%)		
	F1	F2	F3
Nanoparticles of *Centella asiatica* L.	25	25	25
Carbopol 934	1	1.5	2
Glycerin	2	2	2
Methylparaben	0.18	0.18	0.18
Propylparaben	0.02	0.02	0.02
TEA	qs	qs	qs
Aquadest (ad)	100	100	100

Evaluation of nanoparticles gel

The evaluation of the nanoparticle gel included organoleptic tests, homogeneity tests, pH tests, viscosity tests, spreadability tests, and adhesion tests.

Organoleptic and homogeneity test

Organoleptic and homogeneity tests were performed visually. The parameters that were observed included odour, colour, and dosage form of the gel.

pH test

The pH of the nanoparticles gel was measured using a pH meter.

Viscosity test

The viscosity test was carried out using a cup and bob viscometer with a speed of 60 rpm.

Spreadability test

The spreadability test was carried out using a scaled round glass. Measurement of the diameter of the spread is carried out longitudinally and transversely. The load used is from 50 to 150 grams.

Adhesion test

The gel preparation is placed on a slide and covered with a glass of another object, then given a weight of 1 kg for 3 minutes. Determination of adhesion is done by measuring the time it takes for the two slides to come off.

Stability test of nanoparticles gel

The stability test was carried out using the Cycling Test method at a temperature of 4±2°C and 40±2°C. The test was carried out for up to 6 cycles, and observations were made at the end of the cycle. The parameters that were observed included organoleptic and pH.

Measurement of the total flavonoid content of nanoparticles gel

A total of 0.1 sample solution was added with 0.1 mL of 1 M potassium acetate, 0.1 mL of $FeCl_3$, and up to 5 mL of distilled water. The absorbance of the solution was measured at a maximum wavelength for quercetin, which is 425 nm to obtain the total flavonoid content in the sample solution. Quercetin was used as a standard (Indarti et al., 2019).

In vitro release evaluation

In vitro, release evaluation was carried out on the three nanoparticle gel formulas (F1, F2, and F3) and the gel formula which was not formulated into nanoparticles as F4. The membrane used is the cellophane membrane. The receptor compartment solution was phosphate buffer pH 7.4 (Nurleni et al., 2019). The test was carried out at 37°C at a speed of 750 rpm. The number of samples used is 1 gram. Sampling was conducted at 0, 15, 30, 45, 60, 90, and 120 minutes and then the total flavonoid content in the sample was measured. After obtaining the total flavonoid content, the cumulative % drug release was calculated according to equation 1.

$Cumulative~\%~Drug~Release=$

$$\frac{Flavonoid~content~in~receptor~compartment~at~minute~n}{Flavonoid~content~in~nanoparticles~gel}......$$

.... [1]

Furthermore, the cumulative % drug release data is plotted into several models of release kinetics, namely zero order (cumulative % drug release vs time), first order (log cumulative % drug release vs time), Higuchi's model (cumulative % drug release vs squre root of time), and Korsmeyyer Peppas (log cumulative % drug release vs log time) to see the release model that occurs.

Data analysis

Data analysis was performed using SPSS for the evaluation of nanoparticles gel. A normality test was performed using Shapiro Wilk. If the data is normally distributed (p>0.05), then it is continued with the one-way ANOVA test, but if the data is not normally distributed (p<0.05), then it is continued with the Kruskal-Wallis test.

RESULTS AND DISCUSSION

The ethanolic extract of pegagan leaves has a thick texture, blackish green colour, and a distinctive smell. The yield percentage produced is 9.156%. The yield percentage produced is smaller than the previous research conducted by Djoko et al. (2020), namely 16.31%. This difference is due to different extraction processes. The study of Djoko et al. (2020) was sifted at a size of 40 mesh so that the smaller the particle size, the

larger the surface area of the simplicia in contact with the solvent. However, this result still meets the requirements of the Indonesian Herbal Pharmacopoeia, which is not less than 7.2% (Kemenkes RI, 2017).

The ethanol extract of pegagan leaves was then formulated into nanoparticles to increase the stability of the flavonoids. Flavonoids are compounds that are easily degraded in the presence of oxygen, high temperature, and light (Ioannou et al., 2020; Kemit et al., 2019; Ramesova et al., 2011; Sharma et al., 2015). The nanoparticle formula refers to the research of Apriani et al. (2022), where the resulting particle size was 288.1667±3.4195 nm, the polydispersity index was 0.371±0.0045, and the zeta potential was -10.6333±0.1154.

Nanoparticles of pegagan were formulated into gel preparations with varying concentrations of gelling agents. The gelling agent used in this study was Carbopol 934 with a successive concentrations of F1, F2, and F3 were 1; 1.5; and 2%. This concentration refers to the research of Asmi (2013) and Zheng et al. (2016). In Asmi's research (2013), the gel viscosity results obtained at carbopol 934 concentrations below 1% did not meet the requirements for suitable gel viscosity (< 2000 cPs). Meanwhile, in the research conducted by Zheng et al. (2016), the viscosity of the gel at a concentration of 3% carbopol 934 was very high, resulting in a minor release ability of the gel. The results of the evaluation of the nanoparticle gel can be seen in Table 2.

Table 2. Evaluation results of nanoparticles gel

Parameter	Formula			Sig
	F1	F2	F3	
Organoleptic	Yellow, distinctive smell, soft	Yellow, distinctive smell, slightly stiff	Yellow, distinctive smell, stiff	-
Homogeneity	Homogeneous	Homogeneous	Homogeneous	-
pH	6.20 ± 0.08	6.17 ± 0.17	6.00 ± 0.08	0.216
Viscosity (cPs)	3417.42 ± 55.59	3937.46 ± 127.82	4754.67 ± 277.97	0.001*
Spreadability (cm)	5.1 ± 0.08	3.7± 0.08	3.1 ± 0.08	0.000*
Adhesion (sec)	209.33 ± 8.99	249.00 ± 8.29	301.67 ±10.27	0.000*
Stability	No physical changes, pH 6.5	No physical changes, pH 6.4	No physical changes, pH 6.4	0.192

Note: * indicates that there is a significant difference in each test group (p<0.05)

The gel preparation has good characteristic if they have a pH in the skin range of 4.5-6.5 (Okuma et al., 2015; Nikam, 2017), viscosity in the range of 2000-4000 cPs (Ardana et al., 2015), spreadability of 5-7 cm (Apriani et al., 2018), and adhesion of 2-300 seconds (Yusuf et al., 2017). The resulting gel preparation is yellow, has a characteristic odour, homogeneous, and has a soft to stiff texture due to the effect of differences in the concentration of Carbopol 934 used. The pH of

the gel preparation was around 6 due to the addition of TEA to the formula. Carbopol 934 has an acidic pH range of 2.75 – 3.5 (Rowe et al., 2009). When added TEA which has a pH in the range of 7.76 (Fiume et al., 2013), Carbopol 934 will expand and form a gel mass. TEA also makes the pH of the preparation higher so that it meets the pH requirements of the skin range. The gel viscosity shows that F1 and F2 meet the requirements. F1 has the lowest viscosity compared to F2 and F3. The

viscosity can affect the results of spreadability and adhesion. The higher the viscosity, the smaller the spreadability of the gel, but the adhesion will be longer. The viscosity, spreadability, and adhesion statistical results showed a significant difference between groups ($p<0.05$). This is due to differences in the concentration of Carbopol 934 used. The higher the concentration of Carbopol 934 used, the higher the viscosity of the gel preparation. Carbopol 934 is a polymer that has an -OH group; when in contact with water in an alkaline environment, hydrogen bonds will occur, which cause swelling (Kaur et al., 2018). Spreadability and adhesion will affect the release ability of the preparation. Gels that have high spreadability and adhesion allow the drug to be maximally absorbed into the skin (Febrianto & Mia,

2020). The stability test results also showed that the three formulas did not significantly change in physical and pH ($p>0.05$).

The nanoparticle gel was followed by a release test using the Franz Diffusion Cell method using a cellophane membrane. In this test, pegagan gel which was not formulated into nanoparticles, was used as a comparison (F4). This test was carried out to determine the percentage of flavonoid content that was released at time intervals. The results can be seen in Table 3.

The release kinetics constant from zero order, first order, Higuchi's model, and Korsmeyer Peppas were calculated from the slope of the appropriate plots, and the regression coefficient (r^2) was determined in Table 4.

Table 3. Cumulative % Drug Release

Time (min)	Cumulative % Drug Release			
	F1	F2	F3	F4
0	7.93	5.49	0.67	2.31
15	15.19	12.35	3.07	5.26
30	20.65	17.47	5.78	8.12
45	25.62	26.51	10.78	9.37
60	32.87	35.14	16.71	12.45
90	42.19	40.76	21.01	14.57
120	58.17	47.74	23.76	20.62

Table 4. Release Kinetics Model

Release Kinetics Model	F1		F2		F3		F4	
	r2	k	r2	k	r2	k	r2	k
Zero Order	0.9945	0.4033	0.9606	0.3605	0.9582	0.2089	0.9829	0.1433
First Order	0.9137	0.0065	0.8240	0.0072	0.7712	0.0116	0.8483	0.0069
Higuchi	0.8944	4.4214	0.9388	4.2103	0.8991	2.3397	0.9202	1.6024
Korsmeyer-Peppas	0.9101	0.3917	0.9427	0.4602	0.9646	0.7759	0.9531	0.4370

Based on Table 3, F1 has the highest cumulative percentage of drug release. F4 is a gel preparation of pegagan which is not formulated into nanoparticles and has the smallest cumulative percentage of drug release compared to other formulas. The cumulative amount is strongly influenced by the characteristics of the gel preparation made and the nanoparticle carrier used. F1 has the lowest viscosity compared to F2 and F3, so the resistance to release is lower. When the gel is in contact with the phosphate buffer pH 7.4 (receptor compartment solution), the gel will swell so it will break. At medium pH 7.4, the COO- group in Carbopol 934 will experience electrostatic repulsion among –COO groups and a decrease in hydrogen bonding interactions which causes hydrogel swelling (Gaikwad et al., 2012; Suhail et al., 2020).

PLGA will contact with phosphate buffer solution pH 7.4. The solution will enter the nanoparticle system

and cause the nanoparticles to expand to form pores that allow the active substances in them to be constantly released until the degradation process of the PLGA polymer is complete (Fredenberg et al., 2011; Vimal et al., 2016). Furthermore, the drug in the form of nanoparticles will release. Based on Table 4, F1, F2, and F4 have a zero-order release kinetics model because they have the highest linearity with r2 values of 0.9945, 0.9606, and 0.9829, respectively. At the same time, F3 has a release kinetics model of Korsmeyer Peppas with an r2 value of 0.9646. The zero-order rate describes the systems where the drug release rate is independent of its concentration. F1 has a higher reaction kinetics constant (k) than the other formulas, so drug release occurs faster (Figure 1). Based on the results of the evaluation, physical stability, and release ability of the preparation, F1 was determined as the best formula in this study.
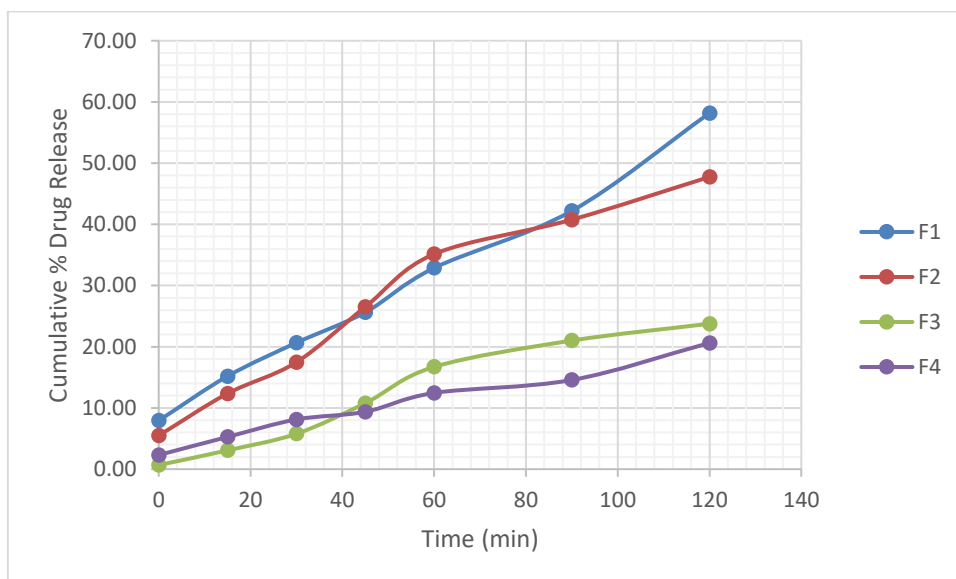
Figure 1. In vitro release curve

CONCLUSION

The concentration of the gelling agent Carbopol 934 influences the evaluation of the gel preparation and the release ability of the gel. The lower the concentration of Carbopol 934 used, the lower the gel's viscosity so that the gel's spreadability will be greater. The low viscosity of the gel will make it easier to release. F1 is the best formula because it has good physical properties and the greatest release ability compared to other formulas.

REFERENCES

Apriani, E.F., Nurleni, N., Nugrahani, H.N. & Iskandarsyah, I. (2018). Stability Testing of Azelaic Acid Cream Based Ethosome. *Asian Journal of Pharmaceutical and Clinical Research*, 11 (5), 270-273.

Apriani, E.F., Ahmadi, A. & Noviani, V. (2021). Formulation and Evaluation of Water Fraction Hair Tonic Containing Flavonoids from Ethanolic Extract of Green Tea Leaves (Camellia sinensis L.). *Traditional Medicine Journal*, 26 (2), 77-83

Apriani, E.F., Mardiyanto, M. & Destiana, R. (2022). Development of Nanoparticles Pegagan Leaves Ethanolic Extract (*Centella asiatica* (L.) Urban) Using Variation Concentration of Poly-Lactic-Co-Glycolic Acid (PLGA) Polymer. *Traditional Medicine Journal*, 27 (1), 67-74.

Ardana, M., Aeyni, V. & Ibrahim, A. (2015). Formulasi dan Optimasi Basis Gel HPMC (Hidroxy Propyl Methyl Cellulose)

dengan Berbagai Variasi Konsentrasi. *J.Trop. Pharm. Chem.,* 3 (2), 101-108.

Arumugam, T., Muniappan, A., Yesudason, J.K. & Sekar, T. (2011). Phytochemical Screening and Antibacterial activity of leaf and callus extracts of *Centella asiatica*. *Bangladesh Journal of Pharmacology*, 6, 55-60.

Asmi, R.P. (2013). Uji Efek Penyembuhan Luka Bakar Gel Ekstrak Herba Pegagan. *Skripsi*, Universitas Muhammadiyah Surakarta, Surakarta, Indonesia

Djoko, W., Taurhesia, S., Djamil, R. & Simanjuntak, P. (2020). Standardisasi Ekstrak Etanol Herba Pegagan (Centella asiatica). *Sainstech Farma*, 13 (2), 118-123.

Febrianto, Y. & Mia, J. (2020). Formulasi Dan Evaluasi Sediaan Gel Ekstrak Etanol Daun Cabai Rawit (*Capsicum frutescens L* .) dengan Variasi Carbopol Dan Cmc Na Sebagai gelling agent. *SCIENTIA Jurnal Farmasi dan Kesehatan,* 10 (2), 136-145.

Fiume, M.M., Heldreth, B., Bergfeld, W.F., Belsito, D.V., Hill, R.A., Klaassen, C.D., Liebler, D., Marks, J.G., Shank, R.C., Slaga, T.J., Snyder, P.W. & Andersen, F.A. (2013). Safety Assessment of Triethanolamine and Triethanolamine-Containing Ingredients as Used in Cosmetics. *International Journal of Toxicology*, *32* (3), 59-83.

Forestryana, D., Surur, F.M. & Novyra, P.A. (2020). Pengaruh Jenis dan Konsentrasi Gelling Agent pada Karakteristik Formula Gel Antiseptik Ekstrak Etanol 70% Kulit Buah Pisang Ambon. *Lumbung Farmasi: Jurnal Ilmu Kefarmasian*, 1 (2), 45.

Fredenberg, S., Wahlgren, M., Reslow, M. & Axelsson, A. (2011). The mechanisms of drug release in poly(lactic-co-glycolic acid)-based drug delivery systems-A review. *International Journal of Pharmaceutics*, 415 (2011), 34-52.

Gaikwad, V., Yadav, V., Dhavale, R., Choudhari, S. & Jadhav, S. (2012). Effect of Carbopol 934 and 940 on Fluconazole Release from Topical Gel Formulation: A Factorial Approach. *Current Pharma Research*, 2, 487-493.

Gelders, G., Baekelandt, V. & Van der Perren, A. (2018). Linking neuroinflammation and neurodegeneration in parkinson's disease. *In J. Immunol. Res.,* 4784268.

Indarti, K., Apriani, E.F., Wibowo, A.E. & Simanjuntak, P. (2019). Antiontioxidant Activity of Ethanolic Extract and Various Fractions from Green Tea (*Camellia sinensis L.*) Leaves. *Pharmacognosy Journal*, 11 (4), 771-776.

Ioannou, I., Hafsa, I. & Ghoul, M. (2012). Review of the effects of food processing and formulation on flavonol and anthocyanin behaviour. *J. Food Eng.*, 2012, 111, 208–217.

Ioannou, I., Chekir, L. & Ghoul, M. (2020). Effect of Heat Treatment and Light Exposure on the Antioxidant Activity of Flavonoids. *Processes*, 8 (1078), 1-17.

Jiang, T., Sun, Q. & Chen, S. (2016). Oxidative stress: A major pathogenesis and potential therapeutic target of antioxidative agents in Parkinson's disease and Alzheimer's disease. *Prog. Neurobiol,* 147, 1–19.

Kaur, G., Grewal, J., Jyoti, K., Jain, U.K., Chandra, R. & Madan, J. (2018). Drug Targeting and Stimuli Sensitive Drug Delivery Systems, India: William Andrew Publishing

Kemenkes RI. (2017). Farmakope Herbal Indonesia Edisi II, Jakarta: Kementerian Kesehatan Republik Indonesia.

Kemit, N., Permana, D.G.M. & Kencana, P.K.D. (2019). Stabilitas Senyawa Flavonoid Ekstrak Daun Alpukat (*Persea americana Mill.*) terhadap Perlakuan pH dan Suhu Flavonoid. *Media Ilmiah Teknologi Pangan (Scientific Journal of Food Technology)*, 6 (1), 34–42.

Liu, S.Y., Duan, X.C., Jin, S., Teng, X., Xiao, L. & Xue, H.M. (2017). Hydrogen Sulfide Improves Myocardial Remodeling via Downregulated Angiotensin II/AT1R Pathway in Renovascular Hypertensive Rats. *Am. J. Hypertens,* 30 (1), 67–74.

Madan, J. & Singh, R. (2010). Formulation and Evaluation of Aloe vera Topical Gels. *International Journal of Pharmaceutical Sciences*, 2 (2), 551-555.

Mardiyanto, M., Apriani, E.F. & Alfarizi, M.H. (2022). Formulation and In-Vitro Antibacterial Activity of Gel Containing Ethanolic Extract of Purple Sweet Potato Leaves (*Ipomoea Batatas* (L.)) Loaded Poly Lactic Co-Glycolic Acid Submicroparticles Against *Staphylococcus aureus*. *Research Journal of Pharmacy and Technology*, 15 (8).

Mardiyanto, M., Fithri, N. A. & Raefty, W. (2018). Optimasi Formula Submikro Partikel Poly (Lactic-co-Glycolic Acid) Pembawa Betametason Valerat dengan Variasi Konsentrasi Poly (Vinyl Alcohol) dan Waktu Sonikasi. *Jurnal Sains Farmasi & Klinis, 5* (1), 55.

Nikam, S. (2017). Anti-acne Gel of Isotretinoin: Formulation and Evaluation. *Asian J. Pharm. Clin. Res.*, 10 (11), 257-266

Nurleni, N., Iskandarsyah, I. & Aulia, A. (2018). Formulation and Penetration Testing of Ethosome Azelaic Acid on Abdominal Skin White Male Rats (*Rattus norvegicus*) With Franz Diffusion Cell. *Asian Journal of Pharmaceutical and Clinical Research*, 11 (4), 327-330.

Okuma, C.H., Andrade, T.A.M., Caetano, G.F., Finci, L.I., Maciel, N.R., Topan, J.F., Cefali, L.C., Polizello, A.C.M., Carlo, T., Rogerio, A.P., Sapadaro, A.C.C., Isaac, V.L.B., Frade, M.A.C. & Rocha-Filho, P.A. (2015). Development of Lamellar Gel phase emulsion containing marigold oil (Calendula officinalis) as a potential modern wound dressing. *Eur. J. Pharm. Sci.,* 71, 62-72.

Panche, A., Diwan, A. & Chandra, S. (2016). Flavonoids: An overview. *Journal of Nutritional Science*, 5 (47), 1-15.

Park, J.H., Choi, J.Y., Son, D.J., Park, E.K., Song, M.J., Hellström, M. & Hong, J. T. (2017). Anti-Inflammatory Effect of Titrated Extract of Centella asiatica in Phthalic Anhydride-Induced Allergic Dermatitis Animal

Model. *International journal of molecular sciences*, *18* (4), 738.

Patel, N.A., Patel, N.J. & Patel, R.P. (2009). Comparative development and evaluation of topical gel and cream formulations of psoralen. *Drug discoveries & therapeutics*, *3* (5), 234–242.

Quyen, N.T.C., Quyen, N.T.N., Quy, N.N. & Quan, P.M. (2020). Evaluation of total polyphenol content, total flavonoid content, and antioxidant activity of *Centella asiatica. IOP Conf. Series: Materials Science and Engineering*, 991, 1-6.

Rameshreddy, P., Uddandrao, V.V.S., Brahmanaidu, P., Vadivukkarasi, S., Ravindarnaik, R., Suresh, P. et al (2018). Obesity-alleviating potential of asiatic acid and its effects on ACC1, UCP2, and CPT1 mRNA expression in high fat diet-induced obese Sprague–Dawley rats. *Mol. Cell. Biochem.,* 442 (1–2), 143–154.

Ramesova, S., Sokolova, R., Degano, I., Bulickova, J., Zabka, J. & Gal, M. (2011). On the stability of the bioactive flavonoids quercetin and luteolin under oxygen-free conditions. *Analytical and bioanalytical chemistry*, 402 (2), 975-982.

Rowe, R.C., Sheskey P.J. & Queen, M.E. (2009). *Handbook of Pharmaceutical Excipients sixth edition*, London: The Pharmaceutical Press.

Sawatdee, S., Choochuay, K., Chanthorn, W. & Srichana, T. (2016). Evaluation of the topical spray containing *Centella asiatica* extract and its efficacy on excision wounds in rats. *Acta Pharm,* 66 (2), 233–244.

Sharma, K., Ko, E.Y., Assefa, A.D., Ha, S., Nile, S.H., Lee, E.T. & Park, S.W. (2015). Temperature dependent studies on the total phenolics, flavonoids, antioxidant activities, and sugar content in six onion varieties. *Journal of Food and Drug Analysis*, 23 (2), 243-252.

Suhail, M., Wu, P.C. & Minhas, M.U. (2020). Using Carbomer-Based Hydrogels for Control the Release Rate of Diclofenac Sodium: Preparation and In Vitro Evaluation. *Pharmaceuticals*, 13 (399), 1-17.

Vimal, P., Bhavesh, A., Anand, D., Manish, G. & Adil, P. (2016). A Review on Long Acting PLGA Based in Situ Forming Microparticles Formulation for a Novel Drug Delivery System. *Res. J. Pharm. Dosage Form. and Tech*, 8 (2), 127-134.

Yusuf, A.L., Nurawaliah, E. & Harun, N. (2017). Uji Efektivitas Gel Ekstrak Etanol Daun Kelor *(Moringa oleifera L.)* sebagai Antijamur Malassezia furfur. *Kartika: Jurnal Ilmiah Farmasi*, 5 (2), 62-67.

Zheng, Y., Ouyang, W.Q., Wei, Y.P., Syed, S.F., Hao, C.S., Wang, B.Z. & Shang, Y.H. (2016). Effects of Carbopol® 934 proportion on nanoemulsion gel for topical and transdermal drug delivery: a skin permeation study. *International journal of nanomedicine*, 11, 5971–5987.

Zheng, Y., Ley, S.H. & Hu, F.B. (2018). Global aetiology and epidemiology of type 2 diabetes mellitus and its complications. *Nat. Rev. Endocrinol,* 14 (2), 88–98.

Analysis of Potential *Cinnamomum zeylanicum* Blume Essential Oil Against Alzheimer's Disease: A Molecular Docking Study

Muhammad Ja'far Shodiq[1], Farmindo Hartono[1], Siti Khaerunnisa[2]*, Abdulloh Machin[3]
[1]Faculty of Medicine, Universitas Airlangga, Surabaya, Indonesia
[2]Departement of Physiology and Medical Biochemistry, Faculty of Medicine, Universitas Airlangga, Surabaya, Indonesia
[3]Departement of Neuorology, Faculty of Medicine, Universitas Airlangga - Dr. Soetomo General Hospital, Surabaya, Indonesia

*Corresponding author: st.khaerunnisa@fk.unair.ac.id

Abstract

Background: Alzheimer's Disease (AD) is a neurodegenerative disorder with progressive impairment of behavioural and cognitive functions and the most common cause of dementia. The pathophysiology of AD is associated with low acetylcholine, accumulation of amyloid beta plaque, and neurofibrillary tangles in the brain. Cinnamomum zeylanicum is known to have many medicinal properties, especially neuroprotective effects. Objective: This research was designed to determine the neuroprotective potential of the phytochemicals C. zeylanicum using an in silico study. Methods: There are 5 phytochemicals compounds of C. zeylanicum used in this study. It's qualified for Lipinski's rules of five and can cross blood brain barrier. The protein targets were AChE, BACE1, and GSK-3. Molecular docking and visualization were performed using Avogadro, AutoDock 4.2 PyMol and Biovia Discovery Studio 2019. Results: In silico results show that the main phytochemical compounds of C. zeylanicum Blume essential oil have great potency as an AD drug. The best interaction model of the compound was shown by trans-cinnamyl acetate and coumaric acid. Although the binding energy of the compounds is lower than AD drugs (donepezil, rivastigmine, galantamine), the binding energy is not much different from rivastigmine and galantamine. Conclusion: The phytochemical compounds of C. zeylanicum Blume essential oil have an effect as a neuroprotective agent for AD and should be investigated in future research.

Keywords: Alzheimer's Disease, Cinnamomum zeylanicum, Molecular Docking Study

INTRODUCTION

Alzheimer's Disease (AD) known as a neurodegenerative disorder that mostly attacks people over 65 years marked by insidious onset and progressive impairment of behavioral and cognitive functions including memory, comprehension, language, attention, reasoning, and judgment (Cassani *et al.*, 2018; Cortes-Canteli and Iadecola, 2020; Kumar *et al.*, 2022). AD is the supreme cause of dementia worldwide (60-80%) and also causes a decline in cognitive ability (Lucey, 2020; Litke *et al.*, 2021). In 2015, around 46.8 million people worldwide suffered from AD; it's predicted to be 82 million in 2030 and 152 million in 2050. About 10 million new cases of AD are reported yearly worldwide (Cassani *et al.*, 2018; Vinicius *et al.*, 2019). In the Asia-Pacific region, AD is estimated to increase from 23 million in 2015 to 71 million in 2050 (Alzheimer's Disease International and Alzheimer's Australia, 2014). In Indonesia, the prevalence of AD patients was about 1.2 million in 2013, and it was estimated to have a rapid increase to 1.9 million in 2030 and 3.9 million in 2050 (Ong *et al.*, 2021). The cause of this increase is due to increasing life expectancy worldwide. In 2015, life expectancy reached 72 years in Indonesia itself (Kumar *et al.*, 2022). This will have an impact on the health and socio-economic sectors (Ong *et al.*, 2021).

One of the pathophysiologies of AD is cholinergic neuron dysfunction caused by cholinergic toxicity. Overactivity of AChE will cause a significant decrease in ACh levels in the synaptic cleft in the cortex, hippocampus, and amygdala. It will disturb cholinergic neurons involved in brain functions such as learning, memory, attention, response, sleep, and the delivery of sensory information (Kumar *et al.*, 2022; Samanta, Ramesh and Govindaraju, 2022). Accumulation of Aβ plaques is also found in AD. This accumulation results in amyloid aggregation that promotes microglial activation and local inflammatory responses and leads to neurotoxicity. Amyloid deposition occurs around the meningeal and cerebral blood vessels and grey matter in AD (Dá Mesquita *et al.*, 2016; Tiwari *et al.*, 2019; Fan *et al.*, 2020; Kumar *et al.*, 2022). The presence of neurofibrillary tangles has been proven to have a relationship with AD. Hyperphosphorylation of the tau protein will form these tangles. The main function of tau protein is to stabilize axonal microtubules in the brain. Neurofibrillary tangles are stored in neurons and occur first in the hippocampus, then they are seen throughout the cerebral cortex (Long and Holtzman, 2019; Tiwari *et al.*, 2019; Kumar *et al.*, 2022). Some drugs that the FDAthe FDA approves approves for AD are donepezil, galantamine, and rivastigmine (Yiannopoulou and Papageorgiou, 2020). However, these drugs have side effects such as gastrointestinal disturbances, dyspepsia, nausea, vomiting, loss of appetite, diarrhea, muscle aches, loss of balance, headache, and hepatotoxicity (Kumar, Chowdhury and Kumar, 2017; Kallel *et al.*, 2019). In recent years, there is many studies to develop new anti-AD drugs with lesser side effects (Kareti and Pharm, 2020).

C. zeylanicum Blume is an aromatic plant from Sri Lanka and the Malabar coasts of India. It was usually us as seasoning in Asian traditional food and herbal medicine in different cultures and systems (Fahad *et al.*, 2018; Kallel *et al.*, 2019). It has many medicinal properties such as anti inflammatory, anti oxidant, analgesic,anti-cancer, anti-diabetic, anti-microbial, cardiovascular protective, cytoprotective, and neuroprotective (Momtaz *et al.*, 2017; Wang *et al.*, 2020). The herbal plants used to treat several diseases have developed rapidly in recent years (Kareti and Pharm, 2020). Plants are considered to be one of the sources of therapeutic active compounds, so this research was conducted to find new anti-AD drugs from herbal plants that might later have fewer side effects. *C. zeylanicum* Blume essential oil was chosen because it is believed to have a useful neuroprotective effect on AD. In previous studies, *C. zeylanicum* had anti-alzheimer's activity by inhibiting the nucleation process and the formation of tau filaments (Dhage *et al.*, 2021). Tepe and Ozaslan (2020) reported that *C. zeylanicum* had AChE inhibitory activity, which plays a role in the pathophysiology of AD. Frydman-Marom *et al.* (2011) also reported that *C. zeylanicum* can inhibit Aβ plaque accumulation in AD.

MATERIAL AND METHODS
System Configuration

This molecular docking study used operating Windows 10 OS 32 bit laptop with an Intel Core i3 processor and 2 GB RAM. Applications in silico research include Avogadro, AutoDock 4.2, Biovia Discovery Studio 2019, and PyMol.

Ligand and Protein Selection

C. zeylanicum Blume essential oil has the main phytochemical compounds namely cinnamaldehyde, *trans*-cinnamyl acetate, 1,4-benzene dicarboxylic acid, 1,8-cineole, α-pinene, coumaric acid, and 9-octadecenoic acid (Kallel *et al.*, 2019). The compound that is qualified for Lipinski's rule of five and can cross blood-brain barrier (BBB) is used in this molecular docking. The terms of Lipinski's rule of five can be checked through the website http://www.swissadme.ch/index.php. The qualified compounds will be compared with donepezil, galantamine, and rivastigmine, which are some of the FDA-approved drugs for AD (Yiannopoulou and Papageorgiou, 2020). The qualified compounds are cinnamaldehyde, *trans*-cinnamyl acetate, 1,8-cineole, α-pinene, and coumaric acid (Table 1). The 3D structure of the phytochemicals is downloaded from the website https://pubchem.ncbi.nlm.nih.gov and will be used as a ligand. The ligands were docked with the acetylcholinesterase/AChE receptor (PDB ID: 7E3H), β-site APP cleaving enzyme 1/BACE1 (GDP ID: 4DJU), and glycogen synthase kinase-3/GSK-3 (PDB ID: 1Q5K). These receptors play an important role in the pathophysiology of AD (Jagust, 2018). The protein structure was downloaded from the protein data bank (PDB) website http://www.rcsb.org.

Ligand Structure Optimization

The compounds downloaded in ".sdf" format are optimized using Avogadro software and saved in ".mol2" format. After that, the compounds in ".mol2"

format was converted to ".pdbqt" format using AutoDock 4.2 software.

Protein Structure Preparation

The macromolecular structure of the protein downloaded in ".pdb" format from Protein Data Bank (PDB) was searched for the active site using the BIOVIA Discovery Studio 2019 software. In AChE, BACE1, and GSK-3 proteins, there are two chains, Chain A and B. Then we choose chain A , which is used for docking using AutoDock 4.2 software. Proteins were optimized by adding polar hydrogens, merging non-polar, adding Kollman charges in proteins, and computing gasteiger in native ligands. After that, the receptor is separated from the native ligand and saved in ".pdbqt" format.

Grid Box Determination
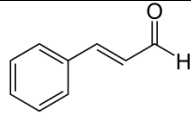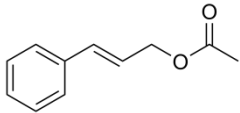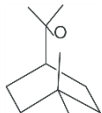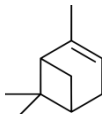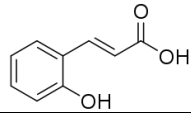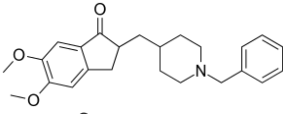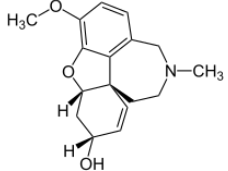
The size, centre coordinates, and spacing of the grid box are determined by the position of the native ligand using AutoDock 4.2 software. In AChE protein, the native ligand E20 grid was set in 40x40x40 (XYZ) point size, -43.74, 37.597, -30.039 centre coordinates, and 0.375 A spacing. In the BACE1 protein, the native ligand 0KK grid was set in 40x40x40 (XYZ) point size, 21,029, 10,689, 22,069 centre coordinates, and 0.375 A spacing. In the GSK-3 protein, the native ligand TMU grid was set in 40x40x40 (XYZ) point size, 23,148, 22.189, 8,978 centre coordinates, and 0.375 A spacing.

Molecular Docking

Proteins and ligands that have been prepared and grid boxes that have been determined are saved in ".gpf" format, and molecular docking is carried out with AutoDock 4.2 software. The ligand conformation output was analyzed using the Lamarckian Genetic Algorithm. Compounds that have the lowest bond energy (ΔG) show strong bonds and favourable conformations for ligand and protein interactions. After that, the results obtained in ".dlg" format are reopened using AutoDock 4.2 software to view the ligand bonds with amino acids and saved in ".pdb" format. The molecular docking results were visualized using the PyMol and BIOVIA Discover Studio 2019 software (Khaerunnisa, Suhartati and Awaluddin, 2020).

Table 1. Ligand Structure of Molecular Docking

Ligand	Molecular Formula	PubChem CID	Molecular Structure
C. zeylanicum blume essential oil			
Cinnamaldehyde	C_9H_8O	637511	
Trans-cinnamyl acetate	$C_{11}H_{12}O_2$	5282110	
1,8-cineole	$C_{10}H_{18}O$	2758	
α-pinene	$C_{10}H_{16}$	6654	
Coumaric acid	$C_9H_8O_3$	637542	
Alzheimer's disease drug			
Donepezil	$C_{24}H_{29}NO_3$	3152	
Galantamine	$C_{17}H_{21}NO_3$	9651	

Rivastigmine	$C_{14}H_{22}N_2O_2$	77991	
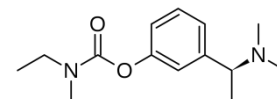
RESULTS AND DISCUSSION

C. zeylanicum Blume essential oil has 23 phytochemical compounds which represent at 99.39% of total essential oil. The main phytochemical compounds were cinnamaldehyde, *trans*-cinnamyl acetate, 1,4-benzene dicarboxylic acid, 1,8-cineole, α-pinene, coumaric acid, and 9-octadecenoic acid (Kallel *et al.*, 2019). Phytochemicals were screened before docking. Five phytochemical compounds were selected for molecular docking analysis. Due to Lipinski's rule of five, all of the ligands have zero violations, but 1,4-benzene dicarboxylic acid and 9-Octadecenoic acid can't cross the BBB, so the ligands are excluded (Table 2). Lipinski's rule of five terms consists of molecular weight <500 Da, log P <5, H-bond donor <5, and H-bond acceptor <10. Lipinski's rule of five can be used to classify the phytochemicals that may be effective in being used as drugs (Lipinski *et al.*, 2001). The compound must cross the BBB because the target receptor being inhibited is located in the brain (Pardridge, 2020).

Table 2. ADME Analysis of *C. zeylanicum* Blume Essential Oil Compound

Phytochemical Compound	Lipinski's Rule of Five					BBB Permeant
	Molecular Weight	Log P	H-bond donor	H-bond acceptor	Violations	
Cinnamaldehyde	132,16	1,97	0	1	0	Yes
Trans-cinnamyl acetate	176,21	2,33	0	2	0	Yes
1,4-benzenedicarboxylic acid	166,13	1,13	2	4	0	No
1,8-cineole	154,25	2,67	0	1	0	Yes
α-pinene	136,23	3,44	0	0	0	Yes
Coumaric acid	164,16	1,26	2	3	0	Yes
9-Octadecenoic acid	282,46	5,71	1	2	0	No

AChE (PDB ID: 7E3H) is a cholinergic enzyme primarily found at postsynaptic neuromuscular junctions (NMJ). AChE immediately breaks down acetylcholine into acetic acid and choline in NMJ. AChE plays a critical role in AD (Trang and Khandhar, 2022). 7E3H has a total structure Weight of 120.37 kDa, an Atom Count of 8437, a Modeled Residue Count of 1054, a Deposited Residue Count of 1080, and one Unique protein chain. This receptor has a native ligand E20 that binds to 14 active site amino acids namely TYR072, ASP074, GLU202, TRP286, VAL294, PHE295, PHE338, TYR341, SER293, TRP086, GLY121, TYR124, TYR337, and HIS447. BACE1 (PDB ID: 4DJU) is a β-secretase involved in the β-amyloid peptide, a dominant component in AD (Gnanaraj *et al.*, 2022). 4DJU has a total structure Weight of 93.33 kDa, an Atom Count of 7068, a Modeled Residue Count of 779, a Deposited Residue Count of 828, and one Unique protein chain. This receptor has a native ligand 0KK that binds to 13 active site amino acids namely LEU091, ASP093, GLY095, SER096, VAL130, TYR132, TRP137, PHE169, TRP176, ILE179, ASP289, GLY291, and THR292 (Cumming *et al.*, 2012). GSK3 (PDB ID: 1Q5K) is a serine/threonine protein kinase that phosphorylates Tau protein, whose expression is associated with AD (Gnanaraj *et al.*, 2022). 1Q5K has a total structure Weight of 92.85 kDa, an Atom Count of 5930, a Modeled Residue Count of 689, a Deposited Residue Count of 828, and one Unique protein chain. This receptor has a nat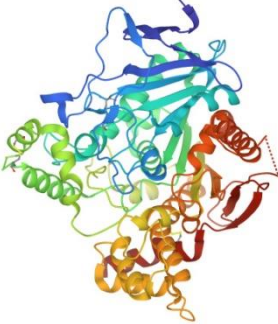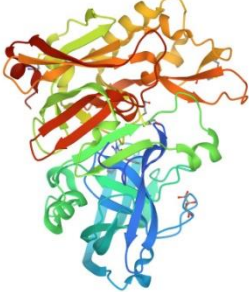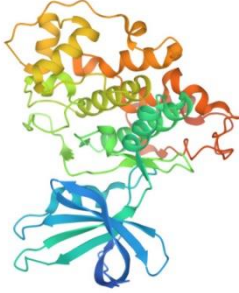ive ligand TMU that binds to 12 active site amino acids, namely VAL061, ILE062, VAL070, ALA083, VAL135, PRO136, LEU132, LEU188, ASP133, TYR134, ARG141, and CYS199 (Bhat *et al.*, 2003). Table 3 also visualizes the 3D structure of each receptor at 2.45, 1.80, and 1.94 Å X-ray diffraction resolutions.

Based on the results of molecular docking, the phytochemical of *C. zeylanicum* Blume essential oil that has the strongest binding energy to the AChE receptor is *trans*-cinnamyl acetate (ΔG: -6.21 kcal/mol) with an inhibition constant of 27.84 µM. The other compounds, α-pinene, 1,8-cineole, coumaric acid, and cinnamaldehyde had binding energies of -5.96, -5.86, -5.76, and -5.50 kcal/mol with inhibition constants of 43.49, 50.56, 60.95, and 92.75 µM. In the AD drug, donepezil, galantamine, and rivastigmine had binding energies of -11.04, -8.05, and -7.29 kcal/mol with inhibition constants of 8.15 nM, 1.26 µM, and 4.52 µM. At the BACE1 receptor, the phytochemical of *C. zeylanicum* Blume essential oil with the strongest binding energy is *trans*-cinnamyl acetate (ΔG: -5.16 kcal/mol) with an inhibitory constant of 164.04 µM. The other compounds, cinnamaldehyde, coumaric acid, α-pinene, and 1,8-cineole have binding energies of -4.62, -4.51, -4.43, and -4.41 kcal/mol with inhibition constants of 408.29, 496.02, 567.62, and 583.24 µM. . Meanwhile, donepezil, galantamine, and rivastigmine had binding energies of -8.50, -6.08, and -5.89 kcal/mol with inhibition constants of 588.62 nM, 34.99 µM, and 47.78 µM. At the GSK-3 receptor, the phytochemical of *C. zeylanicum* Blume essential oil with the strongest

binding energy is coumaric acid (ΔG: -5.61 kcal/mol) with an inhibition constant of 77.41 µM. Other compounds, *trans*-cinnamyl acetate, 1,8-cineole, cinnamaldehyde, and α-pinene have binding energies of -5.47, -4.93, -4.92, and -4.83 kcal/mol with inhibition constants of 97.51, 245.32, 248.03, and 287.66 µM. Meanwhile, donepezil, galantamine, and rivastigmine had binding energies of -8.53, -6.29, and -6.22 kcal/mol with inhibition constants of 562.75 nM, 24.71 µM, and 27.74 µM (Table 4).

Table 3. Protein Target Associated with Alzheimer's Disease

Protein Target	PDB ID	Active Site	3D Structure
AChE (Acetylcholinesterase) Crystal structure of human acetylcholinesterase in complex with donepezil	7E3H	TYR072, ASP074, TRP086, GLY121, TYR124, GLU202, TRP286, SER293, VAL294, PHE295, TYR337, PHE338, TYR341, HIS447	
BACE1 (β-site APP Cleaving Enzyme 1) Structure of BACE bound to 2-imino-3-methyl-5,5-diphenylimidazolidin-4-one	4DJU	LEU091, ASP093, GLY095, SER096, VAL130, TYR132, TRP137, PHE169, TRP176, ILE179, ASP289, GLY291, THR292	
GSK-3 (Glycogen Synthase Kinase-3) crystal structure of glycogen synthase kinase 3 in complexed with inhibitor	1Q5K	VAL061, ILE062, VAL070, ALA083, LEU132, ASP133, TYR134, VAL135, PRO136, ARG141, LEU188, CYS199	

The molecular docking results are then visualized in Table 5. At the AChE receptor, the phytochemical of *C. zeylanicum* Blume essential oil, cinnamaldehyde binds to 9 amino acids with 7 van der Waals bonds, *trans*-cinnamyl acetate binds to 8 amino acids with 4 van der Waals bonds, 1,8-cineole binds to 8 amino acids with 2 van der Waals bonds, α-pinene binds to 8 amino acids with 4 van der Waals bonds, and coumaric acid binds to 12 amino acids with 9 van der Waals bonds. In the AD drug, donepezil binds to 14 amino acids with 6 van der Waals bonds, galantamine binds to 10 amino acids with 6 van der Waals bonds, and rivastigmine binds to 11 amino acids with 5 van der Waals bonds. At the BACE1 receptor, it was found that cinnamaldehyde binds to 11 amino acids with 5 van der Waals bonds, *trans*-cinnamyl acetate binds to 10 amino acids with 6 van der Waals bonds, 1,8-cineole binds to 7 amino acids with 2 van der Waals bonds, α-pinene binds to 7 amino acids with 3 van der Waals bonds, and coumaric acid binds to 10 amino acids with 7 van der Waals bonds. Meanwhile, donepezil binds to 17 amino acids with 11 van der Waals bonds, galantamine binds to 12 amino acids with 6 van der Waals bonds, and rivastigmine binds to 11 amino acids with 1 van der Waals bond. At the GSK-3 receptor, it was found that cinnamaldehyde binds to 12 amino acids with 8 van der Waals bonds, *trans*-cinnamyl acetate binds to 14 amino acids with 9 van der Waals bonds, 1,8-cineole binds to 9 amino acids with 3

van der Waals bonds, α-pinene binds to 11 amino acids with 4 van der Waals bonds, and coumaric acid binds to 11 amino acids with 5 van der Waals bonds. Meanwhile, donepezil binds to 12 amino acids with 6 van der Waals

bonds, galantamine binds to 12 amino acids with 7 van der Waals bonds, and rivastigmine binds to 11 amino acids with 5 van der Waals bonds.

Table 4. Molecular Docking Results of Ligands with The Protein Target

| Ligand | Protein Targets Associated With Alzheimer's Disease | | | | | |
| | AChE | | BACE1 | | GSK-3 | |
	ΔG (kcal/mol)	K_i	ΔG (kcal/mol)	K_i	ΔG (kal/mol)	K_i
C. zeylanicum blume essential oil						
Cinnamaldehyde	-5.50	92.75 μM	-4.62	408.29 μM	-4.92	248.03 μM
Trans-cinnamyl acetate	-6.21	27.84 μM	-5.16	164.04 μM	-5.47	97.51 μM
1,8-cineole	-5.86	50.56 μM	-4.41	583.24 μM	-4.93	245.32 μM
α-pinene	-5.96	43.49 μM	-4.43	567.62 μM	-4.83	287.66 μM
Coumaric acid	-5.76	60.95 μM	-4.51	496.02 μM	-5.61	77.41 μM
Alzheimer's disease drug						
Donepezil	-11.04	8.15 nM	-8.50	588.62 nM	-8.53	562.75 nM
Galantamine	-8.05	1.26 μM	-6.08	34.99 μM	-6.29	24.71 μM
Rivastigmine	-7.29	4.52 μM	-5.89	47.78 μM	-6.22	27.74 μM
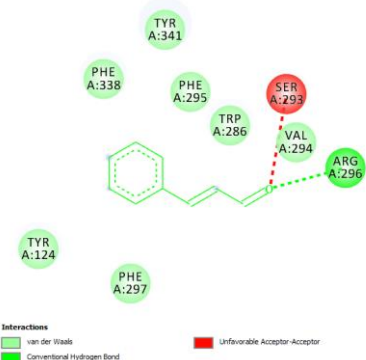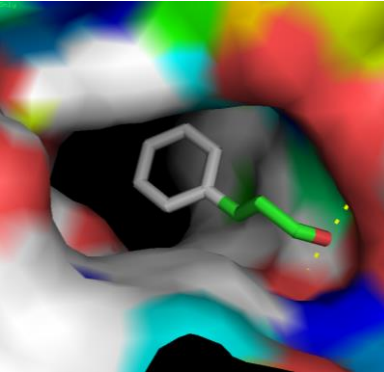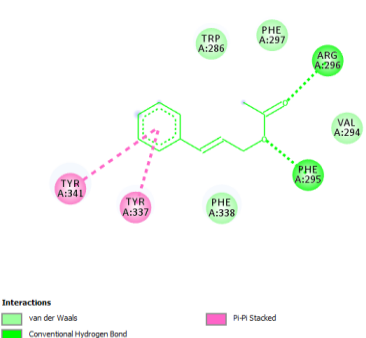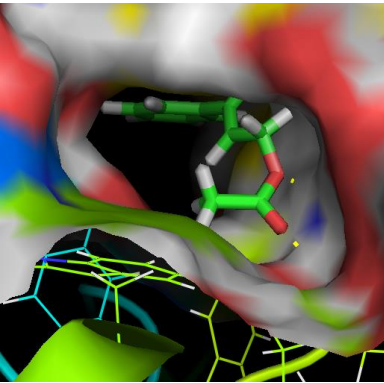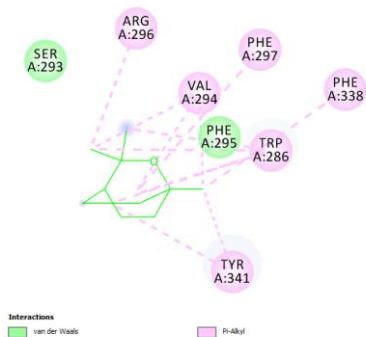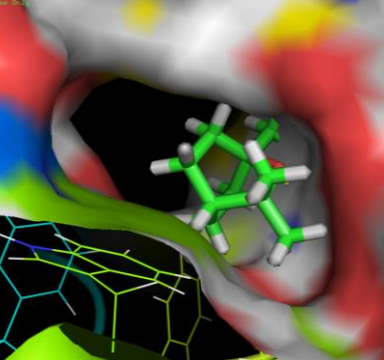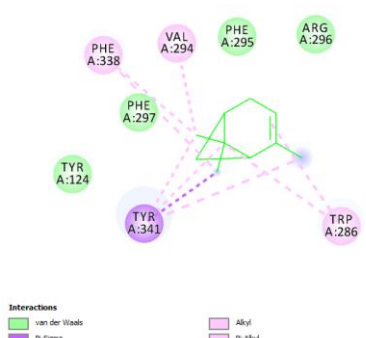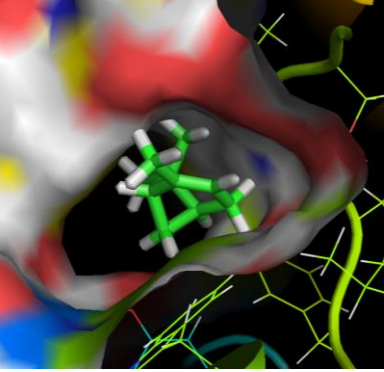
Cinnamaldehyde is a natural flavonoid and derivative compound of the volatile chemical aldehyde that gives cinnamon its flavour and aroma. Cinnamaldehyde is the main phytochemical compound of *C. zeylanicum* Blume essential oil (about 90%) (National Center for Biotechnology Information, 2022c). It has many pharmacological activities, including anti-inflammatory, antimicrobial, anti-cancer, anti-hyperglycemic, and neuroprotection (Zhang *et al.*, 2015). *Trans*-cinnamyl acetate is an acetate ester produced from the condensation of cinnamyl alcohol and acetic acid (National Center for Biotechnology Information, 2022b). Its pharmacological properties include anti-inflammatory, anticancer, antioxidant, antimicrobial, antidiabetic, anti-anxiety, antidepressant, and neuroprotection (Rao and Gan, 2014). Cinnamaldehyde and *trans*-cinnamyl acetate have neuroprotection functions that can be used for preventive and therapeutic nervous system diseases (Zhang *et al.*, 2015). 1,8-Cineole (eucalyptol) is an achiral aromatic component of many plants, including *C. Zeylanicum* (National Center for Biotechnology Information, 2022a). 1,8-Cineole has potential pharmacological properties such as anti-inflammatory, antioxidative, anti-cancer, and neuroprotection. 1,8-Cineole was used to treat nervous system disease (Cai *et al.*, 2020). α-pinene is an organic compound of the polyphenolic group terpene and a component of many aromatic, dietary plants, such as *C. Zeylanicum* (National Center for Biotechnology Information, 2022e). α-pinene has pharmacological properties such as antinociceptive and antioxidant. α-pinene has a strong anti-inflammatory effect in some pathological

conditions. α-pinene also has neuroprotective effect, and it's capable of restoring BBB function and attenuating sensorimotor dysfunctions (Khoshnazar, Parvardeh and Bigdeli, 2020). Coumaric acid is derivative of cinnamic acid mono-hydroxylated at the phenyl group. It is the most abundant isoform and is found at significant levels in many plants, including *C. Zeylanicum* (National Center for Biotechnology Information, 2022d). Coumaric acid has many pharmacological activities, including anti-inflammatory, antidiabetes, antibacterial, hepatoprotective, nephronprotective, and neuroprotective. It has high free radical scavenging. Coumaric acid has potential preventive and therapeutic value for memory-impaired individuals, especially age-related memory-impaired in older people (Ferreira *et al.*, 2018).

C. zeylanicum Blume essential oil, with its main phytochemical compound cinnamaldehyde, *trans*-cinnamyl acetate, 1,8-cineole, α-pinene, and coumaric acid, has a neuroprotective potential function. It was shown from molecular docking that it can inhibit the receptors AChE, BACE, and GSK-3. It prevents acetylcholinesterase from breaking down acetylcholine. The higher concentration of acetylcholine leads to better communication between nerve cells in the brain and may ease some symptoms of AD (Kumar *et al.*, 2022). *C. zeylanicum* Blume essential oil also prevents the accumulation and formation of Aβ plaques and neurofibrillary tangles in neurons from preventing neurotoxicity and worsening AD. It has an antioxidant, neurostimulator function, and prevents neuronal loss (Hamidpour *et al.*, 2015; Momtaz *et al.*, 2017; Hajinejad *et al.*, 2020).
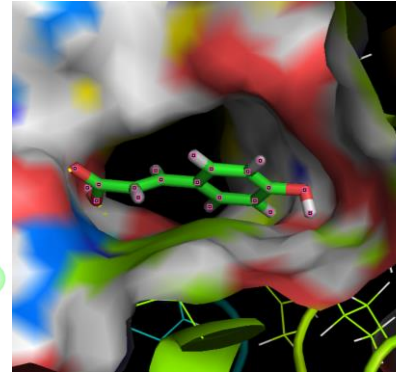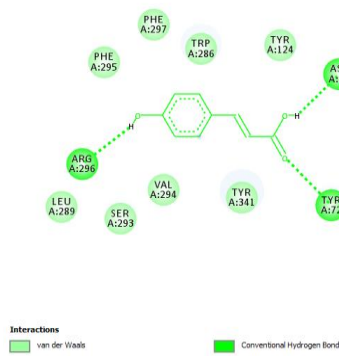
Table 5. Visualization of Ligands with The Protein Target

Protein	Ligand	Amino Acid Bond	2D Visualization	3D Visualization

| Protein	Ligand	Amino Acid Bone	2D Visualization	3D Visualization
AChE	Cinnamaldehyde	TYR124 TRP286 SER293 VAL294 PHE295 ARG296 PHE297 PHE338 TYR341		
	Trans-cinnamyl acetate	TRP286 VAL294 PHE295 PHE297 ARG296 TYR337 PHE338 TYR341		
	1,8-cineole	TRP286 SER293 VAL294 PHE295 ARG296 PHE297 PHE338 TYR341		
	α-pinene	TYR124 TRP286 VAL294 PHE295 ARG296 PHE297 PHE338 TYR341		

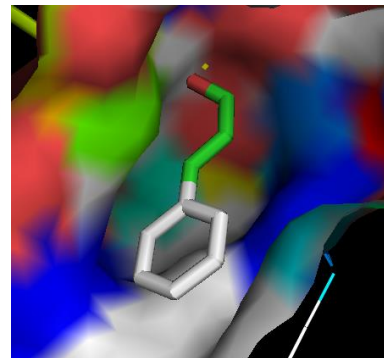|			
	Coumaric acid	TYR072 ASP074 THR075 TYR124 TRP286 LEU289 SER293 VAL294 PHE295 ARG296 PHE297 TYR341	
AChE	Donepezil	TYR072 ASP074 TRP086 GLY121 TYR124 GLU202 TRP286 SER293 VAL294 PHE295 TYR337 PHE338 TYR341 HIS447	
	Galantamine	TYR072 TYR124 TRP286 SER293 VAL294 PHE295 ARG296 PHE297 PHE338 TYR341	
	Rivastigmine	ASP075 TYR124 SER293 PHE295 TRP286 VAL294 ARG296 PHE297 TYR337 PHE338 TYR341	
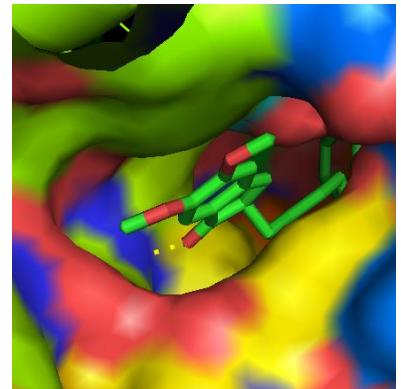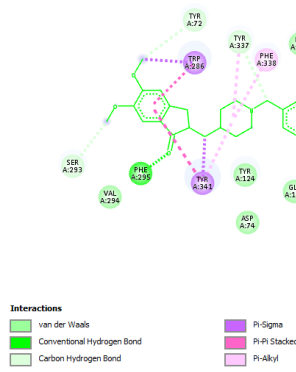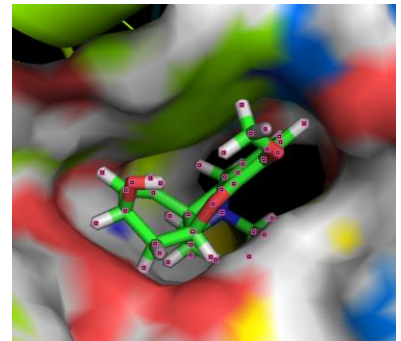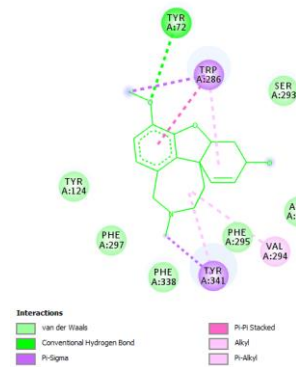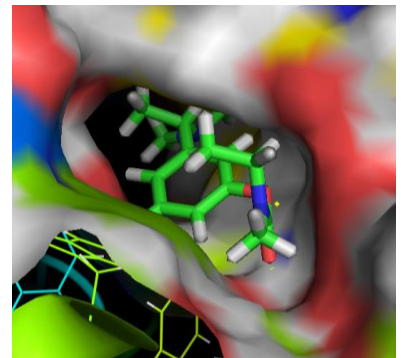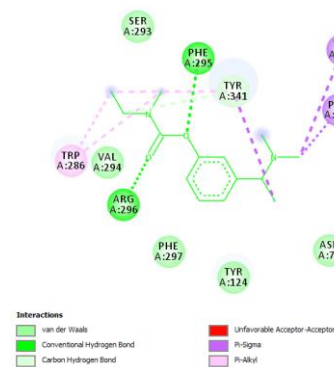
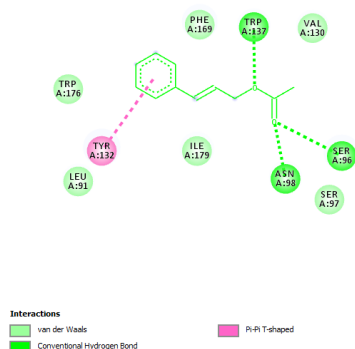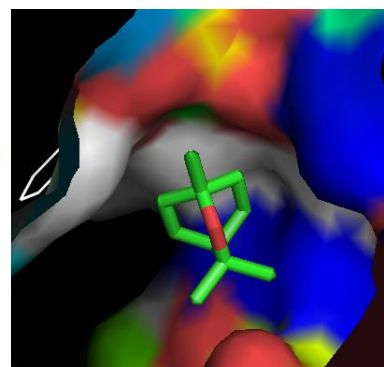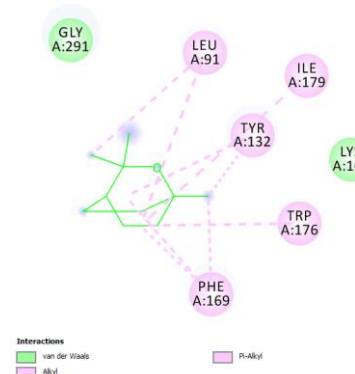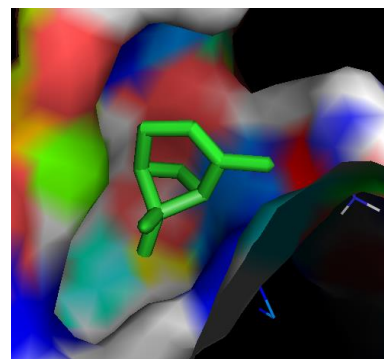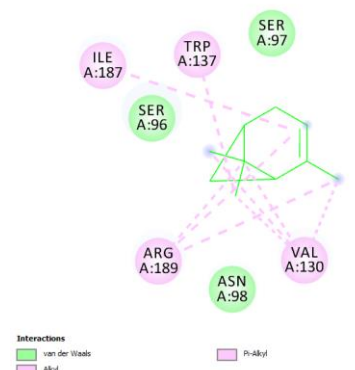|		
Cinnamaldehyde	SER096 SER097 ASN098 VAL130 TYR132 TRP137 PHE169 ILE179 ILE187 ALA188 ARG189	
Trans-cinnamyl acetate	LEU091 SER096 SER097 ASN098 VAL130 TYR132 TRP137 PHE169 TRP176 ILE179	
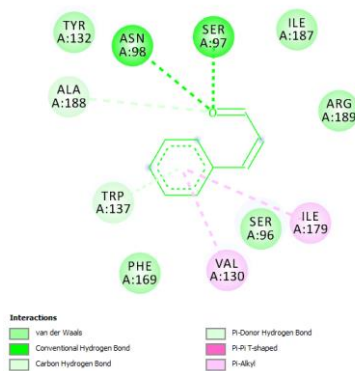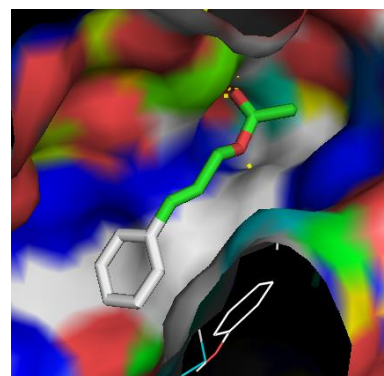
BACE1
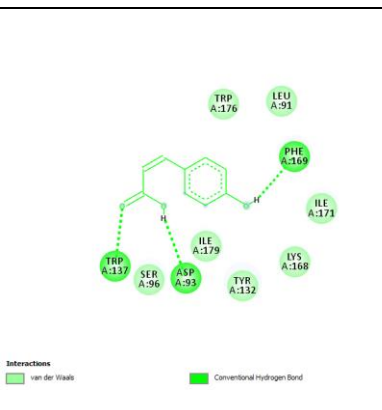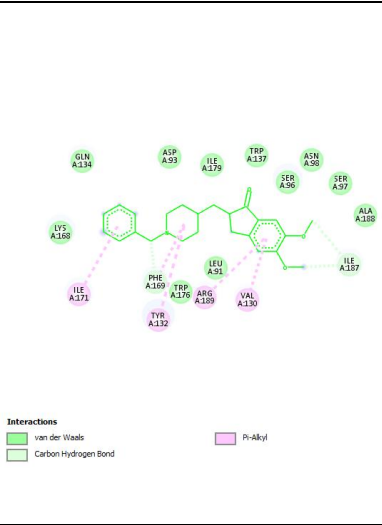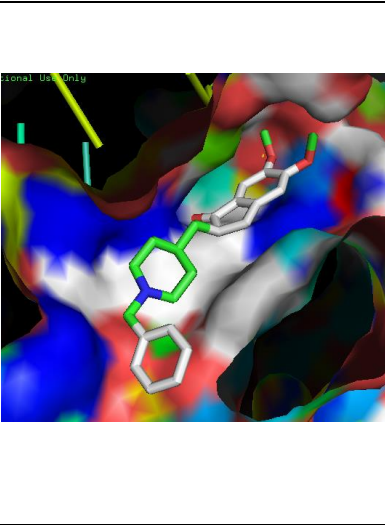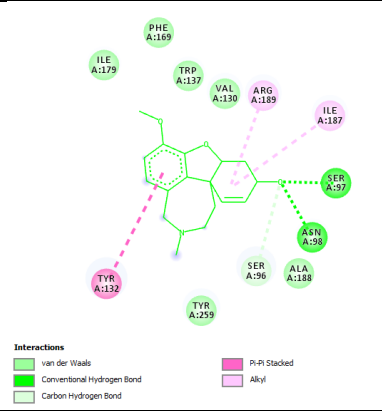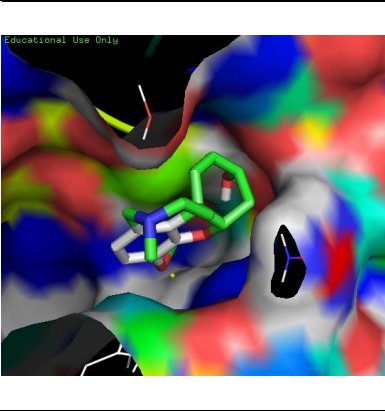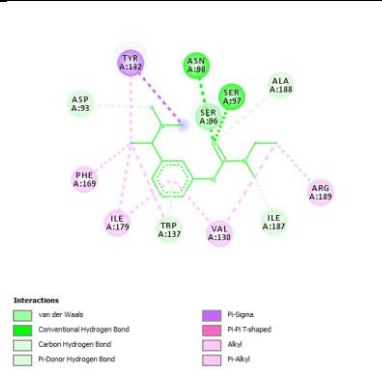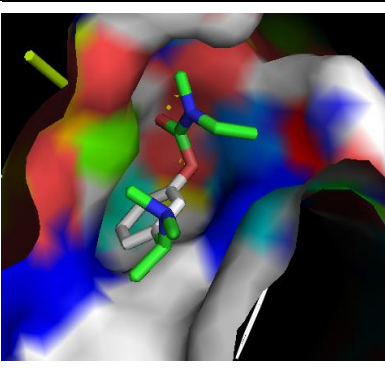
1,8-cineole	LEU091 TYR132 LYS168 PHE169 TRP176 ILE179 GLY291	
α-pinene	SER096 SER097 ASN098 VAL130 TRP137 ILE187 ARG189	

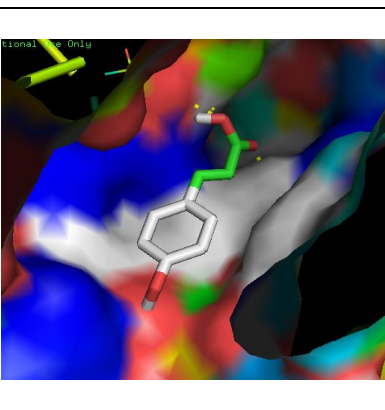| Protein	Ligand	Amino Acid Bone	2D Visualization	3D Visualization
BACE1	Coumaric acid	LEU091 ASP093 SER096 TYR132 TRP137 LYS168 PHE169 ILE171 TRP176 ILE179		
	Donepezil	LEU091 ASP093 SER096 SER097 ASN098 VAL130 TYR132 GLN134 TRP137 LYS168 PHE169 ILE171 TRP176 ILE179 ILE187 ALA188 ARG189		
	Galantamine	ASP093 SER096 SER097 ASN098 VAL130 TYR132 TRP137 PHE169 ILE179 ILE187 ALA188 ARG189		
	Rivastigmine	ASP075 TYR124 SER293 PHE295 TRP286 VAL294 ARG296 PHE297 TYR337 PHE338 TYR341		

	Cinnamaldehyde	ILE062 VAL070 ALA083 LYS085 VAL110 ASP133 LEU132 TYR134 VAL135 LEU188 CYS199 ASP200		
GSK-3	*Trans*-cinnamyl acetate	ILE062 VAL070 ALA083 LYS085 GLU097 VAL110 LEU132 ASP133 TYR134 VAL135 LEU188 CYS199 ASP200 PHE201		
	1,8-cineole	ILE062 ALA083 VAL070 ASP133 TYR134 VAL135 GLU137 THR138 LEU188		
	α-pinene	ILE062 VAL070 ALA083 VAL110 ASP133 TYR134 VAL135 THR138 GLU137 LEU188 CYS199		
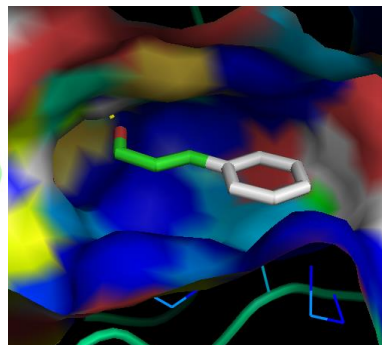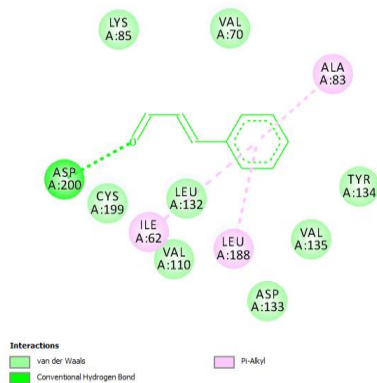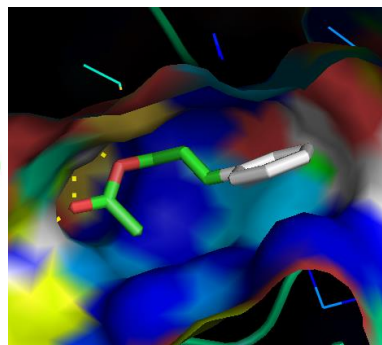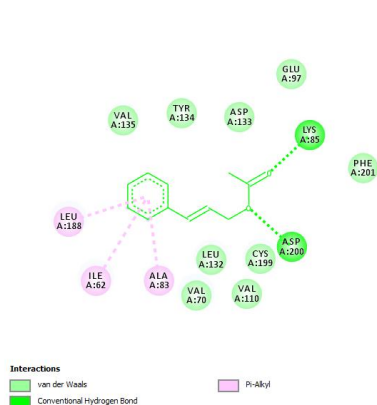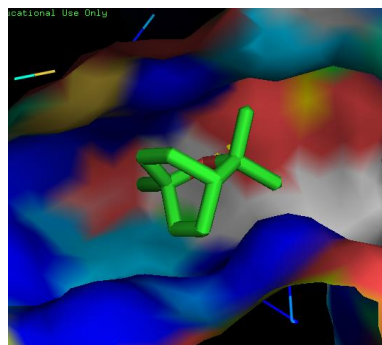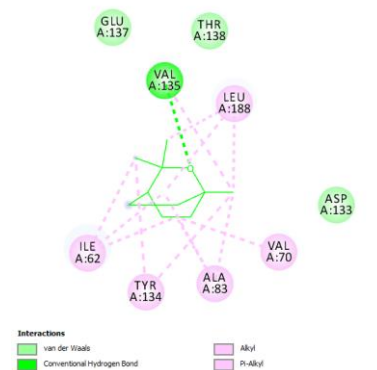
	Coumaric acid	ALA083 LYS085 VAL110 LEU132 ASP133 TYR134 VAL135 LEU188 CYS199 ASP200 PHE201		
	Donepezil	VAL061 ILE062 GLN072 LYS085 LEU132 TYR134 VAL135 PRO136 THR138 LEU188 CYS199 ASP200		
GSK-3	Galantamine	ILE062 VAL070 ALA083 ASP133 TYR134 VAL135 ARG141 PRO136 GLU137 THR138 GLN185 LEU188		
	Rivastigmine	ILE062 VAL070 ALA083 ASP133 TYR134 VAL135 PRO136 GLU137 THR138 ARG141 LEU188		

CONCLUSION

Molecular Docking of main phytochemical compounds of *C. zeylanicum* Blume essential oil has potency as Alzheimer's disease drug. These findings implicated that compounds could actively block the acetylcholinesterase, glycogen synthase kinase-3, and β site APP cleaving enzyme 1 activity. The best interaction model of the compound was shown by *trans*-cinnamyl acetate and coumaric acid. The binding energy of the compounds is lower than AD drugs (donepezil,

rivastigmine, galantamine), but it is not significantly different from AD drugs to inhibit the receptors. Our study can be used as the basis for conducting further research. In vitro studies, in vivo studies, pharmacokinetics and bioavailability of compounds, compound structures, and structure-activity relationships are needed to ensure the potency of *C. zeylanicum* Blume essential oil as an AD drug.

ACKNOWLEDGMENTS

CONFLICT OF INTEREST
There are no potential conflicts of interest to declare in this study.

REFERENCES

Alzheimer's Disease International and Alzheimer's Australia (2014) *Dementia in the Asia Pacific Region*, *Alzheimer's Disease International*. London: Alzheimer'ss Disease International. Available at: https://www.alz.co.uk/dementia-in-the-asia-pacific.

Bhat, R. *et al.* (2003) 'Structural Insights and Biological Effects of Glycogen Synthase Kinase 3-specific Inhibitor AR-A014418', *Journal of Biological Chemistry*, 278(46), pp. 45937–45945. doi: 10.1074/jbc.M306268200.

Cai, Z. M. *et al.* (2020) '1,8-Cineole: a review of source, biological activities, and application', *Journal of Asian Natural Products Research*. Taylor & Francis. doi: 10.1080/10286020.2020.1839432.

Cassani, R. *et al.* (2018) 'Systematic review on resting-state EEG for Alzheimer's disease diagnosis and progression assessment', *Disease Markers*, 2018, pp. 1–26. doi: 10.1155/2018/5174815.

Cortes-Canteli, M. and Iadecola, C. (2020) 'Alzheimer's Disease and Vascular Aging', *Journal of the American College of Cardiology*, 75(8), pp. 942–951. doi: 10.1016/j.jacc.2019.10.062.

Cumming, J. N. *et al.* (2012) 'Structure based design of iminohydantoin BACE1 inhibitors: Identification of an orally available, centrally active BACE1 inhibitor', *Bioorganic and Medicinal Chemistry Letters*. Elsevier Ltd, 22, pp. 2444–2449. doi: 10.1016/j.bmcl.2012.02.013.

Dá Mesquita, S. *et al.* (2016) 'Insights on the pathophysiology of Alzheimer's disease: The crosstalk between amyloid pathology, neuroinflammation and the peripheral immune system', *Neuroscience and Biobehavioral Reviews*. Elsevier Ltd. doi: 10.1016/j.neubiorev.2016.06.014.

Dhage, P. A. *et al.* (2021) 'Leveraging hallmark Alzheimer's molecular targets using phytoconstituents: Current perspective and emerging trends', *Biomedicine and Pharmacotherapy*. Elsevier Masson SAS, 139, pp. 1–16. doi: 10.1016/j.biopha.2021.111634.

Fahad, M. *et al.* (2018) 'Medicinal and pharmacological role of traditional Asian Food condiment : Cinnamomum zeylanicum Blume', *International Journal of Advances in Pharmacy Medicine and Bioallied Sciences*, 6(1), pp. 22–30. Available at: http://biomedjournal.com/medicinal-and-pharmacological-role-of-traditional-asian-food-condiment-cinnamomum-zeylanicum-blume/.

Fan, L. *et al.* (2020) 'New Insights Into the Pathogenesis of Alzheimer's Disease', *Frontiers in Neurology*, 10, pp. 1–12. doi: 10.3389/fneur.2019.01312.

Ferreira, P. S. *et al.* (2018) 'A Review of Analytical Methods for p-Coumaric Acid in Plant-Based Products, Beverages, and Biological Matrices', *Critical Reviews in Analytical Chemistry*. Taylor & Francis. doi: 10.1080/10408347.2018.1459173.

Frydman-Marom, A. *et al.* (2011) 'Orally administrated cinnamon extract reduces β-amyloid oligomerization and corrects cognitive impairment in Alzheimer's disease animal models', *PLoS ONE*, 6(1), pp. 1–11. doi: 10.1371/journal.pone.0016564.

Gnanaraj, C. *et al.* (2022) 'In Silico Molecular Docking Analysis of Karanjin against Alzheimer's and Parkinson's Diseases as a Potential Natural Lead Molecule for New Drug Design, Development and Therapy', *Molecules*, 27. doi: 10.3390/molecules27092834.

Hajinejad, M. *et al.* (2020) 'Natural Cinnamaldehyde and Its Derivatives Ameliorate Neuroinflammatory Pathways in Neurodegenerative Diseases', *BioMed Research International*. doi: 10.1155/2020/1034325.

Hamidpour, R. *et al.* (2015) 'Cinnamon from the selection of traditional applications to its novel effects on the inhibition of angiogenesis in cancer cells and prevention of Alzheimer's disease, and a series of functions such as antioxidant, anticholesterol, antidiabetes, antibacteri', *Journal of Traditional and Complementary Medicine*, 5, pp. 66–70. doi: 10.1016/j.jtcme.2014.11.008.

Jagust, W. (2018) 'Imaging the evolution and pathophysiology of Alzheimer disease', *Nature Reviews Neuroscience*. Springer US, 19, pp. 687–700. doi: 10.1038/s41583-018-0067-3.

Kallel, I. *et al.* (2019) 'Optimization of Cinnamon (Cinnamomum zeylanicum Blume) Essential Oil Extraction: Evaluation of Antioxidant and Antiproliferative Effects', *Evidence-based Complementary and Alternative Medicine*. Hindawi, 2019. doi: 10.1155/2019/6498347.

Kareti, S. R. and Pharm, S. M. (2020) 'In Silico Molecular Docking Analysis of Potential Anti-Alzheimer's Compounds Present in Chloroform Extract of Carissa carandas Leaf Using Gas Chromatography MS/MS', *Current Therapeutic*

Research. Elsevier Inc., 93. doi: 10.1016/j.curtheres.2020.100615.

Khaerunnisa, S., Suhartati and Awaluddin, R. (2020) *Penelitian in silico untuk pemula.* Surabaya: Airlangga University Press.

Khoshnazar, M., Parvardeh, S. and Bigdeli, M. R. (2020) 'Alpha-pinene exerts neuroprotective effects via anti-inflammatory and anti-apoptotic mechanisms in a rat model of focal cerebral ischemia-reperfusion', *Journal of Stroke and Cerebrovascular Diseases.* Elsevier Inc., 29(8). doi: 10.1016/j.jstrokecerebrovasdis.2020.104977.

Kumar, A. *et al.* (2022) 'Alzheimer Disease', in *In: StatPearls [Internet].* Treasure Island (FL): StatPearls Publishing. Available at: https://www.ncbi.nlm.nih.gov/books/NBK4999 22/.

Kumar, Shivani, Chowdhury, S. and Kumar, Suresh (2017) 'In silico repurposing of antipsychotic drugs for Alzheimer's disease', *BMC Neuroscience.* BioMed Central, 18(76), pp. 1–16. doi: 10.1186/s12868-017-0394-8.

Lipinski, C. A. *et al.* (2001) 'Experimental and computational approaches to estimate solubility and permeability in drug discovery and development settings', 46, pp. 3–26. Available at: https://pubmed.ncbi.nlm.nih.gov/11259830/.

Litke, R. *et al.* (2021) 'Modifiable Risk Factors in Alzheimer Disease and Related Dementias: A Review', *Clinical Therapeutics.* Elsevier Inc., 43(6), pp. 953–965. doi: 10.1016/j.clinthera.2021.05.006.

Long, J. M. and Holtzman, D. M. (2019) 'Alzheimer Disease: An Update on Pathobiology and Treatment Strategies', *Cell.* Elsevier Inc., 179(3), pp. 312–339. doi: 10.1016/j.cell.2019.09.001.

Lucey, B. P. (2020) 'It's complicated: The relationship between sleep and Alzheimer's disease in humans', *Neurobiology of Disease.* Elsevier, 144, pp. 1–8. doi: 10.1016/j.nbd.2020.105031.

Momtaz, S. *et al.* (2017) 'Cinnamon, a promising prospect towards Alzheimer's disease', *Pharmacological Research.* Elsevier Ltd. doi: 10.1016/j.phrs.2017.12.011.

National Center for Biotechnology Information (2022a) 'PubChem Compound Summary for CID 2758, Eucalyptol'. Available at: https://pubchem.ncbi.nlm.nih.gov/compound/Eu calyptol.

National Center for Biotechnology Information (2022b) 'PubChem Compound Summary for CID 5282110, Cinnamyl acetate'. Available at: https://pubchem.ncbi.nlm.nih.gov/compound/Ci nnamyl-acetate.

National Center for Biotechnology Information (2022c) 'PubChem Compound Summary for CID 637511, Cinnamaldehyde'. Available at: https://pubchem.ncbi.nlm.nih.gov/compound/Ci nnamaldehyde.

National Center for Biotechnology Information (2022d) 'PubChem Compound Summary for CID 637542, 4-Hydroxycinnamic acid'. Available at: https://pubchem.ncbi.nlm.nih.gov/compound/4-Hydroxycinnamic-acid.

National Center for Biotechnology Information (2022e) 'PubChem Compound Summary for CID 6654, alpha-Pinene'. Available at: https://pubchem.ncbi.nlm.nih.gov/compound/al pha-Pinene.

Ong, P. A. *et al.* (2021) 'Dementia Prevalence, Comorbidities, and Lifestyle Among Jatinangor Elders', *Frontiers in Neurology*, 12. doi: 10.3389/fneur.2021.643480.

Pardridge, W. M. (2020) 'Treatment of alzheimer's disease and blood–brain barrier drug delivery', *Pharmaceuticals*, 13, pp. 1–25. doi: 10.3390/ph13110394.

Rao, P. V. and Gan, S. H. (2014) 'Cinnamon: A multifaceted medicinal plant', *Evidence-based Complementary and Alternative Medicine*, pp. 1–12. doi: 10.1155/2014/642942.

Samanta, S., Ramesh, M. and Govindaraju, H. (2022) 'Chapter 1: Alzheimer's is a Multifactorial Disease', in *Alzheimer's Disease: Recent Findings in Pathophysiology, Diagnostic and Therapeutic Modalities*, pp. 1–34. doi: 10.1039/9781839162732-00001.

Tepe, A. S. and Ozaslan, M. (2020) 'Anti-Alzheimer, anti-diabetic, skin-whitening, and antioxidant activities of the essential oil of Cinnamomum zeylanicum', *Industrial Crops and Products.* Elsevier, 145, pp. 1–8. doi: 10.1016/j.indcrop.2019.112069.

Tiwari, S. *et al.* (2019) 'Alzheimer ' s disease: pathogenesis, diagnostics and therapeutics', *International Journal of Nanomedicine*, Jul 2019(14), pp. 5541–5554. doi: 10.2147/IJN.S200490.

Trang, A. and Khandhar, P. B. (2022) 'Physiology, Acetylcholinesterase', in *StatPearls [Internet].* Treasure Island (FL): StatPearls Publishing. Available at: https://www.ncbi.nlm.nih.gov/books/NBK5397 35/.

Vinicius, M. *et al.* (2019) 'Alzheimer's disease: risk factors and potentially protective measures', *Journal of Biomedical Scienceedical Science.* Journal of Biomedical Science, 26(33), pp. 1–11. Available at: https://www.ncbi.nlm.nih.gov/pmc/articles/PM C6507104/.

Wang, J. *et al.* (2020) 'Traditional uses, phytochemistry and pharmacological activities of the genus Cinnamomum (Lauraceae): A review', *Fitoterapia.* Elsevier, 146. doi: 10.1016/j.fitote.2020.104675.

Yiannopoulou, K. G. and Papageorgiou, S. G. (2020) 'Current and Future Treatments in Alzheimer Disease: An Update', *Journal of Central Nervous System Disease*, 12, pp. 1–12. doi:

10.1177/1179573520907397.

Zhang, L. *et al.* (2015) 'Research progress of trans-cinnamaldehyde pharmacological effects', *China Journal of Chinese Materia Medica*, 40(23), pp. 4568–4572. Available at: https://pubmed.ncbi.nlm.nih.gov/27141665/.

Pharmacological Effects of *Glycyrrhiza glabra* L. as Antihepatitis and Hepatoprotective for Children

Faisal Akhmal Muslikh[1], Puja Adi Priatna[1], Wiwied Ekasari[2*]
[1]Master Program of Pharmaceutical Sciences, Faculty of Pharmacy, Universitas Airlangga, Surabaya, Indonesia
[2]Department of Pharmaceutical Sciences, Faculty of Pharmacy, Universitas Airlangga, Surabaya, Indonesia

*Corresponding author: wiwied-e@ff.unair.ac.id

Abstract
Background: The incidence of hepatitis in children has grown from the normal number of hepatitis cases since January 2022, and it will continue to rise since the etiology and pathophysiology are unknown. This case is distinct from those caused by the hepatitis A, B, C, D, and E viruses. Glycyrrhiza glabra L. is a medicinal herb that has long been used in medicine to treat respiratory, digestive, and immune system problems, but it is also known to have an inhibitory impact on the virus. Coronavirus-associated acute respiratory syndrome, hepatitis, herpes simplex virus, influenza virus. *Objective: This article will look at Glycyrrhiza glabra L.'s antihepatitis and hepatoprotective properties.* *Methods: The Pubmed, Sage Journal, and Sciencedirect databases were searched using the Preferred Reporting Items for Systematic Reviews and Meta-Analyses (PRISMA) standards and the keywords "Glycyrrhiza glabra for hepatitis." The inclusion and exclusion criteria were followed.* *Results: From the search results, 17 publications were discovered that explain how Glycyrrhiza glabra L. can operate as an antihepatitis agent through anti-inflammatory, antiapoptotic, and hepatoprotective mechanisms.* *Conclusion: Glycyrrhiza glabra L. can be used as an anti-hepatitis and hepatoprotective in children at doses ranging from 240-480mg/kg/day.*

Keywords: Glycyrrhiza glabra, Licorine, Pediatric Hepatitis, Hepatoprotective, Toxicity.

INTRODUCTION

Investigations into cases of pediatric hepatitis have been ongoing since January 2022 due to an increase in pediatric hepatitis cases, most of which are found in the United States. Through the end of April 2022, instances were reported on all three continents (North America, Asia, and Europe), with a pronounced concentration in Europe. As of May 11, approximately 450 suspected instances of acute hepatitis of unknown etiology had been documented. The ages of the affected children range from one month to sixteen. Of 31 known children with the syndrome, 15 in the US, 5 in Europe, and 11 in the UK required liver transplants (Branwell, 2022; WHO, 2022).

Due to a lack of data on the causative agent, method of transmission (including silent infection), and risk factors, the rise in severe acute hepatitis of unknown origin in children so cannot be estimated. The absence of a connection between these cases of "acute non-HepA-E hepatitis" and the recognized viral hepatitis agents (HAV (hepatitis A virus), HBV (hepatitis B virus), HCV (hepatitis C virus), HDV (hepatitis D virus), HEV(hepatitis E virus)) stimulated research into this growing disease to determine its aetiology and pathogenesis (ECDC, 2022; WHO, 2022). Other causes of hepatitis in children may be unknown autoimmune diseases, drug toxicity or specific drug reactions, and hidden metabolic or genetic disorders (Alexander and Deep, 2022; Ng *et al.*, 2022).

Frequent gastrointestinal effects such as jaundice (71%), respiratory distress (19%), pale stools (50%), fever (31%), diarrhoea (45%), and vomiting (63%) were noted as symptoms (UKHSA, 2022). Concerning acute hepatitis in children is the high frequency of severe cases demanding liver transplantation in a few affected youngsters. The theory is that cofactors make kids more likely to get a mild adenovirus infection, leading to a more serious infection or liver damage caused by the immune system (ECDC, 2022).

The main challenge in combating diseases, particularly viral infections, is their fast adaptation and development of treatment resistance, along with introducing new hybrid viruses, which pose the greatest threat. Common medications are frequently insufficient and have a variety of negative effects. Natural medicines have grown in popularity in recent years (Cecilia and Thomas, 2012).Liquorice, or *Glycyrrhiza glabra* L., has been used for thousands of years as a herbal cure and is described in ancient Chinese, Indian, and Greek medical writings. It is predominantly employed in clinics to medicate respiratory and gastrointestinal disorders and increase immunity (Huan *et al.*, 2021). Glycyrrhiza has been used to medicate chronic hepatitis for more than 50 years, with improved histology in the liver and decreased serum aminotransferases compared to placebo. For seven days, Glycyrrhiza hydromethanolic root extract at dosages of 300 and 600 mg/kg showed a hepatoprotective effect (Sharma and Agrawal, 2014). Glycyrrhizin has been shown to inhibit viral hepatitis, influenza virus, herpes simplex virus, and coronavirus-associated acute respiratory syndrome (Huan *et al.*, 2021). Glycyrrhizin has been used as a treatment for chronic hepatitis under the brand name SNMC (stronger neo minophagen-C) for more than six decades (Clercq, 2000). It is utilized to treat hepatitis and allergies.

This study will look at hepatitis in children, the active chemicals in the plant, *in vitro*, *in vivo*, and clinical trials of the plant to see how well it fights hepatitis and hepatoprotective.

MATERIALS AND METHODS

This literature review meets the Preferred Reporting Items for Systematic Reviews and Meta-Analyses (PRISMA) criteria. This article looks at hepatitis in children and the benefits of *Glycyrrhiza glabra* as an antihepatitis and hepatoprotective, from pre-clinical trials to clinical trials using *Glycyrrhiza glabra*'s way of working.

Search Methodology

Articles were found using the keywords "*Glycyrrhiza glabra* for hepatitis" and "*Glycyrrhiza glabra* for hepatoprotective" in the Pubmed, Sage Journal, and ScienceDirect databases. The language is English, and the article exploration spans the last ten years (2012-2022). The publications used on the potential of *Glycyrrhiza glabra* as an antihepatitis treatment ranged from preclinical trials to clinical trials, as well as additional liver functions such as hepatoprotective. Two writers each did their own search, using the criteria in table 1 for what to include and what to leave out.

Data extraction

The data was collected and checked by the authors using standard procedures. Information from selected articles on hepatitis in general, hepatitis in children, *Glycyrrhiza glabra*, pre-clinical studies, clinical studies, mechanism of action of *Glycyrrhiza glabra* as antihepatitis and hepatoprotective. There are 17 articles used in this literature review, which can be seen in Figure 1.

Table 1. Inclusion and exclusion criteria in journal searches

Criteria	Inclusion	Exclusion
Plant	*Glycyrrhiza glabra*; Licorine; the active compound of *Glycyrrhiza glabra*	Outside the plant *Glycyrrhiza glabra*
Year	2012-2022	Excluding 2012-2022
Biological activity	Antiviral activity in hepatitis	In addition to antiviral activity in hepatitis
Language	Articles in English	Apart from articles in English

Identification

Records identified from*:
  Databases (n = 3)
  Registers (n = 337)

Pubmed (n = 18)
Sage journal (n = 18)
Sciencedirect (n = 301)

Screening

Records screened
(n = 52)

Records excluded**
(n = 285)

Reports assessed for eligibility
(n = 17)

Reports excluded: (n=35)
  Reason 1 : duplicate article
  Reason 2 : include exclusion criteria
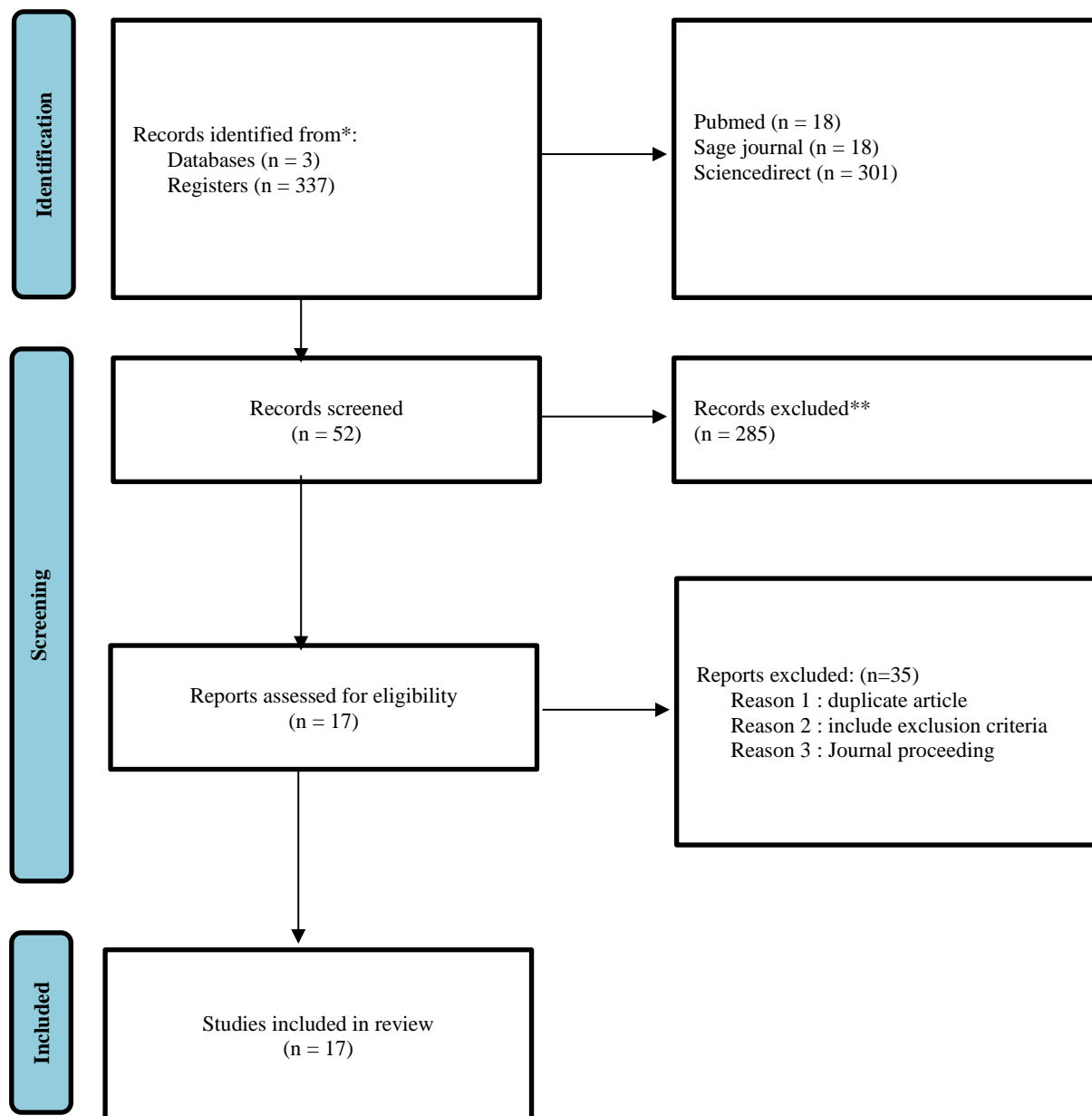 Reason 3 : Journal proceeding

Included

Studies included in review
(n = 17)

Figure 1. PRISMA guidelines flow chart in article search

Table 2. Systematic review data table

Source	Research results		
	In vitro	*In vivo*	**Clinical Trial**
Wang *et al*., 2013	√		
Adianti *et al*., 2014	√		
Sharma and Agrawal, 2014		√	
Yang *et al*., 2016		√	
Chen *et al*., 2017			√
Ali *et al*., 2018	√	√	
Lin *et al*., 2018			√
Maksoud *et al*., 2018		√	
Cao *et al*., 2019		√	
Polansky and Lori, 2020	√		√
Shi *et al*., 2020	√	√	
Zang, 2020	√		
Bell *et al*., 2021			√
Rad *et al*., 2021			√
Richard, 2021		√	
Tan *et al*., 2021	√	√	
Bisht *et al*., 2022	√		

RESULTS AND DISCUSSION
Children's Hepatitis Research

Hepatitis is a condition that causes parenchymal inflammation of the liver. Hepatitis is a disease that causes liver inflammation caused by poisons such as chemicals or medicines, as well as and infectious agents such as viruses. It is possible for inflammation to be either transient, lasting less than six months and resulting in normal liver function, or persistent (Chugh *et al*., 2016).

Children's non-infectious hepatitis can be brought on by chemical or drug exposure, immune system issues (such as autoimmune diseases), metabolic issues (such as Wilson disease and tyrosinemia), and abnormal metabolism (e.g., acetaminophen). Primary hepatotropic viruses cause the majority of infectious diseases. Acute hepatitis can be brought on by the cytomegalovirus (CMV), rubella virus, Epstein-Barr virus (EBV), parvovirus, adenovirus, enterovirus, human immunodeficiency virus (HIV) and herpes virus (HHV-7, HHV-6, HHV-2, HHV-1). *Leptospira*, *Coxiella burnetii*, and other pathogenic organisms that can cause hepatitis include the *Brucella* spp. (ECDC, 2022).

Due to a lack of knowledge regarding the etiologic agent, transmission route (including asymptomatic infection), and risk factors, it is impossible to assess the increase in children with severe acute hepatitis of unclear cause. Current consensus holds that cofactors that predispose children to adenovirus infection, which is generally mild, cause a more severe illness or immune-mediated liver damage (ECDC, 2022).

In the United Kingdom, a rise in the diagnosis of severe hepatitis in young children has been linked to an increase in the prevalence of adenovirus in young children. If adenovirus is found to be the cause or a contributing factor in these instances, an increase in circulating adenovirus could lead to a rise in severe hepatitis in children in other European nations. Although few cases requiring liver transplantation have been reported, they are considered to have a significant potential influence on the affected pediatric population. The ability to transplant and support pediatric liver failure patients differs significantly across EU/EEA nations. Hence, access to highly specialized pediatric intensive care and transplant facilities may influence outcomes, especially as the number of cases rises (ECDC, 2022).

Myalgia, nausea, vomiting, lethargy, tiredness, stomach discomfort, fever, and diarrhoea are some signs and symptoms of acute hepatitis. These signs and symptoms may last for several weeks. A significant fraction of acute viral hepatitis infections are asymptomatic, and children are far more prone than adults to develop mild or silent disease from hepatitis A or B infection (Reider and Beckingham, 2001).

Figure 2. *Glycyrrhiza glabra* L (Sharma and agrawal, 2013; Zadeh *et al.*, 2013)

Glycyrrhiza glabra L. (Fabaceae) is one of the plants that can be used as medicine (IT IS, 2022). Glycyrrhiza is derived from the Greek words glykos, sweet, and rhiza, root. This plant is native to parts of Asia and the Mediterranean (Sharma and Agrawal, 2013; Sharma *et al.*, 2018). Ancient Egypt, Rome, East China, Greece, and the West all used the herbal remedy licorice, since the 16th century has been cultivated in Europe. Different species types of liquorice are grown in Europe, the United States, the Middle East, Southwest Asia, Central Africa, Afghanistan, and northern India (Wahab *et al.*, 2021).

Licorice is a plant that grows to a height of ± 2.5 meters, around 7-15 cm for bearing pinnate leaves, with 9-17 leaves with a yellow-green oval/ellipse shape. The length of the flowers is between 0.8-1.2 cm with purple to pale whitish blue, spiny armpits. The petals are short, and conical in shape. The fruit is pod-shaped with a length of 2-3 cm and contains 3-5 brown seeds. Roots are ± 1 meter long, and usually harvested after 3-4 years (Zadeh *et al.*, 2013; Sharma *et al.*, 2018; Mamedoy and Egamberdieva, 2019).

Licorine has various health benefits, such as anti-tussive, expectorant, antibacterial, antioxidant, anticoagulant, antiviral, antiulcer, hepatoprotective, antitumor, antidiabetic (Sharma and Agrawal, 2013); treatment of chronic hepatitis (Zadeh *et al.*, 2013); anticarcinogenic, antimutagenic (Sharma *et al.*, 2018);

dermatological effects, antidepressants, and memory enhancing activities (Mamedoy and Egamberdieva, 2019). This is due to the chemical compounds contained in licorine.

Glycyrrhiza glabra contains greater than 20 triterpenoids and almost 300 flavonoids. Figure 3 displays the primary, secondary metabolites of *Glycyrrhiza glabra*. The secondary metabolites include triterpenoid saponins, glycyrrhizin, glycosides, 4-methyl coumarin, prenylated biaurone, isoliquiritigenin, 7-acetoxy-2-methyl-isoflavone, licoagrone, 7-methoxy-2-methylisoflavone, glyzaglabrin, 7-hydroxy-2 methyl isoflavone, quercetin-3-glucoside, quercetin, liquiritigenin, and liqcoumarin. Other reported ingredients include vanone rhamnoglucoside, 18α-hydroxy glycyrrhetic acid, isoliquiritin, liquiritoside, liquiritin, licuraside, liquiritic acid, liquoric acid, isoglabrolide, glabrolide glabridin, glabrol, glyzarin, glycyrrhetinic acid, glyzaglabrin, licoisoflavones, licoflavonol, licoisoflavones A, B and glycyrrhizic acid. The primary ingredients in *Glycyrrhiza glabra* are glycyrrhizin and glycyrrhetinic acid. Glycyrrhizin can be transformed into glycyrrhetinic acid in humans through metabolic mechanisms. As a result, glycyrrhizin's pharmacological effects are comparable to those of glycyrrhetinic acid. (Thakur and Raj, 2017; Wahab *et al.*, 2021).
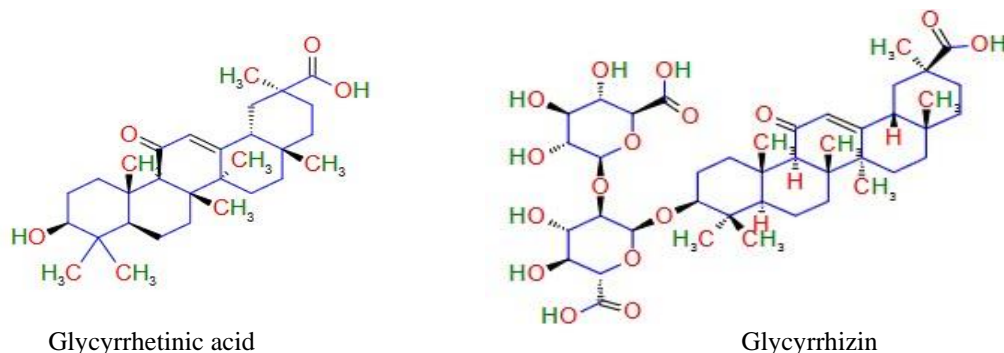
Figure 3. Chemical content of *Glycyrrhiza glabra* (Thakur and Raj, 2017; Wahab *et al*., 2021).

Potential Chemical Content of *Glycyrrhiza glabra* as Hepatitis and Hepatoprotective Antivirus

Since 60 years ago, Glycyrrhizin has been used clinically as an antiallergic and antihepatitic drug under the brand name stronger neo minophagen-C (SNMC) to medicate chronic hepatitis. Due to its ability to prevent viral cells from adhering, glycyrrhizin possesses strong antiviral properties. The antiviral efficacy of ribavirin, mycophenolic acid, pyraziofurin, glycyrrhizin and 6-azauridine against the severe acute respiratory syndrome (SARS) virus's FFM-1 and FFM-2 clinical isolates was recently assessed. Glycyrrhizin was demonstrated to be the most efficient agent for inhibiting viral replication and might be used as a preventive measure. Patients with chronic HCV and HIV-1 have previously received treatment with glycyrrhizin. (Clercq, 2000).

Compared to placebo, glycyrrhizin significantly reduced serum aminotransferase and enhanced liver histology. Additionally, long-term glycyrrhizin use has been linked to reducing the risk of hepatocellular carcinoma in people with chronic HCV. Studies conducted *in vitro* (Ali *et al*., 2018; Sato *et al*., 1996) have demonstrated that glycyrrhizin alters cells' internal movement and can inhibit the HBV surface antigen.

An aglycone of glycyrrhizin called glycyrrhetinic acid (GA) lowers the expression of the P450 E1, sparing the liver. By enhancing GST (glutathione-S-transferase) and CYP1A1 activity, GA can help reduce the liver damage and oxidative brought on by aflatoxins. It may also contribute to anticarcinogenic effects by metabolically inactivating hepatotoxins (Chan *et al*., 2003). Glycyrrhizin and its analogues stimulate the synthesis and proliferation of hepatocyte DNA *in vitro* via activating epidermal growth factor receptors, activating the mitogen activated protein kinase (MAP kinase) pathway (Kimara *et al*, 2001).

Hepatoprotective and Antihepatitis Activities: from Non-Clinical to Clinical Trials

Glycyrrhizin is a primary compound of the Glycyrrhiza family and is reported to have antiviral activity. Glycyrrhizin inhibited HCV infection in Huh-7.5 cells. According to research, glycyrrhizin has receptor ligand binding activity triggered by peroxisome proliferators and has antibacterial activity against *Moraxella catarrhalis*, *Haemophilus influenzae*, and *Streptococcus pyogenes*. According to reports, glycyrol inhibits the function of calcineurin by binding to it and having an anti-inflammatory impact. The following Glycyrrhiza species have substances with anti-HCV action (Adianti *et al*., 2014).

Table 3. Compounds from Glycyrrhiza spp have anti-HCV activity (Adianti *et al*., 2014)

Compounds	IC_{50} (µg/mL)	Concentration (mg/mL)	Anti HCV Activity (% inhibition)		
			During (a)	After (b)	During and after (c)
Glycycoumarin	8,8	20	16,7	100	100
Glycyrin	7,2	15	18,4	98,3	99,6
Glycyrol	4,6	10	21,3	100	100
Liquiritigenin	16,4	30	15,5	90	87,2
Isoliquiritigenin	3,7	8	14,1	91	82,5
Licochalcone A	2,5	5	0	94,4	93,8
Glabridin	6,2	12	0	91	93,8

NB: Treatment is given only during, only after, or during and after virus inoculation. The concentration was determined from the results of $2 \times IC_{50}$. (a) sampling during virus inoculation; (b) sampling after virus inoculation; and (c) sampling both during and after virus inoculation.

The primary bioactive component of *G. glabra*, glycyrrhizin, also known as glycyrrhizic acid, has several pharmacological effects, including the prevention of viral replication in various DNA and RNA viruses, including HAV, HCV, herpes zoster, herpes simplex, HIV, cytomegalovirus and varicella. Glycyrrhizic acid blocks the production of prostaglandins, cyclooxygenase activity, and platelet aggregation, among other components of the inflammatory process (Basar et al., 2015). Glycyrrhizin inhibits aldosterone metabolism in the liver, and has mineralocorticoid and glucocorticoid activity. Other G. glabra secondary metabolites, like hydrocortisone, also have anti-inflammatory properties. The suppression of phospholipase A2, which is implicated in a number of inflammatory processes, may be the cause ofseveral inflammatory processes, may cause the anti-inflammatory activity.

Table 4. *Glycyrrhiza glabra* has the potential as a hepatoprotector and anti-hepatitis *in vitro*.

Source	Sample	Effect	*In vitro* research results
Wang *et al*., 2013	Glycyrrhizic acid	Antiviral	CVA16 inactivates and inhibits EV71 infection via post-viral cell entry.
Adianti *et al*., 2014; Zang, 2020	Glycycoumarin	Antiviral	Decreased translation of the HCV nonstructural protein, NS5A, from HCV replication.
Ali *et al*., 2018	Glycyrrhizin	Hepatitis B Antiviral	The administration of glycyrrhizin to PLC/PRF/5 cells decreased HBsAg generation into the culture medium, leading researchers to believe that glycyrrhizin alters hepatocyte surface characteristics and intracellular transport.
Cheel *et al*., 2010; Polansky and Lori, 2020	Infusion *G. glabra*	Antiviral	Proliferation of human lymphocytes should be activated.
Shi *et al*., 2020	Glycyrrhetinic acid	Antiviral	Repairs liver inflammatory damage via the HMGB1-TLR4 signaling pathway, leading to the release of TNF-α and IL-6.
Tan *et al*., 2021	Licorice root extract and Magnesium isoglycyrrhizinate	Hepatotoxicity	Activates the Nrf2 pathway, increases protein expression of Nrf2 target genes, mRNA and reduces triptolide-induced hepatotoxicity (TP).
Bisht *et al*., 2022	Glycyrrhizin	Hepatitis C Antiviral	When coupled with interferon α 2a, glycyrrhizin lowers HCV titers by resulting in a 50% decrease in HCV at a concentration of 14 ± 2 μg. Glycyrrhizin inhibits the expression of the core HCV 3a gene at the mRNA level.

Glycyrrhizin inhibited HBsAg secretion into culture media in PLC/PRF/5 cells, indicating that glycyrrhizin can decrease HBsAg secretion and exert its effect in hepatocytes chronically infected with HBV (Ali *et al*., 2018). Glycyrrhizin can stop HAV from sticking to and getting into PLC/PRF/5 cells. This means that hepatocytes treated with glycyrrhizin change how they move inside the cells and how they look on the outside (Sato *et al*., 1996).

Using interferon with ribavirin to treat HCV remains with issues, including being expensive, still having significant side effects, and reportedly failing to cure approximately fifty percent of illnesses (Moore *et al*., 2004). Therefore, a combination of interferon with glycyrrhizin was developed, which is cost effective, more efficacious and less toxic. Both its ability to stabilize membranes and its stimulation of endogenous interferon synthesis. When coupled with interferon 2a, glycyrrhizin has a synergistic impact that inhibits the production of the HCV 3a core gene at the mRNA level (Ashfq *et al* 2011; Bisht *et al*., 2022).

Damage generated by reactive oxygen species (ROS) as an effect of oxidative stress is the cause of TP-induced hepatotoxicity (Tan *et al*., 2018). The physiological response to oxidative stress is controlled by the nuclear factor erythroid 2-related factor 2 (Nrf2). Cytosolic Nrf2 is destroyed under physiologically normal conditions by binding to the Kelch-like ECH 1 and the proteasome (Keap1). When under oxidative and electrophilic stress, Nrf2 separates from Keap1, enters the nucleus, dimerizes with Maf-binding protein, and then interacts with the response element antioxidant (ARE) (Tan *et al*., 2018). Then, Nrf2 activates numerous cytoprotective proteins and drug efflux transporters, including hemeoxygenase 1 (HO-1), uridine diphosphate glucuronosyl transferase (UGT), and multidrug resistance-associated protein 2 (MRP2) (Yuan-Jing *et al*., 2016). The Nrf2/ARE signalling

pathway, particularly Nrf2, is thought to be a promising therapeutic target to stop oxidative stress-induced liver damage because it is the most important mechanism underlying cellular defence against oxidative stress (Tan *et al*., 2018).

EV71 and CVA16 are RNA viruses belonging to the genus Enterovirus. The virus can be spread by direct contact with a patient's blisters and other surfaces that can be contaminated with the virus in liquid form, such as by the faecal-oral route. Glycyrrhizic acid can inactivate CVA16 and inhibit EV71 infection through post-virus cell entry so that it can act as an antiviral (Wang *et al*., 2013)

Licorice can stimulate the activation and proliferation of human lymphocytes (B cells, NK cells, CD+, and CD8+). Participation of this type of immune cell, which confers an excess of innate immune cells such as neutrophils and macrophages at the site of infection, is linked to severe death and cases. So, licorice may help the adaptive immune system get rid of viruses early and stop inflammation from getting too bad (Polansky and Lori, 2020).

Table 5. *Glycyrrhiza glabra* has the potential as a hepatoprotector and anti-hepatitis *in vivo*.

Source	Sample	Effect	*In vivo* research results
Sharma and Agrawal, 2014	Glycyrrhiza hidro hydromethanolic root extract	Hepatoprotector	May improve liver histology and decrease serum aminotransferase, rat liver tissue exhibited a effect of hepatoprotective against CCl4-induced oxidative stress at dosages of 300 and 600 mg/kg for 7 days.
Yang *et al*., 2016	Magnesium isoglycyrrhizinate	Hepatoprotector	Capable of eliminating the proliferation of CD25, CD69+ subsets in primary CD4+ T-cells, administration caused a decrease in the expression of NALP3, NLRP6, and caspase-3.
Ali *et al*., 2018	Glycyrrhizin	Hepatoprotector	Intraperitoneally giving mice glycyrrhizin stops liver damage caused by lipopolysaccharide and D-galactosamine by stopping inflammation and the production of IL-18.
	Glycyrrhizin and glycyrrhetinic acid	Hepatoprotector	Administration markedly inhibited α2 (I) activation of the progression of liver fibrosis and the collagen gene promoter in transgenic mice produced by repeated CCl4 injections.
	Glycyrrhizin	Hepatoprotector	Glycyrrhizin stops mice from getting hepatitis caused by anti-Fas antibodies by working before proteases like CPP32.
Maksoud *et al*., 2018	Licorice root extract	Hepatoprotector	Hepatoprotective effect of ethanolic extract of liquorice, 400 mg/kg BW rats, against chronic hepatitis and silymarin through anti-inflammatory and antioxidant mechanisms.
Cao *et al*., 2019	Magnesium isoglycyrrhizinate	Hepatotoxicity	MgIG exerts beneficial effects on intestinal damage and MTX-induced hepatotoxicity.
Shi *et al*., 2020	Glycyrrhetinic acid	Antiviral	Inhibit activation of the hepatic inflammatory response by blocking HMGB1 cytokine activity and suppressing HMGB1 release in mice induced by murine hepatitis virus.
Richard, 2021	Glycyrrhizin	Antiviral	Mice that were given Glycyrrhizin were able to make IFN-γ. This was done by stimulating macrophages, such as by making NK activity go up.
Tan *et al*., 2021	Licorice root extract and Magnesium isoglycyrrhizinate	Hepatotoxicity	Increases protein expression of Nrf2 target and mRNA genes and decreases triptolide-induced hepatotoxicity through activating the Nrf2 pathway (TP).

Another study found that intraperitoneal treatment of glycyrrhizin plus epidermal growth factor (EGF) dramatically promoted liver regeneration and restoration of liver function in rats, which was feasible due to EGF receptor stimulation. Furthermore, glycyrrhizin and EGF stimulated hepatic DNA proliferation and synthesis while decreasing serum aspartate transaminase (AST) and alanine aminotransaminase (ALT) activity. This means that liver function will return quickly after a surgeon

removes a part of the liver. This gives doctors a new way to treat people with acute or chronic hepatitis C or after a live liver transplant (Ali *et al*., 2018).

Serum glutamic oxaloacetic transaminase (SGOT), also known as aspartate aminotransferase (AST), and serum glutamic pyruvic transaminase (SGPT), also known as alanine aminotransferase (ALT), are intracellular enzymes found primarily in the heart, liver, and skeletal tissue that are released from damaged tissue (necrosis) or changes in cell permeability). The normal range for SGOT and SGPT is 5-35 units/ml (Price and Wilson, 2005). Levels will rise if liver cells are damaged or in other conditions, such as a myocardial infarction.

Plasma aminotransferase enzymes might be used to make a diagnosis. Aminotransferases are generally intracellular enzymes, with low plasma levels signifying cellular content release during normal cell turnover. Elevated levels of aminotransferase enzymes may suggest damage to enzyme-rich cells caused by physical trauma or a disease condition that results in cell lysis and the release of intracellular enzymes into the blood. When present in plasma, aminotransferase enzymes such as AST and ALT can be used to make a diagnosis. Plasma AST and ALT levels are raised in practically all liver illnesses, but they are particularly high in situations that cause necrosis, such as severe viral hepatitis, toxic damage, and persistent bleeding. Aminotransferases can be raised in diseases other than the liver, such as myocardial infarction and muscular problems. These illnesses, however, are frequently clinically indistinguishable from liver disease (Champe *et al*., 2009).

A hepatoprotector is a medication that can protect the liver against the harmful effects of endogenous or exogenous causes by reducing inflammation and disease progression (Sulaiman, 2012). Chronic hepatitis is a chronic liver condition that can progress to cirrhosis, hepatocellular cancer, and potentially liver failure. Glycyrrhiza has been used to treat chronic hepatitis for over 50 years, with improved liver histology and decreased serum aminotransferases compared to placebo. In Swiss albino rat liver tissue, Glycyrrhiza hydromethanolic root extract at dosages of 300 and 600 mg/kg/day for seven days was hepatoprotective against CCl4-induced oxidative stress (Sharma and Agrawal, 2014). As shown by a rapid rise in liver function measurements and the formation of toxic compounds from the peroxidation of polyunsaturated fatty acids (MDA) in biological membranes (Maksoud *et al*., 2018), CCl4 damages liver tissue. It causes oxidative stress similar to that seen in humans with chronic hepatitis.

Magnesium isoglycyrrhizinate (MIG) is a novel glycyrrhizic acid stereoisomer that is clinically employed as a hepatoprotective medication with a stronger effect and fewer adverse effects than glycyrrhizic acid. Furthermore, MGL can protect against hepatotoxicity caused by free fatty acid exposure, ischemia/reperfusion-induced liver injury, and decrease ethanol-induced lipid peroxidation (Yang *et al*., 2016; Tan *et al*., 2018).

Interferon (IFN) can cure hepatitis B patients with or without adenine arabinoside. IFNs can reduce hepatitis B and DNA polymerase surface antigen levels in hepatic patients. GL also increased IFN-γ synthesis in human T cells and promoted IFN production in mice, which was produced by stimulation of macrophages and increased natural killer (NK) activity. After GA therapy, spleen IFN-α, IFN-γ, and IL-12 expression increased. Through IFN, GL significantly lowers inflammation. They came to the conclusion that GL's anti-inflammatory effect in enteritis may be linked to its ability to block the IFN signalling pathway (Richard, 2021).

Methotrexate (MTX) was first used to treat juvenile acute leukaemia, and it is now used to treat psoriasis and rheumatoid arthritis worldwide (Jenko *et al*., 2018). However, it has a hazard profile similar to hepatotoxicity (Conway and Carey, 2017). MTX has been linked to an increase in liver transaminases, changes in liver histology, and the development of cirrhosis and fibrosis (Conway and Carey, 2017). Due to hepatotoxicity, MTX's clinical applicability is limited. Aminopterin, the first folate antimetabolite that may prevent the synthesis of purines and pyrimidines and DNA synthesis, repair, and replication, has a stable derivative called MTX. Also, MTX affects the intestinal mucosa, which changes the way the intestinal barrier works and lets bacteria move into the liver (Cao *et al*., 2019). This is called hepatotoxicity.

Table 6. *Glycyrrhiza glabra* has clinical potential as hepatoprotective and antihepatitic.

Source	Sample	Effect	Clinical Trial Research Results
Subrat *et al*., 2012	Interferon (I) α-2b 3 MU/day + Ribavirin (R)	Hepatitis C Antiviral	Ninety-nine patients were given six months of treatment, where the sustained viral response (SVR)

	1000mg/ day (I+R) and Interferon (I) α-2b 3 MU/ day + glycyrrhizin (G) 250 mg (I+G)		was much higher in group I + R than in group I + G (65.7% vs 46.9%, OR = 2.2, P = 0, 03).
Chen *et al.*, 2017	Long-Dan-Xie-Gan-Tang Products (*Glycyrrhiza glabra, Gentiana scabra, Scutellaria baicalensis, Gardenia jasminoides, Plantago asiatica, Alisma orientalis, Clematis montana, Angelica sinensis, Rehmannia glutinosa, and Bupleurum chinense*)	Hepatitis C Antiviral	The 36 chronic hepatitis C patients who received RYJGT treatment for 12 weeks had a significantly higher HCVRNA reduction ratio and better symptoms than those who received placebo.
Lin *et al.*, 2018	Glycyrrhizin 100 mL (200 mg) i.v/day for five days oral entecavir	Hepatitis B Antiviral	A trial in 10 chronic hepatitis B patients with acute-chronic liver failure resulted in ALT levels halving after two days of treatment. Liver compensatory return within 30 days was achieved in 8 patients (80%).
Cheel *et al.*, 2010; Polansky and Lori, 2020	Tincture of *G. glabra*	Antiviral	At 24 hours, 16 people who took the placebo said CD69 expression went up in CD8, CD4+, and NK cells.
Bell *et al.*, 2021	Glycyrrhizin	Hepatoprotector	After 12 weeks of therapy, ALT levels dropped more with glycyrrhizin than with placebo, and necroinflammation and fibrosis got better after 52 weeks of treatment.
	Glycyrrhizin and ursodeoxycholic acid	Hepatitis C Antiviral	The medication is effective and safe in raising specific liver enzyme abnormalities and can be used as an alternative to interferon in chronic HCV infection, particularly for interferon-resistant patients, according to clinical trials involving 170 participants.
Rad *et al.*, 2021	Stronger Neo-Minophagen C (SNMC)	Hepatitis C Antiviral	Giving SNMC to patients can improve liver pathology in chronic hepatitis patients. Besides that, SNMC can inhibit inflammation and liver necrosis in chronic hepatitis C patients.

Compared to the placebo group, using a Long-Dan-Xie-Gan-Tang product, including a wide variety of herbs including *Glycyrrhiza glabra* resulted in a substantially higher reduction in the blood HCV RNA ratio and a better TCM pattern, particularly "Wet Heat" and "Heart Qi Depression." When administered to patients with chronic HCV, this medication is also relatively safe. Only four patients suffered adverse effects (for example, diarrhoea and gastrointestinal problems), which were moderate and resolved spontaneously or with extra therapy (Chen *et al.*, 2017). In a randomized, double-blind study, we provide scientific proof that herbal regimens of this product can be utilized as an alternative therapy option for individuals who do not respond to or are not suitable for ribavirin/interferon treatment in the treatment of patients with chronic HCV (Tang, 2006).

Overall, IFN, in conjunction with ribavirin demonstrated considerably greater SVR than IFN alone. IFN coupled with glycyrrhizin, on the other hand, was found to be less hazardous than ribavirin. As a result, glycyrrhizin may be used instead of ribavirin in combination with IFN as an HCV therapy regimen if ribavirin causes negative effects in the patient (Subrat *et al.*, 2012).

Studies that combined glycyrrhizin and entecavir showed that the combination treatment was safe and effective for about five days. This could mean chronic HBV with acute-chronic liver failure could stay in the hospital less and live longer (Lin *et al.*, 2018).

SNMC is an injectable medication comprising the active component glycyrrhizin, L-cysteine, and glycine. It has been used in Japan for more than 30 years to treat chronic hepatitis and has been demonstrated to be beneficial in preventing the development of

hepatocellular carcinoma in HCV patients. Since 1948, SNMC has been utilized to treat allergy illnesses and chronic liver disease in Japan. SNMC has been shown to dramatically lower serum levels of AST, ALT, and -GTP. Since 1979, SNMC has been approved to treat chronic liver disease in Japan, where there are problems with how the liver works (Saito *et al.*, 2016).

Toxicity study on Glycyrrhiza glabra

A single oral dose of 1000 mg/kg BW female albino rats in an acute toxicity test with aqueous and ethanol extracts of *Glycyrrhiza glabra* did not result in death. A single dose of 1500 mg/kg BW of *Glycyrrhiza glabra* aqueous extract orally administered to Swiss albino mice did not result in mortality after 14 days, but there were physical changes in Swiss albino mice (Chowdhury *et al.*, 2013; Gupta *et al.*, 2016; Nazari *et al.*, 2017). Because of the influence of first-pass metabolism and limited oral absorption, acute toxicity by IV/IP has a considerable variance in LD_{50} values (Nazari *et al.*, 2017).

Subacute toxicity testing of *Glycyrrhiza glabra* aqueous extract (100; 200; 500 mg/kg BW male Wistar rats) revealed a dose-dependent inhibitory effect on the adrenal-pituitary axis, resulting in a hyper mineralocorticoid state with decreased levels of adrenocorticotropic, potassium, aldosterone, and cortisol, as well as increased concentrations of ren (Al-Qawari *et al.*, 2002; Nazari *et al.*, 2017).

Subchronic toxicity experiments on *Glycyrrhiza glabra* aqueous extracts (500; 1000; 2000 mg/kg BW, orally, for nine weeks) revealed no long-term effect in experimental animals. Furthermore, it demonstrates that it has no major harmful effect on reproductive organs (Shin *et al.*, 2008; Nazari *et al.*, 2017). Meanwhile, testing of 12 weeks of subchronic glycyrrhizin (0.1-1mg/mL in drinking water) revealed cardiovascular adverse effects in Sprague-Dawley male rats. This leads to an overabundance of mineralocorticoids, water retention, systemic hypertension, hypokalemia and hypernatremia. This demonstrates glycyrrhizic acid's beneficial effect on boosting right atrial and pulmonary artery pressure. Histological tests (Ruszymah *et al.*,

CONCLUSION

Glycyrrhiza glabra is a medicinal plant with over 20 triterpenoids and over 300 flavonoids. Glycyrrhizin and glycyrrhetinic acid are the primary, secondary metabolites of *Glycyrrhiza glabra*. According to the findings of this study, *Glycyrrhiza glabra* exhibits antihepatitis and hepatoprotective activity with multiple mechanisms, such as anti-inflammatory, antiapoptotic,

1995; Nazari *et al.*, 2017) show that pulmonary hypertension is real.

In male and female rats, chronic toxicity tests on Licorine flavonoid oil (400; 600; 800; 1600 mg/kg, orally, for 90 days) revealed a decrease in hematocrit, erythrocytes, and haemoglobin. Furthermore, there was an increase in mean corpuscular haemoglobin (MCH), white blood cell count (WBC) and mean corpuscular haemoglobin concentration (MCHC), a delay in prothrombin time (PT) and activated partial thromboplastin time (APTT), an increase in Na+ levels in urine and an increase in urine volume (Nakagawa *et al.*, 2008; Nazari *et al.*, 2017). A 45-day chronic toxicity test of G. glabra propylene glycol root extract (1; 2; 4 mg/L) on male black molly fish revealed 100% mortality for 4 mg/L on day 7, 34% mortality for 2 mg/L on day 15, and 17% mortality for 1 mg/L on day 25, followed by a decreased appetite on day 3, weight loss, and liver damage that increased with increasing dose (Radhakrishnan *et al.*, 2005).

Because of the effect of first-pass metabolism and the decreased absorption of oral administration compared to IV/IP administration, *G. glabra* can be administered orally as a therapy. In individuals with hypertension and hypokalemic diseases, long-term therapy of *G. glabra* should be considered. Furthermore, it is contraindicated in pregnant women and neonates since licorine intake during pregnancy might cause premature birth, alterations in the hypothalamic-pituitary-adrenocortical axis, and cognitive impairment in newborns. It should also be taken with caution in women who have a family history of preeclampsia (Nazari *et al.*, 2017).

G. glabra extracts at doses of 300, 400, and 600 mg/kg BW rats per day demonstrated hepatoprotective effects by improving liver histology, lowering serum aminotransferases, and anti-inflammatory and antioxidant activity (Sharma and Agrawal, 2014; Maksound, 2014). To convert a safe dose for children from a rat dose to a human dose, the dose for children per day ranges from 240 mg/kg/BW (equal to a rat dose of 300 mg/kg BW) to 480 mg/kg BW (corresponding to a rat dose of 600 mg).

and hepatoprotective activity in clinical trials, *in vivo*, and *in vitro*. The dose that can be applied to children from the research results described is between 240 and 480 mg/kg/day.

REFERENCES

Adianti, M., Aoki, C., Komoto, M., Deng, L., Shoji, I., Wahyuni, T.S., ... & Hotta, H. (2014). Anti-

hepatitis C virus compounds obtained from *Glycyrrhiza uralensis* and other Glycyrrhiza species. *Microbiology and immunology*; 58(3): 180-187.

Al-Qarawi, A.A., Abdel-Rahman, H.A., Ali, B.H., & El Mougy, S.A. (2002). Liquorice (*Glycyrrhiza glabra*) and the adrenal-kidney-pituitary axis in rats. *Food and chemical toxicology*; 40(10); 1525-1527.

Alexander, E. C., & Deep, A. (2022). Characterization of a Hepatitis Outbreak in Children, 2021 to 2022. *JAMA Network Open*, 5(10), e2237091-e2237091.

Ali, M., Khan, T., Fatima, K., Ali, Q.U.A., Ovais, M., Khalil, A.T., Ullah, I., Raza, A., Shinwari, Z.K., Idrees, M. (2018). Selected hepatoprotective herbal medicines: Evidence from ethnomedicinal applications, animal models, and possible mechanism of actions. *Phytother Res*; 32(2); 199-215. doi: 10.1002/ptr.5957.

Al-Razzuqi, R., Al-Jawad, F., Al- Hussaini, J., Al-Jeboori, A. (2012). Hepatoprotective effect of *Glycyrrhiza glabra* in carbon tetrachloride-induced model of acute liver injury. *J Phys Pharm Adv*; 2; 259-63

Anagha, K., Manasi, D., Priya, L., Meera, M. (2014). Scope of *Glycyrrhiza glabra* (Yashtimadhu) as an Antiviral agent: A Review. *Int.J.Curr.Microbiol.App.Sci*; 3(12); 657-665

Ashfaq, U.A., Masoud, M.S., Nawaz, Z. (2011). Glycyrrhizin as antiviral agent against Hepatitis C Virus. *J Transl Med*; 9; 112. doi:10.1186/1479-5876-9-112

Baker JM, Buchfellner M, Britt W, Sanchez V, Potter JL, Ingram LA, Shiau H, Gutierrez Sanchez LH, Saaybi S, Kelly D, Lu X, Vega EM, Ayers-Millsap S, Willeford WG, Rassaei N, Bullock H, Reagan-Steiner S, Martin A, Moulton EA, Lamson DM, St George K, Parashar UD, Hall AJ, MacNeil A, Tate JE, Kirking HL. 2022. Acute Hepatitis and Adenovirus Infection Among Children – Alabama. *MMWR Morb Mortal Wkly Rep*; 6(18); 638-640. doi: 10.15585/mmwr.mm7118e1.

Basar, N., Oridupa, O. A., Ritchie, K. J., Nahar, L., Osman, N. M. M., Stafford, A., ... & Sarker, S. D. (2015). Comparative cytotoxicity of *Glycyrrhiza glabra* roots from different geographical origins against immortal human keratinocyte (HaCaT), lung adenocarcinoma

(A549) and liver carcinoma (HepG2) cells. *Phytotherapy Research*; 29(6); 944-948.

Bell, R. F., Moreira, V. M., Kalso, E. A., & Yli-Kauhaluoma, J. (2021). Liquorice for pain?. *Therapeutic advances in psychopharmacology*; 11; 20451253211024873.

Bisht, D., Rashid, M., Arya, R.K.K., Kumar, D., Chaudhary, S.K., Rana, V.S., Sethiya, N.K. (2022). Revisiting liquorice (Glycyrrhiza glabra L.) as anti-inflammatory, antivirals and immunomodulators: Potential pharmacological applications with mechanistic insight. *Phytomed Plus*; 2(1);100206. doi: 10.1016/j.phyplu.2021.100206.

Branswell, H. (2022). CDC investigating 109 unusual hepatitis cases in kids in outbreak. https://www.statnews.com/2022/05/06/cdc-looking-at-cases-of-109-children-in-suspected-hepatitis-outbreak/

Cao, Y., Shi, H., Sun, Z., Wu, J., Xia, Y., Wang, Y., ... & Lu, Y. 2019. Protective effects of magnesium glycyrrhizinate on methotrexate-induced hepatotoxicity and intestinal toxicity may be by reducing COX-2. *Frontiers in pharmacology*; 10; 119.

Cecilia, P., Thomas, E., (2012). Antiviral Medicinal Herbs and Phytochemicals. *Journal of Pharmacognosy*; 3(1); 45-48

Chan, H.T., Chan, C., Ho, J.W. (2003). Inhibition of glycyrrhizic acid on alfatoxin B1-induced cytotoxicity of hepatoma cells. *Toxicology*; 188:211–217

Champe PC, Harvey RA, Ferrier DR. *Biochemistry. Edisi ke-4. Philadelphia*: Lippincott Williams & Wilkins; 2009

Cheel, J., Onofre, G., Vokurkova, D., Tůmová, L., & Neugebauerova, J. 2010. Licorice infusion: Chemical profile and effects on the activation and the cell cycle progression of human lymphocytes. *Pharmacognosy Magazine*; 6(21); 26.

Chen, F.P., Chang, C.M., Wu, T.P., Yang, J.L., Kung, Y.Y., Huang, Y.H., Su, C.W., Lan, K.H., Chiang, S.C., Hwang, S.J. (2017). Clinical efficacy of Rong-Yang-Jyh-Gan-Tang on patients with chronic hepatitis C: A double-blinded randomized placebo-controlled crossover study. *J Ethnopharmacol*; 196;1-8. doi: 10.1016/j.jep.2016.12.013.

Chowdhury, B., Bhattamisra, S. K., & Das, M. C. (2013). Anti-convulsant action and

amelioration of oxidative stress by *Glycyrrhiza glabra* root extract in pentylenetetrazole-induced seizure in albino rats. *Indian journal of pharmacology*; 45(1); 40.

Chugh, A., Maximos, M., Perlman, M., Gonzalez-Peralta, R.P. (2016). Viral Hepatitis in Children: A Through E. *Pediatric Annals*; 45(12); e420-e6.

Clercq, E. (2000). Current lead natural products for the chemotherapy of human immunodeficiency virus (HIV) infection. *Med Res Rev*;20;323–349

Conway, R., & Carey, J. J. 2017. Risk of liver disease in methotrexate treated patients. *World Journal of Hepatology*; 9(26);1092.

ECDC (European Centre for Disease Prevention and Control). (2001). *Increase in severe acute hepatitis cases of unknown aetiology in children*, ECDC: Stockholm.

Gupta, M., Sasmal, S. K., Karmakar, N., Sasmal, S., & Chowdhury, S. (2016). Experimental evaluation of antioxidant action of aqueous extract of Glycyrrhiza glabra Linn. roots in potassium dichromate induced oxidative stress by assessment of reactive oxygen species levels. *Inter. J. Pharmacognosy and Phytochem. Res*; 8(8); 1325-1333.

Huan, C., Xu, Y., Zhang, W., Guo, T., Pan, H. and Gao, S. (2021). Research Progress on the Antiviral Activity of Glycyrrhizin and its Derivatives in Liquorice. *Front. Pharmacol*; 12;680674. doi: 10.3389/fphar.2021.680674

ITIS. Accessed on 7 june 2022. https://www.itis.gov/servlet/SingleRpt/Single Rpt?search_topic=TSN&search_value=26718 #null . diakses pada 7 juni 2022

Jenko, B., Tomšič, M., Jekić, B., Milić, V., Dolžan, V., & Praprotnik, S. (2018). Clinical pharmacogenetic models of treatment response to methotrexate monotherapy in Slovenian and Serbian rheumatoid arthritis patients: differences in patient's management may preclude generalization of the models. *Frontiers in pharmacology*; 9; 20.

Kimura, M., Inoue, H., Hirabayahi, K., Natsume, H., Ogihara, M. (2001). Glycyrrhizin and some analogues induce growth of primary cultured adult rat hepatocytes via epidermal growth factor receptors. *Eur J Pharmacol*; 431;151–161

Korenaga, M., Hidaka, I., Nishina, S., Sakai, A., Shinozaki, A., Gondo, T., (2011). A Glycyrrhizin-Containing Preparation Reduces Hepatic Steatosis Induced by Hepatitis C Virus Protein and Iron in Mice. *Liver Int*; 31(4); 552–560. doi:10.1111/j.1478-3231.2011.02469.x

Lin, Chien-Chu; Weng, Meng-Tzu; Chung, Chen-Shuan; Liang, Cheng-Chao. (2019). The dramatic effect of intravenous glycyrrhizin on acute-on-chronic hepatic failure in chronic hepatitis B patients without liver cirrhosis. *Advances in Digestive Medicine*; 6;153–157. doi:10.1002/aid2.13131

Mamedov, N. A., & Egamberdieva, D. (2019). Phytochemical constituents and pharmacological effects of licorice: a review. *Plant and Human Health*; 3; 1-21.

Maksoud, H.A., Magid, A., Mostafa, Y.M., Elharrif, M., Sorour, R., & Sorour, M. (2018). Ameliorative Effect of Liquorice Extract Versus Silymarin in Experimentally Induced Chronic Hepatitis: A Biochemical and Genetical Study. *Clinical Nutrition Experimental*; 23. doi: 10.1016/j.yclnex.2018.10.005.

Matsumoto, Y., Matsuura, T., Aoyagi, H., Matsuda, M., Hmwe, S.S., Date, T., (2013). Antiviral Activity of Glycyrrhizin against Hepatitis C Virus In Vitro. *PLoS One*; 8(7); e68992. doi:10.1371/journal.pone.0068992

Matsuo, K., Takenaka, K., Shimomura, H., Fujii, N., Shinagawa, K., Kiura, K., 2001. Lamivudine and Glycyrrhizin for Treatment of Chemotherapy-Induced Hepatitis B Virus (HBV) Hepatitis in a Chronic HBV Carrier with NonHodgkin Lymphoma. *Leuk. Lymphoma*; 41(1-2);191–195. doi:10.3109/10428190109057970

Moore, M.M., Elpern, D.J., Carter, D.J. (2004). Generalized nummular eczema secondary to interferon alfa-2b plus ribavirin combination therapy in a patient with chronic hepatitis C virus infection. *Arch Dermatol*; 140;215-217.

Nakagawa, K., Kitano, M., Kishida, H., Hidaka, T., Nabae, K., Kawabe, M., & Hosoe, K. (2008). 90-Day repeated-dose toxicity study of licorice flavonoid oil (LFO) in rats. *Food and chemical toxicology*; 46(7); 2349-2357.

Nazari, S., Rameshrad, M., & Hosseinzadeh, H. (2017). Toxicological effects of Glycyrrhiza glabra (licorice): a review. *Phytotherapy research*; 31(11); 1635-1650.

Ng, V., Science, M., Feld, J., *et al*. (2022). Severe acute hepatitis in children of unknown etiology. *Science Briefs of the Ontario COVID-19 Science Advisory Table*. https://doi.org/10.47326/ocsat.2022.03.63.1.0

Polansky, H., & Lori, G. (2020). Effects of Gene-Eden-VIR and Novirin on SARS-CoV: Implications for COVID-19. *Journal of Evidence-Based Integrative Medicine*; 25; 2515690X20932523.

Rad, S.J., Quispe, C., Herrera-Bravo, J., Belén, L.H., Kaur, R., Kregiel, D., ... & Suleria, H.A.R. (2021). Glycyrrhiza Genus: Enlightening Phytochemical Components for pharmacological and health-promoting abilities. *Oxidative medicine and cellular longevity*. 2021.

Radhakrishnan, N., Gnanamani, A., & Sadulla, S. (2005). Effect of licorice (*Glycyhrriza glabra* Linn.), a skin-whitening agent on Black molly (*Poecilia latipinnaa*). *Journal of applied cosmetology*; 23(4); 149.

Richard, S.A. (2021). Exploring the pivotal immunomodulatory and anti-inflammatory potentials of glycyrrhizic and glycyrrhetinic acids. *Mediators of Inflammation*. 2021.

Romero, M.R., Efferth, T., Serrano, M.A., Castaño, B., Macias, R.I.R., Briz, O., (2005). Effect of Artemisinin/artesunate as Inhibitors of Hepatitis B Virus Production in an "In Vitro" Replicative System. *Antiviral Res*; 68(2); 75–83. doi:10.1016/j.antiviral.2005.07.005

Ruszymah, B.H.I., Nabishah, B.M., Aminuddin, S., & Khalid, B.A.K. (1995). Effects of glycyrrhizic acid on right atrial pressure and pulmonary vasculature in rats. *Clinical and Experimental Hypertension*; 17(3); 575-591.

Ryder S, Beckingham I. 2001. Acute hepatitis. BMJ.322(7279):151-3.

Sato, H., Goto, W., Yamamura, J., Kurokawa, M., Kageyama, S., Takahara, T. Shiraki, K. (1996). Therapeutic basis of glycyrrhizin on chronic hepatitis B. *Antiviral Research*; 30(2–3); 171–177.

Saito, Z., Kaneko, Y., Kinoshita, A., Kurita, Y., Odashima, K., Horikiri, T., ... & Kuwano, K. (2016). Effectiveness of hepatoprotective drugs for anti-tuberculosis drug-induced hepatotoxicity: a retrospective analysis. *BMC Infectious Diseases*; 16(1); 1-6.

Sharma, V.A.R.S.H.A., & Agrawal, R.C. (2013). *Glycyrrhiza glabra*-a plant for the future. *Mintage J Pharm Med Sci*; 2(3); 15-20.

Sharma, V., Agrawal, A. (2014). In vivo antioxidant and hepatoprotective potential of *Glycyrrhiza glabra* extract on carbon tetra chloride (CCl 4) induced oxidative-stress mediated hepatotoxicity. *Int. J. Res. Med. Sci*; 2(1);314-320

Sharma, V., Katiyar, A., & Agrawal, R.C. (2018). *Glycyrrhiza glabra*: chemistry and pharmacological activity. Sweeteners, 87.

Shi, X., Yu, L., Zhang, Y., Liu, Z., Zhang, H., Zhang, Y., Liu, P., Du, P. (2020). Glycyrrhetinic acid alleviates hepatic inflammation injury in viral hepatitis disease via a HMGB1-TLR4 signaling pathway. *Int Immunopharmacol*; 84;106578. doi: 10.1016/j.intimp.2020.106578.

Shin, S., Jang, J.Y., Choi, B.I., Baek, I.J., Yon, J.M., Hwang, B.Y., ... & Kim, Y.B. (2008). Licorice extract does not impair the male reproductive function of rats. *Experimental animals*; 57(1);11-17.

Subrat, K.A., Sreenivas, V., Siddharth, D.G., Shakti, K., Yogesh, K.C., Anurag, T., Aejaz, H., Premashish, K., Abhijit, C., Gourdas, C., Shiv, K.S., Amarapurkar, D.N., Vidya, A., Mohan, D.G., Sushma, G., Deepali, M., Divya, S., Rohit, G., Badri, N.T. (2012). Treatment of Chronic Hepatitis due to Hepatitis C Virus (CH-C) in India: A Randomized Controlled Trial Comparing Daily Interferon-alfa-2b and Ribavirin with Daily Interferon-alfa-2b and Glycyrrhizin A Multicenter Study. *Journal of Clinical and Experimental Hepatology*; 2(1); 10-18.

Sulaiman, H.A., Sulaiman, A.S. (2012). *Obat herbal pada penyakit hati. Buku Ajar Ilmu Penyakit Hati*. 1 st ed. Jakarta: Sagung Seto, p:639-45.

Takahara, T., Watanabe, A., and Shiraki, K. (1994). Effects of Glycyrrhizin on Hepatitis B Surface Antigen: a Biochemical and Morphological Study. *J. Hepatol*; 21(4); 601–609. doi:10.1016/s0168-8278(94)80108-8

Tan, Q.Y., Hu, Q., Zhu, S.N., Jia, L.L., Xiao, J., Su, H.Z., ... & Jin, J. (2018). Licorice root extract and magnesium isoglycyrrhizinate protect against triptolide-induced hepatotoxicity via up-regulation of the Nrf2 pathway. *Drug delivery*; 25(1); 1213-1223.

Tang, J.L., 2006. Research priorities in traditional Chinese medicine. *BMJ*; 333(7564); 391–394.

Tang, B., Qiao, H., Meng, F., Sun, X. (2007). Glycyrrhizin attenuates endotoxin-induced acute liver injury after partial hepatectomy inrats. *Braz. J. Med Biol. Res*; 40; 1637–1646.

Thakur, A.K., & Raj, P. (2017). Pharmacological perspective of *Glycyrrhiza glabra* Linn: A mini-review. *J. Anal. Pharm. Res;* 5(5); 00156.

UKHSA. (2022). Investigation into acute hepatitis of unknown aetiology in children in England, technical briefing, https://assets.publishing.service.gov.uk/govern ment/uploads/system/uploads/attachment_data /file/1073704/acute-hepatitis-technical-briefing-2.pdf

Wahab, S., Annadurai, S., Abullais, S.S., Das, G., Ahmad, W., Ahmad, M.F., ... & Amir, M. (2021). *Glycyrrhiza glabra* (Licorice): A Comprehensive Review on Its Phytochemistry, Biological Activities, Clinical Evidence and Toxicology. *Plants*; 10(12); 2751.

Wang, J., Chen, X., Wang, W., Zhang, Y., Yang, Z., Jin, Y., ... & Yang, G. (2013). Glycyrrhizic acid as the antiviral component of Glycyrrhiza uralensis Fisch. against coxsackievirus A16 and enterovirus 71 of hand foot and mouth disease. *Journal of ethnopharmacology*; 147(1); 114-121.

WHO. 2022. COVID-19, Ukraine and other global health issues. Virtual press conference transcript. World Health Organization.

WHO. (2022). Multi-Country—Acute, Severe Hepatitis of Unknown Origin in Children. Available online: https://www.who.int/emergencies/disease-outbreak-news/item/2022-DON376 (accessed on 28 April 2022)

Xi, C., Peng, S., Wu, Z., Zhou, Q., & Zhou, J. (2017). Toxicity of triptolide and the molecular mechanisms involved. *Biomedicine & Pharmacotherapy*; 90; 531-541.

Yang, Q., Wang, J., Liu, R., Wang, Z., Li, Y., Zhang, Y., Hao, X., Huang, Y., Xie, W., Wei, H. (2016). Amelioration of concanavalin A-induced autoimmune hepatitis by magnesium isoglycyrrhizinate through inhibition of CD4+CD25-CD69+ subset proliferation. *Drug Des Devel Ther*; 10;443-453. doi:10.2147/DDDT.S92440.

Zadeh, J.B., Kor, Z.M., & Goftar, M.K. (2013). Licorice (*Glycyrrhiza glabra* Linn) as a valuable medicinal plant. *International journal of Advanced Biological and Biomedical Research*; 1(10); 1281-1288.

Zhang, H., Ya, G., & Rui, H. (2017). Inhibitory effects of triptolide on human liver cytochrome P450 enzymes and P-glycoprotein. *European journal of drug metabolism and pharmacokinetics*; 42(1); 89-98.

Ziaei, S., & Halaby, R. (2016). Immunosuppressive, anti-inflammatory and anti-cancer properties of triptolide: A mini review. *Avicenna journal of phytomedicine*; 6(2); 149.